

**NUMERICAL MODELLING AND UNDERLYING
ELECTROCHEMICAL MECHANISM CHARACTERISATION
OF CATHODIC PROTECTION FOR CHLORIDE
CONTAMINATED REINFORCED CONCRETE STRUCTURES**

Nan Xiang

School of Computing, Science and Engineering
University of Salford, Manchester, UK

Submitted in Partial Fulfilment of the Requirements for the Degree of
Doctor of Philosophy

June 2019

CONTENTS

PAGE

LIST OF CONTENTS.....	1
LIST OF TABLES.....	5
LIST OF FIGURES.....	6
LIST OF SYMBOLS AND ABBREVIATIONS.....	13
LIST OF PUBLICATIONS.....	17
CONTRIBUTIONS.....	18
ACKNOWLEDGEMENTS.....	19
ABSTRACT.....	20

CHAPTER 1 INTRODUCTION

1.1 Background.....	21
1.2 Problem Statement.....	22
1.3 Aim and Objectives.....	24
1.4 Thesis Layout.....	24

CHAPTER 2 LITERATURE REVIEW

2.1 Steel Corrosion in Concrete.....	26
2.2 Electrochemical Mechanism of Steel Corrosion.....	27
2.2.1 Principle of Steel Corrosion in Concrete.....	27
2.2.2 Controlling Factors of Steel Corrosion Process.....	29
2.2.3 Steel Depassivation Phenomenon.....	30
2.3 Thermodynamics of Steel Corrosion.....	34
2.4 Kinetics of Steel Corrosion.....	36
2.5 Cathodic Protection for Reinforced Concrete Structure.....	38
2.5.1 Sacrificial Anode Cathodic Protection.....	40

2.5.2 Impressed Current Cathodic Protection	41
2.6 Electrochemical Mechanism of Cathodic Protection.....	43
2.6.1 Principle of Cathodic Protection of Reinforced Concrete Structures	43
2.6.2 Beneficial and Negative Influences Induced by Cathodic Protection.....	47
2.7 Numerical Modelling of Cathodic Protection for Reinforced Concrete Structure	50
2.7.1 Boundary Condition of Numerical Modelling of Cathodic Protection	51
2.7.2 Development State of Numerical Modelling of Cathodic Protection	57

CHAPTER 3 RESEARCH METHODOLOGY

3.1 Introduction.....	61
3.2 Numerical Model for Cathodic Protection Process	62
3.2.1 Mathematical Modelling of Ionic Transport in Concrete.....	62
3.2.2 Numerical Modelling of Cathodic Protection	64
3.3 Case Study of Preliminary Simulation of Cathodic Protection	65
3.3.1 Model Description.....	65
3.3.2 Electric Field Distribution in Concrete	66
3.3.3 Boundary Condition	66
3.3.4 Case I (Constant Electrical Resistivity)	67
3.3.5 Case II (Variable Electrical Resistivity).....	71
3.3.6 Discussion and Summary	74
3.4 Electrochemical Mechanism of Steel-Concrete Interface in Cathodic Protection Process	75
3.4.1 Interfacial Electrochemical Mechanism.....	75
3.4.2 Research Idea on A New Butler-Volmer Equation Based Steel Polarisation Characterisation.....	78
3.5 Conclusions.....	79

CHAPTER 4 CONCRETE ELECTRICAL RESISTIVITY CHARACTERISATION

4.1 Introduction.....	80
4.2 Influence of Water Content.....	82
4.2.1 Characterisation in Terms of Water Saturation.....	82
4.2.2 Characterisation in Terms of Water Content.....	83
4.2.3 Characterisation in Terms of Water Loss.....	85
4.3 Influence of Chloride Content	86
4.4 Characterisation on Concrete Electrical Resistivity	87
4.4.1 Two Empirical Models.....	87
4.4.2 A New Semi-Empirical Model.....	90
4.4.3 Model Test.....	92
4.5 Conclusions.....	103

CHAPTER 5 BOUNDARY CONDITION CHARACTERISATION

5.1 Introduction.....	105
5.2 Reinforcement Polarisation — Butler-Volmer Equation.....	106
5.3 Reinforcement Polarisation — Real-Time Polarisation Curve.....	107
5.4 Analysis on Existing Polarisation Model.....	107
5.4.1 Butler-Volmer Polarisation Model.....	107
5.4.2 Real-Time Polarisation Model	108
5.5 Selection of the Polarisation Model.....	109
5.6 A New Butler-Volmer Equation based Polarisation Characterisation on Experiments	109
5.6.1 Background of the Experimental Data Used.....	109
5.6.2 Steel Polarisation under Cathodic Protection.....	111
5.6.3 Characterisation of Steel Polarisation under Cathodic Protection	113
5.7 Conclusions.....	120

CHAPTER 6 MODELLING OF CATHODIC PROTECTION FOR CHLORIDE CONTAMINATED REINFORCED CONCRETE STRUCTURES

6.1 Introduction.....	122
6.2 Numerical Modelling Setup.....	123
6.2.1 Model Description.....	123
6.2.2 Electric Field Distribution in Concrete	127
6.2.3 Boundary Condition	128
6.3 Results and Analysis	129
6.3.1 Ionic Distribution under Cathodic Protection	129
6.3.2 Ionic Condition under Cathodic Protection.....	134
6.3.3 Steel Corrosion Rate under Cathodic Protection.....	139
6.3.4 Comparison with Experimental Study	144
6.3.5 Parameter Study	146
6.4 Discussion.....	149
6.4.1 Ionic Distribution and Concentration Variation.....	149
6.4.2 Steel Corrosion.....	150
6.4.3 Effect of Concrete Pore Saturation on Cathodic Protection.....	152
6.5 Conclusion	153

CHAPTER 7 CONCLUSIONS AND RECOMMENDATIONS FOR FUTURE WORK

7.1 Conclusions.....	154
7.2 Recommendation for Future Research Work	155

REFERENCES	157
APPENDIX A.....	168
APPENDIX B.....	174
APPENDIX C.....	180

LIST OF TABLES

Table 2.1 Steel corrosion state at various pH levels (Berkeley and Pathmanaban, 1990).....	31
Table 2.2 Allowable values of chloride content in RC concrete (Kerkhoff, 2007).....	33
Table 3.1 Initial ionic concentrations (C_i) and diffusion coefficients (D_i) (Wang and Li, 2000).....	66
Table 4.1 Electrical resistivity of concrete (Ω -m) made by different cement type under different exposure condition (Polder, 1996).....	81
Table 4.2 Concrete specimen composition in case I.....	93
Table 4.3 Concrete specimen composition and exposure conditions in case II.....	97
Table 5.1 Specimen composition for rebar polarisation test.....	110
Table 6.1 Specimen composition for CP test (Oleiwi, 2018).....	124
Table 6.2 Initial ionic concentrations and diffusion coefficients (Buffle et al., 2007; Chang et al., 2018).....	126
Table 6.3 Model input parameters (Morgan and Lahav, 2007; Wang and Li, 2000; Oleiwi, 2018; Jiang and Yuan, 2013).....	126
Table 6.4 Constants of concrete electrical resistivity characterisation model.....	128
Table 6.5 Constants of steel polarisation characterisation model.....	129
Table 6.6 Results of numerical simulation and experimentation about the required CP current density for steel corrosion protection(mA/m^2).....	145

LIST OF FIGURES

Figure 2.1 Schematic illustration of steel corrosion in offshore RC structures.....	26
Figure 2.2 Schematic illustration of the steel corrosion in concrete (Hansson, 1984).	27
Figure 2.3 Electrochemical mechanism of steel corrosion in concrete (Pedferri and Bertolini, 2000).....	29
Figure 2.4 Schematic illustration of microcell corrosion (Cheung and Cao, 2013).....	31
Figure 2.5 Schematic illustration of macrocell corrosion (Cheung and Cao, 2013).	32
Figure 2.6 Schematic illustration of steel corrosion potential (Jan, 2003).	34
Figure 2.7 Schematic illustration of steel state in concrete as a function of potential and chloride content (Bertolini et al., 1998).....	35
Figure 2.8 Schematic illustration of active-passive anodic polarisation of steel in concrete (Pedferri, 1996).....	37
Figure 2.9 Schematic illustration of anodic behaviour of steel in concrete under different chloride contents (Bertolini et al., 1998)..	38
Figure 2.10 Schematic illustration of anodic polarisation curve of steel in concrete under different chloride contents (Angst et al., 2009).	38
Figure 2.11 Schematic diagram of SACP system of RC structure (Byrne et al., 2016).....	40
Figure 2.12 Application of zinc sheet anode in SACP for RC structure (Chess and Broomfield, 2014).	41
Figure 2.13 Application of SACP to protect the sheet steel piles.	41
Figure 2.14 Schematic diagram of ICCP system of RC structure (Byrne et al., 2016).....	42
Figure 2.15 Application of Ti/MMO anode and mortar cover (Araujo et al., 2013).....	43
Figure 2.16 Application of ICCP to protect the steel tubular piles.	43
Figure 2.17 Schematic illustration of steel state in concrete as a function of potential and chloride content under CP condition (Bertolini et al., 1998).....	44
Figure 2.18 Schematic illustration of CP application for RC concrete.	45
Figure 2.19 Schematic illustration of steel behaviour in concrete under CP.....	48
Figure 2.20 Schematic illustration of the variation of anodic (left) and cathodic behaviour (right) of steel bar affected by pH increase, chloride removal and oxygen consumption (Pedferri, 1996).....	48
Figure 2.21 Development of pH value of corrosion model with time under different impressed current density (Polder et al., 2011).	49

Figure 2.22 Polarisation curve of electrode reaction at equilibrium potential. (a) Linear scale for current density (Jan, 2003), (b) Logarithmic scale for current density.....	52
Figure 2.23 Combination of activation and concentration controlled kinetics (Frankel 2016).	55
Figure 2.24 Polarisation curve of electrode corrosion in acidic electrolyte. (a) Linear scale for current density (Jan, 2003), (b) Logarithmic scale for current density (Frankel, 2016).	56
Figure 3.1 Schematic diagram of control volume concrete.....	62
Figure 3.2 Model geometry ($x_1=20\text{mm}$, $x_2=45\text{mm}$, $y_1=50\text{mm}$, $y_2=150\text{mm}$, diameter of steel bar is 10mm).....	65
Figure 3.3 Profile of chloride concentration in concrete under 2.5A/m^2 . (a) $\rho_c = 1\Omega\text{-m}$, (b) $\rho_c = 10\Omega\text{-m}$	68
Figure 3.4 Profile of chloride concentration in concrete under 5A/m^2 . (a) $\rho_c = 1\Omega\text{-m}$, (b) $\rho_c = 10\Omega\text{-m}$	68
Figure 3.5 Profile of electric potential in concrete under 2.5A/m^2 . (a) $\rho_c = 1\Omega\text{-m}$, (b) $\rho_c = 10\Omega\text{-m}$	69
Figure 3.6 Profile of electric potential in concrete under 5A/m^2 . (a) $\rho_c = 1\Omega\text{-m}$, (b) $\rho_c = 10\Omega\text{-m}$	70
Figure 3.7 Profile of electric potential along the circumference of steel bar cross section under 2.5A/m^2 . (a) $\rho_c = 1\Omega\text{-m}$, (b) $\rho_c = 10\Omega\text{-m}$	71
Figure 3.8 Profile of electric potential along the circumference of steel bar cross section under 5A/m^2 . (a) $\rho_c = 1\Omega\text{-m}$, (b) $\rho_c = 10\Omega\text{-m}$	71
Figure 3.9 Profile of chloride concentration in concrete under 5A/m^2 . (a) $\rho_c = \frac{A}{c_{Cl+B}}$, (b) $\rho_c = \frac{c}{c_{Cl+OH}}$	73
Figure 3.10 Profile of electric potential in concrete under 5A/m^2 . (a) $\rho_c = \frac{A}{c_{Cl+B}}$, (b) $\rho_c = \frac{c}{c_{Cl+OH}}$	73
Figure 3.11 Profile of electric potential along the circumference of steel bar cross section under 5A/m^2 . (a) $\rho_c = \frac{A}{c_{Cl+B}}$, (b) $\rho_c = \frac{c}{c_{Cl+OH}}$	74
Figure 3.12 Profile of interfacial electric potential of chloride contaminated RC structure under CP application.	76
Figure 4.1 Effect of water saturation on concrete electrical resistivity (Gjørsv et al., 1977). .	83

Figure 4.2 Water exits in capillary pores under equilibrium condition (Bertolini et al., 2014).	84
Figure 4.3 Water adsorption isotherm of concrete refers to capillary pore radius (Hunkeler, 1996).	85
Figure 4.4 Hysteresis in water isotherm curve (Andrade et al., 2011).	86
Figure 4.5 Relative change of concrete electrical resistivity with chloride state (Hunkeler, 1996).	87
Figure 4.6 Experimental data of the study by Shaikhon (2015).	89
Figure 4.7 Comparison of three models on data by Saleem et al. (1996) at certain chloride contents. (a) Chloride content: 0 kg/m ³ , (b) Chloride content: 2.4 kg/m ³ , (c) Chloride content: 4.8 kg/m ³ , (d) Chloride content: 9.6 kg/m ³ , (e) Chloride content: 19.2 kg/m ³	94
Figure 4.8 Modelling the coupling effect of water and chloride contents on concrete electrical resistivity for the data by Saleem et al. (1996). (a) Modelling result of Equation (4.3), (b) Modelling result of Equation (4.9), (c) Modelling result of Equation (4.14).....	95
Figure 4.9 Modelling statistics for the data by Saleem et al. (1996). (a) RMSE, (b) R-squared.	96
Figure 4.10 Configuration of concrete specimen for concrete electrical resistivity measurements (Oleiwi, 2018). (a) Dimension, (b) Concrete specimen.	96
Figure 4.11 Comparison of the three models on data by Oleiwi (2018) (w/c = 0.4) at certain total chloride contents. (a) NaCl: 0%, (b) NaCl: 0.197%, (c) NaCl: 0.358%, (d) NaCl: 0.502%.....	97
Figure 4.12 Comparison of the three models on data by Oleiwi (2018) (w/c = 0.5) at certain total chloride contents. (a) NaCl: 0%, (b) NaCl: 0.217%, (c) NaCl: 0.389%, (d) NaCl: 0.517%.	98
Figure 4.13 Comparison of the three models on data by Oleiwi (2018) (w/c = 0.6) at certain total chloride contents. (a) NaCl: 0%, (b) NaCl: 0.223%, (c) NaCl: 0.402%, (d) NaCl: 0.53%.	98
Figure 4.14 Residuals of the three models from cases in Figures 4.11, 4.12 and 4.13. (a) w/c=0.4, (b) w/c=0.5, (c) w/c=0.6.	99
Figure 4.15 Modelling chloride effect on concrete electrical resistivity using the exponential weighting term in Equation (4.14).....	99
Figure 4.16 Modelling the coupling effect of water and chloride contents on concrete resistivity using Equation (4.3) for the data by Oleiwi (2018). (a) w/c=0.4, (b) w/c=0.5, (c) w/c=0.6.	100

Figure 4.17 Modelling the coupling effect of water and chloride contents on concrete resistivity using Equation (4.9) for the data by Oleiwi (2018). (a) w/c=0.4, (b) w/c=0.5, (c) w/c=0.6.	101
Figure 4.18 Modelling the coupling effect of water and chloride contents on concrete resistivity using Equation (4.14) for the data by Oleiwi (2018). (a) w/c=0.4, (b) w/c=0.5, (c) w/c=0.6.	102
Figure 4.19 Modelling statistics for the data by Oleiwi (2018). (a) w/c=0.4, (b) w/c=0.5, (c) w/c=0.6.	103
Figure 5.1 Configuration of CP experimental specimen (Oleiwi, 2018).....	110
Figure 5.2 Relation of total and free chloride concentration under different NaCl contents.	111
Figure 5.3 Variation trend of steel potential under CP application (Oleiwi, 2018).....	112
Figure 5.4 Rebar polarisation versus applied CP current density at different chloride contents. (a) Free chloride: 0%, (b) Free chloride: 0.666%, (c) Free chloride: 1.056%, (d) Free chloride: 1.872%, (e) Free chloride: 2.747%.....	114
Figure 5.5 Variation of anodic and cathodic Tafel slopes at different chloride contents (in term of molar concentration converted by free chloride content by cement mass). (a) Anode Tafel slope (b_a), (b) Cathodic Tafel slope (b_c).....	117
Figure 5.6 Polarisation curves of active and passive steel bars (Redaelli et al., 2006)	118
Figure 5.7 Relation between rebar corrosion state and applied CP current densities under different chloride contents (by cement mass).....	119
Figure 5.8 Relation between rebar corrosion state and its fitting curve under different CP current densities and chloride contents (by cement mass).	119
Figure 5.9 Variation of slope and intercept value under different chloride contents. (a) Slope (a), (b) Intercept (b).	119
Figure 6.1 Configuration of CP experimental specimen (Oleiwi, 2018).....	123
Figure 6.2 Model geometry (dimensions in mm).	124
Figure 6.3 Rate constants for oxidation of ferrous ions in different aqueous solutions as a function of pH (Morgan and Lahav, 2007)..	126
Figure 6.4 Redistribution of chloride ion concentration in concrete under 10mA/m ² (1% NaCl). (a) $t = 24$ hours, (b) $t = 10$ days, (c) $t = 30$ days, (d) $t = 90$ days.....	130
Figure 6.5 Redistribution of chloride ion concentration in concrete under 20mA/m ² (1% NaCl). (a) $t = 24$ hours, (b) $t = 10$ days, (c) $t = 30$ days, (d) $t = 90$ days.....	131

Figure 6.6 Distribution of chloride and hydroxyl ion concentration at steel-concrete interface under 25mA/m ² (1% NaCl). (a) <i>t</i> = 24 hours (b) <i>t</i> = 10 days.	133
Figure 6.7 Distribution of chloride and hydroxyl ion concentration at steel-concrete interface under 45mA/m ² (1% NaCl). (a) <i>t</i> = 24 hours (b) <i>t</i> = 10 days.	134
Figure 6.8 Variation of chloride ion concentration at steel-concrete interface remote from the anode under different current densities for CP operation time of 90 days (1, 2, 3.5 and 5% NaCl).	136
Figure 6.9 Variation of chloride and hydroxyl ion concentrations at steel-concrete interface under different CP operation time at current density of 15mA/m ² (1% NaCl). (a) steel-concrete interface near anode (b) steel-concrete interface remote from anode.	136
Figure 6.10 Variation of chloride and hydroxyl ion concentrations at steel-concrete interface under different CP operation time at current density of 75mA/m ² (1% NaCl). (a) steel-concrete interface near anode (b) steel-concrete interface remote from anode.	137
Figure 6.11 Variation of chloride and hydroxyl ion concentrations at steel-concrete interface under different CP operation time at current density of 15mA/m ² (2% NaCl). (a) steel-concrete interface near anode (b) steel-concrete interface remote from anode.	138
Figure 6.12 Variation of chloride and hydroxyl ion concentrations at steel-concrete interface under different CP operation time at current density of 75mA/m ² (2% NaCl). (a) steel-concrete interface near anode (b) steel-concrete interface remote from anode.	138
Figure 6.13 Distribution of steel corrosion rate along the circumference of steel bar cross section under 35mA/m ² (1% NaCl). (a) <i>t</i> = 24 hours, (b) <i>t</i> = 10 days, (c) <i>t</i> = 30 days, (d) <i>t</i> = 90 days.	140
Figure 6.14 Distribution of steel corrosion rate along the circumference of steel bar cross section under 75mA/m ² (1% NaCl). (a) <i>t</i> = 24 hours, (b) <i>t</i> = 10 days, (c) <i>t</i> = 30 days, (d) <i>t</i> = 90 days.	141
Figure 6.15 Variation of steel corrosion rate under different CP current densities for 24 hours. (a) 1, 2% NaCl, (b) 3.5, 5% NaCl.	142
Figure 6.16 Variation of ferric ion concentrations at steel-concrete interface under different CP current densities for 24 hours. (a) 1, 2% NaCl, (b) 3.5, 5% NaCl.	144
Figure 6.17 Comparison of the numerical and experimental results of required current density under different chloride contents.	145
Figure 6.18 Four hours steel potential decay versus applied current density.	148
Figure 6.19 Variation of steel corrosion rate under 5mA/m ² for 24 hours (1% NaCl). (a) PS = (1~100)%, (b) PS = (20~100)%..	147

Figure 6.20 Variation of steel corrosion rate under 10mA/m ² for 24 hours (1% NaCl). (a) PS = (1~100)%, (b) PS = (20~100)%.....	147
Figure 6.21 21Variation of steel corrosion rate under 15mA/m ² for 24 hours (1% NaCl). (a) PS=(1~100)%, (b) PS=(20~100)%.....	147
Figure 6.22 Variation of steel corrosion rate under 10mA/m ² for 24 hours (2% NaCl). (a) PS = (1~100)%, (b) PS = (20~100)%.....	148
Figure 6.23 Variation of steel corrosion rate under 15mA/m ² for 24 hours (2% NaCl). (a) PS = (1~100)%, (b) PS = (20~100)%.....	148
Figure 6.24 Variation of steel corrosion rate under 20mA/m ² for 24 hours (2% NaCl). (a) PS=(1~100)%, (b) PS=(20~100)%.....	149
Figure A.1 Redistribution of chloride concentration in concrete under 10mA/m ² (2% NaCl). (a) <i>t</i> = 24 hours, (b) <i>t</i> = 10 days, (c) <i>t</i> = 30 days, (d) <i>t</i> = 90 days.....	168
Figure A.2 Redistribution of chloride concentration in concrete under 20mA/m ² (2% NaCl). (a) <i>t</i> = 24 hours, (b) <i>t</i> = 10 days, (c) <i>t</i> = 30 days, (d) <i>t</i> = 90 days.....	169
Figure A.3 Redistribution of chloride concentration in concrete under 10mA/m ² (3.5% NaCl). (a) <i>t</i> = 24 hours, (b) <i>t</i> = 10 days, (c) <i>t</i> = 30 days, (d) <i>t</i> = 90 days.....	170
Figure A.4 Redistribution of chloride concentration in concrete under 20mA/m ² (3.5% NaCl). (a) <i>t</i> = 24 hours, (b) <i>t</i> = 10 days, (c) <i>t</i> = 30 days, (d) <i>t</i> = 90 days.....	171
Figure A.5 Redistribution of chloride concentration in concrete under 10mA/m ² (5% NaCl). (a) <i>t</i> = 24 hours, (b) <i>t</i> = 10 days, (c) <i>t</i> = 30 days, (d) <i>t</i> = 90 days.....	172
Figure A.6 Redistribution of chloride concentration in concrete under 20mA/m ² (5% NaCl). (a) <i>t</i> = 24 hours, (b) <i>t</i> = 10 days, (c) <i>t</i> = 30 days, (d) <i>t</i> = 90 days.....	173
Figure B.1 Distribution of chloride and hydroxyl ions concentration at steel-concrete interface under 25mA/m ² (2% NaCl). (a) <i>t</i> = 24 hours (b) <i>t</i> = 10 days.	174
Figure B.2 Distribution of chloride and hydroxyl ions concentration at steel-concrete interface under 45mA/m ² (2% NaCl). (a) <i>t</i> = 24 hours (b) <i>t</i> = 10 days.	175
Figure B.3 Distribution of chloride and hydroxyl ions concentration at steel-concrete interface under 25mA/m ² (3.5% NaCl). (a) <i>t</i> = 24 hours (b) <i>t</i> = 10 days.	176
Figure B.4 Distribution of chloride and hydroxyl ions concentration at steel-concrete interface under 45mA/m ² (3.5% NaCl). (a) <i>t</i> = 24 hours (b) <i>t</i> = 10 days.	177
Figure B.5 Distribution of chloride and hydroxyl ions concentration at steel-concrete interface under 25mA/m ² (5% NaCl). (a) <i>t</i> = 24 hours (b) <i>t</i> = 10 days.	178

Figure B.6 Distribution of chloride and hydroxyl ions concentration at steel-concrete interface under 45mA/m^2 (5% NaCl). (a) $t = 24$ hours (b) $t = 10$ days.	179
Figure C.1 Distribution of steel corrosion rate along the circumference of steel bar cross section under 35mA/m^2 (2% NaCl). (a) $t = 24$ hours, (b) $t = 10$ days, (c) $t = 30$ days, (d) $t = 90$ days.	180
Figure C.2 Distribution of steel corrosion rate along the circumference of steel bar cross section under 75mA/m^2 (2% NaCl). (a) $t = 24$ hours, (b) $t = 10$ days, (c) $t = 30$ days, (d) $t = 90$ days.	181
Figure C.3 Distribution of steel corrosion rate along the circumference of steel bar cross section under 35mA/m^2 (3.5% NaCl). (a) $t = 24$ hours, (b) $t = 10$ days, (c) $t = 30$ days, (d) $t = 90$ days.....	182
Figure C.4 Distribution of steel corrosion rate along the circumference of steel bar cross section under 75mA/m^2 (3.5% NaCl). (a) $t = 24$ hours, (b) $t = 10$ days, (c) $t = 30$ days, (d) $t = 90$ days.....	183
Figure C.5 Distribution of steel corrosion rate along the circumference of steel bar cross section under 35mA/m^2 (5% NaCl). (a) $t = 24$ hours, (b) $t = 10$ days, (c) $t = 30$ days, (d) $t = 90$ days.	184
Figure C.6 Distribution of steel corrosion rate along the circumference of steel bar cross section under 75mA/m^2 (5% NaCl). (a) $t = 24$ hours, (b) $t = 10$ days, (c) $t = 30$ days, (d) $t = 90$ days	185

LIST OF SYMBOLS AND ABBREVIATIONS

Abbreviation/Symbol	Definition
CP	Cathodic Protection
CPre	Cathodic Prevention
SACP	Sacrificial Anode Cathodic Protection
ICCP	Impressed Current Cathodic Protection
RC	Reinforced Concrete
CF	Carbon Fibre
ER	Electrochemical Realkalisation
ECR	Electrochemical Chloride Removal
FEA	Finite Element Analysis
FE	Finite Element
DC	Direct Current
FHWA	Federal Highway Administration
CIA	Central Intelligence Agency
ASCE	American Society of Civil Engineers
BS EN	British adoption of European Standard
ACI	American Concrete Institute
GDP	Gross Domestic Product
GNP	Gross National Product
C ₃ A	Tricalcium Aluminate
C-S-H	Calcium-Silicate-Hydrate
ASR	Alkali-Silica Reaction
Ti/MMO	Titanium Mixed Metal Oxide
SCE	Saturated Calomel Electrode
W/C	Water/Cement ratio
RH	Relative Humidity
PS	Pore Saturation
NaCl	Sodium Chloride
AgCl	Silver Chloride

KCl	Potassium Chloride
FEM	Finite Element Method
FDM	Finite Difference Method
BEM	Boundary Element Method
RMSE	Root Mean Square Error
$[M^{n+}]$	Ionic molar concentration, mol/m ³
R	Gas constant, J/(mol·k)
T	Absolute temperature, K
F	Faraday's constant, C/mol
δ	Nernst diffusion layer
n	Electrons number
N	Total number
α	Charge transfer coefficient
η	Polarisation, V
E	Electrochemical potential, V
E_{eq}	Equilibrium potential, V
E_{corr}	Corrosion potential, V
E_{pit}	Pitting potential, V
E_{pro}	Protection potential, V
E_a	Polarised anodic potential, V
E_c	Polarised cathodic potential, V
E_0	Standard potential, V
ΔE_{app}	Applied voltage under CP, V
E_{cp}	Steel potential under CP, V
I	Current, A
i_{corr}	Corrosion rate, A/m ²
i_{lim}	Limiting current density, A/m ²
i_o	Exchange current density, A/m ²
i_a	Anodic current density, A/m ²
i_c	Cathodic current density, A/m ²
i_n	Net current density, A/m ²

i_{ion}	Ions formed current density in concrete pore solution, A/m ²
i_{app}	Applied CP current density, A/m ²
i_{Fe}	Iron oxidation rate, A/m ²
i_{O_2}	Oxygen reduction rate, A/m ²
R_p	Steel polarisation resistance
b_a	Anode Tafel slope, V
b_c	Cathode Tafel slope, V
ρ_c	Concrete electrical resistivity, Ω -m
ρ_p	Electrical resistivity of cement paste, Ω -m
ρ_w	Electrical resistivity of pore water solution, Ω -m
R_r	Rock electrical resistivity, Ω -m
R_b	Brine electrical resistivity, Ω -m
S_w	Concrete pore water saturation, %
S_b	Brine saturation degree, %
ε	Rock porosity
ϑ	Concrete porosity
τ	Tortuosity of pore structure
ϵ	Volume fraction of porosity
φ	Volume fraction of cement paste
θ	Volume fraction of pore water
P_w	Total pore volume average pressures of the water phase
P_v	Total pore volume average pressures of the vapour phase
D_i	Ionic diffusion coefficient, m ² /s
C_i	Ionic concentration, mol/m ³
C_{Cl}	Chloride ions concentration, mol/m ³
$C_{Cl_{th}}$	Chloride threshold concentration, mol/m ³
$C_{Fe^{2+}}$	Ferrous ion concentration, mol/m ³
C_{OH}	Hydroxyl ion concentration, mol/m ³
ϕ	Static electric potential in concrete, V
ϕ_{bar}	Electric potential of steel bar, V
ϕ_{anode}	Electric potential of anode, V

ψ	Externally applied electric potential, V
C_{O_2}	Oxygen concentration
J	Ionic flux, mol/m ² ·s
A	Cross section area, m ²
v	velocity of bulk solution, m/s
z_i	Charge number
∇	Gradient operator
Cl/W	Chloride to water mass ratio
Φ	Steel bar diameter
p_{O_2}	Partial pressure of oxygen, bar

LIST OF PUBLICATIONS

Xiang, N., Y. Wang, H. M. Oleiwi, E. Chadwick, G. W. Yao, L. Augustus-Nelson, X. Y. Chen, and I. Shabalin. "Modelling the electrical resistivity of concrete with varied water and chloride contents." *Magazine of Concrete Research*, 2019

Xiang, N., Y. Wang, and H. M. Oleiwi. "Characterization of concrete electrical resistivity at varied pore structures, water and chloride contents." 38th Cement and Concrete Science Conference, 10-11 September 2018, University of Coventry, UK

Oleiwi, H. M., Y. Wang, N. Xiang, L. Augustus-Nelson, X. Y. Chen, and I. Shabalin. "An experimental study of concrete resistivity and the effects of electrode configuration and current frequency on measurement." 6th International Conference on Durability of Concrete Structures, 18-20 July 2018, University of Leeds, UK

Xiang, ZH. F., ZH. P. Guan, J. CH. Wang, F. ZH. Zhang, D. J. Xu, L. Jiang, and N. Xiang. "Research and engineering application on the control technology of prestressed construction for bridge structure." submitted for *Chongqing Architecture*, 2019

CONTRIBUTIONS

1. A semi-empirical mathematical model of concrete electrical resistivity taking account of the coupling effect of the varied water and chloride contents in concrete, it highlights the intrinsic linkage between concrete electrical resistivity and water content and the pore size distribution of concrete.
2. A new Butler-Volmer Equation based rebar polarisation model under cathodic protection condition taking account of the coupling effect of the varied chloride contents and applied cathodic protection current densities.
3. An improved cathodic protection numerical model for reinforced concrete structures which can directly characterise the steel corrosion state under the cathodic protection process.

ACKNOWLEDGEMENTS

First and foremost, I am deeply indebted to my supervisor Dr. Yu Wang, for his keen supervision, encouragement and continuous support throughout this PhD study, special appreciations on his guidance on numerical modelling. I believe that it would be hard to complete this study without his valuable guidance.

I am particularly grateful to my colleagues, Dr. Hayder Majeed Oleiwi, for his valuable experimental data given to support my numerical modelling study. Also, I would like to thank my best friend Mr. Chengzhang Liu for standing by me and supporting me all these years.

I would like to thank my family, Zhongfu Xiang and Li Xiao who have unconditionally supported and encouraged me over the years of my PhD studies.

Finally, I would like to thank my beloved husband Dr. Theo Theodoridis for his love, endless patience and continuous support.

ABSTRACT

Cathodic Protection (CP) as an effective electrochemical repair technique has been widely employed in the rehabilitation of deteriorated Reinforced Concrete (RC) structures worldwide. However, the quantitative specifications of CP technology for RC structures in national and international standards mainly depend on empirical experience and qualitative assessment, which lead to conservative results and poor economic benefits.

Numerical modelling and simulation have been proved as the effective tools to help understand the CP fundamental electrochemical mechanisms. They are useful to investigate the effects of environmental and operational factors on the performance of the CP system providing the optimum operation. A large number of CP numerical studies for RC structures have been carried out in the past couple of decades. However, most of the previous CP numerical studies, in terms of the literature research in this study, have some deficiencies of concern. For example, most CP numerical modelling cases neglected the variability of the concrete electrical resistivity and the steel polarisation resistance. Meanwhile, many modelling works did not consider the coupling effect of the transportation of different ionic species in concrete and the applied CP electric field effect.

This research aims to improve the CP numerical modelling for the RC structures to comprehensively take into account the major electrical and electrochemical mechanisms involved in CP process. Three major contributions have been made in this study. 1) Based on a previous experimental research, this study proposed and developed a concrete electrical resistivity model taking account of the coupling influence of the varied water and chloride contents; 2) presented a characterisation for the steel polarisation state under CP conditions; 3) considered the coupling effect of the ionic behaviour and electric field action in the process of CP numerical simulation. At last, combining these two developed models, put forward an improved CP numerical modelling of RC structures.

CHAPTER 1

INTRODUCTION

1.1 Background

Reinforced Concrete (RC) has been used as a structural material in civil engineering for hundreds of years due to the cheap cost, convenient construction, and excellent durability (Gao et al., 2011). It is well known that RC can present good performance over its service life is attributed to the steel bars in concrete are protected from corrosion attack by the high alkalinity environment of concrete pore solution, and the concrete cover isolates the steel bars with the external harmful species (Hansson et al., 2012). However, in recent decades the premature deterioration of RC structures due to corrosion of reinforcement has become a serious worldwide issue, which severely degrades the structural durability, poses a major problem in the economy, and even causes the loss of people's lives (Sun et al., 2010).

Reinforcement corrosion is the major cause induces the damage of RC structures, and directly influences the sustainability of infrastructure. Concerning the causes of steel corrosion has been the main research subject for many durability studies. For the concern, a large number of previous research have identified at chloride attack plays a critical role in steel corrosion in both newly-built and existing RC structures (Bertolini et al., 2004). Chloride induced steel corrosion in concrete is a serious problem, which can be very dangerous, and the repair cost can be extremely costly (Olewi, 2018). Trethewey and Chamberlain (1995) reported that the annual cost of corrosion in the US was first estimated in 1949 to be \$5 billion which is equivalent to 2.1% of the Gross National Product (GNP). In North America the estimated cost for structural restoration is about 10 billion dollars (Hansson and Hansson, 1993). A similar situation was been seen in Europe, and the worse situation found in Middle East due to the severe environment (Wang, 2001). The US Federal Highway Administration (FHWA) had estimated the annual cost for maintain of highway bridges in 2002 to be \$8.3 billion (Koch et al., 2002), and the necessary annual maintenance investment used for improving bridge

conditions reached US \$17 billion (ASCE, 2009). It has been reported that the worldwide annual corrosion cost approximately occupied 3-4% of the Gross Domestic Product (GDP) of industrialised countries (Schmitt, 2009; CIA, 2009).

In recent decades, many different corrosion prevention technologies have been developed, including structural quality control (high-performance concrete), barrier separation (coating, anti-corrosion painting), chemical additives (corrosion inhibitor), and electrochemical prevention. The electrochemical prevention methods include Cathodic Protection (CP), Electrochemical Realkalisation (ER), and Electrochemical Chloride Removal (ECR) (Berkeley and Pathmanaban, 1990; Qiao et al., 2016). However, most of the non-electrochemical repair techniques have been found that which are not very effective in mitigating the steel corrosion rate with little or no success in practice (Hong et al., 1993), meanwhile, lots of long-term experimental studies have demonstrated that the electrochemical prevention methods are the most effective and reliable ones in arresting the corrosion condition (Hong et al., 1993), among them, the CP technique is the most popular one, which has been increasingly applied in the practice of repairing and maintaining RC structures worldwide (Wilson et al., 2013). The USA Federal Highway Administration had stated that the CP is the only rehabilitation technique, which has been proven to stop corrosion in salt contaminated bridge decks regardless of chloride content (FHWA, 1982).

Although the CP effectiveness has been verified by a large number of scientific experimental research and successful project cases, not all the knowledge obtained from these studies has been expanded into practical engineering applications (Helm and Raupach, 2016); moreover, the understanding of the fundamental electrochemical mechanism of CP process in RC structures is still insufficient. So far, the design and maintenance of CP system primarily depends on empirical experiences (Polder et al., 2008) with a great number of assumptions. The situation presents a big challenge to the CP designer to obtain an optimum and reliable CP installation and operation for effectiveness and cost saving.

1.2 Problem Statement

Nowadays, numerical technology has been used to help understand the fundamental electrochemical mechanisms of the CP process in order to investigate the effects of

environmental and operational factors on the performance of CP systems. The advantage of computer-aided simulation was proven feasible to replace complex experiments (Qiao et al., 2015). However, in terms of the literature research in this study, the existing numerical models for the CP process still present some deficiencies, which distance them from the practical problem at a concerned level.

1. Most of the studies on the CP numerical modelling for the RC structures had taken the concrete electrical resistivity by default as constant; in other words, the variation of concrete conductivity had been neglected in most of the previous works. Such hypothesis leads to the fact that the Laplace Equation has been widely used as the governing equation in the CP numerical simulation to evaluate the current and potential distribution in the concrete domain. In reality, the concrete electrical resistivity is directly influenced by concrete state and the exposure environment, which can vary dramatically by changing from tens to thousands ($\Omega\cdot\text{m}$) under aggressive environments (Hornbostel et al., 2013).
2. Few researchers considered the long-term effects of protection current of CP, such as the steel polarisation resistance changes caused by chloride ion removal and hydroxyl ion production at the steel-concrete interface. In reality, the steel polarisation resistance will increase if the steel state transfers from the corrosion into the passive state. In many previous works the steel polarisation resistance was defined in terms of the Butler-Volmer Equation or the measured polarisation curve, which have been adopted to describe the boundary conditions for the electrochemical reactions occurring at the steel-concrete interface. However, most of the work did not consider the variations of the polarisation curve itself which was influenced by the state or condition change at the steel-concrete interface. As a result, its application in CP simulation could not reflect the long-term effect.
3. The majority of the CP numerical modelling of RC structures did not consider the coupling effect of the transportation of different ionic species in concrete, and the applied CP electric field effect; therefore, the CP effectiveness could not be evaluated by the actual steel corrosion rate but the steel potential.

1.3 Aim and Objectives

This research aims to make a contribution to address the three issues seen above. To achieve that, there are four objectives planned for this study.

1. Mathematically characterise a concrete electrical resistivity model considering the coupling influence of the varied water and chloride contents.
2. Propose a steel polarisation model taking account of the coupling influence of the varied chloride contents and applied CP current densities.
3. Consider the coupling effect of the ionic behaviour in concrete and the applied electric field action in the process of CP numerical simulation.
4. Implement these two developed models into a Finite Element Analysis (FEA) CP numerical model, and validate the CP numerical model on an experimental work.

1.4 Thesis Layout

This thesis is divided into seven chapters as below:

Chapter 1 — Introduction covers the background of this study, the existing problems, and the research aims and objectives are briefly described.

Chapter 2 — Literature review goes over the fundamental electrochemical theory of steel corrosion in concrete, the thermodynamics and kinetics of steel corrosion, the fundamental principle of CP for RC structures, and the application and development of numerical modelling of CP RC structures.

Chapter 3 — Research methodology introduces the mathematical model adopted for the numerical modelling of CP process, presents a preliminary CP numerical case study to verify the effect of concrete electrical resistivity, and puts forward the research idea on the steel polarisation characterisation.

Chapter 4 — Concrete electrical resistivity characterisation introduces a mathematical characterisation model for the electrical resistivity of concrete for varied water and chloride contents.

Chapter 5 — Boundary condition characterisation describes a new steel polarisation model, which considers the varied chloride contents and applied CP current densities.

Chapter 6 — CP numerical modelling of chloride contaminated RC structures, in which the two models in Chapters 4 and 5 are implemented into the CP modelling, which considers the coupling effect of ionic transportation and applied electric field. The numerical model has been validated with an experimental work, and a parameter study has been conducted.

Chapter 7 — Conclusions and recommendations for future research work.

CHAPTER 2

LITERATURE REVIEW

2.1 Steel Corrosion in Concrete

Steel corrosion in concrete has been recognised as the predominant factor to bring about structural premature failures and consequent costly repairs for many decades, especially for coastal and offshore structures where the Reinforced Concretes (RC) structures, subjected to chloride contaminated seawater, are the most susceptible to corrosion due to aggressive environments, as shown in Figure 2.1.



Figure 2.1 Schematic illustration of steel corrosion in offshore RC structures.

In general, the concrete acts as both physical and chemical barrier to provide the embedded steel bar a high degree of protection (Gjørsv et al., 1977; Broomfield, 1997). The chemically passive film is formed on the steel surface under the high alkaline environment due to the pH value of concrete pore solution in the range of 12.5 to 13.2. However, on condition that the passive film has been destroyed, steel corrosion subsequently takes place. The following phenomena can be expected. The steel corrosion results in not only the loss of rebar section which reduces the structural carrying capacity but, more importantly, the corrosion products expand several times bigger than the original steel size and the deposit in a restricted space between the rebar and concrete, which creates tensile stresses in concrete, and leads to the loss

of bond between the rebar and concrete as well as cracking and spalling of concrete cover. In addition, these phenomena accelerate the ingress of harmful ions into concrete by aggravating the further corrosion and ultimately threatening the durability and security of engineering structures (Al-Sulaimani et al., 1990; Andrade et al., 2001).

2.2 Electrochemical Mechanism of Steel Corrosion

2.2.1 Principle of Steel Corrosion in Concrete

Steel corrosion in concrete is an essential electrochemical process, which contains the chemical and electrical species. It can be seen from Figure 2.2 that the process of steel corrosion at least contains a coupled anodic (at anode) and cathodic (at cathode) reactions on the steel surface exposed to the concrete environment.

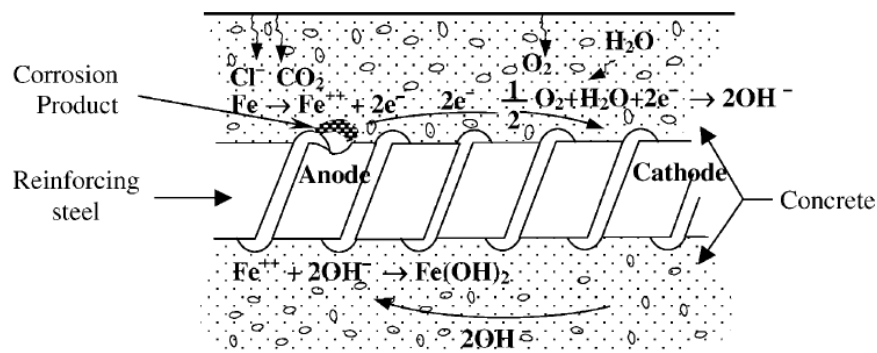


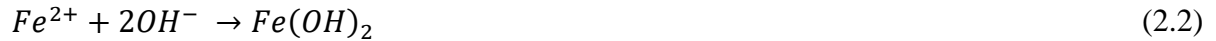
Figure 2.2 Schematic illustration of the steel corrosion in concrete (Hansson, 1984).

Anodic reaction is the actual iron oxidation (dissolution) and the cathodic reaction is commonly the oxygen reduction. The cathode has a more positive electrochemical potential in comparison with the anode resulting in the driving force for the steel corrosion (Warkus and Raupach, 2008). In detail, the steel corrosion in concrete includes the following four partial processes (Bertolini et al., 2014):

- **Anodic Reaction**

It is the iron oxidation reaction (Equation 2.1), in which the iron atoms pass into the concrete pore solution in the form of ferrous ion and the electrons are liberated in the steel phase

(Ahmad, 2003; Chess and Broomfield, 2014), subsequently, the ferrous ions react with the hydroxyl ions from the concrete pore solution to produce the ferrous hydroxide (Equation 2.2). When the quantity of ferrous ions exceed its solubility in pore solution, the ferrous hydroxide will be further oxidised to ferric hydroxide (Equation 2.3) and finally converted to hydrated ferric oxide (Equation 2.4), which is also commonly known as rust.



PH value of anode will drop due to the acidity formed by hydrolysis of iron ions (Equation 2.5) (Polder et al., 2011; Bertolini et al., 2014), and the inflow of chloride ions to anode due to its flow in the opposite direction of the corrosion current will both bring a further attack.



- **Cathodic Reaction**

It is the oxygen reduction reaction (Equation 2.6), in which the dissolved oxygen in concrete pore solution reacts with the water molecules and the liberated electrons from the steel phase to generate hydroxyl ion and then produce alkalinity (Ahmad, 2003; Cicek, 2013; Chess and Broomfield, 2014). However, there is a series of cathodic reactions, which can couple with the steel corrosion in neutral aerated environment, such as the water reduction reaction (Equation 2.7) accompanied by the formation of hydrogen. But in reality, oxygen is the most universal cathodic reactant which exists in the natural environment, and hence, the oxygen reduction is much more thermodynamically preferred and kinetically easier than water reduction. Even if the oxygen is absent, the water reduction reaction rate is so slow that the corresponding steel corrosion rate is very marginal, for example, the steel corrosion of underwater concrete structures is negligible. Therefore, the oxygen reduction is dominantly represented as the reduction reaction for the steel corrosion in concrete (Ashworth, 2010).





- **Electron Transfer in Steel Bar**

The steel itself (metallic path) is the location which contacts both the anode and cathode, and permits the electrons to flow. The released electrons from the anode, where the oxidation reaction occurs (production of electrons), transfer to the cathode, where the reduction reaction occurs (consumption of electrons), through the metallic path, leading to an electric current flow from the cathode to the anode inside the steel bar.

- **Current Flow in Concrete**

The concrete (electrolyte) is the location which contacts both the anode and cathode, and permits the charged ions to migrate. For the sake of completing the corrosion electric circuit, the electric current will flow from the anode to the cathode through the concrete and this is achieved by the movement of charged carrier ions in concrete pore solution.

2.2.2 Controlling Factors of Steel Corrosion Process

Steel corrosion is a cyclic process, the above four partial processes must all be present and function in order for the electrochemical reactions to occur. In case of any of the four partial processes is prevented the whole corrosion process will be stopped. Meanwhile, the four partial processes occur simultaneously and complementarily, in other words, the formed corrosion current between the anode and cathode through concrete and steel itself is equal in value and the relation is shown in Figure 2.3.

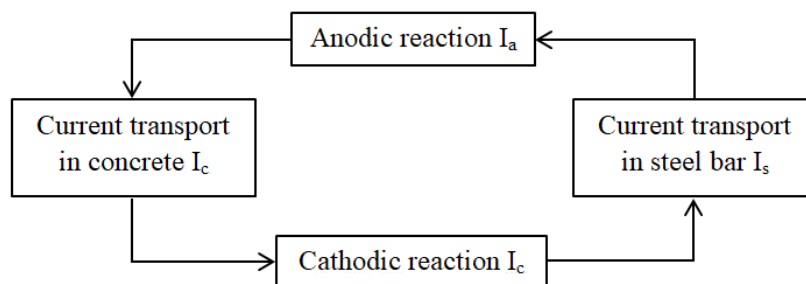


Figure 2.3 Electrochemical mechanism of steel corrosion in concrete (Pedefferri and Bertolini, 2000).

Customarily, the corrosion current is decided by the size of iron oxidation, so the equivalence relation of current among the four partial processes can be expressed by Equation (2.8):

$$I_{corrosion} = I_{anode} = I_{concrete} = I_{cathode} = I_{steel} \quad (2.8)$$

In reality, the reaction rate of each partial process can be controlled by many factors, due to the collateral effect between each partial process, these controlling factors will further affect the corrosion rate. The steel corrosion rate is dependent on the slowest rate of the four partial processes (Bertolini et al., 2014). Steel has very good electrical conductivity, apart from the current flow in steel itself, the corrosion rate will be negligible if any of the following phenomena occurs. The embedded rebar is in a passive state and the anodic reaction rate is very slow; this is called passive control. The oxygen content at the steel-concrete interface is insufficient and the cathodic reaction rate becomes very slow; this is called oxygen diffusion control. For the high concrete electrical resistivity the corrosion current flow in concrete is very slow; this is called ohmic control.

2.2.3 Steel Depassivation Phenomenon

Concrete carbonation and chloride attack are the main causes of steel corrosion in concrete, which are widely prevailing in civil infrastructure around the world (Zhou et al., 2014). Chloride ions can directly destroy rebar passive film, Acidic gases can carbonate the concrete nearby the rebar and indirectly destroy rebar passive film (Hornbostel et al., 2013).

- **Concrete Carbonation**

The concrete carbonation process starts as the acidic gas of carbon dioxide dissolved in pore solution (Equation 2.9), which reacts with the alkaline hydroxides presented in the concrete matrix to produce the calcium carbonate (Equation 2.10), this reaction is also called neutralisation reaction (Broomfield, 1997; Chess and Broomfield, 2014):



Concrete carbonation can induce the pH value of concrete pore solution to drop from about 13 to less than 9, which may cause the loss of steel passivity and then give rise to severe steel corrosion. Table 2.1 shows the effects of pH values on steel corrosion.

Table 2.1 Steel corrosion state at various pH levels (Berkeley and Pathmanaban, 1990).

pH value of concrete	State of steel corrosion
Below 9.5	Corrosion initiation (depassivation)
At 8.0	Passive film on the steel surface disappears
Below 7	Catastrophic steel corrosion occurs

Concrete carbonation induced steel corrosion generally occurs over a large area of steel surface, this is called uniform corrosion (generalised corrosion). The uniform corrosion belongs to the microcell corrosion in which pairs of anodic and cathodic reactions occur at the adjacent position. The anodic current is thus supported by the local cathodic current (Montemor et al., 2003; Cheung and Cao, 2013), as shown in Figure 2.4.

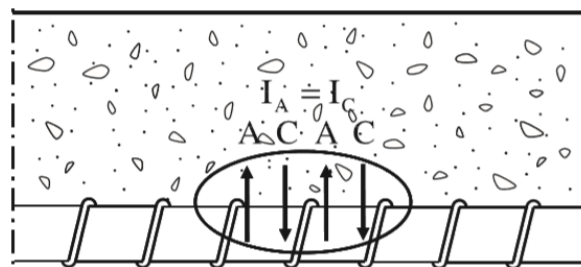


Figure 2.4 Schematic illustration of microcell corrosion (Cheung and Cao, 2013).

The probability of concrete carbonation induced steel corrosion is related to the carbon dioxide content in the atmosphere and the diffusion rate of carbon dioxide from the external environment to the internal concrete. At first, it usually occurs in urban and industrial areas where a large amount of carbon dioxide exists in the atmosphere and is discharged by the public transport systems or industries. Secondly, it is closely linked with the environmental relative humidity (RH), and the diffusion rate of carbon dioxide that is extremely slow in wet concrete ($RH > 90\%$) due to the gas transport in liquid. On the contrary, the carbonation reaction will not occur in very dry concrete ($RH < 40\%$) owing to the water content being a necessity for the carbonation reaction (Schutter, 2012). Tuutti (1980) stated that the highest carbonation rate can be expected at the RH of about 50%, and the alternative cycle of drying and wetting climates will provide the most aggressive environment for carbonation induced

steel corrosion in concrete. However, concrete carbonation is a very slow process and does not exceed several millimetres in concrete if the concrete quality is good (Sims, 1994).

- **Chloride Attack**

Chloride attack plays the most significant role in steel corrosion in concrete and chloride induced steel corrosion is the main concern for the deterioration of RC structures. The chloride ions can get into the RC structure from different sources, either from concrete raw materials (contaminated aggregates, mixing water), concrete admixtures (used for accelerating or impeding the cement hardening), or penetrate into concrete from the artificially applied de-icing salts or aggressive environments (seawater).

Chloride ions have little influence on the pH value of the concrete pore solution, but they can destroy the steel passive film even in highly alkaline environments (Bertolini et al., 2013). The penetration rate of chloride ions in concrete varies due to the heterogeneity of concrete, if the quantity of chloride ions at the steel-concrete interface exceeds the threshold concentration value, the directly contacting region will act as the anode, which will start to corrode and the remaining region will act as the cathode, resulting in localised corrosion (pitting corrosion). Pitting corrosion belongs to the macrocell corrosion in which the anodic and cathodic reactions are isolated spatially. The anodic current in the active zone is supported by the cathodic current in the passive zone (Lambert, 1995; Cheung and Cao, 2013), as shown in Figure 2.5. Pitting corrosion is the most common corrosion form, which is more dangerous than the uniform corrosion due to the high cathode to anode ratio, and can cause the high corrosion rate to reduce the rebar section, and then the rebar cannot sustain the external loading and this will lead to a catastrophic structural failure (Ahmad, 2003; Helm and Raupach, 2016).

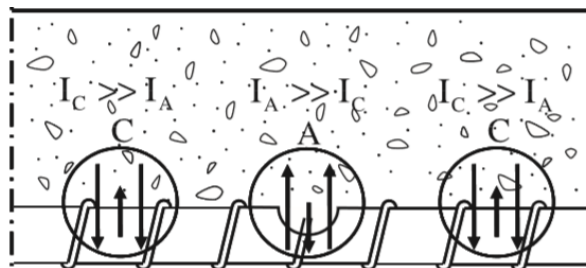


Figure 2.5 Schematic illustration of macrocell corrosion (Cheung and Cao, 2013).

Chloride ions in concrete may bind with the hydration products of cement, such as Tricalcium Aluminate (C_3A) and Calcium-Silicate-Hydrate (C-S-H) gel, by the physical and chemical forces, therefore, the chloride ions exist in concrete either in free form, dissolved in concrete pore solution or bound form, adsorbed or bound to the constituents of cement paste (Alonso and Sanchez, 2009). Nevertheless, only the free ions can destroy the rebar passive film and then promote the steel corrosion (Berkeley and Pathmanaban, 1990).

Moreover, the quantity of free ions in concrete is alterable, and a dynamic equilibrium that exists between the free and bound chloride ions in concrete pore solution depends on the cement type (binding capacity), and the varying concrete internal environment (Bertolini et al., 2014). For instance, there are amounts of bound chloride ions will be released back to the free form only if the pH value of concrete internal environment falls (Glass and Buenfeld, 1997; Montemor et al., 2003); therefore, if the RC structure is contaminated by both chlorides and carbonation, the steel corrosion effect will be superimposed. Blended cement (fly ash, slag or silica fume blended cement) has higher binding capacity than ordinary Portland cement in hydrated products and the free chloride concentration observed in the former cement is lower than the latter even with lower pH values (Page et al., 1986); so, blended cement is a better choice for the concrete material than ordinary Portland cement in terms of corrosion protection.

The chloride content in RC structures is an very important parameter indicator that refers to the structural quality control. There are several national standards that have different quantitative specifications for the limit value of chloride content in RC structures as shown in Table 2.2.

Table 2.2 Allowable values of chloride content in RC concrete (Kerkhoff, 2007).

Structural Type	BS EN 206	ACI 318	ACI 222R
	total chloride	water soluble chloride	acid-soluble chloride
RC structure	0.2-0.4%	0.15%	0.2%
Prestressed structure	0.1-0.2%	0.06%	0.08%

2.3 Thermodynamics of Steel Corrosion

If presuming that there is no reaction between the steel and the contacted water, the steel redox system (Equation 2.11) is in the equilibrium condition that the quantity of steel oxidised into the ionic form equals to the quantity of steel formed in its reduction reaction. At this moment, the steel presents the equilibrium potential ($E_{eq,steel}$) and there is no steel corrosion. The steel corrosion only occurs if the steel redox system is in contact with a different redox system and the equilibrium potential of that redox system is higher than the equilibrium potential of steel redox system, then the steel will be oxidised and that redox system will be reduced (Jan, 2003).



For the corroding steel in concrete, steel corrosion (anodic reaction) and oxygen reduction (cathodic reaction) randomly take place on the steel-concrete interface due to the complex natures of the rebar and concrete. The steel presents a corrosion potential (E_{corr}), which is a mixed potential between the equilibrium potential of steel redox system ($E_{eq,steel}$), and the equilibrium potential of oxygen redox system (E_{eq,O_2}), as shown in Figure 2.6. Under this circumstance, the steel corrosion potential is higher than the equilibrium potential of the steel redox system, the steel has the tendency to be oxidised to the iron ions. The corrosion potential is lower than the equilibrium potential of the oxygen system, which has a tendency to be reduced to the hydroxyl ions (Pedferri, 1996).

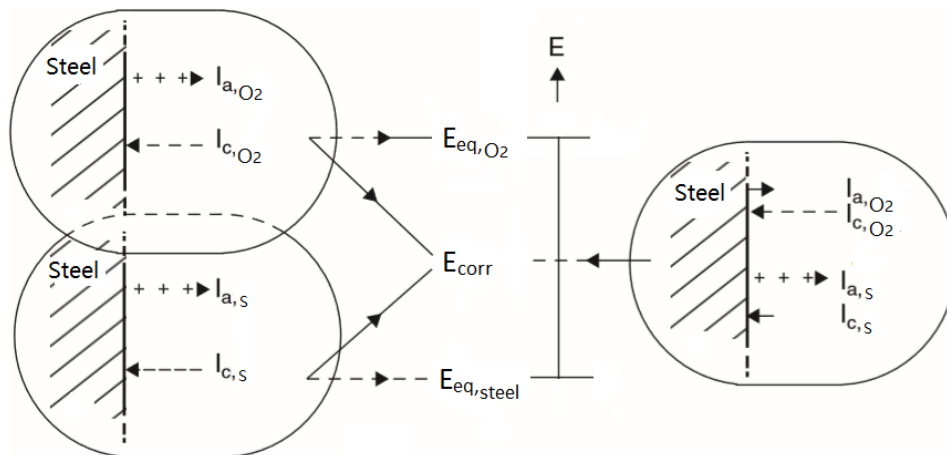


Figure 2.6 Schematic illustrate of steel corrosion potential (Jan, 2003).

The tendency of steel corrosion under the given various conditions has been studied by Pourbaix, who defined both the pitting potential (E_{pit}), it refers to the least potential at which the corrosion pit initiates on the steel surface, and the protection potential or repassivation potential (E_{pro}), below it the steel corrosion stops, shown by a graphical representation of the steel stability as a function of the potential and chloride content (Figure 2.7).

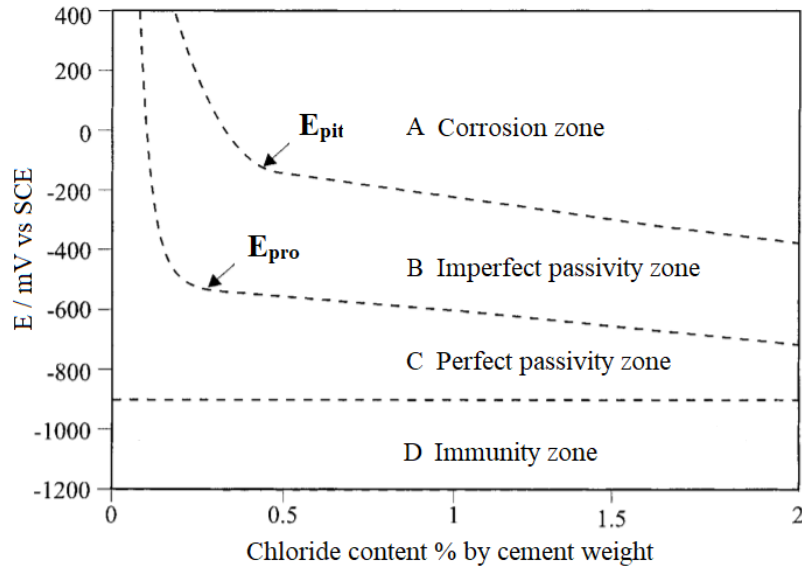


Figure 2.7 Schematic illustration of steel state in concrete as a function of potential and chloride content (Bertolini et al., 1998).

The steel potential can be determined by the Nernst Equation (2.12), which relates the electrochemical reaction potential to the concentrations of participating ions (Pedferri, 1996; Bertolini et al., 1998).

$$E = E_0 + \frac{RT}{nF} \ln[M^{n+}] \quad (2.12)$$

where E is the electrochemical potential (V), E_0 is the standard potential (V), R is the gas constant ($\text{J}\cdot\text{mol}^{-1}\cdot\text{k}^{-1}$), T is the absolute temperature (K), F is the Faraday's constant (C/mol), n is the involved electrons number, and $[M^{n+}]$ is the ionic molar concentration (mol/m^3). The thermodynamics for the steel corrosion was discussed by Pourbaix who showed four zones related to the possible steel states (Pedferri, 1996), as depicted in Figure 2.7:

1. Corrosion zone A: in which the steel corrosion can initiate and propagate.

2. Imperfect passivity zone B: in which the steel corrosion cannot initiate but can propagate, if move the potential from pitting potential (E_{pit}) to protection potential (E_{pro}) the steel corrosion rate decreases.
3. Perfect passivity zone C: in which the steel corrosion cannot initiate and propagate.
4. Immunity zone D: in which the hydrogen embrittlement of prestressed steel can occur.

Figure 2.7 shows that the steel corrosion can be decreased by moving the steel potential from corrosion zone to imperfect passivity zone, arrested by lowering the steel potential to the perfect passivity zone, where the passive film will be formed on the steel surface (Schweitzer, 2009). The mechanism of Cathodic Protection (CP) to control the steel corrosion in concrete is directly associated with that negatively shifting the steel potential to the perfect passivity zone while, combining the beneficial effect of the pH production to promote the steel repassivation. However, the Pourbaix diagram can only be used to predict the tendency of steel corrosion (thermodynamics nature) but not the steel corrosion rate (kinetics nature).

2.4 Kinetics of Steel Corrosion

Steel corrosion rate is determined by the steel polarisation curve, which describes the coupling effect between the steel exchange current density and the corresponding steel polarisation. The steel polarisation curve represents the characteristic curve of iron oxidation reaction, which is obtained experimentally, based on the steel equilibrium potential. Steel polarisation is the deviation of potential induced by the flow of electric current on the steel surface, which is equal to the potential shift and it is quantified in terms of overpotential. The exchange current density is the current in the absence of net electrolysis and at zero overpotential, where the cathodic current is balanced by the anodic current, and the ongoing current in both directions is called the exchange current density. In general, the steel corrosion rate is determined by the Butler-Volmer Equation (2.13):

$$i_{corr} = i_o \cdot \left\{ \exp \left[\frac{\alpha n F}{RT} (E - E_{eq,steel}) \right] \right\} \quad (2.13)$$

where i_{corr} is the steel corrosion rate (A/m^2), i_o is the steel exchange current density (A/m^2), α is the anodic charge transfer coefficient, $E_{eq,steel}$ is the steel equilibrium potential. When the steel is embedded in concrete the anodic reaction will present the active-passive behaviour shown in Figure 2.8, which can be classified into three phases (Pedferri, 1996):

1. Activity phase: when the steel potential is above its equilibrium potential ($E_{eq,steel}$), the steel starts to corrode and the corrosion rate increases with the growing potential.
2. Passivity phase: the corrosion rate decreases to a negligible value with the increasing potential owing to the passive film formed on the steel surface.
3. Transpassivity phase: the corrosion rate increases again at a higher critical potential – the pitting potential (E_{pit}).

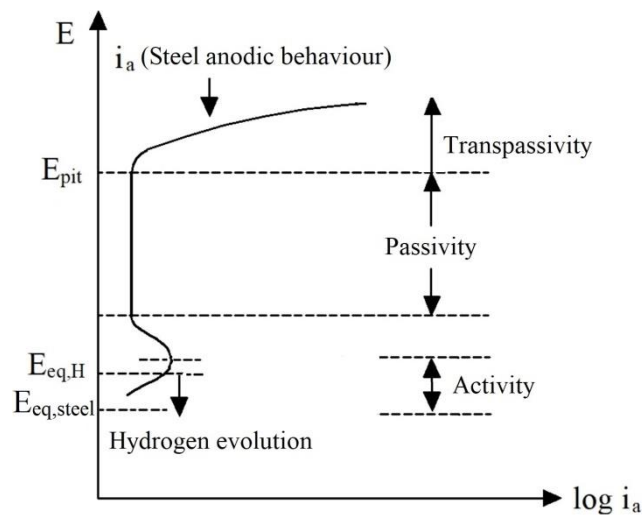


Figure 2.8 Schematic illustration of active-passive anodic polarisation of steel in concrete (Pedferri, 1996).

However, the chloride contents have a significant effect on the steel active-passive anodic behaviour. As shown in Figure 2.9, with the increasing chloride ions (Cl^-) the passivity region will be reduced and the corresponding pitting potential decreases and vice versa (Pedferri, 1996; Bertolini et al., 1998). As seen in Figure 2.10, with the increasing chloride ions the corresponding pitting potential (E_{pit}^A) drops to (E_{pit}^B), the steel corrosion potential (E_{corr}^A) drops to (E_{corr}^B), and the steel corrosion rate (i_{corr}^A) increases to (i_{corr}^B).

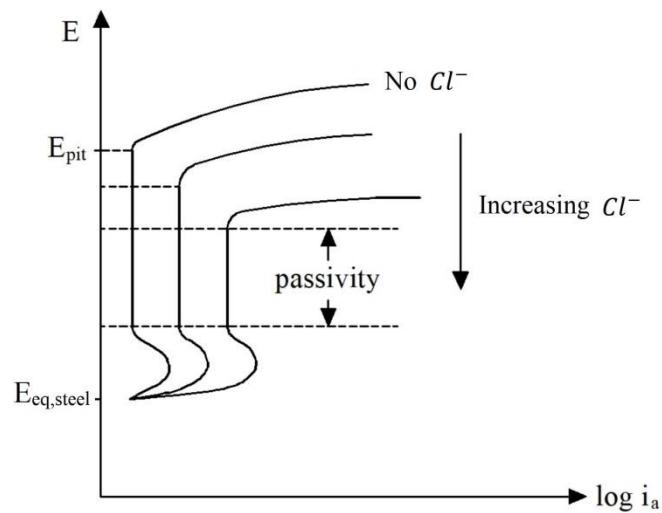


Figure 2.9 Schematic illustration of anodic behaviour of steel in concrete under different chloride contents (Bertolini et al., 1998).

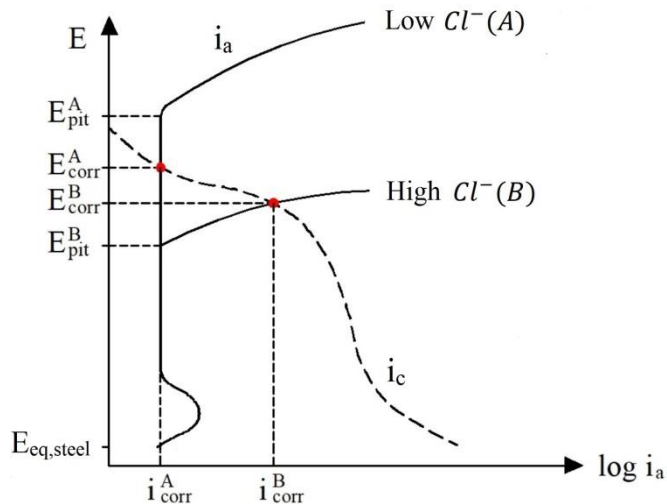


Figure 2.10 Schematic illustrate of anodic polarisation curve of steel in concrete under different chloride contents (Angst et al., 2009).

2.5 Cathodic Protection for Reinforced Concrete Structure

CP is an anti-corrosion electrochemical technology that has been widely used in many fields, including buried elements in soil, submerged ones in seawater, but to a lesser degree, in RC structures. The CP technique for RC structures has been developed in the last few decades in three stages (Pedferri, 1996).

- The first stage started with the first successful attempt of CP on chloride contaminated bridge decks that was conducted by Stratfull in North America in 1973 (Stratfull, 1974). Since the 1970s, various investigations have been dedicated to the application of CP on RC structures, which were mainly focused on the protection of bridge decks contaminated by chloride with simple anode materials.
- In the second stage, CP techniques began to be introduced outside North America and the application was extended to protect the bridge piles and slabs, parking lots, and industrial buildings affected by chloride induced corrosion. In the meantime, the more reliable anodes composed of mixed metal oxide activated titanium and carbon containing paints were developed.
- In the last stage, CP was applied to RC structures was not only limited to effectively reduce or stop the ongoing corrosion rate for existing structures but also used to improve the steel corrosion resistance for newly-built structures. This type of CP is called cathodic prevention (CPre), it is a particular case of CP, which is applied before the corrosion initiation and mainly during the construction period. CPre is capable of keeping the rebar in the passivation state for new RC structures (Pedefferri, 1996; Byrne et al., 2016; Carmona et al., 2017).

Conventional repair techniques used for RC structures, which is a laborious and time-consuming process by necessarily removing the affected concrete and reconstructing the structure, is accompanied by huge expense. A European inventory has shown that approximately half of the conventional repairs fail in about 10 years (Tilly and Jacobs, 2007), but the CP technique normally presents a shorter execution time, a longer service life but a significant advantage on the capital cost saving and lower maintenance costs than conventional repair (Polder et al., 2011). At present, the CP technology has been broadly applied to RC structures worldwide and in the United State and Canada more than 275 bridges introduced CP until 1989 (Barthalomew et al., 1993). In the early 1990s in Italy about 150,000m² of newly-built and prestressed RC structures employed CP. In North America more than 600,000m² of RC structures used CP and in Australia, Asia (Japan, Middle East and Korea) and Europe (UK, Italy and Norway) more than 500 bridges had installed CP until 1998 (Bertolini et al., 1998). There are two different way to supply the protection current, these are Sacrificial Anode Cathodic Protection (SACP) and Impressed Current Cathodic Protection (ICCP).

coating ones, adhesive zinc sheet anodes and discrete anodes (BSI, 2012). Figure 2.12 shows the practical application of zinc foil anode in SACP system. Figure 2.13 shows the application of SACP (aluminium alloy anode) at Campbeltown old quay wall (left) and Westway Dock in Glasgow (right).



Figure 2.12 Application of zinc sheet anode in SACP for RC structure
(Chess and Broomfield, 2014).

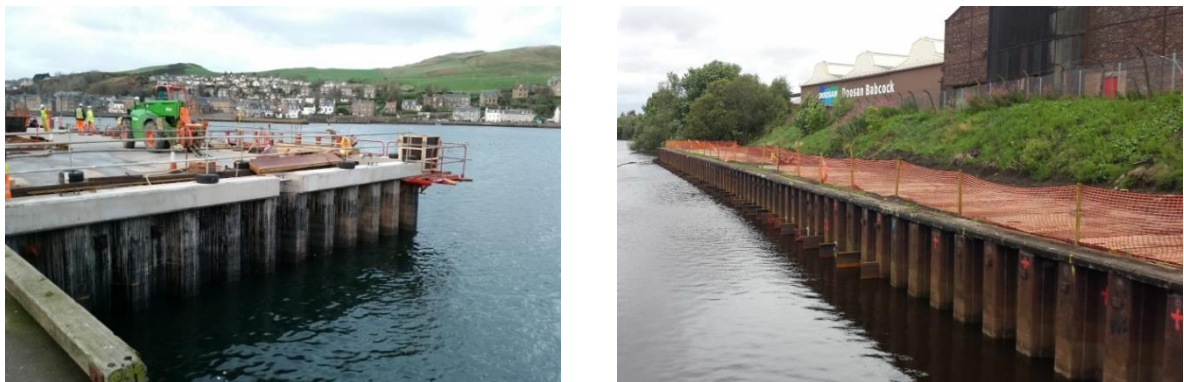


Figure 2.13 Application of SACP to protect the sheet steel piles.

2.5.2 Impressed Current Cathodic Protection

The basic setup of ICCP system of RC structure is shown in Figure 2.14. The predetermined anode connected to the positive terminal of the power supply and the protected reinforcement (cathode) connected to the negative terminal, a positive current will flow from the anode toward the rebar through concrete.

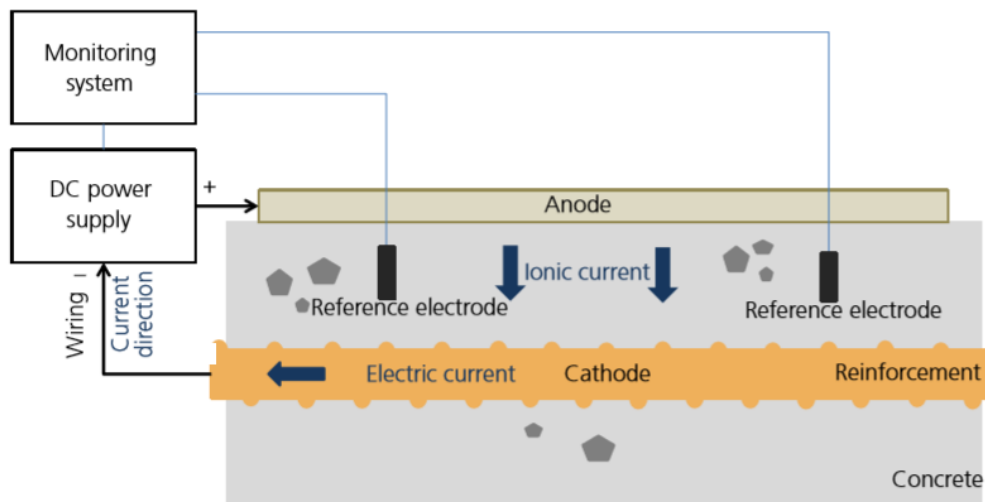


Figure 2.14 Schematic diagram of ICCP system of RC structure (Byrne et al., 2016).

In the ICCP system, the driving force between the anode and cathode is urged by the energy of rectifier, or Direct Current (DC) power supply which forces the electrons flow. The anode plays the role of electrons source, the anodic electrochemical reaction and the desired current can be adjusted by the rectifier (Paul Guyer et al., 2014). In consequence, the ICCP system can be used for the RC structure regardless of structural size and chloride contamination level, but according to the available high current supply the consideration also should be taken into account is the likelihood of hydrogen embrittlement and the interaction on adjacent structure (stray current corrosion). In practice, the ICCP has been applied widely on RC structure due to the high resistance of concrete environment requires the sufficient, enduring and controllable protection current, meanwhile, it is more appropriate for the large - scale structures with more serious corrosion condition and longer service life expectancy than SACP system (Wilson et al., 2013; Byrne et al., 2016).

The anode system provides protection current, occupies the crucial position that the corroding part of system and primarily determines the durability of ICCP system (Pedferri, 1996). To date, the new anode types are focus on the characteristics of easy installation, bonding efficiency and lower cost (Zhu et al., 2014). Plenty of research had conducted on ICCP anode, such as the most regularly used activated titanium mesh co5ated with inert metal oxides (Ti/MMO), organic coating anode and conductive cementitious anode (BSI, 2012). Figure 2.15 shows the application of Ti/MMO anode (left) and the mortar cover application (right) for ICCP. Figure 2.16 shows the practical application of ICCP (Ti/MMO anodes) at the new Kirkwall Harbour Development in 2012 (left) and Liverpool in 2016 (right).



Figure 2.15 Application of Ti/MMO anode and mortar cover (Araujo et al., 2013).



Figure 2.16 Application of ICCP to protect the steel tubular piles.

2.6 Electrochemical Mechanism of Cathodic Protection

2.6.1 Principle of Cathodic Protection of Reinforced Concrete Structures

The corroding rebar in concrete remains at a corrosion potential, the anodic oxidation (iron dissolution) and cathodic reduction (oxygen reduction) simultaneously occur on the steel surface at equal rates. Once the corrosion potential is polarised to its positive direction, iron dissolution is accelerated and oxygen reduction is decelerated, polarised to its negative direction the increasing oxygen reduction and decreasing iron corrosion can be observed (Srinivasan et al., 1996). The electrochemical mechanism of CP for RC concrete is based on applying the protection current by the external anode to pass through the concrete onto the protected rebar and forcing the steel potential shift to the negative direction, where the steel corrosion is thermodynamically impossible to take place (Christodoulou et al., 2010). The CPre for RC concrete is based on supplying a small current onto the passive rebar, this small current normally can provide at least 100-200mV steel potential drop to increase the chloride threshold concentration of rebar (which can induce the initiation of steel corrosion) by at least

one order of magnitude to further prevent or postpone the initiation of pitting corrosion (Pedferri, 1996; Bertolini et al., 1998).

Figure 2.17 shows the rebar state under different CP conditions related to the potential and chloride content. (1 → 4 → 6) and (1 → 4 → 5) represent the typical CP evolution paths where the steel corrosion decreases and stops (rebar repassivation occurs), respectively. (1 → 2 → 3) shows the typical CPRe evolution paths where the chloride threshold concentration of rebar increases.

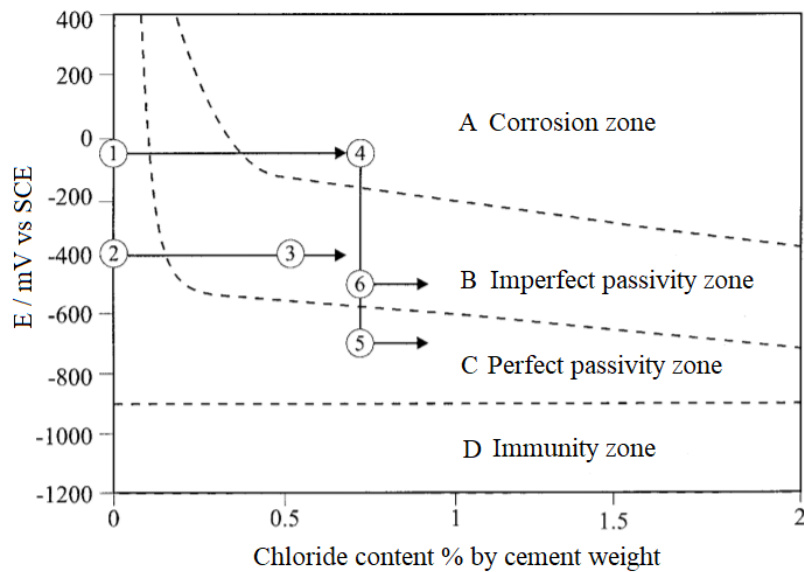


Figure 2.17 Schematic illustration of steel state in concrete as a function of potential and chloride content under CP condition (Bertolini et al., 1998).

The CP process of RC structures is also an electrochemical process which contains the chemical and electrical species. It can be seen from Figure 2.18, when the protection current density (i_{app}) is applied to rebar, the steel corrosion potential (E_{corr}) drops to more negative potential (E_{cp}) which is in the passivity region, resulting in the steel corrosion rate (i_{corr}) decreasing to (i'_a) and the corresponding oxygen reduction rate increasing from (i_{corr}) to (i'_c), the different value between the steel corrosion rate and oxygen reduction rate is balanced by the protection current density (i_{app}).

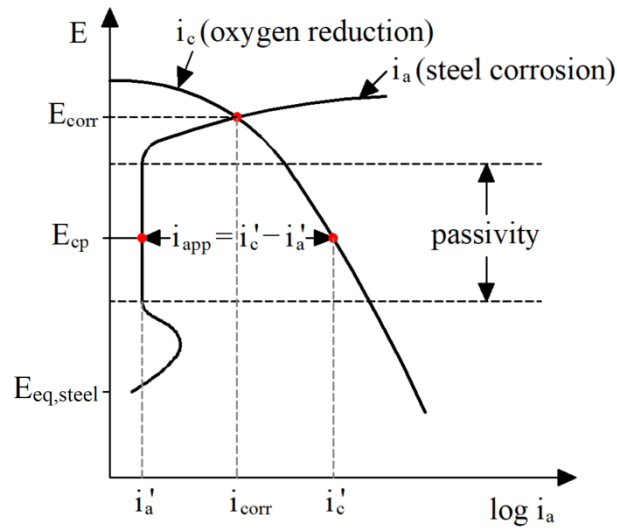


Figure 2.18 Schematic illustration of CP application for RC concrete.

When the CP is applied on RC structures, on condition that the oxygen and moisture are available around rebar in concrete, the following electrochemical reactions will occur at the steel/anode-concrete interface (Chess and Broomfield, 2014):

- **Cathodic and Anodic Reactions of Rebar (Cathode)**

There are two electrochemical reactions that take place at rebar, the steel corrosion (Equation 2.14) and reduction reaction of dissolved oxygen in concrete pore solution (Equation 2.15). If the rebar received inadequate protection current from the external anode, the steel corrosion decreased but still proceed and the oxygen reduction increased; if rebar received excess protection current, the steel corrosion stopped and the oxygen reduction increased greatly. The produced hydroxide ions by oxygen reduction can increase the alkalinity of concrete around rebar and enhance the rebar passive film, meanwhile, the chloride ions will be repelled due to the negatively shifted steel potential.



As mentioned before, in the cathodic reactions of steel corrosion, the hydrogen evolution (Equation 2.16) barely participates in steel corrosion in neutral aerated environment. However, the hydrogen evolution occupied a very important position in CP for RC structure. Under CP application, if the steel potential becomes increasingly negative and the oxygen has been completely consumed, hydrogen evolution could occur, which can lead to severe hydrogen

embrittlement, especially for prestressed RC structures. This should be taken into consideration when design CP for applications on RC structure.

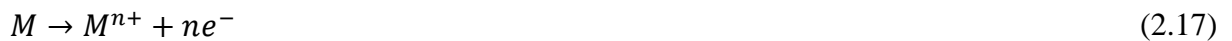


- **Anodic Reaction of External Anode**

Nowadays there are three generic types of anode in service they are consumable, semi-consumable and non-consumable (Ashworth, 2010). If the anode is consumable, the protection current will be produced by anode oxidation (Equation 2.17). If non-consumable anode, anodic reaction (Equation 2.18) by decomposing the aqueous environment will replace the anode oxidation, this is the predominant oxidation reaction expected in CP application, which together with the oxygen formation and accumulation of hydrogen ions at the anode-concrete surface and then increases the acidity, the acidic condition may lead to concrete degradation (Berkeley and Pathmanaban, 1990). If semi-consumable anode, anodic reaction comprise the anode oxidation and environment oxidation.

Moreover, if the RC concrete is chloride contaminated, the applied electric field will also drive the chloride ions in concrete to move from the rebar (cathode) toward the external anode, where chloride evolution may take place (Equation 2.19). Furthermore, if there are plenty of hydroxide ions generated from the cathodic reaction which migrate to the anode, the hydroxide ions may be oxidised (Equation 2.20).

Therefore, for continued anodic operation, the selected anode should chemically resist its own products, especially the gaseous product should be discharged instantly to avoid interfering with anode operation (Ashworth, 2010).



2.6.2 Beneficial and Negative Influences Induced by Cathodic Protection

Under the CP application for RC structures, there is a current circulation built between the external anode and the protected steel bar through the concrete, which can principally induce the steel cathodic polarisation, electrochemical reactions at the steel/anode-concrete interface, and the ions transportation in concrete, respectively, these resultant phenomena will further cause both beneficial and negative influences .

- **Primary Beneficial Influences**

The impressed protection current will give rise to the steel cathodic polarisation and this polarisation phenomenon can induce the beneficial influences in respective thermodynamic and kinetics aspects:

1. Decrease the driving force (potential difference between steel corrosion potential and steel equilibrium potential) for anodic reaction.
2. Increase the resistance of anodic reaction.

As shown in Figure 2.19, when the steel corrodes, the steel corrosion potential (E_{corr}) is higher than its equilibrium potential ($E_{eq,steel}$), the difference between these two potentials forms the driving force which impels steel corrosion to occur. Under the CP action, cathodic polarisation will shift the steel corrosion potential to a more negative value (E_{cp}), which reduces the driving force from $(E_{corr} - E_{eq,steel})$ to $(E_{cp} - E_{eq,steel})$, and then the steel corrosion rate decreases.

The anodic resistance (steel resistance to oxidation) will become extremely high if the steel potential drops into the passivity region and the passive film formed on steel surface (repassivation), and then the corrosion rate becomes negligible.

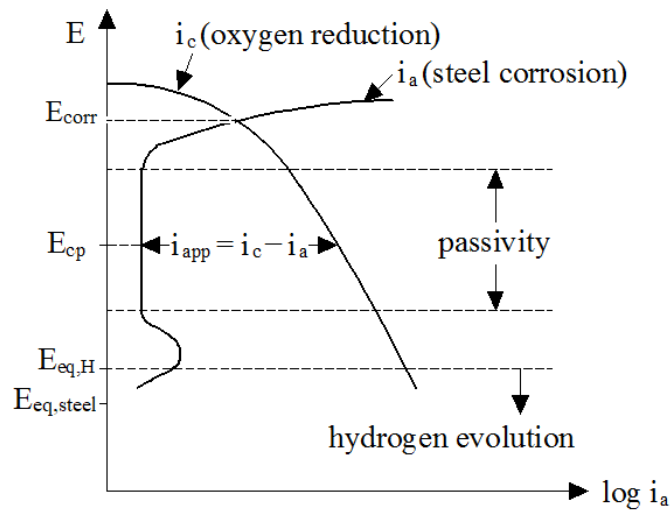


Figure 2.19 Schematic illustration of steel behaviour in concrete under CP.

- **Secondary Beneficial Influences**

Under CP the induced electrochemical reaction at the steel-concrete interface is mainly the oxygen reduction reaction which is accompanied by alkalinity production and oxygen consumption, the generated hydroxyl ions can neutralise the acidity of the corrosion site and further increase the pH value of the immediate environment of steel surface. It can be seen from Figure 2.20 that these two effects can stop and prevent steel corrosion by widening the passivity region of steel in concrete and depolarising the cathodic reaction (Pedferri, 1996).

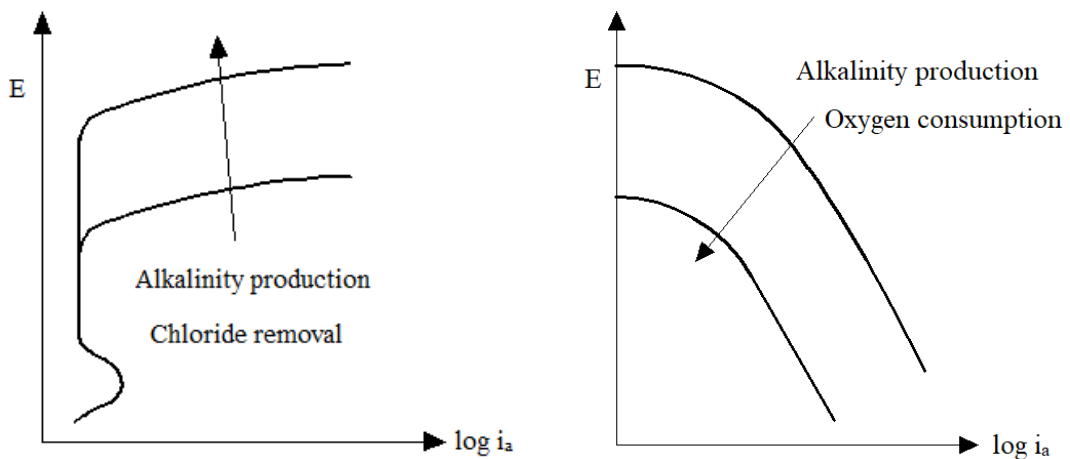


Figure 2.20 Schematic illustration of the variation of anodic (left) and cathodic behaviour (right) of steel bar affected by pH increase, chloride removal and oxygen consumption (Pedferri, 1996).

Under the applied CP electric field, the current flowing between the anode and the steel bars in concrete is carried directly by the ions in the pore solution related to the ionic mobility and

concentration, the negatively charged ions will migrate in the opposite direction of protection current. Thus for chloride contaminated concrete, the chloride ions will be repelled from the rebar to the anode, namely, the benefits in decreasing the chloride content near the steel surface and building a barrier to slow down the ingress of chloride ions from the external environment (Pedferri, 1996; Liu and Shi, 2012).

Polder et al. (2011) had studied the early stage benefits of CP for RC structure, their work suggested that under CP application the pH value of a corrosion site will increase up to the level where the corrosion rate will be significantly reduced or steel passivity restoration on the time scale of hours to days. As shown in Figure 2.21, at high and low current densities, a corrosion model reached pH of 7 after about 2.8 hours and 28 hours, respectively; and a reached pH of 12 after about 6.4 days and 81 days, respectively.

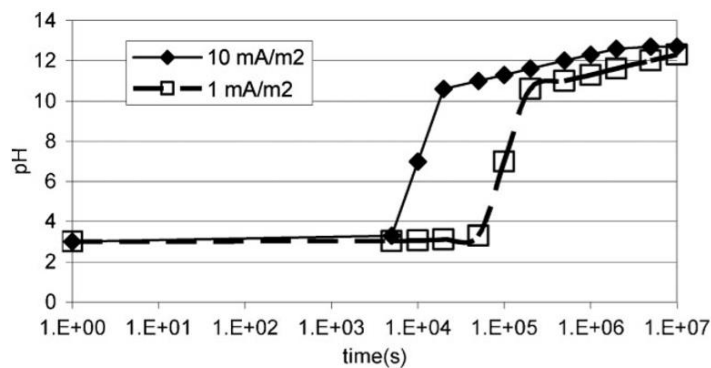


Figure 2.21 Development of pH value of corrosion model with time under different impressed current densities (Polder et al., 2011).

- **Negative Influences**

The impressed protection current can also cause negative influences in the following three aspects (Pedferri, 1996):

1. Steel hydrogen embrittlement, which is the most critical negative influence caused by the generated atomic hydrogen from cathodic reaction, enters the steel structure bringing about steel embrittlement. Due to the susceptibility of prestressing steel to steel embrittlement, only the prestressed structure should be considered to be subjected to this phenomenon if the steel potential drops to the level where hydrogen evolution can occur.

2. Concrete degradation, the concrete swelling reaction induced by alkali-silica reaction (ASR) can be expected once a large amount of alkali is produced in concrete which contains alkali-reactive aggregates.
3. Adhesion loss between rebar and concrete, may occur if the rebar is overprotected or the oxygen content is not available around the steel surface, the resultant very negative potential can cause adhesion loss between rebar and concrete, especially for plain round bars.

2.7 Numerical Modelling of Cathodic Protection for Reinforced Concrete Structure

In the past, the development of CP technology for RC structure was mainly promoted by indoor and site experiments, and the engineering experiences. However, the acquisition of experimental data and experiences both are time-consuming processes and the results apply to unique conditions, leading to the lack of understanding in the fundamental mechanism of CP process in RC structures and then bring in a slow CP development. Nowadays, the demand for CP applied on RC structure is increasingly high and it is urgent to accelerate its development.

The numerical technology based on sound principles is used to predict the feasibility of CP applied on RC structures, it is an important and valid tool to provide an insight into the fundamental processes of CP systems. One of the most significant advantages is the possibility that it can substitute complicated experiments by numerical simulation and then investigate the effects of environmental conditions, the protection levels and better operational conditions for CP application, further provide guidance for the future optimal design and operation of CP systems for RC structure (Koretsky et al., 1999; Muehlenkamp et al., 2005).

The application of CP numerical technology for RC structure should address the following issues (Muehlenkamp et al., 2005): solve the differential equations of ionic species transportation in concrete pore solution with spatially varying properties; incorporate the nonlinear boundary conditions which describe the electrochemical reaction kinetics at the

steel-concrete interface; provide adequate resolution at steel-concrete interface to assess the steel corrosion uniformity. The Finite Element Method (FEM), Finite Difference Method (FDM) and Boundary Element Method (BEM) have been used for the CP numerical simulation. However, the FDM (Koretsky et al., 1999), with uniform grids, is difficult to achieve adequate resolution around the steel bar; the BEM (Fonna et al., 2018), with various complex boundary conditions, is failing to describe the spatially varying properties of concrete domain; only the FEM can address all the issues.

2.7.1 Boundary Condition of Numerical Modelling of Cathodic Protection

In most cases of current CP numerical modelling studies for RC structures (Koretsky et al., 1999; Liu and Shi, 2012; Cheung and Cao, 2013), the Butler-Volmer Equation based polarisation curve is used as the boundary condition to describe the electrochemical reaction at the steel-concrete interface. In a few cases, the measured real-time polarisation curve is adopted (Warkus and Raupach, 2008; Bruns and Raupach, 2010; Qiao et al., 2016). The Butler-Volmer Equation is one of the most fundamental relationships in electrochemical kinetics, which considers both the anodic and the cathodic reaction simultaneously occurring on the same electrode and defines that the current density on the electrode depends upon the level of the electrode polarisation (potential shift, quantified in terms of overpotential).

In corrosion electrochemistry the electrode polarisation can be classified into two categories: activation and concentration polarisations (Roberge, 2008):

1. If the concentration of the reactants at the electrode surface is sufficient, a situation when the rate of reactant transport (mass transport) to the electrode surface is faster than the electrode reaction rate (charge transfer rate) at the electrode surface, the potential difference between the electrode corrosion potential and the corresponding equilibrium potential is called activation polarisation (Frankel, 2016).
2. If the concentration of the reactants at the electrode surface is insufficient, a situation when the rate of reactant transport to the electrode surface is slower than the electrode reaction rate, the difference between the corrosion potential and the corresponding equilibrium potential is called concentration polarisation (Frankel, 2016).

- **Butler-Volmer Equation under Activation Controlled Kinetics**

In the situation of activation polarisation, due to the sufficient reactant content, the electrode reaction rate primarily depends on the charge transfer rate. For example, for an electrode reaction $M \rightleftharpoons M^{n+} + ne^-$, under the equilibrium potential (E_{eq}), the anodic reaction rate (i_a) and the cathodic reaction rate (i_c) are the same, equals to the exchange current density (i_o), therefore, the net current density (i_n) on the electrode surface will be zero, where $i_n = i_c - i_a$, as shown in Figure 2.22.

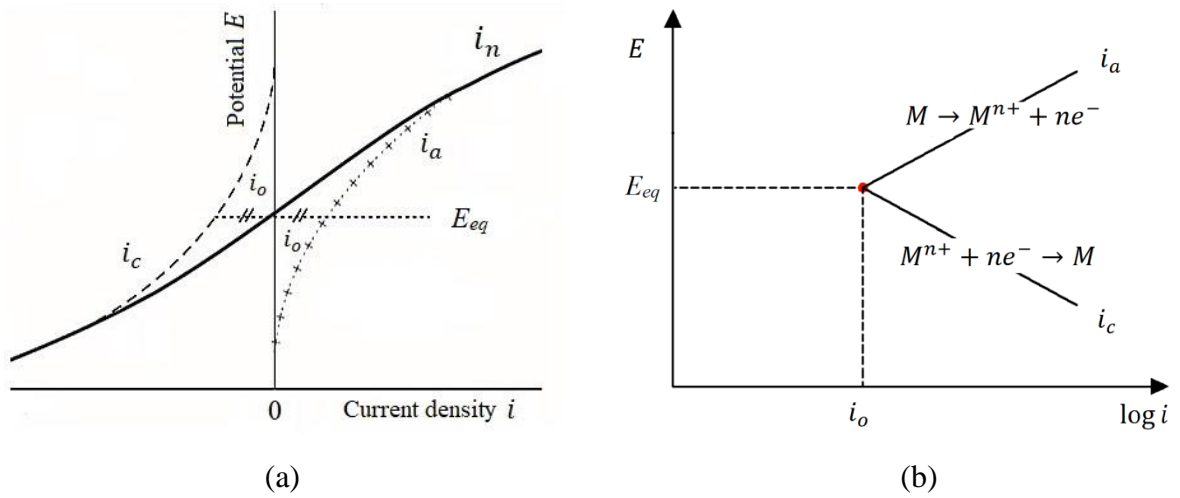


Figure 2.22 Polarisation curve of electrode reaction at equilibrium potential. (a) Linear scale for current density (Jan, 2003), (b) Logarithmic scale for current density.

When the electrode potential deviates from the equilibrium potential to the anodic (oxidation) or cathodic (reduction) reaction dominated direction, the net current density of the anodic or cathodic reaction can be described by the following Butler-Volmer Equation (Gulikers, 2005):

$$i_n = i_o \cdot \left\{ \exp \left[\frac{\alpha_a n F}{RT} (E_a - E_{eq}) \right] - \exp \left[\frac{-(1 - \alpha_a) n F}{RT} (E_a - E_{eq}) \right] \right\} \quad (2.21)$$

$$i_n = i_o \cdot \left\{ \exp \left[\frac{\alpha_c n F}{RT} (E_c - E_{eq}) \right] - \exp \left[\frac{-(1 - \alpha_c) n F}{RT} (E_c - E_{eq}) \right] \right\} \quad (2.22)$$

Where i_n is the net current density (A/m^2) of electrode reaction, E_{eq} is the equilibrium potential (V) of the electrode reaction, E_a and E_c are the polarised anodic and cathodic potential (V), $E_a - E_{eq}$ and $E_c - E_{eq}$ are the anodic and cathodic polarisation (V), α_a and α_c

are the anodic and cathodic charge transfer coefficient, usually close to 0.5, but must be between 0 and 1 (Frankel, 2016).

If the electrode potential significantly deviates from the equilibrium potential, the Butler-Volmer Equation can be simplified to the following Tafel Equation forms (Gulikers, 2005):

The net anodic current density:

$$i_{n_a} = i_o \cdot \exp \left[\frac{\alpha_a n F}{RT} (E_a - E_{eq}) \right] \quad (2.23)$$

or

$$i_{n_a} = i_o \cdot \exp \left[\frac{2.303}{b_a} (E_a - E_{eq}) \right] \quad (2.24)$$

The net cathodic current density:

$$i_{n_c} = -i_o \cdot \exp \left[\frac{-(1 - \alpha_c) n F}{RT} (E_c - E_{eq}) \right] \quad (2.25)$$

or

$$i_{n_c} = -i_o \cdot \exp \left[\frac{-2.303}{b_c} (E_c - E_{eq}) \right] \quad (2.26)$$

where

$$b_a = \frac{2.303 \cdot RT}{\alpha_a n F} \quad (2.27)$$

$$b_c = \frac{2.303 \cdot RT}{(1 - \alpha_c) n F} \quad (2.28)$$

where i_{n_a} and i_{n_c} are the net anodic and cathodic current density (A/m^2), b_a and b_c are the Tafel slopes (V) for the anodic and cathodic reaction.

- **Butler-Volmer Equation under Concentration Controlled Kinetics**

In the situation of concentration polarisation, due to inadequate reactant content, the reaction rate depends upon the rate of reactant mass transport. For instance, the cathodic reaction of steel corrosion in water saturated concrete involves oxygen reduction. Owing to the fact that the oxygen molecules are present in a small amount in the concrete pore solution and are consumed quickly in the cathodic reaction at the steel surface, the oxygen transfers more easily in gas phase than liquid phase that $C_{O_2,air}/C_{O_2,water} \approx 33$ (Koretsky et al., 1999), resulting in the oxygen diffuses through the bulk water saturated concrete to the steel surface

is slower than the reaction rate, and there is an oxygen concentration gradient formed in the bulk concrete. Therefore, the cathodic reaction is affected by concentration polarisation, for which the Equation (2.26) is revised to the Equation (2.29), the net current density of cathodic reaction at the electrode-electrolyte interface depends not only on the polarised potential but also on the reactant concentration prevailing at the electrode surface (Frankel, 2016).

$$i_{n_c} = -i_o \left(\frac{C_s}{C_e} \right) \cdot \exp \left[\frac{-2.303}{b_c} (E_c - E_{eq}) \right] \quad (2.29)$$

where C_s and C_e are the reactant concentrations (mol/m^3) at the electrode surface and in the bulk electrolyte, respectively. Assuming that there is a Nernst diffusion layer (δ) at the electrode-electrolyte interface, within the layer the diffusion mechanism contributes to the reactant flux, as a result, the reactant transport from the bulk electrolyte to the electrode surface through the Nernst diffusion layer can be described by the Fick's first law below (Frankel, 2016):

$$i_{n_c} = \frac{-nFD_r(C_e - C_s)}{\delta} \quad (2.30)$$

Where i_{n_c} is the net cathodic current density (A/m^2) which is associated with the reduction of reactant, D_r is the reactant diffusion coefficient (m^2/s). An increasing cathodic reaction rate will decrease reactant concentration at the electrode surface, until the reactant concentration is completely consumed by introducing a limiting current density (i_{lim}) denotes the maximum possible cathodic reaction rate associated with this condition. Finally the Equation (2.30) can be rearranged as:

$$i_{lim} = \frac{-nFD_r C_e}{\delta} \quad (2.31)$$

Dividing the Equation (2.30) by Equation (2.31) to yield the following one:

$$\frac{C_s}{C_e} = 1 - \frac{i_{n_c}}{i_{lim}} \quad (2.32)$$

Then substituting the Equation (2.32) into the Equation (2.29) to yield a new Equation (2.33) which has described the relation of current density and electrode polarisation for a cathodic

reaction under the combined action of activated and concentration controlled kinetics, as shown in Figure 2.23.

$$i_{n_c} = - \frac{i_o \cdot \exp\left(\frac{-2.303}{b_c} E_c - E_{eq}\right)}{1 + \frac{i_o}{i_{lim}} \cdot \exp\left(\frac{-2.303}{b_c} E_c - E_{eq}\right)} \quad (2.33)$$

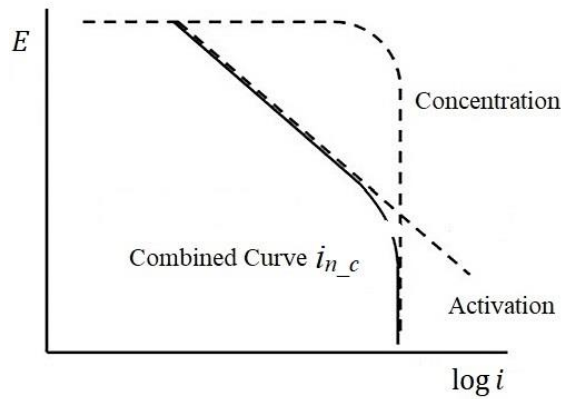


Figure 2.23 Combination of activation and concentration controlled kinetics (Frankel, 2016).

- **Butler-Volmer Equation based Steel Polarisation Curve**

For the corroding rebar in concrete, there are at least two coupled different half reactions simultaneously take place on the steel surface, they are the anodic reaction or the iron oxidation ($Fe \rightarrow Fe^{2+} + 2e^-$) and the cathodic reaction or the oxygen reduction ($O_2 + 2H_2O + 4e^- \rightarrow 4OH^-$). The formed steel corrosion potential (or mixed potential) follows the theory of mixed potential and which is in between the equilibrium potentials (E_{eq}^a, E_{eq}^c) of above two half reactions (Jan, 2003). At the corrosion potential (E_{corr}), the net current density (i_n) on the steel surface will be zero and the corresponding iron oxidation rate is defined as the corrosion rate (i_{corr}). Figure 2.24 illustrates the mechanism.

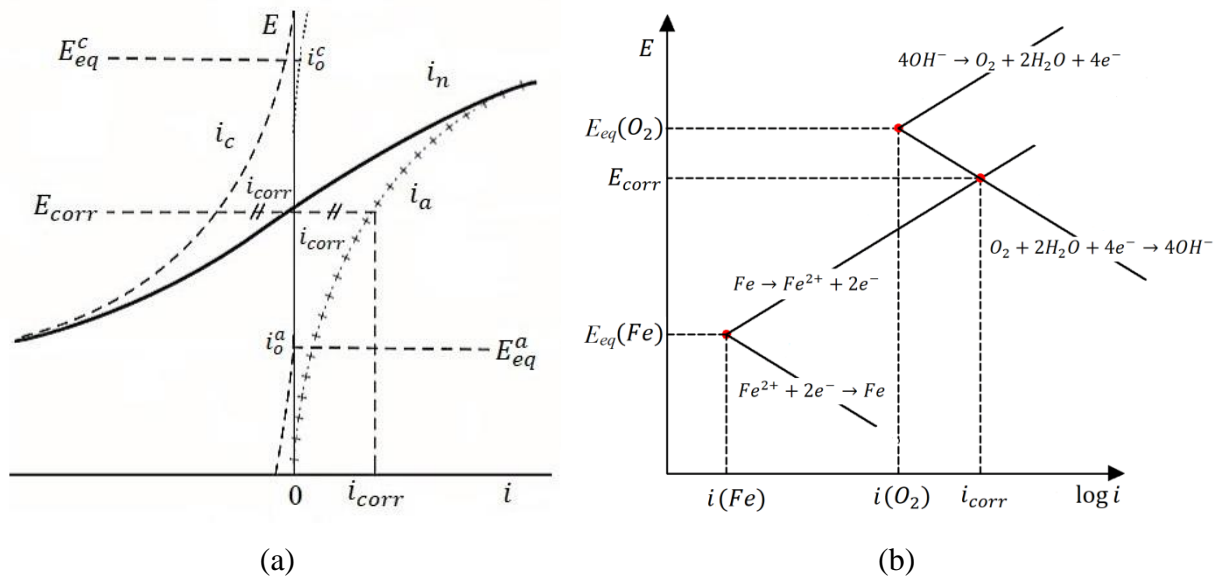


Figure 2.24 Polarisation curve of electrode corrosion in acidic electrolyte. (a) Linear scale for current density (Jan, 2003), (b) Logarithmic scale for current density (Frankel, 2016).

We can use the simplified Butler-Volmer Equations of Equation (2.24) and (2.26) to describe the kinetics of the oxidation and reduction reaction occur on the steel surface (or electrochemical kinetics at the rebar-concrete interface). In the Butler-Volmer Equation the potential shift takes the equilibrium potentials of the two different half reactions and the corresponding respective exchange current densities as the reference points. The Equations (2.34) and (2.35) represent the activation and the combined activation and concentration controlled kinetics respectively.

$$i_n = i_o^a \cdot \exp\left(2.303 \frac{E - E_{eq}^a}{b_a}\right) - i_o^c \cdot \exp\left(-2.303 \frac{E - E_{eq}^c}{b_c}\right) \quad (2.34)$$

$$i_n = i_o^a \cdot \exp\left(2.303 \frac{E - E_{eq}^a}{b_a}\right) - \frac{i_o^c \cdot \exp\left(-2.303 \frac{E - E_{eq}^c}{b_c}\right)}{1 + \frac{i_o^c}{i_{lim}} \cdot \exp\left(-2.303 \frac{E - E_{eq}^c}{b_c}\right)} \quad (2.35)$$

where i_n is the net current density (A/m^2) on the steel surface, i_o^a and i_o^c are the exchange current density (A/m^2) of anodic and cathodic reaction, E is the polarised potential (V) under CP, E_{eq}^a and E_{eq}^c are the equilibrium potential (V) of anodic and cathodic reaction, i_{lim} is the limiting current density (A/m^2).

Moreover, Butler-Volmer Equation can also take the other form as the Equations (2.36) and (2.37), which are equivalent to the aforementioned Equations (2.34) and (2.35), where the potential shift takes the corrosion potentials and the corresponding corrosion rate as the reference point.

$$i_n = i_{corr} \left\{ \exp \left(2.303 \frac{E - E_{corr}}{b_a} \right) - \exp \left(-2.303 \frac{E - E_{corr}}{b_c} \right) \right\} \quad (2.36)$$

$$i_n = i_{corr} \cdot \exp \left(2.303 \frac{E - E_{corr}}{b_a} \right) - \frac{i_{corr} \cdot \exp \left(-2.303 \frac{E - E_{corr}}{b_c} \right)}{1 + \frac{i_{corr}}{i_{lim}} \cdot \exp \left(-2.303 \frac{E - E_{corr}}{b_c} \right)} \quad (2.37)$$

where i_{corr} is the corrosion current density (A/m^2) at the steel surface, E_{corr} is the free corrosion potential (V).

2.7.2 Development State of Numerical Modelling of Cathodic Protection

At the present stage, the numerical studies of CP for RC structures are mainly focus on two aspects: protection current and potential distribution as well as numerical optimisation. Many CP numerical studies of RC structures are based on investigating the effects of various influencing factors (structural, environmental, and operational factors) on the protection current and potential distribution on steel surface, and finally provide relevant suggestions. A small number of studies are related to numerical optimisation, in order to present not only effective but also economical CP model.

- **Research on Protection Current and Potential Distribution**

Koretsky et al. (1999) studied the effect of concrete pore water saturation on the behaviour of CP systems for corroding RC structures. The research shows concrete pore saturation presents a significant influence on the performance of CP system, which is mainly reflected in the effects of concrete electrical resistivity and oxygen transport on the protection current and potential distribution of rebar. Hassanein et al. (2002) studied the influences of steel conditions (corrosion rate, oxygen limiting rate, anodic and cathodic Tafel slopes), applied protection current, and concrete resistance on the current and potential distribution in RC concrete under CP. The study indicates increasing corrosion rate, concrete resistance, and

applied current have marked adverse effects; greatly polarised cathode (greater cathodic Tafel slope) has a beneficial effect; and anodic Tafel slope and limiting current density have little influence on the current and potential distribution respectively. When the RC structure has two or more rows of steel bars, most of the protection current (about 70%) will be received by the first row which is closest to the anode. Muehlenkamp et al. (2005) studied the influence of moisture content on the spatial uniformity of a CP system for RC structures. Polder et al. (2008) investigated the current and potential distribution of different states (active, passive) of steel bars in concrete under CP process. The research shows the active rebar can only be protected directly under the anode coverage area, and if outside it by even only a few centimetres will obtain less current and be less polarised. The polarisation of passive rebar is much higher than the corroding rebar even those which are far away from the anode. Bruns and Raupach (2010) studied the effects of different concrete electrical resistivities (dry, wet) on the CP effect for distant rebar in concrete. The research indicates the fraction of total protection current of the rear rebar is significantly depending on the concrete electrical resistivity and applied current density. Liu and Shi (2012) researched the effects of applied potential, surface chloride concentration and concrete mix design on CPre system for unconventional concrete under salting environment. The findings confirmed the benefits of CPre which can extend the service life of new concrete structures. Cheung and Cao (2013) studied the effect of macrocell corrosion on the CP effectiveness for RC structures. The study results show the uniformity of protection current around rebar is significantly dependent on not only the geometry, and concrete electrical resistivity but also the different corrosion model, the macrocell corrosion may exacerbate the CP non-uniformity, a much more uniform potential distribution can be observed around the passive bars. Loziquez (2018) investigated the useful contribution of sacrificial anode in improving CP for RC patch repair. The research results propose the installation position of sacrificial anode that which should be set in concrete substrate rather than patch concrete, and also evaluate the effect of electrical resistivity of the repairing concrete. Fonna et al. (2018) studied the influence of anode type and anode-cathodic displacement on potential distribution of RC structures under CP process. The findings show that the anode type affects the steel potential value and the anode-cathode displacement influences the potential distribution on steel surface.

- **Research on Numerical Optimisation**

Qiao et al. (2016) presented a numerical optimisation method of CP system for RC structure by considering the structural life expectancy and protection potential as the constraint

conditions and optimising the location and area of anode and the output voltage amplitude to minimise the total cost of CP system. This research provided an idea to optimise the anode setting and output power by reducing the total cost and meeting the protection requirement simultaneously. Qiao et al. (2017) proposed a CP optimisation design scheme for RC structure by illustrating a 3D-FEM model with the complexity of structural geometry, and multiple corrosion boundaries. The research results reveal the optimised CP system can control the steel corrosion very well; the geometrical arrangement of anodes greatly influences the CP corrosion-controlling effect regardless of the adjustment of the impressed voltage or current; besides, the junction regions among different rebars and stirrups are the most difficult location to protect.

Overall, at first, in all the CP numerical studies of RC structures, the Laplace Equation is adopted as the governing equation to characterise the potential and current distribution in concrete, in other words, the concrete electrical resistivity is considered as constant in the numerical model; secondly, the model boundary conditions (electrochemical reactions at the steel-concrete interface), in most cases, using the Butler-Volmer Equation based polarisation curve, in a few cases, adopting the measured real-time polarisation curve; thirdly, the assessment of simulated results for the steel corrosion protection under CP condition is based on the CP standard (BS EN ISO, 2016). The CP standard states that the steel protection is achieved when any representative steel in concrete meets any one of the following criterion (Laurens and Francois, 2017):

1. An instant-off potential more negative than -720mV (with respect to $\text{Ag/AgCl}/0.5\text{ M KCl}$ reference electrode); which corresponds to -680mV/SCE (Saturated Calomel Electrode); no instant-off potential more negative than -1100mV for plain reinforcing bar or -900 mV for prestressed bar (with respect to $\text{Ag/AgCl}/0.5\text{ M KCl}$ reference electrode).
2. A potential decay over 24 hours of at least 100mV from instant-off potential;
3. A potential decay over an extended period (typically 24 hours or longer) of at least 150mV from instant-off potential subject to a continuing decay and the use of reference electrodes for the measurement extended beyond 24 hours.

This is an empirical based CP standard, the criteria do not provide any specific recommendation on the applicable environment (variability of concrete state) and rebar condition (active or passive). In general, the CP application for RC structures adopts the first and the second criterion.

CHAPTER 3

RESEARCH METHODOLOGY

3.1 Introduction

There are two fundamental inadequacies in the existing numerical modelling of Cathodic Protection (CP) for Reinforced Concrete (RC) structures, one is that, in general, almost all numerical modelling works regards the concrete electrical resistivity as a constant by default, neglecting its variation under different states of concrete; the other one is the boundary condition at the steel-concrete interfaces, for which the knowledge of the effects of CP current on steel corrosion state is still limited, resulting in neglecting the change of steel polarisation state in the CP numerical modelling. This research will focus on the two issues and the corresponding characterisation model development.

This chapter introduces the mathematical model adopted for the numerical modelling of the CP process, which describes the ionic transport behaviour in the concrete pore solution under the applied CP current. Thereafter, a preliminary CP numerical study based on the mathematical model has been conducted, it aims to investigate the effect of concrete electrical resistivity on the chloride ions distribution, potential value, as well as profile in concrete under CP process. A subsequent detailed study on the characterisation of concrete electrical resistivity that links to the concrete state is discussed in Chapter 4.

This chapter introduces the electrochemical mechanism of steel-concrete interface under CP process. In view of the Butler-Volmer Equation based polarisation curve which is broadly used as the boundary condition in the CP numerical modelling, but most of the existing models could not reflect the dynamic change of steel state in CP processes. This research is to suggest a new characterisation model for the Butler-Volmer Equation, based on the measured corrosion parameters and polarisation values of steel bar embedded in chloride contaminated concrete specimens. A subsequent detailed study on this topic is discussed in Chapter 5.

3.2 Numerical Model for Cathodic Protection Process

3.2.1 Mathematical Modelling of Ionic Transport in Concrete

For RC structures under implemented CP, the impressed protection current flows from the external anode to the protected steel bars within the concrete, in which the flow of electric current is formed by the migration of charged ions in the concrete pore solution under the action of the externally applied electric field.

Supposing there is an ionic species passes through the concrete, taking a small control volume in concrete for analysis as illustrated in Figure 3.1, in terms of the law of mass conservation, the incremental mass of the ionic species in the control volume should be equal to the difference value of the ions mass flowed in and flowed out the volume. The ionic mass balance can be expressed using the Equation (3.1) or (3.2):

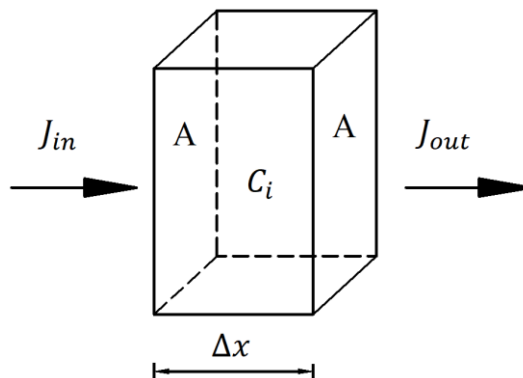


Figure 3.1 Schematic diagram of control volume concrete.

$$\Delta C_i \cdot A \cdot \Delta x = J_{in} \cdot A \cdot \Delta t - J_{out} \cdot A \cdot \Delta t \quad (3.1)$$

$$\frac{\Delta C_i}{\Delta t} = \frac{J_{in} - J_{out}}{\Delta x} \quad (3.2)$$

where C_i is the ionic concentration (mol/m^3) in the control volume concrete and the subscript i represents different ionic species, ΔC_i is the ionic concentration variation (mol/m^3) in time Δt (s), J is the ionic flux ($\text{mol}/\text{m}^2 \cdot \text{s}$) through a cross section, and A is the cross section area (m^2). When the size of the control volume is extremely small, the Equation (3.2) can be rewritten into a differential form as follow:

$$\frac{\partial C_i}{\partial t} = -\nabla J_i \quad (3.3)$$

where ∇ is the gradient operator. Assuming that the concrete pore solution is an ideal electrolyte, the governing equation for ionic mass transfer of individual ionic species in the pore solution is known as the Nernst-Planck Equation, shown as the following expression (Cussler, 2009; Newman, 1973), which takes account of the internal ionic diffusion (ionic concentration gradient effect), ionic migration (electric field effect), and the ionic convection (flow effect of bulk solution):

$$J_i = -D_i \nabla C_i - \frac{F}{RT} z_i D_i C_i \nabla \phi + C_i v \quad (3.4)$$

where D_i is the ionic diffusion coefficient (m^2/s), z_i is the charge number, ϕ is the static electric potential (V), and v is the velocity (m/s) of bulk solution. Without the flow effect of bulk solution in the concrete pore structures, the Governing equation (3.4) can be simplified as below (Masuda et al., 2004):

$$J_i = -D_i \nabla C_i - \frac{F}{RT} z_i D_i C_i \nabla \phi \quad (3.5)$$

The first term on the right side of Equation (3.5) represents the ionic diffusion due to its own concentration gradient; the second term represents the ionic migration driven by the internal electric potential gradient. The Equation (3.5) is applicable for all the different ionic species dissolved in the concrete pore solution, which all together will meet the condition of the electric neutrality at any local points. Substituting the Equation (3.5) into (3.3) yields the following one:

$$\frac{\partial C_i}{\partial t} = \nabla \left[z_i D_i \left(\frac{F}{RT} \nabla \phi \right) C_i \right] + \nabla (D_i \nabla C_i) \quad (3.6)$$

Moreover, the total fluxes of charged ions at any point in concrete pore solution will form a current density which is defined as follow (Faraday's Law):

$$i_{ion} = F \sum_{i=1}^N z_i J_i \quad (3.7)$$

where i_{ion} is the current density (A/m^2) at any point in concrete pore solution, and N is the total number of the ionic species in pore solution. Substituting the Equation (3.5) into (3.7) and rearranging yield:

$$\frac{F}{RT} \nabla \phi = - \left(\frac{i_{ion}}{F} + \sum_{i=1}^N z_i D_i \nabla C_i \right) / \sum_{i=1}^N z_i^2 D_i C_i \quad (3.8)$$

Equations (3.6) and (3.8) together describe the mutual ionic transport behaviour in the ideal concrete pore solution under a static electric potential gradient and an ionic concentration gradient, and these two are influenced by the applied current density in the case of CP.

3.2.2 Numerical Modelling of Cathodic Protection

According to the Ohm's law and the local electric neutrality, the current density in concrete should satisfy the following Equations respectively:

$$i_{ion} = - \frac{1}{\rho_c} \nabla \psi \quad (3.9)$$

$$\nabla i_{ion} = 0 \quad (3.10)$$

where ψ is the potential (V) of the externally applied electric field on concrete, ρ_c is the concrete electrical resistivity ($\Omega\cdot m$). By substituting the Equation (3.9) into (3.10), the potential distribution inside concrete complies with the following ohm-charge conservation Equation:

$$\nabla \cdot \frac{1}{\rho_c} (\nabla \psi) = 0 \quad (3.11)$$

So far, most of the existing CP numerical studies have presented a deficiency, which simply takes the concrete electrical resistivity as a constant and simplifies the Equation (3.11) into the Laplace Equation:

$$\nabla^2 \psi = 0 \quad (3.12)$$

On account of the fact that concrete electrical resistivity varies under real environmental conditions, this study will take the original form of the Equation (3.11), in which the

variation of concrete electrical resistivity is considered to be linked to the chloride and water content in concrete.

To justify the necessity of this work, a preliminary comparison using two hypothetical cases studies, which use Equations (3.11) and (3.12) respectively, is to be presented in the next section to demonstrate the concrete electric resistivity effect on the chloride ions distribution, electric potential value, and profile in concrete during the CP operation process. All these numerical calculations were conducted using software, COMSOL Multiphysics, a FEM numerical simulation package.

3.3 Case Study of Preliminary Simulation of Cathodic Protection

3.3.1 Model Description

- **Model Geometry and Material Properties**

A simplified two-dimensional Finite Element (FE) model describes a concrete specimen with an anode and three embedded steel bars (cathode) has been investigated, as shown in Figure 3.2. The specimen height and width were 150mm and 90mm, respectively, the steel bars diameter was 10mm, corresponding to the concrete cover of 20mm.

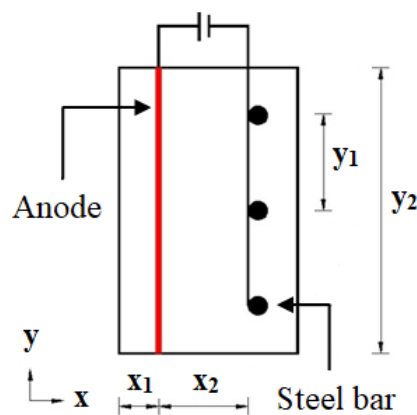


Figure 3.2 Model geometry

($x_1=20\text{mm}$, $x_2=45\text{mm}$, $y_1=50\text{mm}$, $y_2=150\text{mm}$, diameter of steel bar is 10mm).

In the study, the major ionic chemical species observed in the pore solution of chloride contaminated conventional Portland cement concrete will be taken into account, they are

hydroxyl (OH^-), sodium (Na^+), potassium (K^+) and chloride (Cl^-) ions. The initial conditions and diffusion coefficients of the four ionic species considered in concrete pore solution are given in Table 3.1, and the initial concentrations of ionic species are assumed to be evenly distributed in concrete solution. In the numerical simulation, the chloride, sodium, and potassium ions concentration are calculated by solving the Equations (3.6) and (3.8), while the hydroxyl ion concentration is determined in terms of the electric neutrality, $\sum_i^n z_i C_i = 0$. The preliminary numerical simulation of the CP operation process will be conducted for 60 days.

Table 3.1 Initial ionic concentrations (C_i) and diffusion coefficients (D_i)
(Wang and Li, 2000).

Species	Chloride (Cl^-)	Hydroxyl (OH^-)	Sodium (Na^+)	Potassium (K^+)
C_{i_ini} (mol/m ³)	380	620	900	100
D_i (m ² /s)	0.406e-9	1.056e-9	0.266e-9	0.392e-9

3.3.2 Electric Field Distribution in Concrete

As regards the governing equation for concrete domain, the mathematical models of ionic transportation are given by Equations (3.6) and (3.8). To describe the concrete condition under CP application, if the concrete electrical resistivity is considered as constant, Equation (3.12) is adopted; if the concrete electrical resistivity is treated as variable, Equation (3.11) is utilised.

3.3.3 Boundary Condition

- **Anode-Concrete Interface**

The anode-concrete interface in this study was assumed to be non-polarisable, any aging effects and building up of electrical resistance at the anode-concrete interface had been neglected. Thus, the anode was fixed at a zero as the reference potential:

$$\phi_{anode} = 0 \quad (3.13)$$

- **Steel-Concrete Interface**

The electrochemical reactions at the steel-concrete interface under the CP process are directly related to the applied current density, therefore, there are two sets of constant current densities represent the applied CP current density are approximately applied on all the steel bars, respectively.

- **RC Specimen Boundary**

All the other boundaries were characterised as insulating conditions, both the fluxes of all the ionic species and the electric current were assumed to be zero on all these boundaries of RC specimen.

3.3.4 Case I (Constant Electrical Resistivity)

Two sets of concrete electrical resistivity values of $1\Omega\text{-m}$ and $10\Omega\text{-m}$, as well as two sets of current densities of 2.5A/m^2 and 5A/m^2 were assumed in the CP case study respectively. Figures 3.3 and 3.4 show the chloride ion concentration profile in concrete with different concrete electrical resistivity values under the different applied current densities.

It can be seen that the chloride ions have been redistributed under the applied electric field, and those ions are driven to the region near the anode, whereas the ionic concentration around the steel bar decreases (compared to the initial concentration).

Comparing Figures 3.3 with 3.4, we can see that there are more chloride ions migrated to the anode due to the increased current density. However, under the same CP current density, the chloride redistribution profiles in concrete can be observed to be the same for the two different concrete electrical resistivity values.

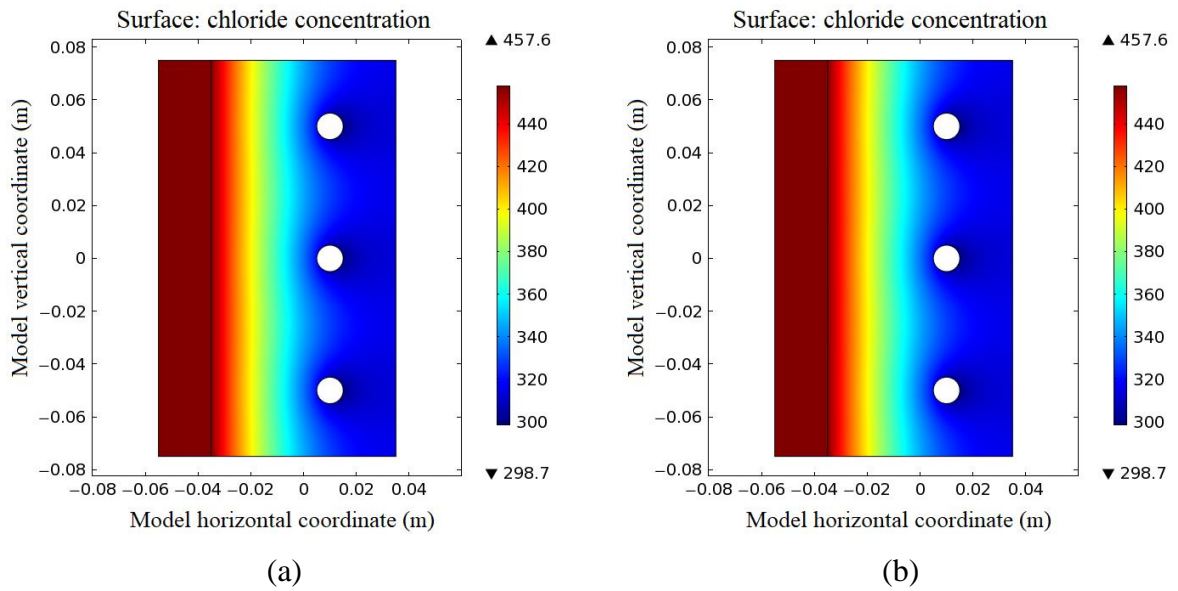


Figure 3.3 Profile of chloride concentration in concrete under 2.5A/m^2 .

(a) $\rho_c = 1\Omega\text{-m}$, (b) $\rho_c = 10\Omega\text{-m}$.

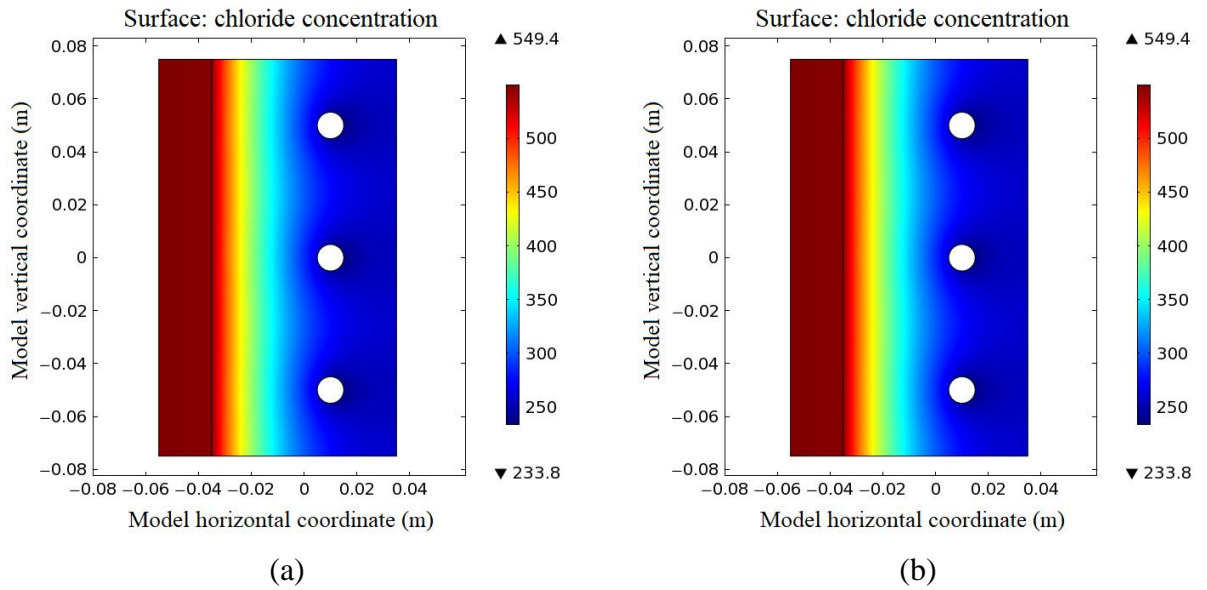


Figure 3.4 Profile of chloride concentration in concrete under 5A/m^2 .

(a) $\rho_c = 1\Omega\text{-m}$, (b) $\rho_c = 10\Omega\text{-m}$.

Figures 3.5 and 3.6 show the electric potential profile in concrete with different concrete electrical resistivity values under the different applied current densities.

It can be seen that the electric potential in concrete under the applied electric field, which displays a progressively increasing trend, and is in line with the distance that comes closer to the anode, resulting in the electric potential around the surface of the steel bar shows the lowest value.

Comparing Figures 3.5 with 3.6, we can see that the electric potential value around the surface of the steel bar decreases with the applied current density and the concrete electrical resistivity. For the condition of applied current density of 2.5A/m^2 , when the concrete electrical resistivity is $1\Omega\text{-m}$ the electric potential around the rebar is -0.086V , whilst when the concrete electrical resistivity is at $10\Omega\text{-m}$ its electric potential around the rebar is -0.856V , which is about ten times smaller. For the condition of applied current density of 5A/m^2 , when the concrete electrical resistivity is at $1\Omega\text{-m}$ the electric potential around the rebar is -0.171V , whilst when the concrete electrical resistivity is $10\Omega\text{-m}$ its electric potential around the rebar is -1.711V , which is still about ten times smaller.

However, the electric potential profiles in concrete are very similar for the two different concrete electrical resistivity values under the same CP current densities, but slightly different under the different current densities.

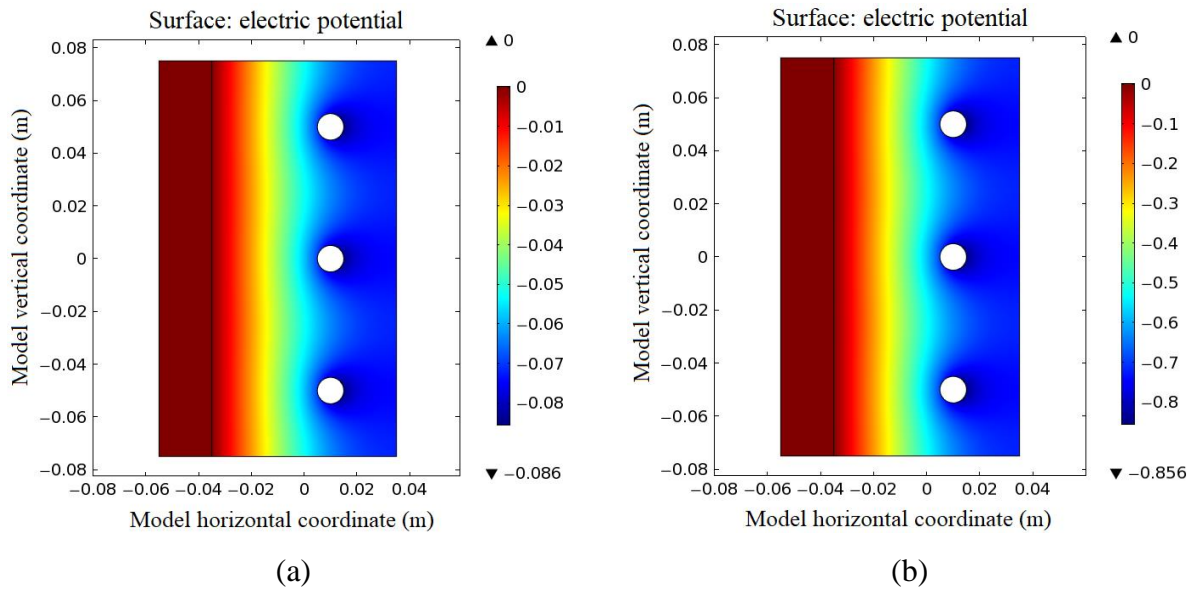


Figure 3.5 Profile of electric potential in concrete under 2.5A/m^2 .

(a) $\rho_c = 1\Omega\text{-m}$, (b) $\rho_c = 10\Omega\text{-m}$.

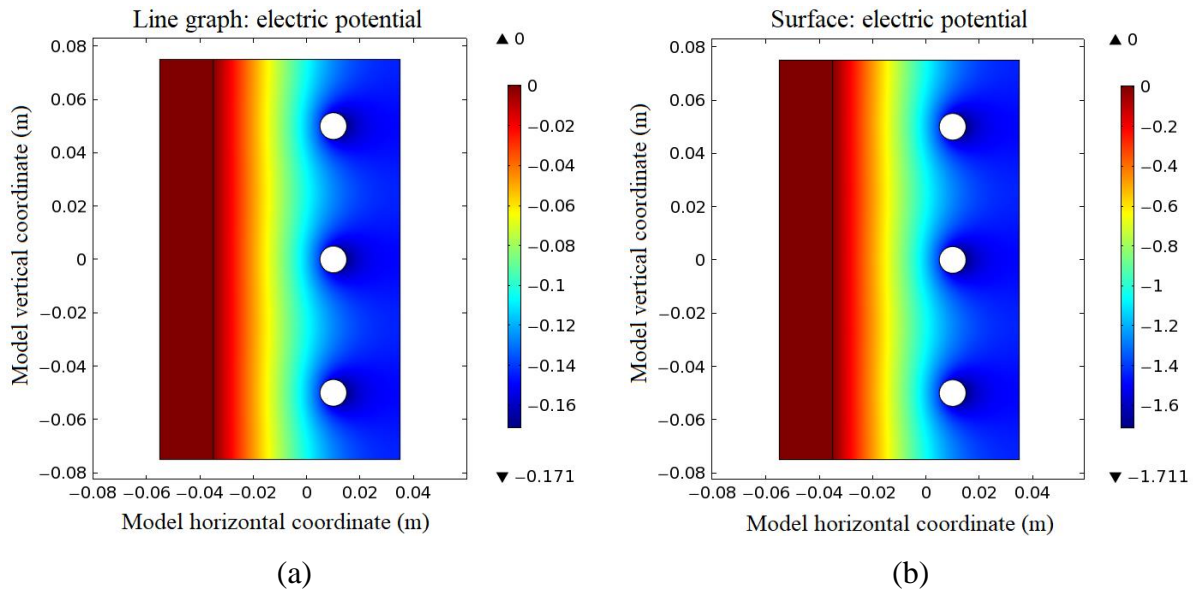


Figure 3.6 Profile of electric potential in concrete under $5A/m^2$.

(a) $\rho_c = 1\Omega\cdot m$, (b) $\rho_c = 10\Omega\cdot m$.

Figures 3.7 and 3.8 show the electric potential distribution along the circumference of the cross section of the middle steel bar at different time under the applied current density of $2.5A/m^2$ and $5A/m^2$, respectively.

The horizontal axis shows the positions on the circumference of the steel cross section, starting anticlockwise from the point near to the anode ($x = 0$). The curve displays the electric potential distribution along the cross section circumference of the rebar, which presents a similar sine function shape, showing the electric potential along the rebar circumference that is not uniform. The closest point to anode has the largest electric potential value, whilst the furthest point to the anode has the smallest value.

Comparing Figures 3.7 with 3.8, it can be seen that the electric potential value along the cross section circumference of the steel bar decreases with the increase of the applied electric field. However, the electric potential profiles along with the cross section circumference of steel bar are closely similar under the different concrete electrical resistivity values and the same current density, but slightly different under the same concrete electrical resistivity and different applied current densities. Moreover, the legends in the figures demonstrate that there are no developmental stages of the numerical model with time.

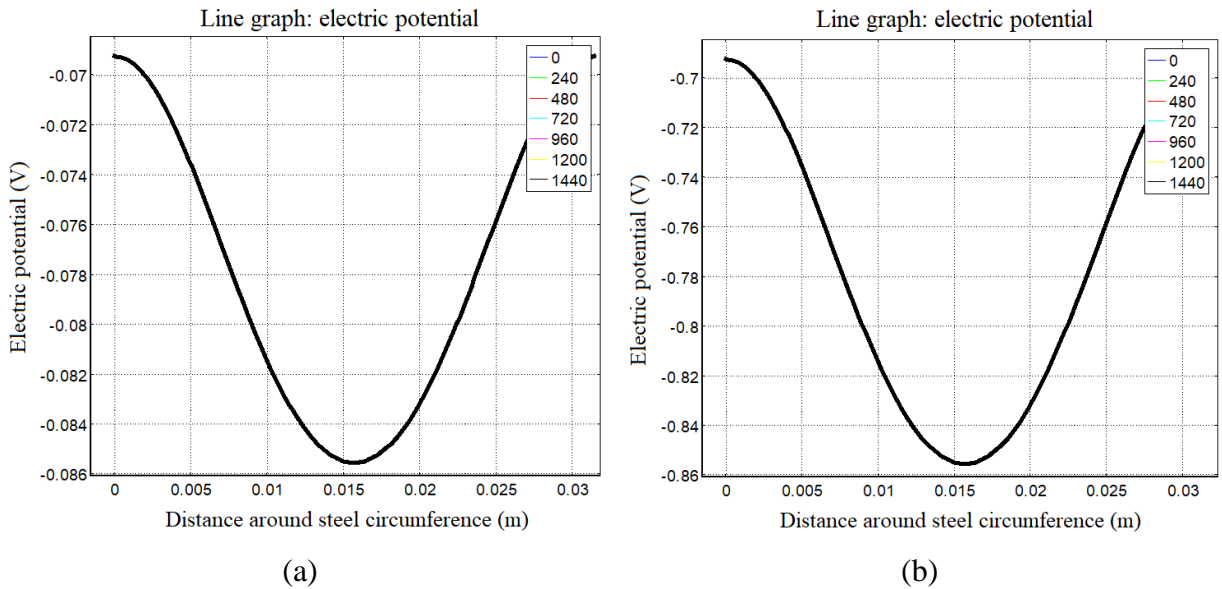


Figure 3.7 Profile of electric potential along the circumference of steel bar cross section under 2.5A/m^2 . (a) $\rho_c = 1\Omega\cdot\text{m}$, (b) $\rho_c = 10\Omega\cdot\text{m}$.

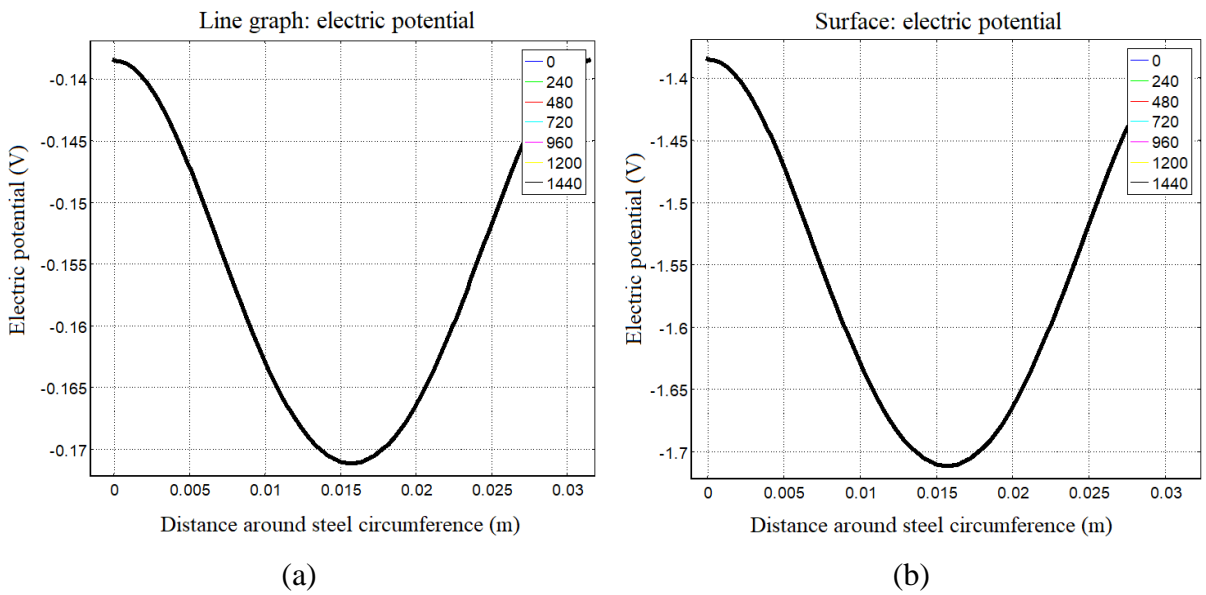


Figure 3.8 Profile of electric potential along the circumference of steel bar cross section under 5A/m^2 . (a) $\rho_c = 1\Omega\cdot\text{m}$, (b) $\rho_c = 10\Omega\cdot\text{m}$.

3.3.5 Case II (Variable Electrical Resistivity)

In this case study two variable concrete electrical resistivity values were compared under a current density of 5A/m^2 . Two hypothetical concrete electrical resistivity models were adopted as below:

$$\rho_c = \frac{A}{C_{Cl} + B} \quad (3.14)$$

$$\rho_c = \frac{C}{C_{Cl} + C_{OH}} \quad (3.15)$$

where C_{Cl} is the chloride ion concentration (mol/m^3) in concrete pore solution, C_{OH} is the hydroxyl ion concentration (mol/m^3) in concrete pore solution, A , B and C are three constants (nonzero and nonnegative number). These assumptions are based upon the fact that there exists an inverse relationship between concrete electrical resistivity and ionic concentration in concrete pore solution, whilst the chloride and hydroxyl ions are both highly variable in concrete under the CP process; these constants make these two equations have generality. Figures 3.9 to 3.11 show the results using different variable concrete electrical resistivity values under the same applied current density.

Figure 3.9 shows the chloride ion concentration profile in concrete under the applied current density of 5A/m^2 . Similar phenomenon as that can be noticed in Case I before. The chloride ions in concrete have been redistributed under the applied electric field by the migration of chloride ions from the steel bars to the anode. Figures 3.4 and 3.9 show the same chloride profile under the same applied current density. This result can be concluded that the ionic redistribution depends on the applied current density only, but is less affected by the concrete electrical resistivity.

Figure 3.10 shows the electric potential profile in concrete under the applied current density of 5A/m^2 . It can be seen that both the electric potential value and profile display a big difference under the two variable concrete electrical resistivity values.

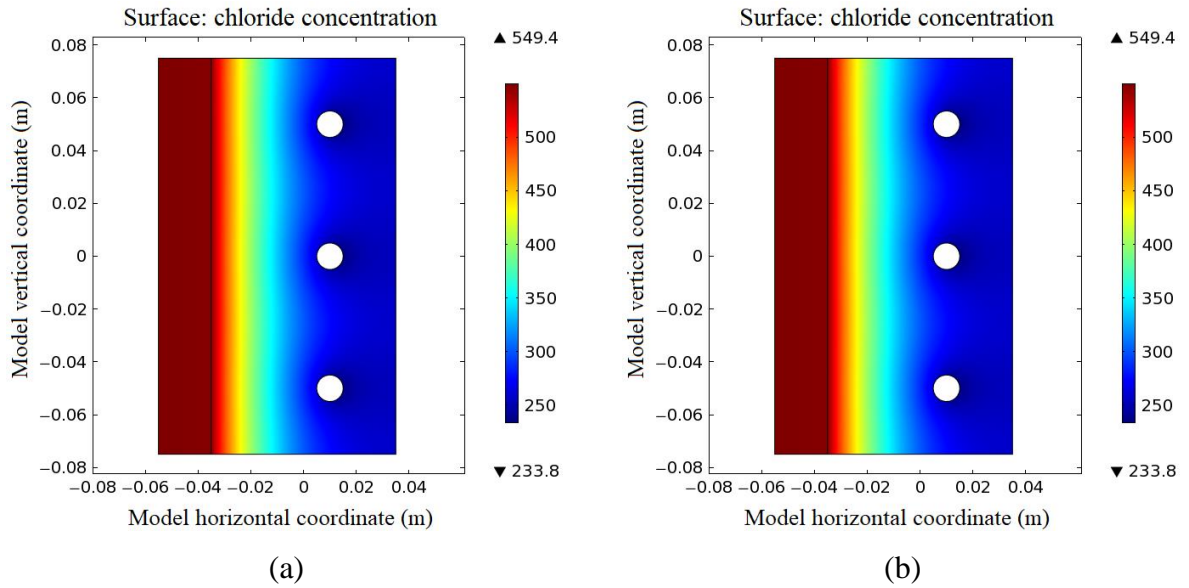


Figure 3.9 Profile of chloride concentration in concrete under $5A/m^2$.

$$(a) \rho_c = \frac{A}{C_{Cl}+B}, (b) \rho_c = \frac{C}{C_{Cl}+C_{OH}}.$$

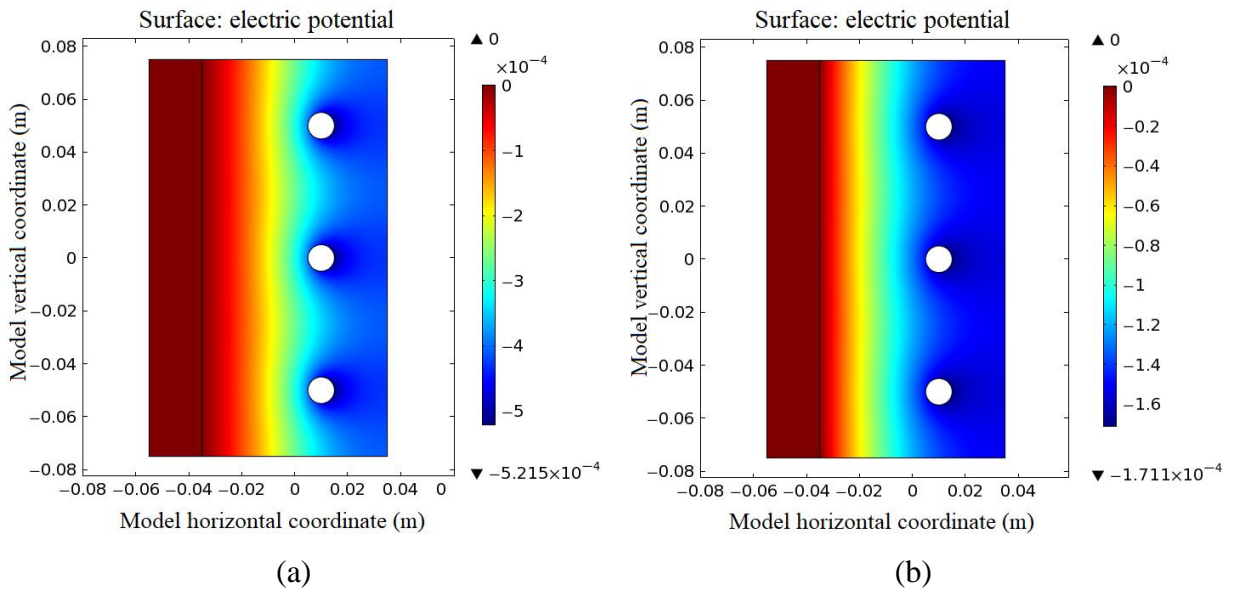


Figure 3.10 Profile of electric potential in concrete under $5A/m^2$.

$$(a) \rho_c = \frac{A}{C_{Cl}+B}, (b) \rho_c = \frac{C}{C_{Cl}+C_{OH}}.$$

Figure 3.11 shows the electric potential distribution along the cross section circumference of the steel bar under the applied current density of $5A/m^2$. A similar phenomenon can also be seen in Case I, the electric potential distribution along the cross section circumference of the rebar is not uniform, but present different shapes of sine functions and different electric potential values. Moreover, the legends in the figures demonstrate the developmental stages of the numerical model with time presented by multiple curve variation.

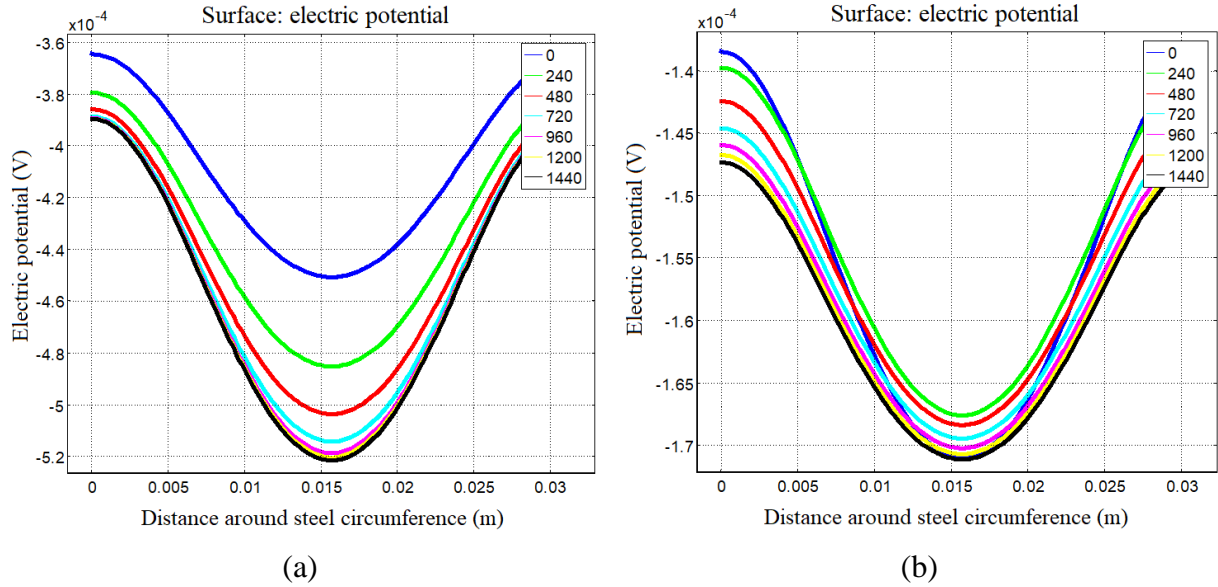


Figure 3.11 Profile of electric potential along the circumference of steel bar cross section

under 5A/m^2 . (a) $\rho_c = \frac{A}{C_{Cl}+B}$, (b) $\rho_c = \frac{C}{C_{Cl}+C_{OH}}$.

3.3.6 Discussion and Summary

Based on the above two preliminary hypothetical case studies, the following information can be obtained regarding the effect of concrete electrical resistivity:

1. Chloride ion concentration distribution

- The chloride ion concentration in concrete has been redistributed under the applied current density by the migration of chloride ions from the steel bar towards the anode.
- The chloride ion concentration redistribution profile in concrete is only depended on the implemented current density not the concrete electrical resistivity.

2. Electric potential value and profile (Case I)

- The electric potential values in concrete and along the cross section circumference of steel bar are both dependent on the concrete electrical resistivity and the applied current density.

- The electric potential profiles in concrete and along the cross section circumference of steel bar are slightly affected by the impressed current density only.

3. Electric potential value and profile (Case II)

- The electric potential value and profiles are both related to the concrete electrical resistivity variable and the applied current density.

For Case I, it can be seen that, by neglecting the influences of concrete pore structures, water content and ionic concentration on the concrete electrical resistivity, the electric potential profiles in concrete and along the cross section circumference of steel bar all depend on the implemented current density only. However, for Case II that considers the variable concrete electrical resistivity, the results are determined by the concrete electrical resistivity and the applied current density, which is the phenomenon that in line with the actual situation.

In conclusion, owing to the fact that concrete electrical resistivity depends on the concrete conditions, and by taking the concrete electrical resistivity as constant by default in the CP modelling could not reflect the actual state of the real structure. Hence, these results could not provide the correct information and effective guidelines for the future development of CP technology. The preliminary studies confirmed that in order to obtain accurate CP modelling, the electrical resistivity must be correctly characterised with concrete conditions, which is one of the critical points that needs to be addressed.

3.4 Electrochemical Mechanism of Steel-Concrete Interface in Cathodic Protection Process

3.4.1 Interfacial Electrochemical Mechanism

As shown in Figure 3.12, when CP is applied on a chloride contaminated RC structure, there is a voltage (ΔE_{app}) is imposed between the anode and steel bar (cathode), which makes the anode, steel bar and the concrete domain (between the anode and steel bar) present different potential values.

Assuming a point A in concrete, which approaches the anode infinitely, there is a potential difference ($\Delta E_{anode_concrete}$) at the anode-concrete interface exists between the anode surface and the contacting concrete surface point A, it is defined by the Equation (3.16). Similarly, assuming a point B in concrete, which approaches the steel bar infinitely, there is a potential difference ($\Delta E_{bar_concrete}$) at steel-concrete interface exists between the steel surface and the contacting concrete surface point B, it is defined by the Equation (3.17). The imposed voltage (ΔE_{app}) reflects the potential difference between the anode and the steel bar (Equation 3.18). The potential difference of $\phi_{anode_concrete}$ and $\phi_{bar_concrete}$ is the imposed voltage on the concrete domain between the anode and the steel bar. The interfacial potential difference of $\Delta E_{anode_concrete}$ controls the electrochemical reactions occurring at the anode-concrete interface; while the interfacial potential difference of $\Delta E_{bar_concrete}$ controls the electrochemical reactions occurring at the steel-concrete interface.

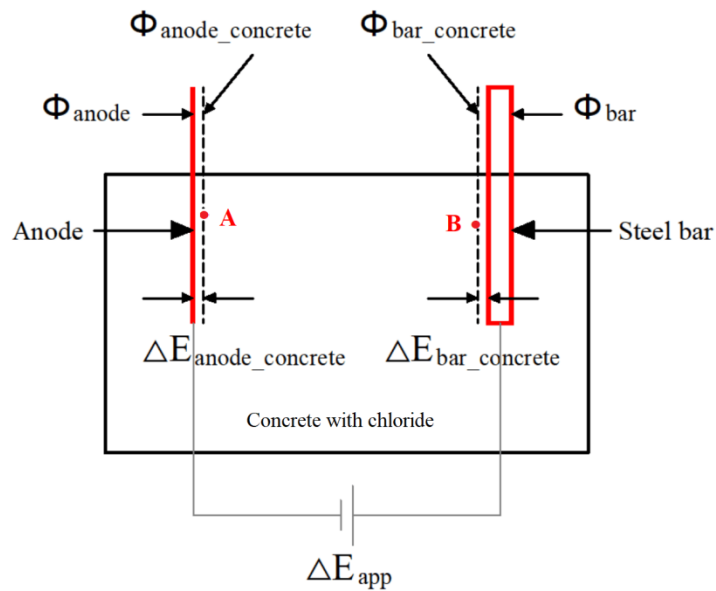


Figure 3.12 Profile of interfacial electric potential of chloride contaminated RC structure under CP application.

$$\Delta E_{anode_concrete} = \phi_{anode} - \phi_{anode_concrete} \quad (3.16)$$

$$\Delta E_{bar_concrete} = \phi_{bar_concrete} - \phi_{bar} \quad (3.17)$$

$$\Delta E_{app} = \phi_{anode} - \phi_{bar} \quad (3.18)$$

where $\Delta E_{anode_concrete}$ is the interfacial potential difference (V) at anode-concrete interface, ϕ_{anode} is the anode potential (V), $\phi_{anode_concrete}$ is the electric potential (V) of point A

which approaches the anode infinitely in concrete, $\Delta E_{bar_concrete}$ is the interfacial potential difference (V) at steel-concrete interface, $\phi_{bar_concrete}$ is the electric potential (V) of point B which approaches the rebar infinitely in concrete, ϕ_{bar} is the rebar potential (V), ΔE_{app} is the applied voltage under CP.

In this study, the CP numerical modelling takes no account of the electrochemical reaction at the anode-concrete interface because it is set to as a reference point. At the steel-concrete interface, two reactions are considered: the anodic reaction ($Fe \rightarrow Fe^{2+} + 2e^{-}$) and the cathodic reaction ($O_2 + 2H_2O + 4e^{-} \rightarrow 4OH^{-}$).

For a chloride contaminated RC structure without implemented CP, as reviewed in Chapter 2, the anodic reaction (iron oxidation) and the cathodic reaction (oxygen reduction) take place simultaneously on the steel surface where the rebar presents an electric potential value, a corresponding iron oxidation rate (i_{Fe}) and an oxygen reduction rate (i_{O_2}), we have the following relation:

$$i_{O_2} - i_{Fe} = 0 \quad (3.19)$$

At this moment, we indicate the i_{Fe} as i_{corr} , the corrosion rate if there is no CP current density ($i_{app} = 0$), the corresponding rebar potential as corrosion potential (E_{corr}). If there is a CP current density (i_{app}) applied on the chloride contaminated RC structure, we have:

$$i_{app} = i_{O_2} - i_{Fe} \quad (3.20)$$

For a chloride contaminated RC structure with implemented CP, the protection current will push the rebar potential (E_{corr}) to a more negative potential value (E_{cp}), so the steel polarisation (potential shift) η under the externally applied voltage (ΔE_{app}) corresponding to a CP current density (i_{app}) can be expressed as below:

$$\eta = E_{cp} - E_{corr} \quad (3.21)$$

Here the polarised steel potential (E_{cp}) is the steel interfacial potential ($\Delta E_{bar_concrete}$) in Figure 3.12 under the externally applied voltage (ΔE_{app}) or the applied CP current density (i_{app}); the corrosion potential (E_{corr}) is the steel interfacial potential ($\Delta E_{bar_concrete}$) in

Figure 3.12 without implemented CP; the steel polarisation (η) controls the electrochemical reactions occurring at the steel-concrete interface under CP.

As discussed in Chapter 2, for the corroding rebar in concrete under CP application, the respective anodic and cathodic reaction rate (i_{F_e}, i_{O_2}) can be described using simplified Butler-Volmer Equations (3.22) and (3.23), which involve the relevant anodic and cathodic Tafel slopes (b_a, b_c) and steel polarisation (η). Combine Equations (3.20), (3.22) and (3.23) to yield Equation (3.24), a derived Butler-Volmer Equation representing the steel polarisation curve under CP. Equation (3.24) describes the kinetics of the anodic and cathodic reaction occurring on the steel surface, here the net current density on the steel surface is balanced by the applied protection current density (i_{app}) under CP application, and the increasing protection current density will result in the increasing oxygen reduction rate and the decreasing iron oxidation. Equation (3.24) is widely adopted as the boundary condition in the CP numerical modelling for RC structures.

$$i_{F_e} = i_{corr} \cdot \exp\left(2.303 \frac{\eta}{b_a}\right) \quad (3.22)$$

$$i_{O_2} = i_{corr} \cdot \exp\left(-2.303 \frac{\eta}{b_c}\right) \quad (3.23)$$

$$i_{app} = i_{O_2} - i_{F_e} = i_{corr} \cdot \exp\left(-2.303 \frac{\eta}{b_c}\right) - i_{corr} \cdot \exp\left(2.303 \frac{\eta}{b_a}\right) \quad (3.24)$$

3.4.2 Research Idea on A New Butler-Volmer Equation Based Steel Polarisation Characterisation

In terms of the literature review in this study, most of the previous works on CP modelling for RC structures had no consideration of the coupling effect of the ionic transport in concrete and the applied electric field effect. Therefore, when implementing the boundary condition by taking the Equation (3.24), most of these works can only describe the potential state of steel-concrete interface and the simulated result could not provide the actual steel corrosion rate.

In consequence, the information and knowledge of the effects of CP current on steel corrosion state, drawn from the CP numerical simulation are still limited, resulting in the lack of understanding of the electrochemical mechanism of the CP process in RC structures, there is

limited applicable quantitative specification in a few CP standards, such as BS EN ISO (2016). At the present stage, the evaluation of the CP efficiency so far is based on the steel instant-off potential, or the potential decay value over a certain period, in which the potential value as a criterion, is an indirect approach based on the thermodynamics of steel corrosion. Moreover, to define the boundary condition by the Equation (3.24) in CP numerical modelling, the anodic and cathodic Tafel slopes (b_a, b_c), which reflect the steel polarisation states under CP process, are generally considered as constants. With the constant Tafel slopes the Butler-Volmer Equation is unable to represent the different steel polarisation curves to reflect the dynamic change of steel corrosion state in the CP process.

This study aims to characterise the variation of anodic and cathodic Tafel slopes under CP application for the concrete of different chloride contents. It is to propose a new characterisation model for the Butler-Volmer Equation, which can not only consider the dynamic Tafel slopes, but also can directly describe the variation of steel corrosion rate referring to the applied different CP current density.

3.5 Conclusions

This research need to focus on two contributions for the numerical modelling of CP process on RC structure. It is going to investigate the characterisation for the concrete electrical resistivity and the rebar polarisation state under CP. The two characterisation models are to be developed and validated using the experimental data available. At the end, the two developed models are to be implemented to optimise CP numerical simulation for RC structures. The simulation results will be compared with an experimental study completed early.

CHAPTER 4

CONCRETE ELECTRICAL RESISTIVITY CHARACTERISATION

4.1 Introduction

The electrical resistivity is a fundamental property of concrete, which describes the ability of concrete to oppose the flow of electric current. It is an important indicator in the assessment of reinforcement corrosion in concrete, which controls the steel corrosion current flow in concrete. Moreover, it is an essential parameter in the design and operation of Cathodic Protection (CP) for Reinforced Concrete (RC) structures, which governs the applied current and potential distribution in concrete, and influences the potential distribution at the steel-concrete interface under the CP process.

The electric current flow in concrete is achieved by the motion of dissolved charged ions in the concrete pore solution, thus, the concrete electrical resistivity fundamentally depends upon the formation of concrete pore structure (the pore connectivity, tortuosity and the pore size distribution), pore water content (transport medium), as well as the chemical composition (the actual carriers of electric current) of the pore water solution (Layssi et al., 2015; Banea, 2015; Azarsa and Gupta, 2017).

These factors are consequently determined by the nature of the component materials (cement type, aggregates and mixing water), mixture proportion, water/cement (w/c) ratio, curing methods, and the exposed environment (Elkey and Sellevold, 1995; Whiting and Nagi, 2003). Table 4.1 shows the significant variation of concrete electrical resistivity under the different chemical compositions and exposed situations.

Table 4.1 Electrical resistivity of concrete ($\Omega\text{-m}$) made by different cement type under different exposure condition (Polder, 1996).

Different type of cement	Atmospheric area	Immersed and splash area
Portland cement	300-700	135
5% silica fume	300-2000	250
70% blast furnace slag	2200	800

CP so far has been proven to be the most effective and reliable anti-corrosion technique for RC structures and has been increasingly used in civil engineering for structural repair and maintenance (Wilson et al., 2013). Nowadays, numerical modelling and simulation has been popularly employed for the CP design and operation analysis of RC structure (Liu and Shi, 2012; Qiao et al., 2015; Qiao et al., 2016).

In theory, the mathematical model adopted for the numerical modelling, which describing CP process running in RC structures are generally based on the Nernst-Planck Equation (3.4) describing the principles of ionic transportation in concrete pore solution and Ohm's law (Equation 3.9) describing the implemented DC current flow in concrete (Wang, 2001). To solve the two equation models, the concrete electrical resistivity as a material property is required at the first hand. For the reason, the accurate estimation of concrete electrical resistivity at varied conditions is important to help assess the steel state under the CP operation or for CP design.

In spite of the important role of concrete electrical resistivity, in terms of the literature research in this study, most of the previous works on numerical modelling and simulation of the CP process on the RC structures neglected the variation of concrete electrical resistivity with changing water content and ionic concentration in concrete under varying environmental situations, those works assume the concrete electrical resistivity as a constant by default, so that the electric current and potential distribution in concrete was simply described using the Laplace Equation.

However, in order to accurately evaluate the potential distribution of steel-concrete interface under CP conditions, and to help understand and optimise CP numerical modelling for RC structures, the variation of concrete electrical resistivity needs to be considered by developing an appropriate concrete electrical resistivity model to evaluate its relationship with concrete conditions. Water and chloride contents in concrete are highly variable for RC structures in

real world hostile environments, which leads to interest in the characterisation of their coupling effects on the concrete electrical resistivity. So far, a few researchers have reported the combined influence of water and chloride contents on concrete electrical resistivity, but the characterisation and modelling of the concrete electrical resistivity under the coupling influence of the two important factors are still open for discussion for accuracy, reliability, and fundamental underlying mechanisms.

To provide an efficient parameter for numerical modelling of CP process in RC structure, this chapter will focus on the mathematical characterisation of the coupling effects of water and chloride contents on concrete electrical resistivity based on the previous experimental research (Oleiwi, 2018), a new semi-empirical model based on the understanding that the relationship between concrete electrical resistivity and water content has an intrinsic linkage to the pore size distribution of concrete pore structures, and the chloride content will be put forward.

4.2 Influence of Water Content

Numerous studies have been completed on the effect of water content on concrete electrical resistivity by different representations: water saturation, water content, and water loss.

4.2.1 Characterisation in Terms of Water Saturation

The concrete electrical resistivity varies widely in the natural environment, for mature concrete, the degree of pore water saturation has been identified as the most important influencing factor for the concrete electrical resistivity.

It has been found that the degree of pore water saturation varying from 20% to 100% causes the concrete electrical resistivity to decrease in three orders from 6×10^6 to $7 \times 10^3 \Omega\text{-cm}$ (Gjørsv et al., 1977). A study about the effect of water saturation on concrete electrical resistivity made by different w/c ratios is illustrated in Figure 4.1, and the results show that the concrete electrical resistivity decreases with increasing degree of water saturation and w/c ratio. However, Lopez and Gonzalez (1993) proposed two critical limits, 70% and 35%, when the

degree of pore water saturation is over 70% or below 35%, concrete electrical resistivity value is either too small or too large to be detected.

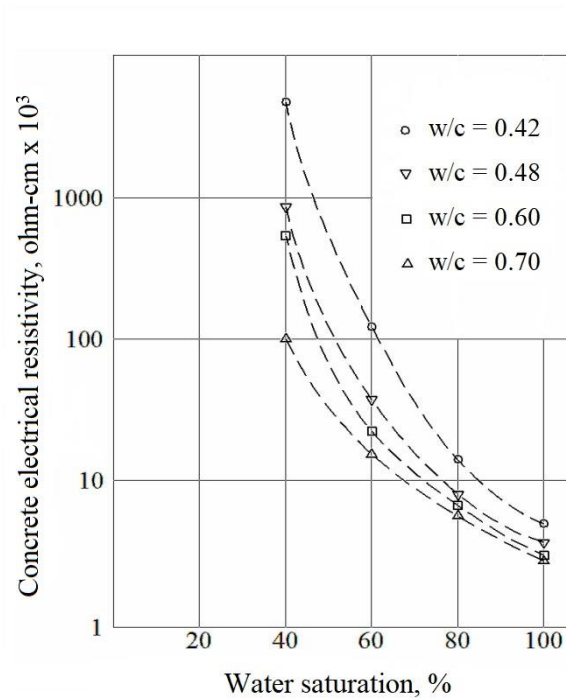


Figure 4.1 Effect of water saturation on concrete electrical resistivity (Gjørsv et al., 1977).

It should be noted that the degree of pore water saturation is a relative value, which is the ratio of water volume to concrete pore volume, to characterise the concrete electrical resistivity in terms of the degree of pore water saturation only is not efficient. Also, its coupled effect needs to be considered with the concrete porosity to reflect the total water content (Villagran and Di Maio, 2014). For instant, in the case of fully saturated concrete (underwater structure) with the constant saturation degree of pore water, due to the total water content is directly proportional to the concrete porosity, so the concrete electrical resistivity decreases with an increase in porosity.

4.2.2 Characterisation in Terms of Water Content

The electric current transport in concrete is essentially carried by the mobile charged ions in pore water so that the water content, as the transport medium in the pore network, plays a significant role in influencing the concrete electrical resistivity.

Concrete contains interlinked pore structures with different sizes, which are formed in the cement hydration process. In general, the pores are categorised into three types (Brandt, 2014;

Roy et al., 1993; Bertolini et al., 2014): air voids, the air entrapped in the cement paste that cannot be removed by concrete vibration; capillary pores, the voids not filled with solid hydration products in the hardened cement paste; gel pores, the interlayer spacing within C-S-H gel layer, which is hydrates of cement composition silicates.

When the concrete is exposed to the atmospheric environment, the actual water content in the pore network is related to the concrete hygroscopic equilibrium and the relative humidity (RH) of the surrounding environment (Villagran and Di Maio, 2014). The water content in capillary pores occupies the largest proportion of water content in concrete and in bigger pores only as a layer of water film adsorbed on the pore wall (Bertolini et al., 2014), as shown in Figure 4.2.

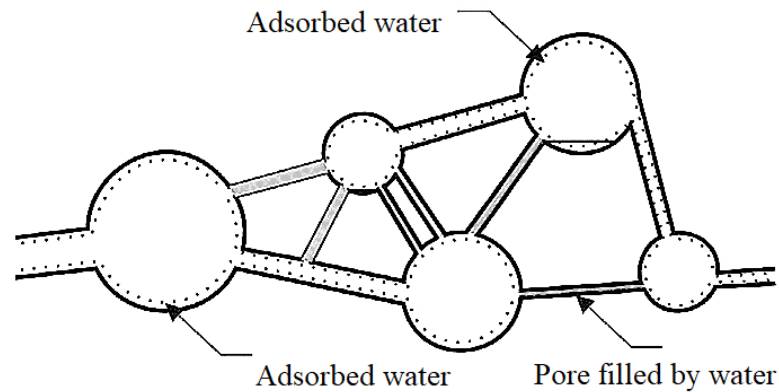


Figure 4.2 Water exits in capillary pores under equilibrium condition (Bertolini et al., 2014).

Concrete can absorb water from the air with high RH. The equilibrium relation of the water content in air and the water content in concrete pore structure can be depicted by an adsorption isotherm shown in Figure 4.3. It can be seen from the graph that when the RH below 40%, the water content is adsorbed on the wall of capillary pores or filled in the gel pores. Also, Chen et al. (2014) confirmed that when concrete is exposed to RH below 40%, the concrete electrical resistivity was too large to be stable. The large electrical resistivity at low RH may be explained by the fact that the water in the gel pores is much less electrically conductive due to the strong chemical bond with the inner surfaces of gel pores and the disconnected distribution of gel pores (Zaccardi and Maio, 2014; Hunkeler, 1996).

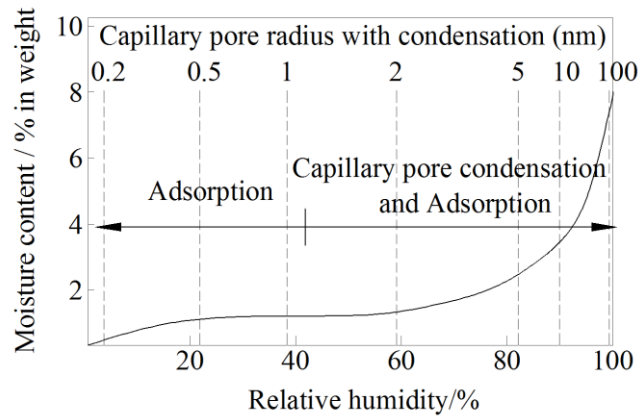


Figure 4.3 Water adsorption isotherm of concrete refers to capillary pore radius (Hunkeler, 1996).

As depicted by Figure 4.3, when RH exceeds 40%, condensation (the gaseous phase changes into the aqueous phase) in capillary pores takes place and the relevant concrete electrical resistivity will exponentially decrease with the increase of water content (Villagran et al., 2009; Hunkeler, 1996; Saleem et al., 1996; Zaccardi and Maio, 2014). Also Saleem, et al. (1996) found that the decreasing tendency of concrete electrical resistivity will become negligible after a certain amount of water content, which is similar to the description of Lopez and Gonzalez (1993) in Section 4.2.1.

4.2.3 Characterisation in Terms of Water Loss

When the RC structure is located in the environment with either the high temperature or the low RH, the water evaporation in concrete pore network (the aqueous phase changes into the gaseous phase) takes place.

Su et al. (2002) pointed out that concrete electrical resistivity increases with the increase of water loss ratio. In general, water evaporation is closely related to the pore size distribution of concrete. During the process of pore water evaporation, due to the “ink-bottle” effect, the water exists in the larger pores and if connected with the smaller pores cannot evaporate until the water exists in the smaller pores has dried out. For instant, as shown in Figure 4.4, the water desorption curve shows higher water content than the water adsorption curve under the same RH and presents a hysteresis phenomenon.

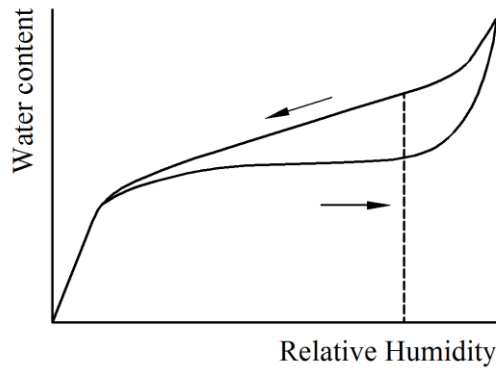


Figure 4.4 Hysteresis in water isotherm curve (Andrade et al., 2011).

In summary, the water loss is an influencing factor for concrete electrical resistivity, however, the characterisation of the concrete electrical resistivity in terms of water loss may not reflect the real concrete electrical resistivity value due to the hysteresis phenomenon of the “ink-bottle” effect during the evaporation process and then leads to a deviation. Andrade et al. (2011) studied the effect of water content and water loss on concrete electrical resistivity under different RHs. They have demonstrated that the electrical resistivity of concrete is better related to water content than water loss.

4.3 Influence of Chloride Content

The chloride ions in concrete have been identified as another important factor, influencing the concrete electrical resistivity due to its wide presence in the exposed environments, and high mobility in concrete. The influence of chloride content on concrete electrical resistivity has been investigated qualitatively by Henry (1964) reporting an inverse proportional correlation between chloride content and concrete electrical resistivity. Some other similar research results have been summarised in Figure 4.5.

In terms of the steel corrosion mechanism, chloride ions play an important role in breaking the passive film formed on the steel surface, so corrosion researchers had paid intense attention to the chloride threshold concentration, which can induce the initiation of steel corrosion. The concrete electrical resistivity considerably affects the steel corrosion condition, thus Morris et al. (2004) suggested a relationship between the chloride threshold concentration ($C_{Cl_{th}}$) and concrete electrical resistivity (Equation 4.1):

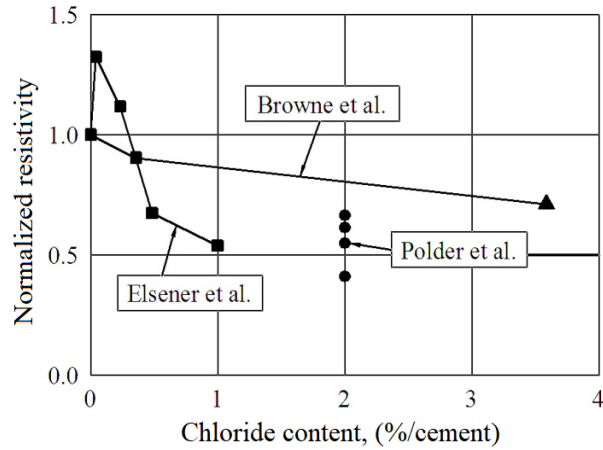


Figure 4.5 Relative change of concrete electrical resistivity with chloride state (Hunkeler, 1996).

$$C_{Cl_{th}}(\%) = 0.019\rho_c + 0.401 \quad (4.1)$$

In addition to the chloride threshold concentration, the general relationship between the concrete electrical resistivity and the chloride content also has a significant interest. Although extensive experimental studies have been conducted on the topic, the mathematical characterisation is still open to questions. So far, there has not been a widely recognised quantitative model to characterise their relationship.

4.4 Characterisation on Concrete Electrical Resistivity

4.4.1 Two Empirical Models

Jiang and Yuan (2012) have suggested a concrete electrical resistivity model as expressed in Equation (4.2), which considers the effects of w/c ratio, pore water saturation, chloride content, and temperature.

$$\rho_c = [750,605(w/c) - 106,228] \times \exp\left[-0.4417C_{Cl} - 7.7212S_w + 2889\left(\frac{1}{T} - \frac{1}{303}\right)\right] \quad (4.2)$$

where C_{Cl} is the total chloride ions content (% the mass percentage of cement), S_w is the degree of pore water saturation of concrete near the surface of the steel bar. For a specific concrete under a certain temperature condition, the Equation (4.2) may be rewritten into a general form as:

$$\rho_c = A \exp(aC_{Cl} + bS_w + c) \quad (4.3)$$

where A , a , b and c are constants depending on the formation and temperature of concrete.

Another attempt was to use the purely empirical Archie's law (Zaccardi et al., 2009; Atkins and Smith, 1961; Whittington et al., 1981). The formula, shown by Equation (4.4), was firstly proposed to describe the electrical resistivity of rocks for the effects of the rock porosity and the saturation degree of brine (Archie, 1942).

$$R_r = a\varepsilon^{-m} S_b^{-n} R_b \quad (4.4)$$

where R_r is the electrical resistivity ($\Omega\text{-m}$) of rock saturated with brine, R_b is the brine electrical resistivity ($\Omega\text{-m}$), S_b is the degree of brine saturation (%) in rocks, a is a factor for tortuosity, ε is the rock porosity, m and n are two constants. Considering that the concrete electrical resistivity is primarily decided by the cement paste, Atkins and Smith (1961) revised Archie's law into the form Equation (4.5) and applied it to concrete:

$$\rho_c = A\varphi^{-m} \rho_p \quad (4.5)$$

where ρ_p is the electrical resistivity ($\Omega\text{-m}$) of the cement paste in concrete, φ is the volume fraction of cement paste, A and m are two constants. Later, having recognised that the electrical conductivity of the pore solution is several orders higher than that of all the other phases (air, aggregates and cement paste) in concrete, Archie's law was further revised into the form of the Equation (4.6) to explicitly consider the effect of water content variation in concrete (Zaccardi et al., 2009; Whittington et al., 1981).

$$\rho_c = A\theta^{-m} \rho_w \quad (4.6)$$

where ρ_w is the electrical resistivity ($\Omega\text{-m}$) of pore water solution, which depends upon the composition of the pore water solution, θ is the pore water volume fraction of concrete, A and m are two redefined constants.

For a chloride contaminated concrete, the electrical resistivity of pore water solution will be influenced by the chloride ion concentration dissolved in the pore water. Therefore, to explicitly describe the effect of the variation of the chloride content in concrete pore water solution, Equation (4.6) was rewritten into the following form:

$$\rho_c = AS_w^{-n} \rho_w(C_{Cl}) \quad (4.7)$$

where $\rho_w(C_{Cl})$ is the electrical resistivity ($\Omega\text{-m}$) of pore water solution, which is simply assumed to depend on the chloride content, A and n are two constants related to the pore structure, such as porosity and tortuosity. To find out the explicit expression of $\rho_w(C_{Cl})$, a study by Shaikhon (2015) investigated the influence of chloride concentration on concrete electrical resistivity was employed. The experimental data is presented in Figure 4.6.

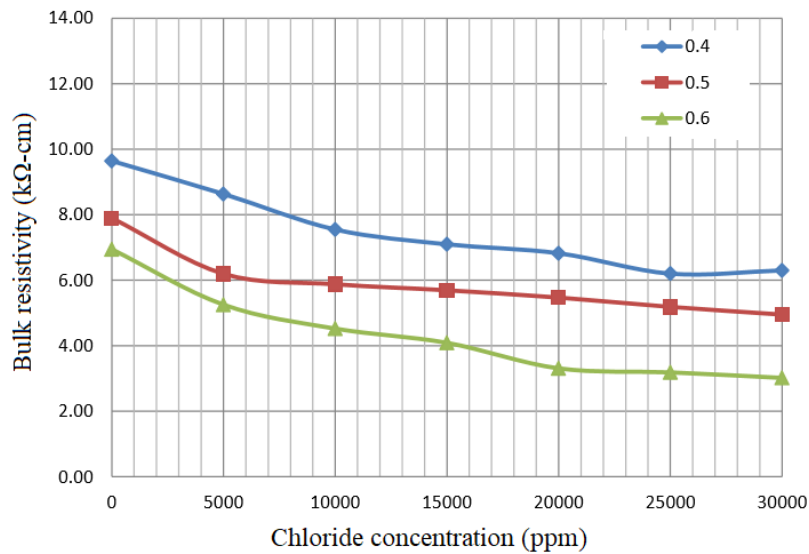


Figure 4.6 Experimental data of the study by Shaikhon (2015).

By fitting the above experimental data, a non-linear relationship was observed, for which an exponential function is suggested to express the electrical resistivity of pore water solution in terms of chloride concentration:

$$\rho_w(C_{Cl}) = ae^{bC_{Cl}} + c \quad (4.8)$$

where a , b and c are three constants depending on the other condition of the concrete pore solution such as temperature, pH etc. Substituting Equation (4.8) into Equation (4.7) yields a new revision of Archie's law:

$$\rho_c = S_w^{-n}(ae^{bc_{cl}} + c) \quad (4.9)$$

where a and c are two redefined constants merged with A in Equation (4.7).

4.4.2 A New Semi-Empirical Model

Although two empirical models (Equation 4.3 and 4.9) provide the expected explicit form to describe the coupling influence of the water and chloride content variation on concrete electrical resistivity, they have little fundamental explanation for the underlying mechanism. Fundamentally, the pore water solution in concrete acts solely as the medium for the electrical conductivity, and the greater the water content the higher the concrete conductivity, or the lower the concrete electrical resistivity. In addition to the absolute pore water quantity, the water distribution in the concrete pore structure also plays an important role in deciding the concrete electrical conductivity.

When the concrete is in the unsaturated state, the bulk water phase presents two configurations in pores. The major part of water predominantly occupies the pore space of small sizes, while a water film covers all the empty pore surfaces (shown in Figure 4.2). Such water occupying configuration state is due to the physicochemical adsorption of pore surfaces and capillary condensation (Wang et al., 2008; Wang and Wu, 2008). Consequently, the water distribution or configuration at varied pore water saturation degrees depends upon the pore size distribution. As a result, the influence of water content on concrete electrical conductivity or resistivity is intrinsically related to concrete pore size distribution. Such an intrinsic relationship is similar to that between the thermal conductivity of unsaturated soils and soil water saturation (Jin et al., 2017). To reflect the underlying mechanism, the work by Jin et al. (2017) was revised to characterise and model concrete electrical resistivity at varied water content. Based on the physical chemistry theory of interfacial phenomena, for unsaturated porous media in general, the total pore volume average pressure of the bulk water phase in filled pores, and the total pore volume average pressure of the bulk vapour phase in empty pores can be expressed respectively using two functions of water saturation (Wang and Li, 2000; Wang et al., 2012; Jin et al., 2017), i.e.:

$$P_w = \frac{P_0}{\alpha} [\exp(\alpha S_w) - 1] \quad (4.10a)$$

$$P_v = \frac{P_0}{\beta} \{ \exp[\beta(1 - S_w)] - 1 \} \quad (4.10b)$$

where P_w and P_v are the total pore volume average pressures of the water phase and the vapour phase in porous media, P_0 , α , β are three constants related to the nature of the interfacial phenomenon at pore surfaces. Under thermodynamic equilibrium, the pressure difference of the two phases will be balanced by the interfacial menisci between the bulk water phase and the bulk vapour phase, and is related to the pore size distribution (Wang and Li, 2000; Wang et al., 2012).

Water pressure and water electrical conductivity has an intrinsic thermodynamic relationship. Both of them relate to the water molecular and ionic dynamics. The same form of the Equation (4.10) is adopted to describe the electrical conductivity or resistivity of the bulk water in filled pores, and the water film on the empty pore surfaces (the water film thickness relates to the vapour pressure in the empty pores) respectively. Consequently, the concrete electrical resistivity at varied water saturation degree may be expressed as:

$$\rho_c = \rho_w + \rho_{wf} = \frac{\rho_0}{\alpha} [\exp(\alpha S_w) - 1] + \frac{\rho_0}{\beta} \{ \exp[\beta(1 - S_w)] - 1 \} \quad (4.11)$$

where ρ_w and ρ_{wf} indicate the electrical resistivity ($\Omega\cdot m$) of the bulk water phase and the water film phase in concrete respectively, ρ_0 , α and β are constants. By explicitly distinguishing the two water configuration phases, Equation (4.11) has naturally taken account of the effect of pore size distribution. Rearranging Equation (4.11) generates:

$$\rho_c = \rho_0 \left\{ -\frac{1}{\beta} - \frac{1}{\alpha} + \exp(\alpha S_w)/\alpha + \exp[\beta(1 - S_w)]/\beta \right\} \quad (4.12)$$

A similar form as the Equation (4.12) has been successfully used to model the water vapour adsorption isotherm of concrete materials for pore size distribution analysis (Wang et al., 2012). Based on the Equation (4.12), for easy implementation and memorisation, a simplified form was suggested as:

$$\rho_c = f_0 + \rho_0 \{ \exp(\alpha S_w) + \exp[\beta(1 - S_w)] \} \quad (4.13)$$

where f_0 , ρ_0 , α and β are four redefined constants. The form of Equation (4.13) has proved to generate a close result on water vapour adsorption isotherm compared with that of the similar

form of Equation (4.12) (Wang et al., 2012). For this reason, the simplified form of Equation (4.13) was used, to describe the effect of water saturation on concrete electrical resistivity.

To characterise the coupling effect of water and chloride contents on concrete electrical resistivity, an exponential form function was used to account for the chloride effect as shown in Equation (4.14):

$$\rho_c = \exp(aC_{cl}^b) \{f_0 + \rho_0 [\exp(\alpha S_w) + \exp(\beta(1 - S_w))]\} \quad (4.14)$$

where a and b are two constants.

4.4.3 Model Test

To validate the new developed semi-empirical model of concrete electrical resistivity, Equations (4.3), (4.9) and (4.14) are used to model two sets (cases) of experimental data respectively, which have been selected to compare their performance. One case is from a published reference (Saleem et al., 1996), and another case is based on an experimental study made by (Oleiwi, 2018).

The MATLAB curve fitting tool was employed for the modelling study. The model performance (goodness-of-fit) was evaluated in terms of two statistical measures, they are the Root Mean Square Error (RMSE) and the R-squared (coefficient of determination), which are defined as below:

$$RMSE = \sqrt{\frac{\sum_{i=1}^N (y_i - f_i)^2}{n}} \quad (4.15)$$

$$R - \text{squared} = \sqrt{1 - \frac{\sum_{i=1}^N (y_i - f_i)^2}{\sum_{i=1}^N (y_i - \bar{y}_i)^2}} \quad (4.16)$$

where \bar{y}_i is the average of all the experimental data y_i , N is the total number of the experimental data, f_i is the modelling value from data fitting.

RMSE is the standard deviation of the residuals. Residuals are a measure of how far from the regression line data points are. RMSE is a measure of how spread out these residuals are,

which describe how concentrated the data is around the line of best fit. The lower the RMSE value the better the modelling. R-squared statistical measure describes how close the experimental data are to the fitting regression line, its value always lies between 0 and 1, a value of R-squared closer to 1 indicates that almost all the observed variation can be explained by the inputs of model.

- **Case I**

Saleem et al. (1996) conducted a series of studies on the effects of both chloride and water contents on the electrical resistivity of concrete. All the parameter values related to the concrete specimens are provided in Table 4.2. The water content was accounted in terms of the mass percentage to the oven dry specimens, while the chloride content was accounted in terms of the weight in 1 m³ volume of the specimens. In the current study, with an estimation that the dry concrete specimens have a density of 2000kg/m³ and a porosity of 0.13, the data were converted to pore water saturation (S_w) and chloride to water mass ratio (Cl/W).

Table 4.1 Concrete specimen composition in case I.

Parameter	Value
Cement content	350 kg/m ³
Water/cement ratio (w/c)	0.45
Chloride content (by concrete volume)	0, 2.4, 4.8, 9.6 and 19. 2kg/m ³
Dry specimen porosity	0.13
Dry specimen density	2000kg/m ³

Figure 4.7 compares Equations (4.3), (4.9) and (4.14) to model the variation of concrete electrical resistivity at different water contents under certain chloride contents. A good agreement between these equations and experimental data can be observed clearly, especially that Equations (4.14) and (4.9) outperformed Equation (4.3) and both of them have produced good fitting results. It shows that the electrical resistivity of concrete decreases with increasing saturation degree of pore water.

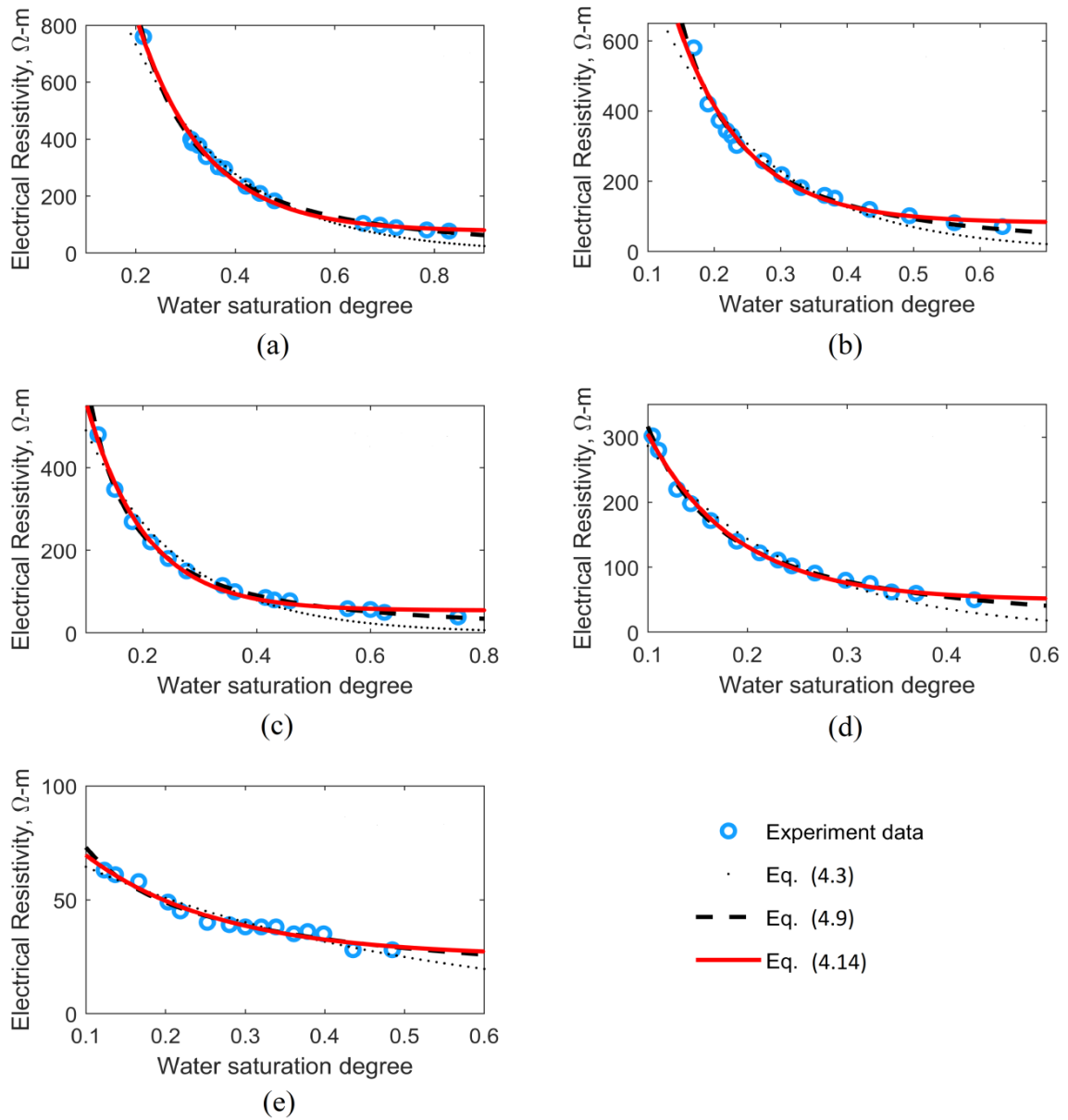
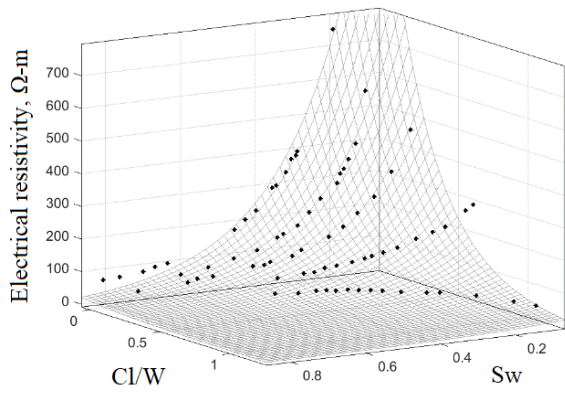
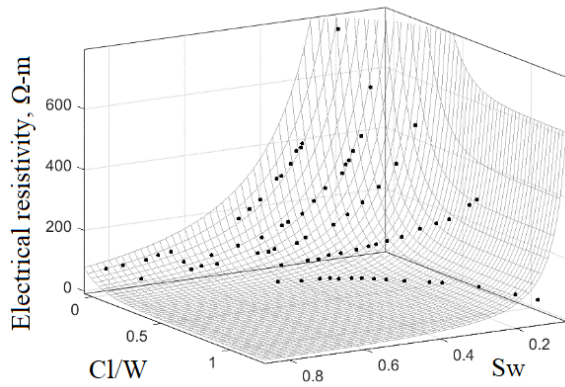
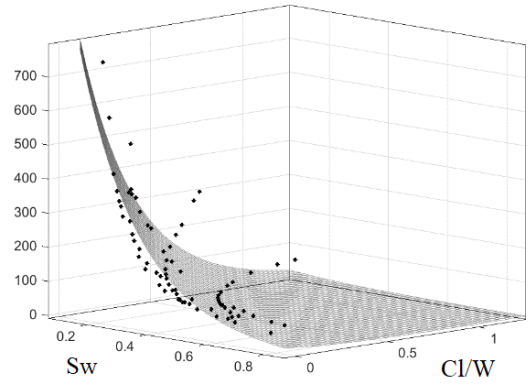


Figure 4.7 Comparison of three models on data by Saleem et al. (1996) at certain chloride contents. (a) Chloride content: 0 kg/m^3 , (b) Chloride content: 2.4 kg/m^3 , (c) Chloride content: 4.8 kg/m^3 , (d) Chloride content: 9.6 kg/m^3 , (e) Chloride content: 19.2 kg/m^3 .

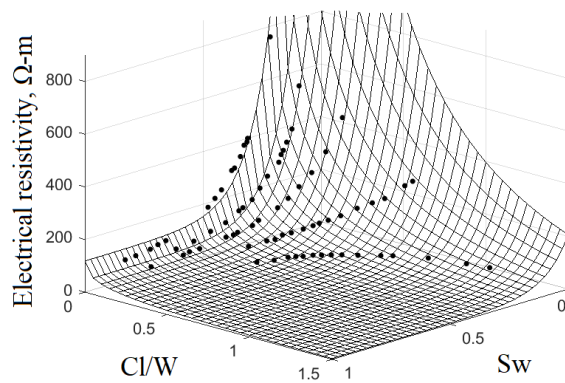
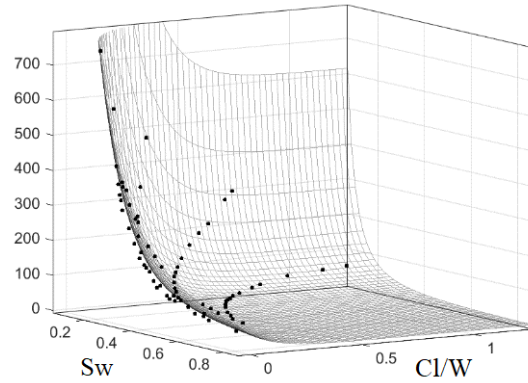
Figure 4.8 compares the modelling results using Equations (4.3), (4.9) and (4.14) to fit all the reported experimental data in the linear scale 3D space of electrical resistivity against the pore water saturation, and the chloride to water mass ratio respectively. Although all three models present a surface fitting to the measurement points, it can be seen that Equations (4.9) and (4.14) have produced much better, stable, and reliable results than Equation (4.3), which fails to represent all the experimental data involved.



(a)



(b)



(c)

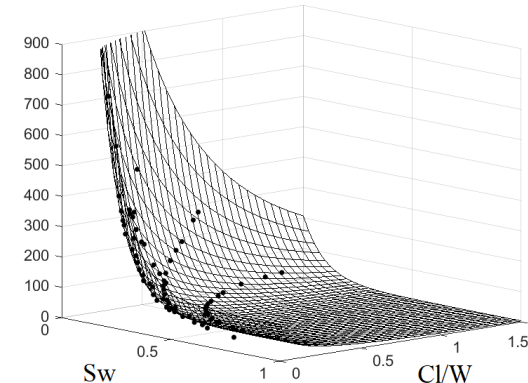


Figure 4.8 Modelling the coupling effect of water and chloride contents on concrete electrical resistivity for the data by Saleem et al. (1996). (a) Modelling result of Equation (4.3), (b) Modelling result of Equation (4.9), (c) Modelling result of Equation (4.14).

Figure 4.9 compares the modelling statistics of the three models. It shows that the RMSEs of the Equations (4.9) and (4.14) are about half of that of Equation (4.3). The R-squared values of Equations (4.9) and (4.14) are very close to 1, which indicate that deviation around the mean value is small as well. Overall, the model Equation (4.14) presents the best performance.

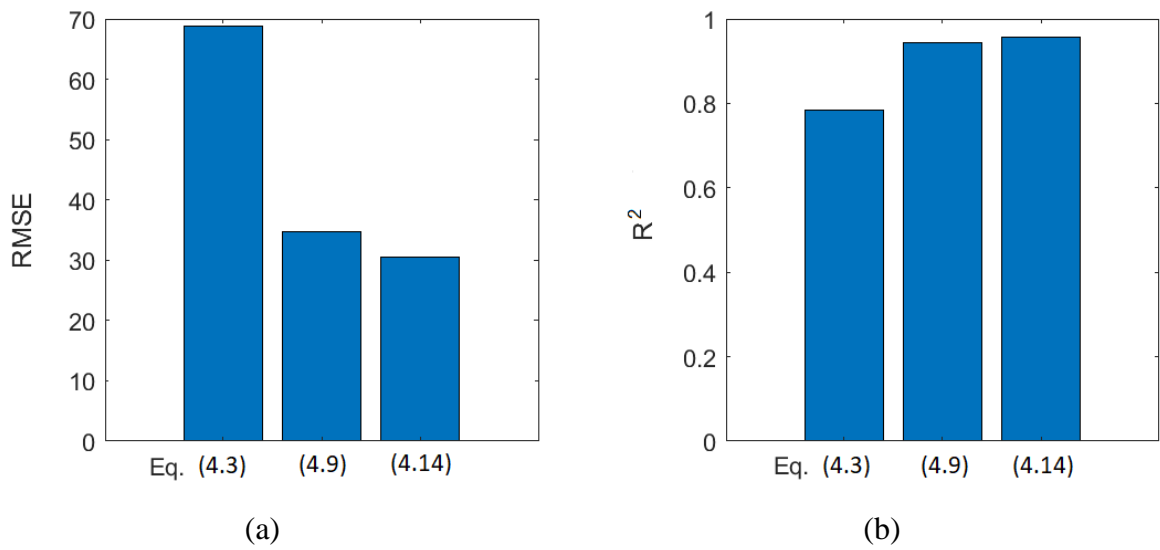
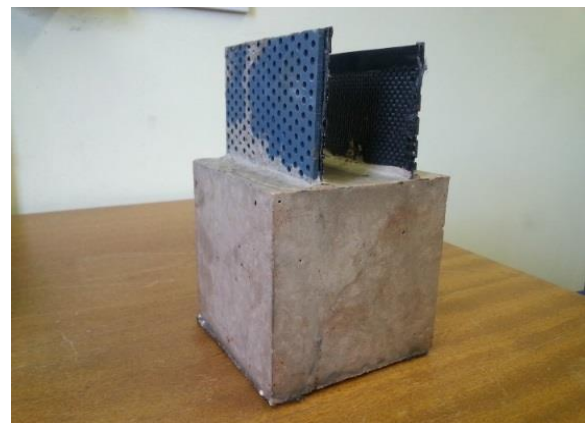
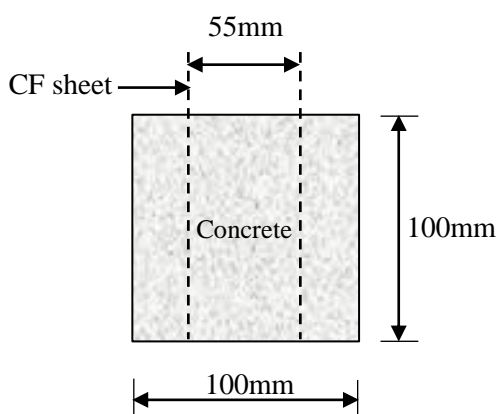


Figure 4.9 Modelling statistics for the data by Saleem et al. (1996). (a) RMSE, (b) R-squared.

- **Case II**

Olewi (2018) investigated the concrete electrical resistivity under different chloride contents and RHs. Concrete specimen configuration is presented in Figure 4.10 and all the parameter values related to the concrete specimen and exposure conditions are provided in Table 4.3. The actual total chloride contents in the cured concrete samples for each mixture were measured specifically.



(a)

(b)

Figure 4.10 Configuration of concrete specimen for concrete electrical resistivity measurements (Olewi, 2018). (a) Dimension, (b) Concrete specimen.

Table 4.3 Concrete specimen composition and exposure conditions in case II.

Parameter	Value
Cement content	390 kg/m ³
Water/cement ratio (w/c)	0.4, 0.5 and 0.6
Added NaCl content	0, 1.5, 3, and 4.5% (by cement mass)
Relative humidity	35, 60, 80, and 100%

Figures (4.11), (4.12) and (4.13) compares the Equations (4.3), (4.9) and (4.14) to model the variation of the concrete electrical resistivity at different water contents under certain chloride contents (total chloride content by concrete weight), where the electrical resistivity presented in log scale to show difference more clearly. Figure 4.14 shows the residuals of the modelling, and the differences between the fitting results to the experimental data (i.e. $f_i - y_i$). It can be seen that apart from an extremely low water saturation ($\ll 0.1$) Equation (4.14) produced the best fitting (close to the neutral line, 0) compared to all other data. The underperformance at very low water saturation may be due to the unstable measurement of concrete electrical resistivity under the situation.

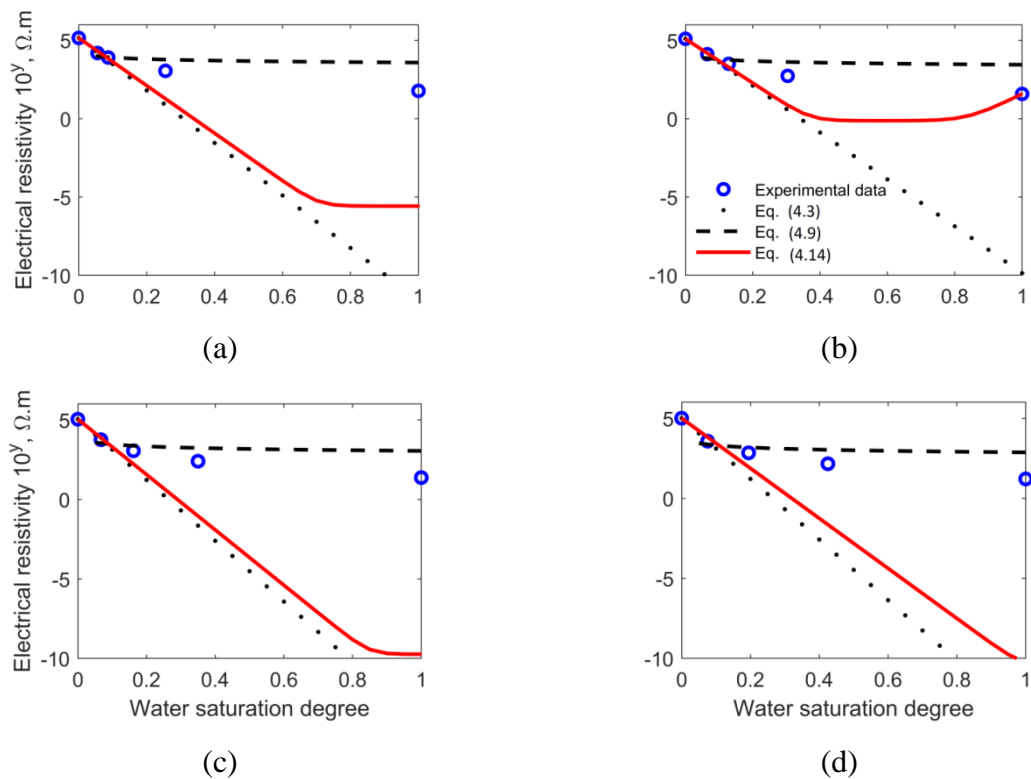


Figure 4.11 Comparison of the three models on data by Oleiwi (2018) ($w/c = 0.4$) at certain total chloride contents. (a) NaCl: 0%, (b) NaCl: 0.197%, (c) NaCl: 0.358%, (d) NaCl: 0.502%.

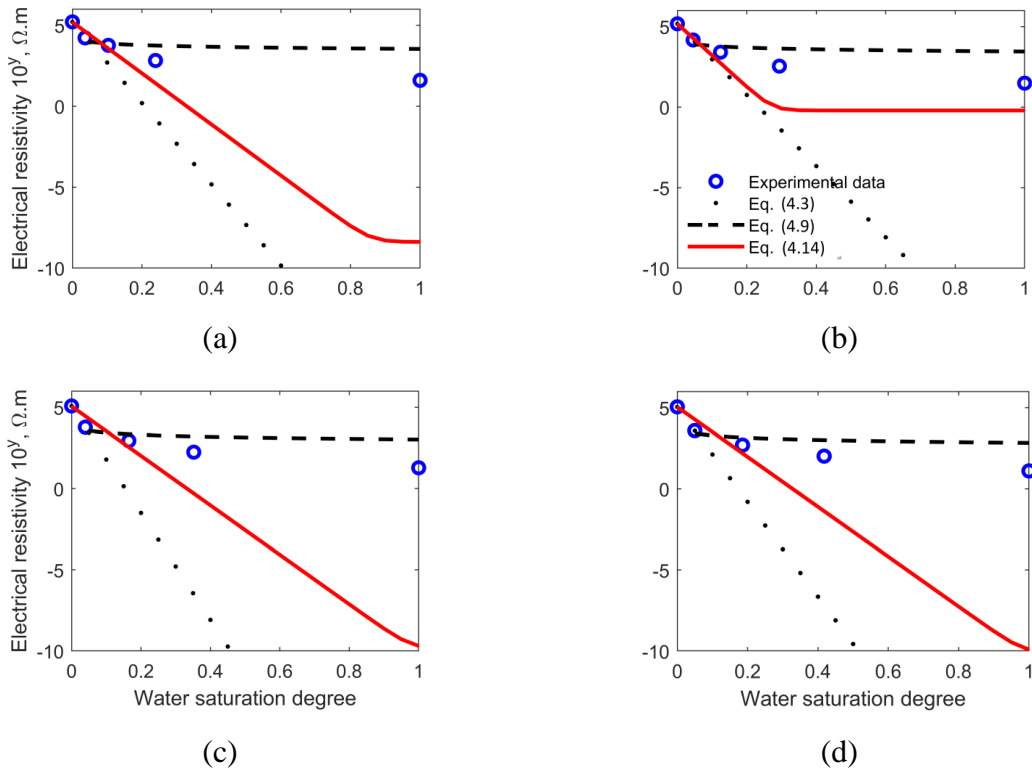


Figure 4.12 Comparison of the three models on data by Oleiwi (2018) ($w/c = 0.5$) at certain total chloride contents. (a) NaCl: 0%, (b) NaCl: 0.217%, (c) NaCl: 0.389%, (d) NaCl: 0.517%.

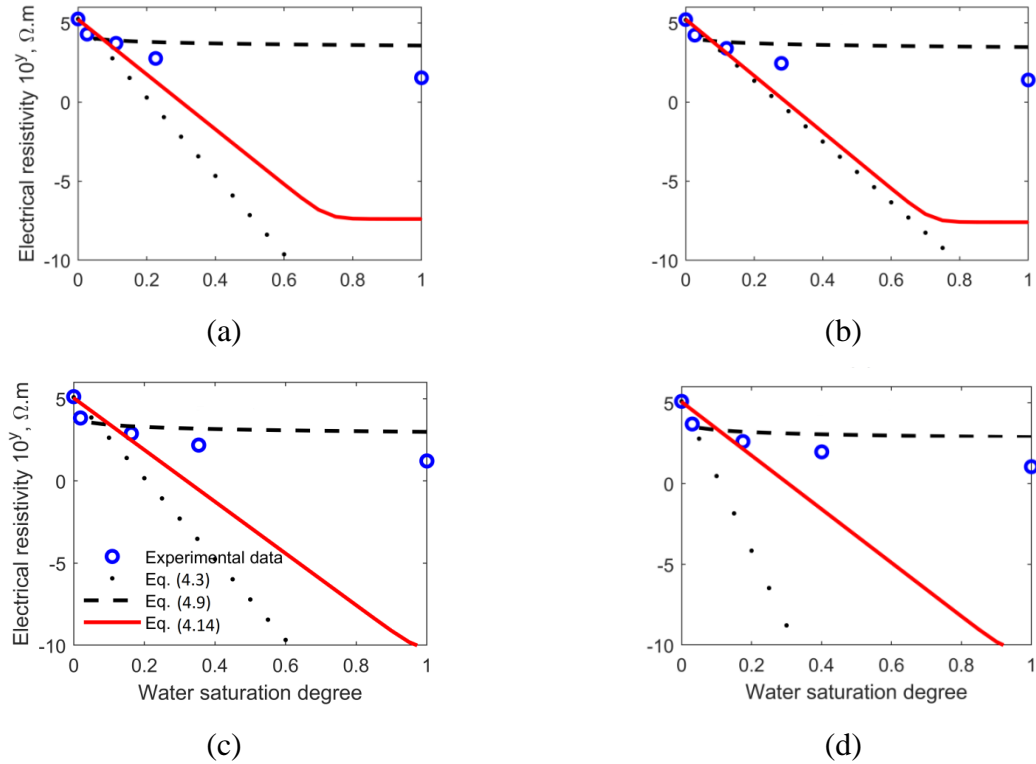


Figure 4.13 Comparison of the three models on data by Oleiwi (2018) ($w/c = 0.6$) at certain total chloride contents. (a) NaCl: 0%, (b) NaCl: 0.223%, (c) NaCl: 0.402%, (d) NaCl: 0.53%.

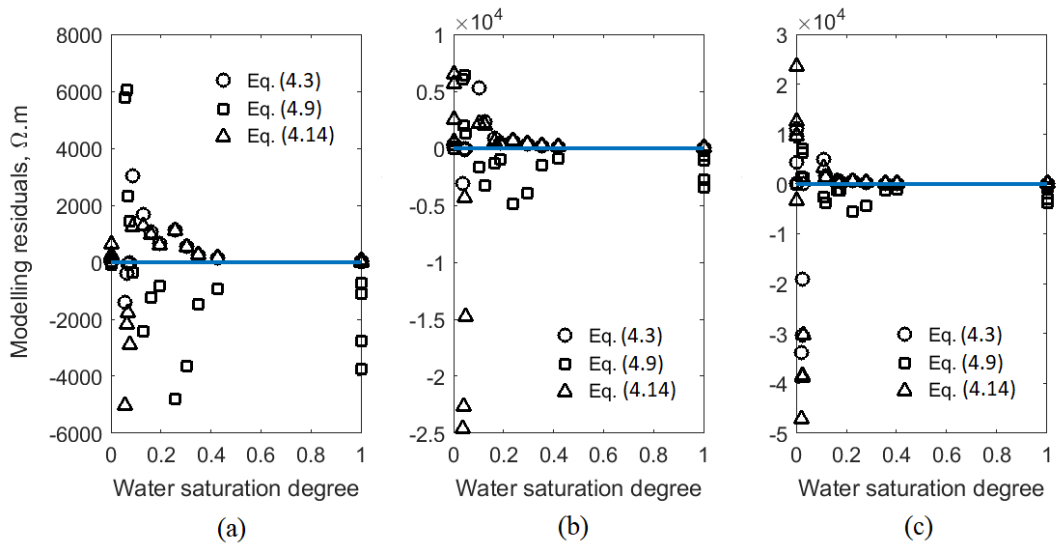


Figure 4.14 Residuals of the three models from cases in Figures 4.11, 4.12 and 4.13.

(a) $w/c=0.4$, (b) $w/c=0.5$, (c) $w/c=0.6$.

Figure 4.15 shows the exponential weighting term as used in Equation (4.14) to model the chloride effect on concrete electrical resistivity of fully saturated samples, which proves a good performance.

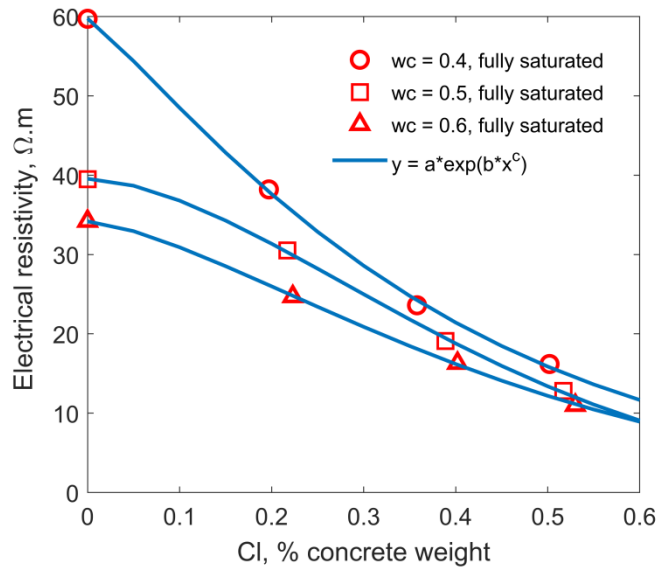
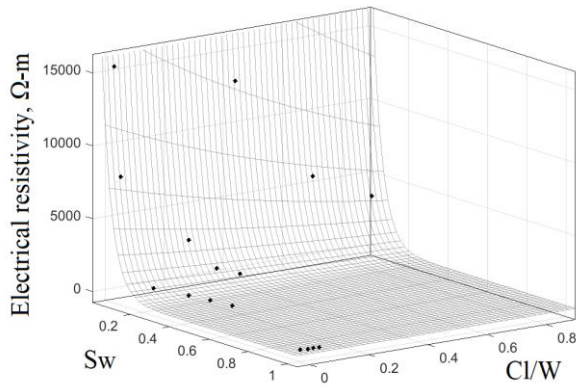


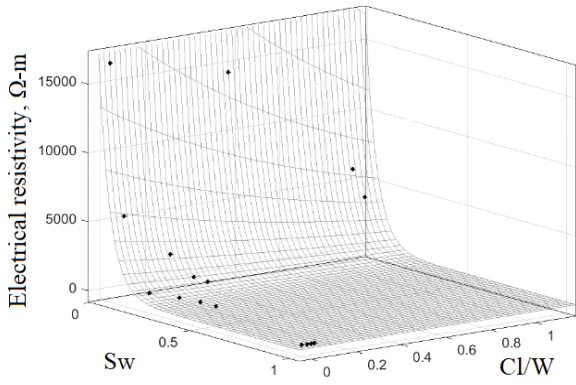
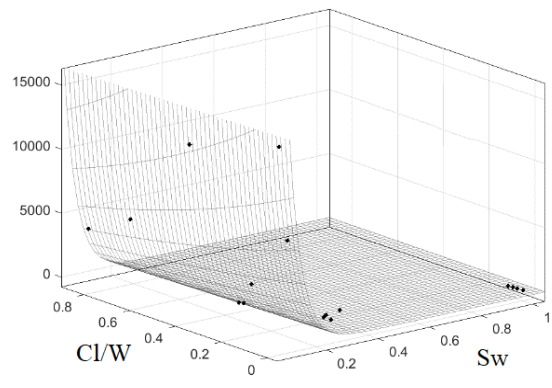
Figure 4.15 Modelling chloride effect on concrete electrical resistivity using the exponential weighting term in Equation (4.14).

Figure 4.16 shows the results using the Equation (4.3) to fit all the experimental data in the linear scale 3D space of concrete electrical resistivity against the pore water saturation and

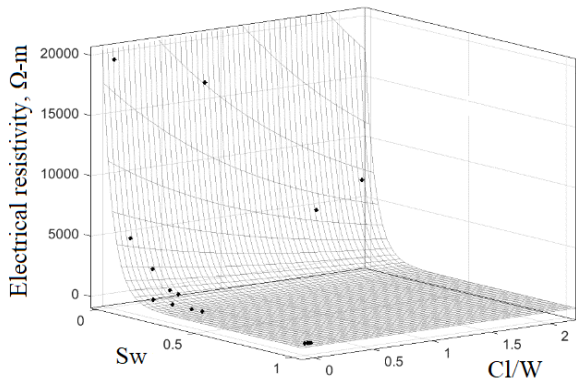
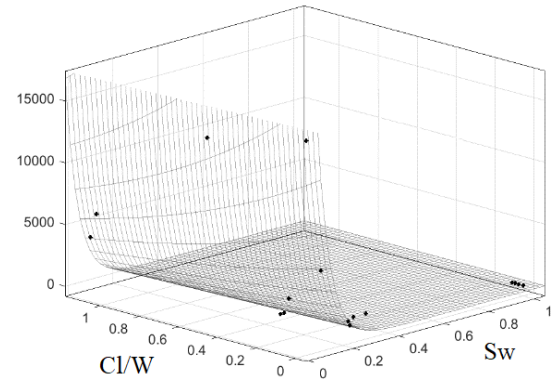
total chloride content in terms of pore water content. Visually, the fitting surfaces for the concrete with different w/c ratios have shown a good agreement with the experimental data.



(a)



(b)



(c)

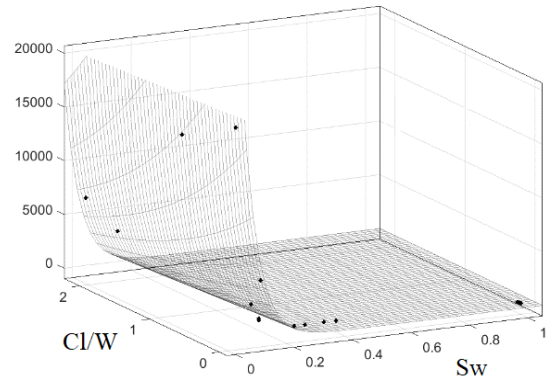
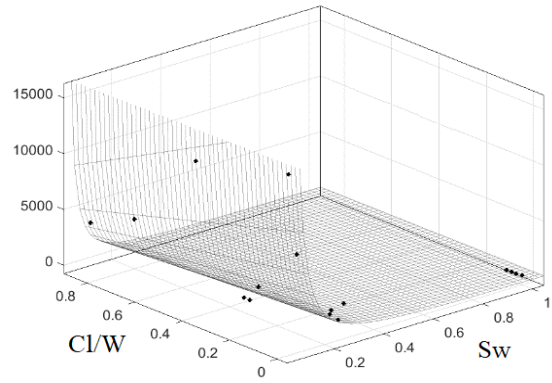
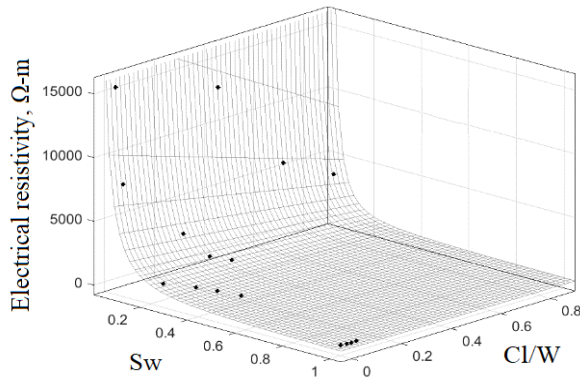


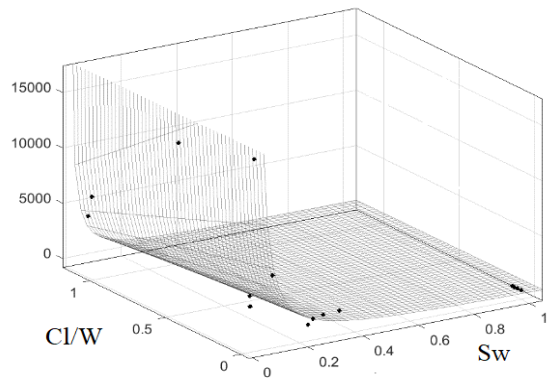
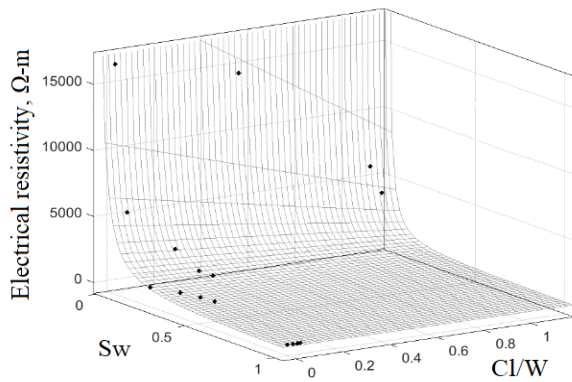
Figure 4.16 Modelling the coupling effect of water and chloride contents on concrete resistivity using Equation (4.3) for the data by Oleiwi (2018).

(a) w/c=0.4, (b) w/c=0.5, (c) w/c=0.6.

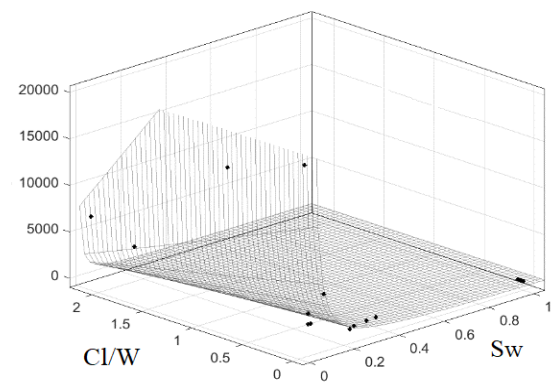
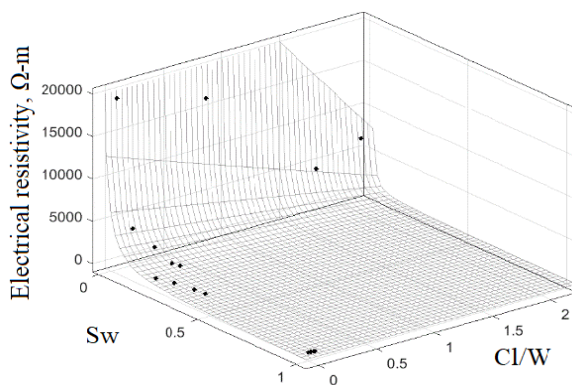
Figure 4.17 shows the results using Equation (4.9) to fit these experimental data in the same way. A visual inspection shows that the fitting surfaces for the three concretes of different w/c ratios are close to that presented by Equation (4.3) in Figure 4.15.



(a)



(b)

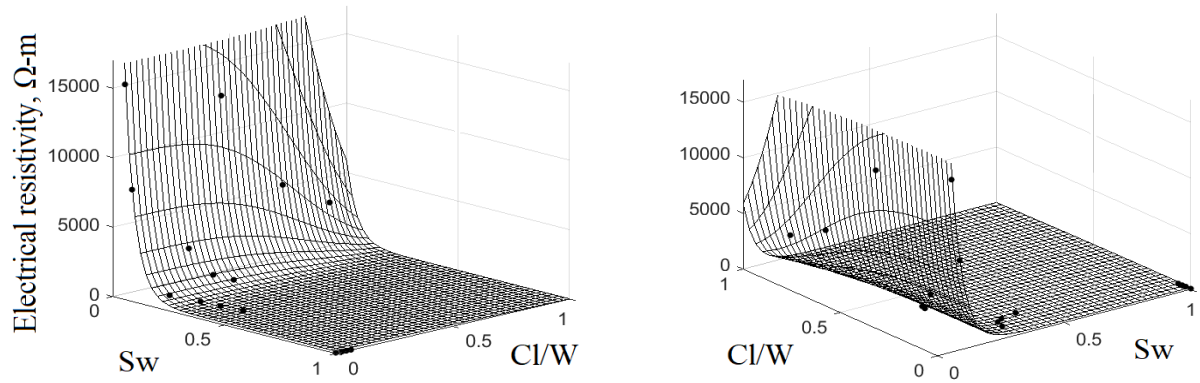


(c)

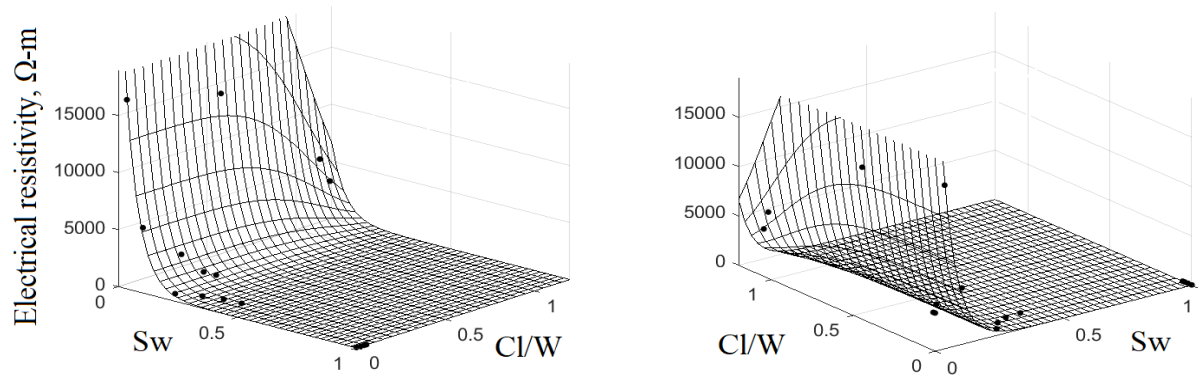
Figure 4.17 Modelling the coupling effect of water and chloride contents on concrete resistivity using Equation (4.9) for the data by Oleiwi (2018).

(a) w/c=0.4, (b) w/c=0.5, (c) w/c=0.6.

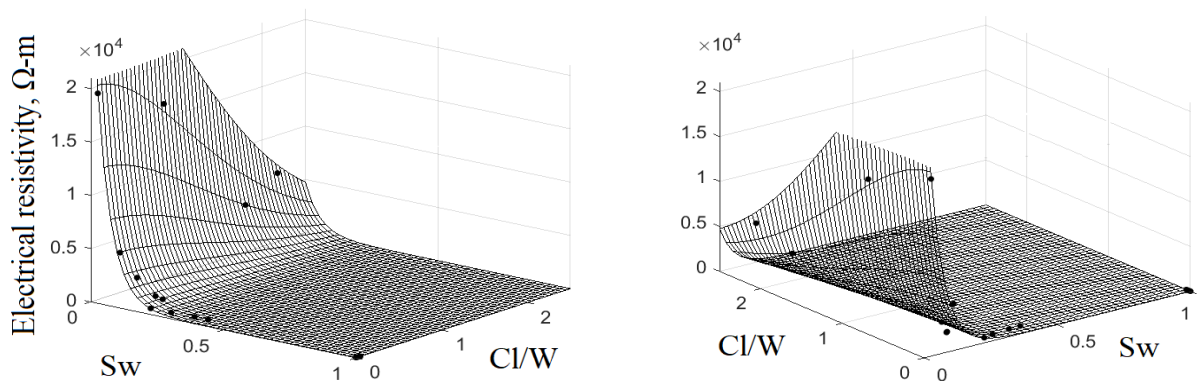
Figure 4.18 shows the results using Equation (4.14) to fit all the experimental data again in same way. A visual inspection shows that Equation (4.14) has produced a better performance than Equations (4.3) and (4.9) in representing the experimental measurements over all.



(a)



(b)



(c)

Figure 4.18 Modelling the coupling effect of water and chloride contents on concrete resistivity using Equation (4.14) for the data by Oleiwi (2018).

(a) $w/c=0.4$, (b) $w/c=0.5$, (c) $w/c=0.6$.

Figure 4.19 compares the modelling statistics of the three models for this set of data. It shows that in all cases the R-squared values of the three models are very close to 1. However, the model Equation (4.14) presents the best performance with a quite small RMSE. In fact, it produces the smallest RMSE and the highest R-squared value in all the cases.

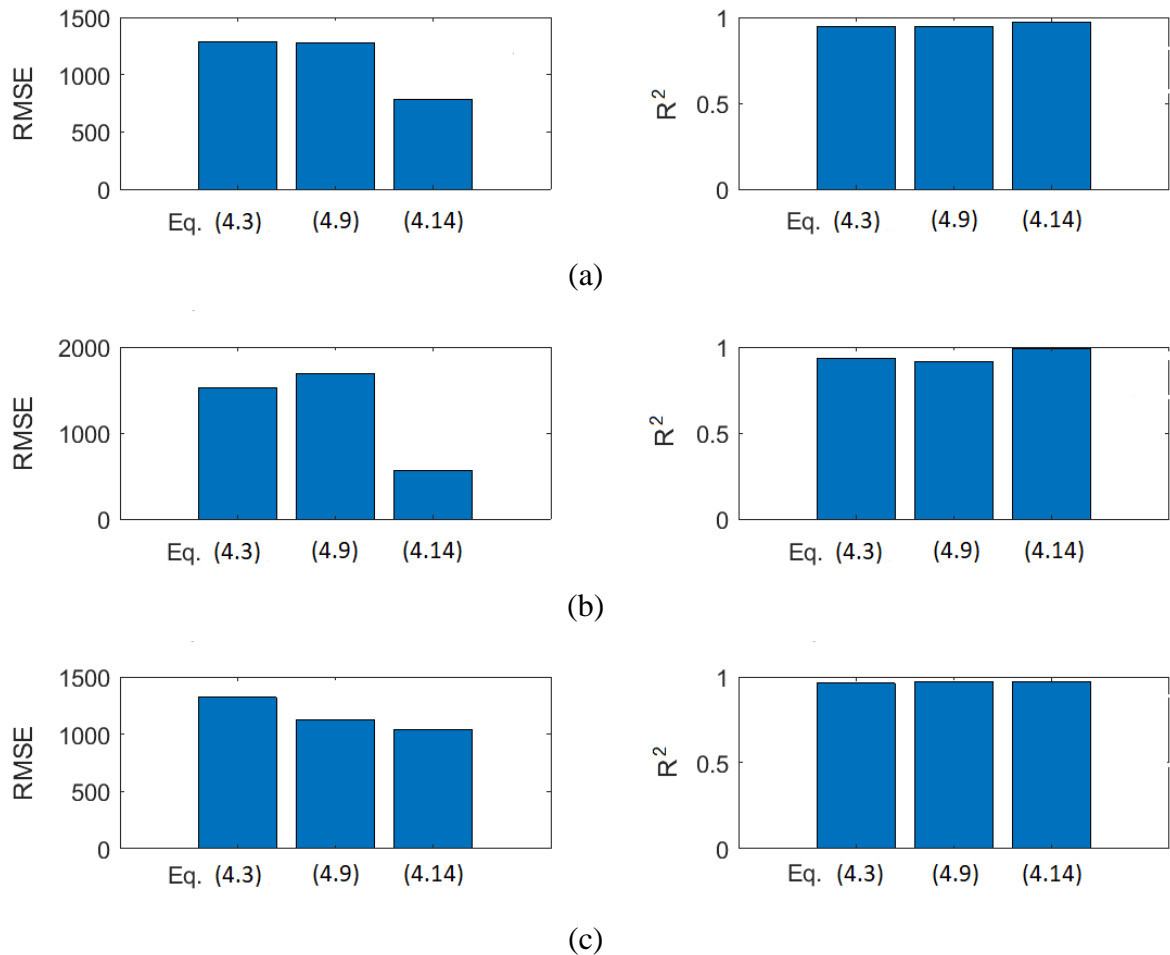


Figure 4.19 Modelling statistics for the data by Oleiwi (2018).

(a) $w/c=0.4$, (b) $w/c=0.5$, (c) $w/c=0.6$.

4.5 Conclusions

This chapter investigated the characterisation models for the coupled effect of water and chloride contents on the electrical resistivity of concrete of different pore structures (related to different w/c ratios). It proposed a semi-empirical model based on the understanding that

concrete electrical resistivity at varied water content is related to the pore size distribution of the pore structure as below:

$$\rho_c = \exp(-2.211C_{cl}^{3.322}) \times \{168.1 + 1.649e - 5[\exp(-71.33S_w) + \exp(21.9(1 - S_w))]\} \quad (4.17)$$

Comparison of the three different models has been conducted on two sets of experimental data. From the investigation, we can draw the following conclusions:

1. Archie's law demonstrates a good representation for the effect of degree of pore water saturation on the concrete electrical resistivity, while an exponential function well represents the effect of chloride content.
2. The proposed semi-empirical model established on the water phase configurations in pore network highlights the important role of the pore size distribution of pore structures in the electrical resistivity of unsaturated concrete.
3. The semi-empirical model has demonstrated a more accurate and reliable performance compared to the other two empirical models to characterise the coupling effect of the variation of water and chloride contents on concrete electrical resistivity.
4. The proposed semi-empirical model provides a useful parameter for the numerical modelling of the CP process in concrete to describe the coupling effect of the water and chloride variation when RC structures are exposed to varying severe environments.

CHAPTER 5

BOUNDARY CONDITION CHARACTERISATION

5.1 Introduction

The efficiency of Cathodic Protection (CP) systems for Reinforced Concrete (RC) structures depends on the protection current transport in concrete and the steel polarisation phenomenon. To implement the numerical simulation technology of CP for RC structures with satisfactory accuracy, there are two issues which need to be addressed, they are the redistribution of the different kinds of ions in concrete, and the details of electrochemical reactions at the steel-concrete interface. The first issue has been discussed in Chapters 3 and 4 regarding the Nernst-Planck Equation, which describes the motion of the charged chemical species in the concrete pore solution and the variation of concrete electrical resistivity. For the second issue, it is necessary to choose the appropriate mathematical models to reflect the electrochemical reaction kinetics at the steel-concrete interface.

According to the specific steel state (active or passive state) in concrete, in CP numerical modelling of RC structures, the electrochemical reaction kinetics at the steel-concrete interface is represented by the different polarisation curve, which describes the coupled effect between the current density on the steel surface and the steel polarisation. In general, the polarisation curve based on the Butler-Volmer Equation has been widely adopted as the boundary condition in CP numerical model of RC structures to describe the electrochemical reaction at steel-concrete interface under the CP process (Koretsky et al., 1999; Hassanein et al., 2002; Muehlenkamp et al., 2005; Polder et al., 2008; Cheung and Cao, 2013), also the measured real-time polarisation curve has been used in several research investigations (Warkus and Raupach, 2008; Bruns and Raupach, 2010; Qiao et al., 2016).

5.2 Reinforcement Polarisation — Butler-Volmer Equation

As reviewed in Chapter 2, the simplified Butler-Volmer Equations can be used to describe the kinetics of the oxidation and reduction reaction simultaneously occurring on the steel surface (Equation 5.1), in which the potential shift takes the equilibrium potentials (E_{eq}^a, E_{eq}^c) of the two different half reactions and the corresponding respective exchange current densities (i_o^a, i_o^c) as the reference points.

$$i_n = i_o^a \cdot \exp\left(2.303 \frac{E - E_{eq}^a}{b_a}\right) - i_o^c \cdot \exp\left(-2.303 \frac{E - E_{eq}^c}{b_c}\right) \quad (5.1)$$

The Butler-Volmer Equation represents the steel polarisation curve, which has been widely adopted in the numerical simulation to study the process of CP implemented on RC structures. For instant, Koretsky et al. (1999) studied the influence of degree of concrete pore saturation on CP behaviour for a corroding RC bridge. Liu and Shi (2012) modelled the effects of design parameters of cathodic prevention for unconventional concrete under aggressive environments. Cheung and Cao (2013) simulated the effect of macrocell corrosion on CP protection current distribution in RC structures.

Butler-Volmer Equation can also take the form shown in Equation (5.2), in which the potential shift takes the corrosion potential (E_{corr}) and the corresponding corrosion rate (i_{corr}) as the reference point.

$$i_n = i_{corr} \left\{ \exp\left(2.303 \frac{E - E_{corr}}{b_a}\right) - \exp\left(-2.303 \frac{E - E_{corr}}{b_c}\right) \right\} \quad (5.2)$$

This form of the Butler-Volmer Equation has also been broadly applied in the numerical research of CP for RC structures to characterise the steel polarisation curve. For example, Hassanein et al. (2002) studied the effects of the structural, environmental, and operational factors on the performance of CP/RC systems. Polder et al. (2008) used the advanced numerical design to study the current and potential distribution of rebar in concrete under CP application.

5.3 Reinforcement Polarisation — Real-Time Polarisation Curve

In terms of the literature research in this study, most of the numerical simulations of CP for RC structures treated the boundary conditions at steel-concrete interface using a unitary polarisation curve, which is based on the Butler-Volmer Equation and accompanied by a variety of experimentally measured parameters, such as Tafel slope, corrosion potential, etc. On the other hand, in order to describe a more direct steel-concrete interfacial electrochemical behaviour, a real-time polarisation curve, which is measured from the potentiodynamic test had also been adopted.

The real-time polarisation curve is obtained by forcing the electrode polarisation under a certain scanning potential rate, and then the resultant current density and the real-time potential are recorded simultaneously. Due to the size limitation of RC structures, and the intricate arrangement of embedded rebar, it is not applicable to directly conduct measurements on the prototype structures. For convenient measurements and accurate results, the test specimens with simple geometry which are consistent with the prototype structures (identical composition, curing condition and post-treatment conditions) are used. Up to now, a few researchers adopted this method, such as Masuda et al. (2004) who measured the polarisation curves of titanium anode plate and steel rod immersed in saturated calcium hydroxide solution. Bruns and Raupach (2010) tested polarisation curves on prepared RC test specimens Qiao et al. (2016) and Qiao et al. (2017) both characterised the polarisation curves of the anode specimens immersed in simulated concrete pore solution and prepared RC test specimens respectively.

5.4 Analysis on Existing Polarisation Model

5.4.1 Butler-Volmer Polarisation Model

The application of Butler-Volmer Equation based polarisation curves has a relatively good record in CP numerical studies but which still present deficiencies.

In CP numerical modelling, the use of the Butler-Volmer Equation based polarisation curve needs to be defined by various constant corrosion parameters beforehand, and then the

solution by the simulation is based on the set of input constant parameters. However, in the actual condition of CP process in RC structures, the steel negative polarisation effect and the long-term effects of CP applications will significantly change these parameters. For example, the Tafel slope of active bar is different from that of the passive bar. So far, the conventional application of Butler-Volmer Equation based polarisation curves in CP numerical modelling does not take into account the time-dependent effects. Consequently, the associated simulation is unable to precisely describe the actual electrochemical behaviour at the steel-concrete interface. Therefore, to select the proper Butler-Volmer polarisation model, which can truly reflect the time-dependent steel state under CP application is directly connected to the accuracy of the CP numerical study results, which is also a challenging task for researchers (Ge and Isgor, 2007).

5.4.2 Real-Time Polarisation Model

The real-time polarisation curve acts as an alternative and has been used recently for the boundary condition in CP numerical modelling of RC structures (Qiao et al., 2016; Qiao et al., 2017). The real-time polarisation curve can truly reflect the actual dynamic variation of the electrochemical behaviour of steel-concrete interface under the action of CP; nevertheless, it is demonstrated that the measured real-time polarisation curve still presents insufficient accuracy.

Warkus and Raupach (2008) had numerically studied the steel macrocell corrosion in concrete with real-time polarisation curves as the boundary condition. The measured polarisation curves of active bars were highly scattered, and this was attributed to the amount of macrocell corrosion area, which is unknown as well as it is different for different steel bars, so their numerical modelling replaced the polarisation curves of active rebars by a simplified linear equation. Bruns and Raupach (2010) modelled CP applied to RC structures with real-time polarisation curves as the boundary condition. Their results showed that there exists a wide variation of real-time polarisation curves on identical specimens which were subjected to uniform corrosion. The variation may be ascribed to the heterogeneity of concrete and the micro difference of the steel surface states, so their numerical modelling used the polarisation curves obtained by fitting the measured data with the Butler-Volmer Equation. Qiao et al. (2016) and Qiao et al. (2017) measured real-time polarisation curves of rebars which were subjected to uniform corrosion, and then they used them to represent the rebar state in their numerical modelling, in which the rebars were subjected to macrocell corrosion.

In conclusion, the measurement results of real-time polarisation curves of steel bars in concrete, for the rebar either undergoing macrocell or microcell corrosion, both present a great scattering. As a result, the application of real-time polarisation curves in CP numerical modelling will superimpose the deviation and bring in significant error in the numerical research results.

5.5 Selection of the Polarisation Model

In order to optimise the CP numerical modelling for RC structures, in regard to the selection of the appropriate boundary conditions to describe the electrochemical reactions occurring at steel-concrete interface under CP process, real-time polarisation curve is ruled out, due to its measuring results that are divergent so that it is very difficult to determine the accurate expression.

In this study, the steel dynamic polarisation state will be described by fitting the Butler-Volmer Equation based polarisation curve with CP experimental data (Oleiwi, 2018), to investigate the variation of Tafel slopes for RC of different chloride contents and then characterise their change trend under the CP process. A new Butler-Volmer Equation based characterisation model, which considers the dynamic Tafel slopes is to be proposed, this improved polarisation model can be used to describe the variation of rebar corrosion state under different chloride contents and applied CP current densities.

5.6 A New Butler-Volmer Equation based Polarisation Characterisation on Experiments

5.6.1 Background of the Experimental Data Used

An experimental study for RC rebar polarisation under applied CP currents has been carried out at the University of Salford (Oleiwi, 2018). The study investigated the effect of CP on the RC specimens subjected to different chloride conditions under an atmospheric environment. The specimen configuration is presented in Figure 5.1. The experimental study measured the

actual total and free chloride contents in the concrete at different added chloride contents after wet curing, and all the parameter values related to the CP experimental specimens are listed in Table 5.1. The relation between the total and free chloride concentration has been plotted in Figure 5.2.



Figure 5.1 Configuration of CP experimental specimen (Oleiwi, 2018).

Table 5.1 Specimen composition for rebar polarisation test.

Parameter	Value
Cement content	390 kg/m ³
Water/cement ratio (w/c)	0.4
Added NaCl content (by cement mass)	0, 1, 2, 3.5 and 5%
Free chloride content (by cement mass)	0, 0.666, 1.056, 1.872 and 2.747%
Steel bar diameter (Φ)	10mm
Carbon fibre sheet (specific area weight)	375g/m ²

Figure 5.2 shows a linear relationship between the actual total and free chloride contents with increasing added NaCl contents. Since only free chloride ions can induce the steel corrosion, the numerical model in this study is to use the free chloride concentration (mol/m³) in the concrete pore solution, in relation to the electrochemical properties of RC structure such as the rebar polarisation.

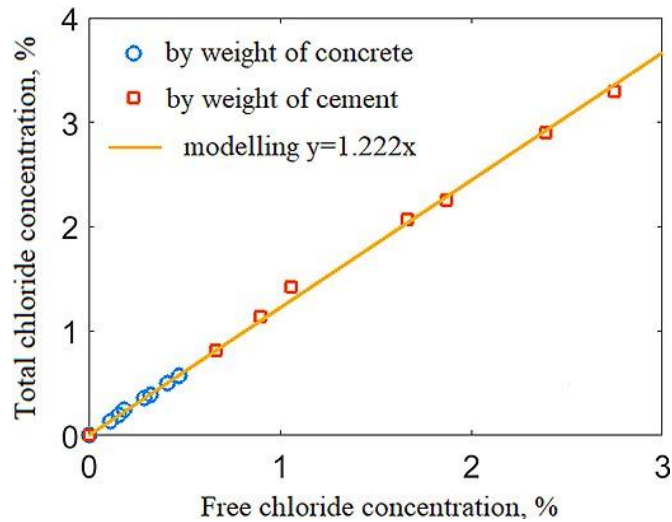


Figure 5.2 Relation of total and free chloride concentration under different NaCl contents.

5.6.2 Steel Polarisation under Cathodic Protection

- **Mechanism of Steel Polarisation**

When a CP is applied to RC structures, the impressed protection current flows into the reinforcing steel, the steel potential will be shifted artificially to a more negative value and the steel anodic polarisation and corrosion rate will be reduced. In addition, CP current has the long-term effects on the removal of chloride content and the increase of alkalinity (increase of pH value) in the region around the rebar, which can further decrease the corrosion rate and helps steel repassivation.

Both the steel potential shift (polarisation) and the long-term effects of CP protection current play the critical roles in CP efficiency. The polarisation degree of steel potential is closely related to the steel polarisation resistance (R_p), the transition resistance at the steel-concrete interface, which can be defined as the steel resistance to oxidation under the application of an external potential, it is quantified using the Equation (5.3):

$$R_p = \frac{\Delta E}{\Delta i_{(\Delta E \rightarrow 0)}} \quad (5.3)$$

where ΔE is the variation of impressed potential (V) around the steel corrosion potential, Δi is the resulting current density (A/m^2). The higher the steel polarisation resistance the larger the steel corrosion resistance and vice versa. Therefore, the relationship between the steel

polarisation resistance and the corresponding corrosion current density can be expressed by the Stern-Geary Equation (Pradhan, 2014):

$$R_p = \frac{B}{i_{corr}} = \frac{1}{2.3} \cdot \frac{b_a b_c}{b_a + b_c} \cdot \left(\frac{1}{i_{corr}} \right) \quad (5.4)$$

where B is the Stern-Geary constant in connection with the Tafel slopes. As shown in Equation (5.4) the steel polarisation resistance is inversely proportional to the steel corrosion rate, thus it can be concluded that the polarisation resistance of passive steel bar is greater than the corroded steel bar due to the corrosion rate of the passive steel bar being smaller, as a result, the polarisation degree of passive steel bar will be larger than the corroded steel bar under the same applied CP current.

- **Steel Polarisation Behaviour**

Figure 5.3 shows that when the protection current is impressed on the steel bar embedded in concrete, an immediate polarisation (potential shift) from the initial steel corrosion potential (E_{corr}) to a more negative value can be observed, and then the steel polarisation will increase continually at a slowed speed with the time until the steel potential finally reaches a stable potential, which is also called on potential.

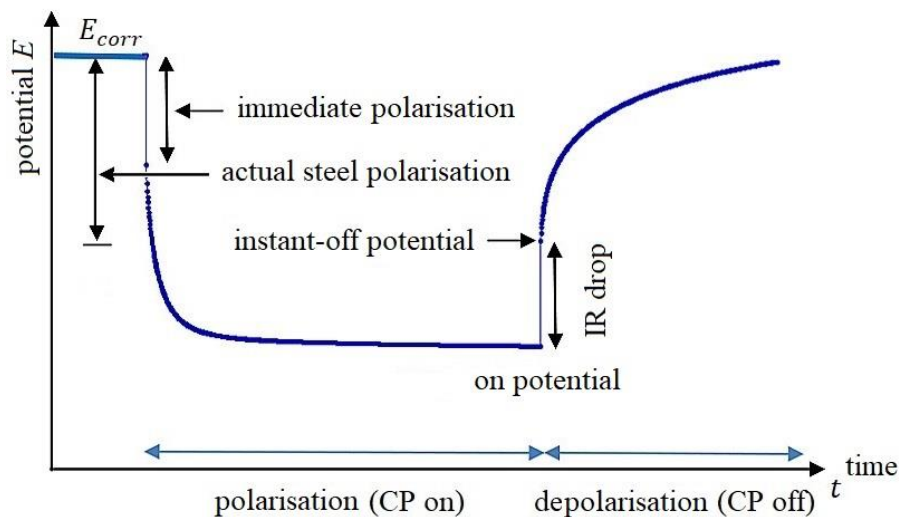


Figure 5.3 Variation trend of steel potential under CP application (Olewi, 2018).

Under the CP process, the actual steel polarisation is the potential difference between the initial corrosion potential and the instant-off potential. The instant-off potential is the actual

steel polarised potential which has eliminated the effect of IR drop. For example, the voltage drop inside the bulk concrete, induced by the applied current and the concrete resistance. Therefore, only the actual steel polarisation is directly related to the rebar corrosion state and the efficiency of CP applied on RC structures.

5.6.3 Characterisation of Steel Polarisation under Cathodic Protection

This study used the CP experimental data by Oleiwi (2018) to characterise the dynamic polarisation state at the steel-concrete interface for the concretes of different chloride contents under CP process, which has been given five sets of applied protection current densities, they are 5, 10, 15, 20 and 25 mA/m², respectively, in terms of the total surface area of reinforcing steel bars.

- **Plotting of Steel Polarisation State**

Figure 5.4 shows the actual rebar polarisation under the five different applied CP current densities for concrete of different chloride contents (free chloride content by cement mass). For experimental data, we use the Butler-Volmer Equation based polarisation curve (Equation 5.2) to fit them in each case, where Tafel slopes (b_a, b_c) were taken as two fitting parameters, corrosion rate (i_{corr}) and corrosion potential (E_{corr}) were the measured data by Oleiwi (2018). The curves are the fitting results using the MATLAB curve fitting tool.

It can be seen that the Butler-Volmer Equation based fitting curves have shown a good agreement with each set of experimental data, and the actual rebar polarisation increases with increasing CP current density.

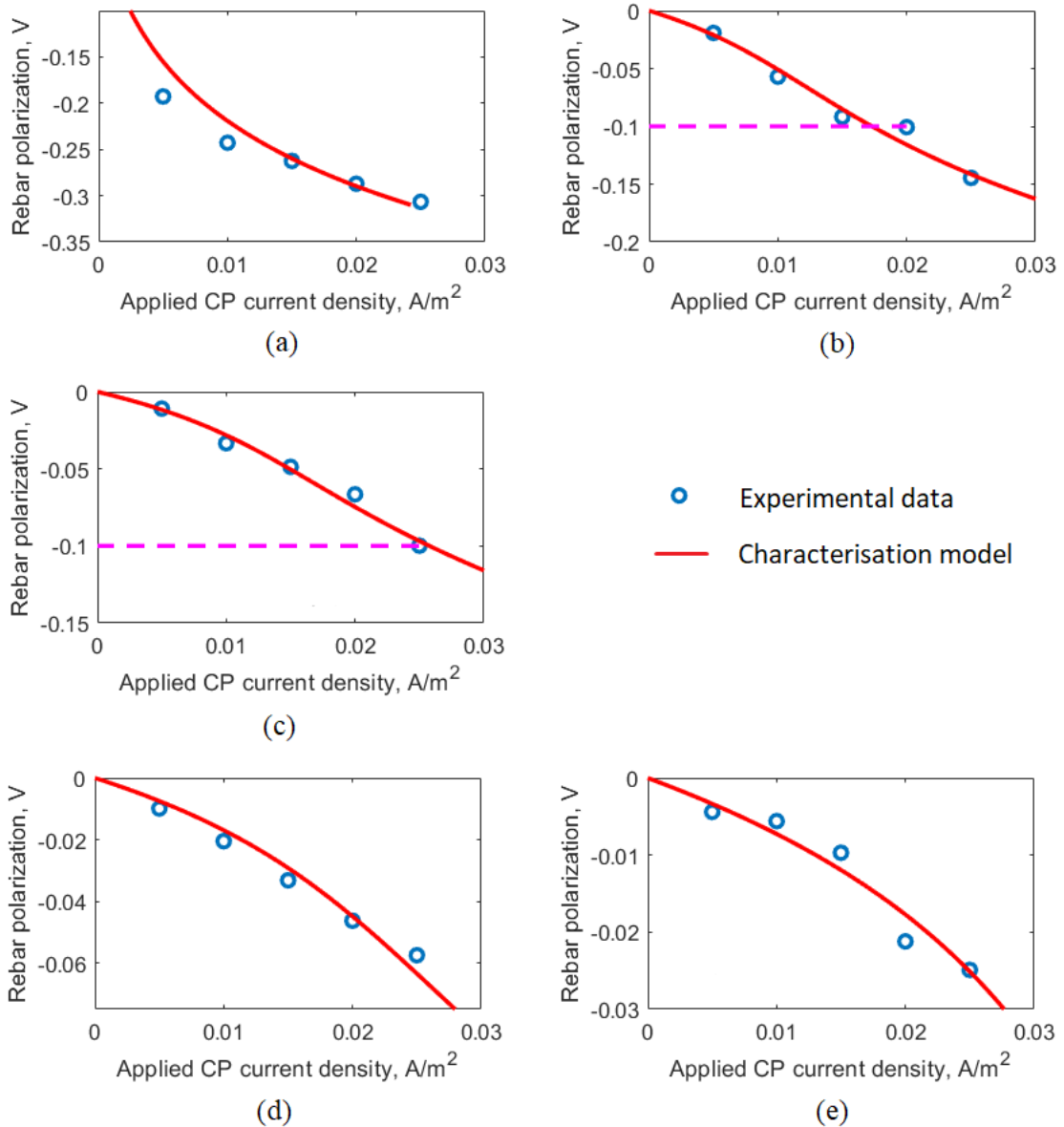


Figure 5.4 Rebar polarisation versus applied CP current density at different chloride contents. (a) Free chloride: 0%, (b) Free chloride: 0.666%, (c) Free chloride: 1.056%, (d) Free chloride: 1.872%, (e) Free chloride: 2.747%.

Firstly, Figure 5.4 shows that the rebar polarisation decreases with increasing chloride contents. For instance, when there is no chloride added to concrete and the rebar is supposed to be in passive state (which has been confirmed by the measured corrosion rate of 1.59 mA/m^2 is lower than 2 mA/m^2), the rebar polarisation attains 262.4 mV under the CP current density of 15 mA/m^2 ; in contrast, when the free chloride content increases to 1.872% by cement mass, the rebar polarisation of only 33.2 mV can be observed under the same CP current density.

Secondly, in terms of the CP design and operation standards for RC structure (BS EN ISO, 2016), the depolarisation of 100 mV or more under a certain amount of time is taken as the protection criterion. Figure 5.4 shows that for rebar under passive condition (0% free chloride), only the CP current density of 2.5 mA/m^2 can provide the required 100 mV polarisation, whilst for the concrete of free chloride content of 0.666%, 1.056% by cement mass, the minimum required CP current density is 18 mA/m^2 , 25 mA/m^2 , respectively. When the free chloride content increases to 2.747% by cement mass, the minimum required CP current density is even larger than 30 mA/m^2 .

In conclusion, under a certain amount of chloride content, the polarisation degree of rebar increases with the applied CP current density. Under a particular CP current density the polarisation degree of rebar reduces with the increasing chloride contents, and the polarisation degree of passive rebar is much higher than that of corroded rebar. Therefore, for the practical application of CP to RC structures, the higher the rebar corrosion rate the higher the CP current density required to achieve the protection purpose.

- **Variation of Tafel Slopes under Different Chloride Contents**

According to the electrochemical mechanism of steel corrosion in concrete, steel corrosion rate increases with chloride content at the steel-concrete interface, combined with the inverse relation between steel polarisation resistance and corrosion rate shown in Equation (5.4), it can be concluded that polarisation resistance of passive steel bar is greater than that of the corroded bar. When apply CP to a corroding RC structure, steel bar will experience the active/passive transition process, which will transform from corroding state to passive state. In other words, steel polarisation resistance will gradually change from small to large under CP process.

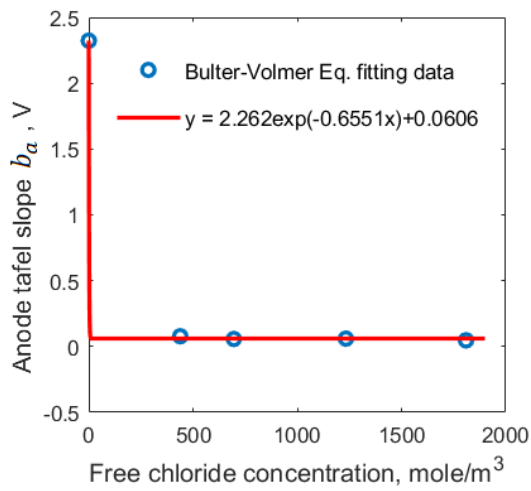
For Tafel Equations of Equations (2.24) and (2.26), in which Tafel slope represents the slope of the polarisation curve of anodic or cathodic reaction (polarisation versus the logarithm of current density). Based on Equation (5.3) it can be seen that steel polarisation is directly affected by steel polarisation resistance, as a result, change in steel polarisation resistance under CP will indirectly influence Tafel slope. That is to say, the values of Tafel slope can indirectly reflect the steel polarisation state, and there is a relation between Tafel slopes and chloride content can be expected. By analysing two fitting parameters, anodic and cathodic

Tafel slopes (b_a , b_c) of the Butler-Volmer Equation (Equation 5.2) seen in the Figure 5.5, are observed to be related to electrolyte conditions, which mainly depend on chloride contents.

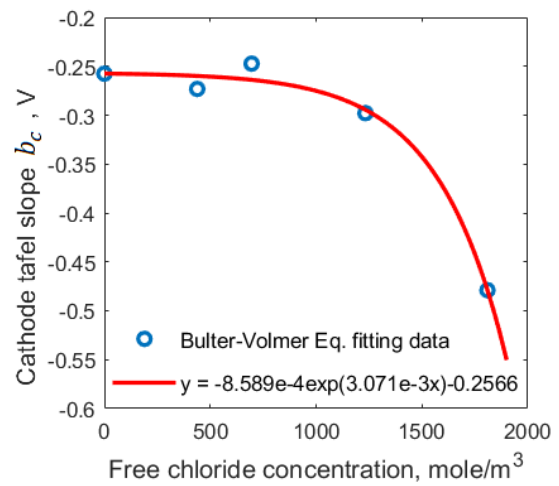
Figure 5.5 shows the obtained Tafel slopes (b_a , b_c) for the fitting curves in Figure 5.4 at different chloride contents, for which the exponential function has presented a good characterisation. It can be seen that two exponential functions have shown a good agreement with the two parameters, b_a and b_c , respectively. Looking at the variation of the anodic Tafel slope (b_a), when there is no chloride content in concrete, it is very large, a situation meaning that the steel corrosion rate is very small, this fact matches the polarisation curve of the passive steel bar observed in experimentation as shown in Figure (5.6). When the free chloride concentration increases the anodic Tafel slope sharply plunges to about 60 mV and remains constant thereafter regardless of further increases in chloride content. These values of anodic Tafel slope are consistent with the research from Ge and Isgor (2007).

Figure 5.5(b) shows that the cathodic Tafel slope (b_c) increases with increasing free chloride concentration in an exponential form, in which it varies in a range of 250mV when the chloride concentration is small. The values of cathodic Tafel slope are slightly higher than the previously proposed range of 120-230mV (Hassanein et al., 2002; Ge and Isgor, 2007). The difference can be explained by the fact that the added excess chloride content in this study results in a higher steel corrosion rate, which then further accelerated the oxygen consumption at the steel surface, and eventually led to the oxygen reduction reaction under the combined effect of the activation and concentration controlled kinetics, this resulted in a high cathodic Tafel slope, this is in accordance with the phenomenon shown in Figure (2.23).

In summary, the exponential form function can well reflect the variation of anodic and cathodic Tafel slopes (b_a , b_c) under different chloride contents.



(a)



(b)

Figure 5.5 Variation of anodic and cathodic Tafel slopes at different chloride contents (in term of molar concentration converted by free chloride content by cement mass).

(a) Anode Tafel slope (b_a), (b) Cathodic Tafel slope (b_c).

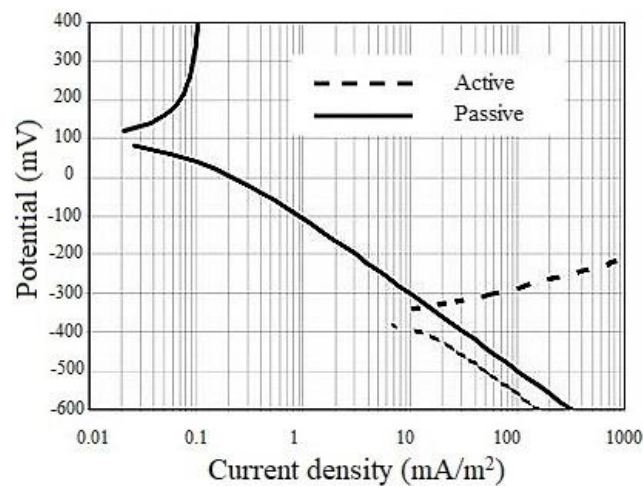


Figure 5.6 Polarisation curves of active and passive steel bars (Redaelli et al., 2006)

- **Steel Corrosion State versus CP Current Density**

Based on the Butler-Volmer Equation (5.2), the coupling effect of anodic reaction rate (rebar corrosion rate) and cathodic reaction rate is balanced by the applied CP current density. Under a fixed applied electric potential, in terms of the obtained variable Tafel slope data under different chloride contents, the corresponding relation between the applied CP current density (expressed by Equation 5.2) and rebar corrosion state (expressed by the first term in Equation 5.2) can be plotted out, as shown in Figure 5.7.

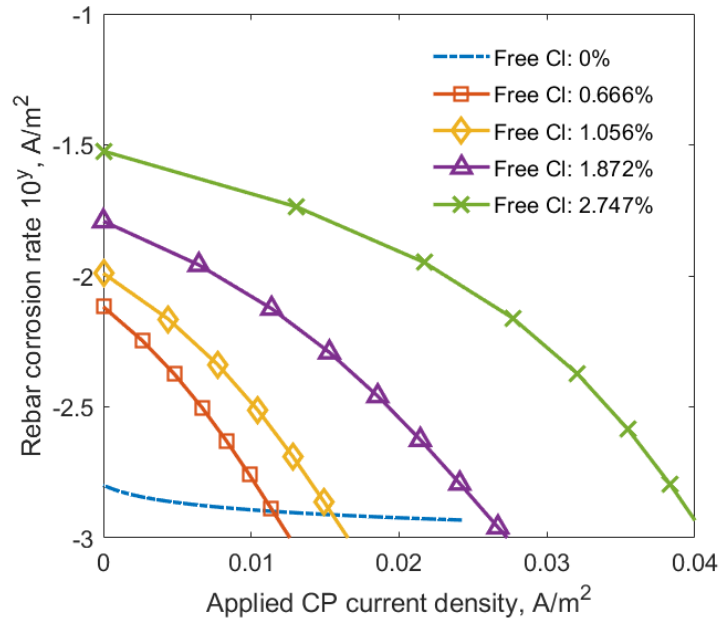


Figure 5.7 Relation between rebar corrosion state and applied CP current densities under different chloride contents (by cement mass).

From Figure 5.7, it can be seen that the higher the free chloride contents the higher the rebar corrosion rate. Meanwhile, all the rebar corrosion rate decreases gradually with the increasing applied CP current density. When there is no chloride contamination (0% chloride), no matter the different values of the applied CP current density, the rebar corrosion rate stays around a low value about 1.5mA/m^2 due to the rebar being in a passive state. For this reason, the corrosion rate of the passive rebar can be regarded as a baseline, and when the rebar corrosion rates are below this specific value (into the region below the dash line), for all the other curves, the corroded rebar can be considered as being protected (repassivation), and the corresponding CP current density is the minimum requirement for steel protection. It also can be seen from the Figure 5.7 that the higher the steel corrosion rate the higher the protection current density is required.

- **A Corrosion Model of Rebar in Chloride Contaminated Concrete under CP**

To characterise the relationship between the steel corrosion rate and the impressed CP current density for the chloride contaminated concrete, a simple linear function ($y = ax + b$) was adopted to represent the curve shown in Figure 5.7.

Figure 5.8 shows the fitting results, where a and b are fitting parameters when used the linear function to fit each curve.

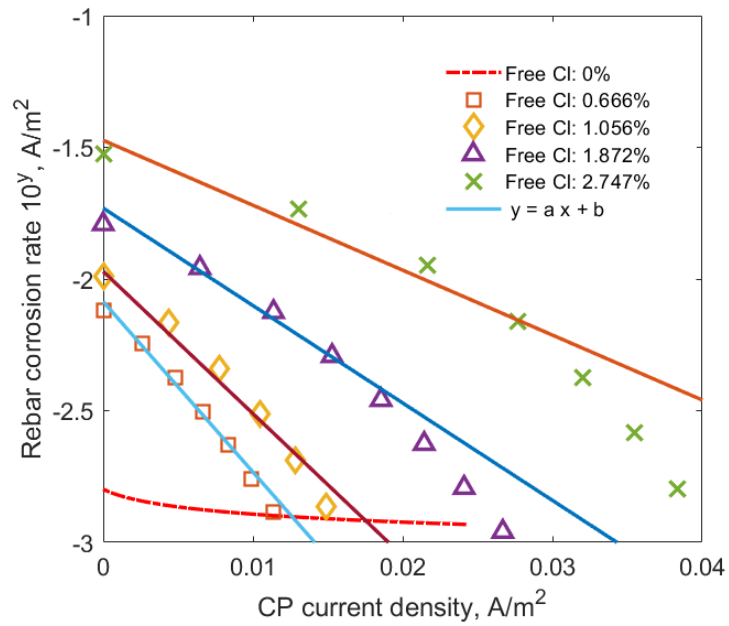


Figure 5.8 Relation between rebar corrosion state and its fitting curve under different CP current densities and chloride contents (by cement mass).

Figure 5.9 shows the variation of the slope (a) and intercept (b) of the linear equation for these curves of different chloride contents. It can be seen that Equations (5.5) and (5.6) have shown a good agreement with the variation of a and b at different chloride contents.

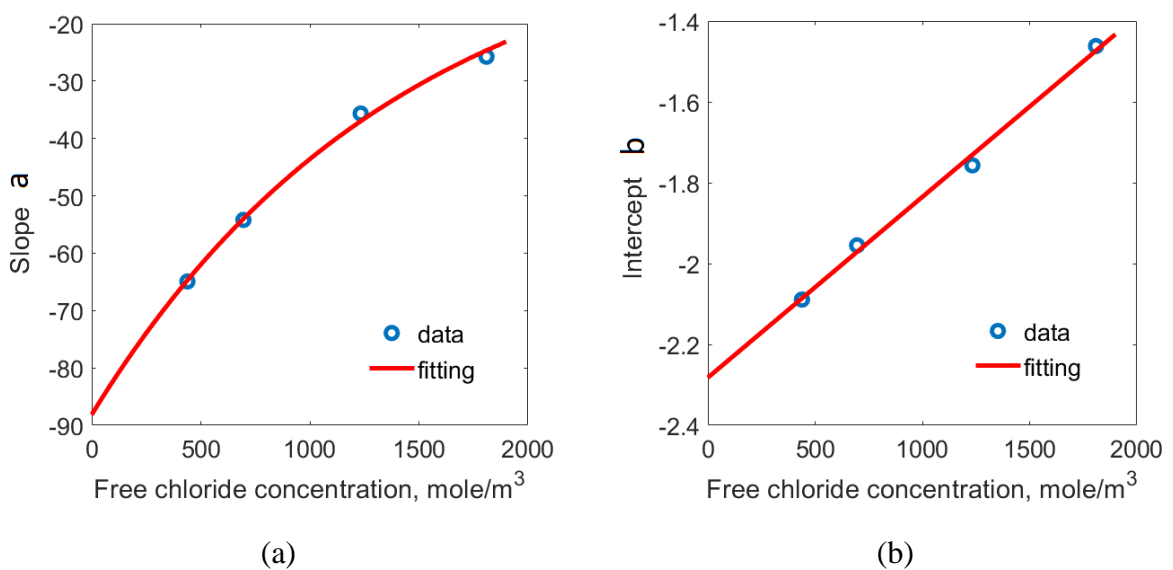


Figure 5.9 Variation of slope and intercept value under different chloride contents.

(a) Slope (a), (b) Intercept (b).

$$a = -88.15 \exp(-0.0007041 C_{Cl}) \quad (5.5)$$

$$b = 0.0004469 C_{Cl} - 2.282 \quad (5.6)$$

where a and b are the slope and intercept of the linear Equation.

At last, substituting the characterised a and b into the linear formula, a model for the relationship between the steel corrosion rate and the concrete chloride contents and the implemented CP current density is obtained:

$$\log_{10} i_{corr} = [-88.15 \exp(-0.0007041 C_{Cl})] i_{app} + 0.0004469 C_{Cl} - 2.282 \quad (5.7)$$

5.7 Conclusions

As it can be seen from Figure 5.8, the proposed linear polarisation model (Equation 5.7) has shown a good agreement with the rebar corrosion state especially for the cases when chloride contents are small. However, the goodness deteriorates when concrete chloride content increases, these curves shift to the upper right corner.

The deterioration can be explained by the following reasons. Due to the concrete with the nature of the spatially non-homogeneous property and the internal varying microenvironment, under the high chloride content environment, the rebar corrosion state is very complex and may be subjected to serious uniform corrosion, in addition, a greater possibility is that the rebar is subjected to severe macrocell corrosion, all the unknown macrocell corrosion area and corrosion current size lead to an unpredictable rebar corrosion state. Besides, the higher chloride contents are impossible to reach in real chloride contaminated RC structures exposed to atmospheric environment. Also, for the possible range of chloride content, the proposed linear polarisation model has showed a good degree of matching with the rebar corrosion state.

Furthermore, as it can be seen from Figure 5.8, under the same chloride content, the proposed linear polarisation model requires more CP current density to achieve the protection (rebar corrosion rate drops to the predefined baseline) than the curve of actual rebar corrosion state, which means that this proposed model is more conservative and reliable.

In conclusion, the Butler-Volmer Equation based linear polarisation model can well reflect the steel polarisation state under different chloride contents and applied current densities. The proposed polarisation model will be applied to CP numerical modelling research for RC structures in the following chapter.

CHAPTER 6

MODELLING OF CATHODIC PROTECTION FOR CHLORIDE CONTAMINATED REINFORCED CONCRETE STRUCTURES

6.1 Introduction

In the past decade, numerical simulation based on the FEM as a convenient and economical tool to help understand the underlying electrochemical mechanisms of CP applied to RC structures, has been extensively used to investigate the effects of various influencing factors on CP performance and evaluating the efficiency of CP application (Hassanein et al., 2002; Polder et al. , 2008; Bruns and Raupach, 2010; Helm and Raupach, 2016). In order to promote the development of CP techniques for RC structures, it is desirable to develop and improve CP numerical modelling and simulation from a theoretical basis of the electrochemical mechanism.

As reviewed in Chapter 3, most of the current research on CP numerical modelling for RC structures, had considered the concrete electrical resistivity as a constant in the model, leading to the use of Laplace Equation and associated inaccurate numerical results. Most of these works also had not taken into account the long-term beneficial effects of CP current and ignored the variability of steel polarisation state under the CP process, resulting in the conservative simulated results and poor economic benefits. Some numerical studies did not combine the ionic behaviour in concrete pore solution and the applied electric field effect in the simulation, so the results could not show the specific steel corrosion state, instead, in general, they used the resulting potential of the steel-concrete interface to indirectly reflect the CP efficiency.

This chapter presents the CP numerical modelling of chloride contaminated RC structures using the proposed mathematical models described in the Chapters 4 and 5, and considers the

coupling effect between the ionic behaviour and the electric field effect. Thereafter, the simulated results were compared with the corresponding CP experimental data and then a parameter study was carried out. All these numerical calculations were conducted using software, COMSOL Multiphysics, a FEM numerical simulation package.

6.2 Numerical Modelling Setup

6.2.1 Model Description

- **Background of Experiment**

An experimental study was conducted to investigate the CP effect on chloride contaminated RC specimens under atmospheric environment at the University of Salford (Oleiwi, 2018). The CP experimental specimen consists of three rebars and an embedded carbon fibre (CF) sheet shown in Figure 6.1. Different chloride contents were added into the concrete by dissolving (NaCl) salt in the mix water at casting time to create different corrosion environments for the rebars. Experimental specimens were placed in the water containing the same chloride concentration with the mixing water for curing.



Figure 6.1 Configuration of CP experimental specimen (Oleiwi, 2018).

In the CP experiment, ten different current densities were applied to the rebars of each specimen, they are 5, 10, 15, 20, 25, 35, 45, 55, 65, and 75mA/m², in terms of the total surface area of rebars; each test applied a certain CP current density for 24 hours. All the parameter values related to the CP specimen are listed in Table 6.1.

Table 6.1 Specimen composition for CP test (Oleiwi, 2018).

Parameter	Value
Cement content	390 kg/m ³
Water/cement ratio (w/c)	0.4
Added NaCl (by cement mass)	0, 1, 2, 3.5 and 5%
Steel bar diameter (Φ)	10mm
CF sheet (specific area weight)	375g/m ²

- **Model Geometry and Material Properties**

A two-dimensional FE model was set up, which describes a rectangular concrete specimen with three embedded steel bars (cathode) and a CF sheet (anode), as illustrated in Figure 6.2. The specimen height and width were 150mm and 90mm, respectively, the steel bars diameter was 10mm, corresponding to the concrete cover of 20mm. The numerical model represented a chloride contaminated RC specimen, there were five different initial chloride ion concentrations (in terms of free chloride ion concentration, converted by chloride content by cement mass) considered in the CP simulation, they are 0, 439, 696, 1233, and 1809mol/m³, respectively, and the initial concentrations of chloride ions were assumed to be uniform in the model.

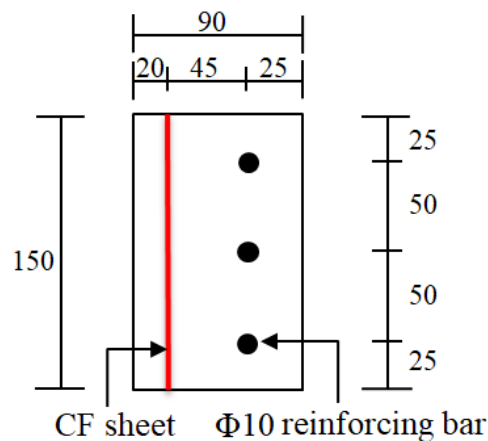


Figure 6.2 Model geometry (dimensions in mm).

In the study, the proposed new Butler-Volmer Equation based steel polarisation model, which is related to the steel corrosion rate was adopted as the boundary condition in the model, based on the new boundary condition the production history of ferrous ions through the

simulated results can be directly track. Therefore, in the modelling, in addition to the major ionic chemical species observed in the pore solution of chloride contaminated concrete, which are hydroxyl (OH^-), sodium (Na^+), potassium (K^+) and chloride (Cl^-) ions, ferrous (Fe^{2+}) ions will also be considered. Due to the fact that the ferrous ions in the chloride contaminated RC structure are only accumulated at the corroding steel-concrete interface not inside concrete before the CP energisation, hence, there are no initial ferrous ions in the bulk concrete, but an initial value of ferrous ions is set at the steel-concrete interface region. In the process of numerical simulation, the hydroxyl ion concentration is determined in terms of the electric neutrality.

For the electrochemical mechanism of steel corrosion in concrete, the increasing chloride ion concentration will accelerate the steel corrosion rate, the correspondingly ferrous ion concentration in concrete pore solution will also increase. However, the ferrous ion solubility in the concrete pore solution is fixed, as reviewed in Chapter 2, when the ferrous ion concentration exceeds its solubility, the extra ferrous ions will be oxidised to the ferric ions (in the form of ions or/and rust) in pore solution.

Equation (6.1) for the oxidation from ferrous ions to ferric ions (Stumm and Morgan, 1996) under alkaline conditions was adopted in the numerical model together with the Butler-Volmer Equation based steel corrosion characterisation to define the boundary condition of the ferrous ions at the steel-concrete interface.

$$\frac{-dC_{Fe^{2+}}}{dt} = k \cdot p_{O_2} \cdot (C_{Fe^{2+}}) \cdot (C_{OH^-})^2 \quad (6.1)$$

where $C_{Fe^{2+}}$ and C_{OH^-} are the ferrous and hydroxyl ion concentration (mol/m^3) in concrete pore solution respectively, k is the rate constant of ferrous ion oxidation in concrete pore solution and can be obtained from Figure 6.3, p_{O_2} is the partial pressure of oxygen (bar). Tables 6.2 gives the initial data of all ionic species and their diffusion coefficients used in the simulation. Table 6.3 lists the other parameters adopted.

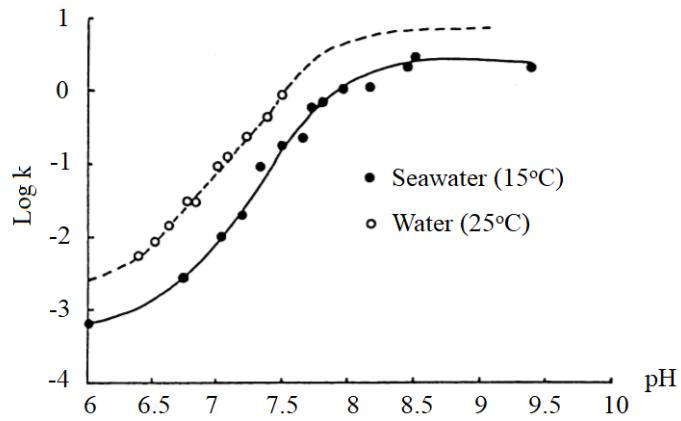


Figure 6.3 Rate constants for oxidation of ferrous ions in different aqueous solutions as a function of pH (Morgan and Lahav, 2007).

Table 6.2 Initial ionic concentrations and diffusion coefficients
(Buffle et al., 2007; Chang et al., 2018).

Parameters	Cl^-	Na^+	OH^-	K^+	Fe^{2+}
C_{i_ini} (mol/m ³)	* Cl^-	* $Cl^- + 160$	550	390	50
D_i (m ² /s)	2.03e-9	1.334e-9	5.27e-9	1.957e-9	7.19e-10

*Note: Cl^- is set to different values in the simulation study, Na^+ initial concentration varies with Cl^- (according to the NaCl adding method)

Table 6.3 Model input parameters

(Morgan and Lahav, 2007; Wang and Li, 2000; Oleiwi, 2018; Jiang and Yuan, 2013).

Parameter	Value
Pore saturation degree (S_w)	0.6
Tortuosity coefficient (τ)	10
Chloride bound coefficient	0.222
Concrete porosity (ϑ)	0.167
Rate constant of ferrous ions oxidation (k)	1.995
Partial pressure of oxygen (p_{O_2})	0.2 (bar)
Model run time (t)	24 (hours)

6.2.2 Electric Field Distribution in Concrete

The concrete is a heterogeneous electrolyte with porous property, to model the transportation behaviour of different species of ions in chloride contaminated concrete pore solution, Equations (3.6) and (3.8) were modified by taking into account the influence of porosity and tortuosity of the pore network and the binding effect (chemically and physically) between the chloride ions and pore wall in the cement matrix (Wang and Li, 2000) as the following forms:

$$\tau^2 \vartheta S_w \frac{\partial(C_i + S_i)}{\partial t} = \nabla \left[z_i D_i \left(\frac{F}{RT} \nabla \phi \right) C_i \right] + \nabla(D_i \nabla C_i) \quad (6.2)$$

$$\frac{F}{RT} \nabla \phi = - \left(\frac{\tau i_{ion}}{F \epsilon^{2/3}} + \sum_{i=1}^N z_i D_i \nabla C_i \right) / \sum_{i=1}^N z_i^2 D_i C_i \quad (6.3)$$

where S_i is the concentration (mol/m³) of bound ions, τ is the tortuosity of pore structure, ϵ is the volume fraction of porosity.

Assuming the concrete electrolyte domain is adequately dilute so that the activity of every ionic species is equivalent to its concentration (Liu and Shi, 2012). Under the action of an externally applied electric field, the ionic motion in the electrolyte domain should obey the charge conservation law and Ohm's law, the potential distribution inside concrete can be described by (details shown in Chapter 3):

$$\nabla \cdot \frac{1}{\rho_c} (\nabla \psi) = 0 \quad (6.4)$$

In this study the concrete electrical resistivity (ρ_c) is treated as a variable, its variation is considered to be linked to the chloride and water content in concrete and expressed as (details shown in Chapter 4):

$$\rho_c = \exp(a C_{Cl}^b) \{ f_0 + \rho_0 [\exp(\alpha S_w) + \exp(\beta(1 - S_w))] \} \quad (6.5)$$

where the constants of f_0 , ρ_0 , α , β , a and b which have been determined in Chapter 4 are listed in Table 6.4.

Table 6.4 Constants of concrete electrical resistivity characterisation model

Constant	f_0	ρ_0	α	β	a	b
Value	168.1	1.649e-5	-71.33	21.9	-2.211	3.322

6.2.3 Boundary Condition

- **CF Sheet-Concrete Interface**

The CF sheet-concrete interface in this study was assumed to be non-polarisable, and any aging effects induced by, for example, the generated chloride gas ($2Cl^- \rightarrow Cl_2(\uparrow) + 2e^-$), oxygen gas and hydrogen ions ($2H_2O \rightarrow O_2(\uparrow) + 4H^+ + 4e^-$), or the building up of electrical resistance at the CF sheet-concrete interface had been neglected (Muehlenkamp et al., 2005).

To solve the electric field governing equation (6.4), the CP current density (i_{app}) will be applied on the CF sheet anode.

- **Steel-Concrete Interface**

At the steel-concrete interface, before the CP energisation, the steel corrosion rate ($Fe \rightarrow Fe^{2+} + 2e^-$) is commonly balanced by the oxygen reduction rate ($O_2 + 2H_2O + 4e^- \rightarrow 4OH^-$); after the CP energisation, the decreasing steel corrosion rate is coupled with the increasing oxygen reduction rate and the net current density (the current density difference between steel corrosion rate and oxygen reduction rate) on the steel surface is balanced by the applied CP current density.

In this study we used the proposed new Butler-Volmer Equation based steel polarisation model (Equation 6.6) as the boundary condition at the steel-concrete interface to solve the ionic governing equations (6.2) and (6.3), which is considered to be linked to the chloride content in concrete and the applied current density (details shown in Chapter 5). To solve the electric field governing equation (6.4), the electric potential of steel bar (ϕ_{bar}) is fixed at a constant and acted as the reference potential (Equation 6.7):

$$\log_{10}(i_{corr}) = [a \exp(bC_{Cl})]i_{app} + cC_{Cl} - d \quad (6.6)$$

$$\phi_{bar} = 0 \quad (6.7)$$

where the constants of a , b , c and d which have been determined in Chapter 5 are listed in Table 6.5.

Table 6.5 Constants of steel polarisation characterisation model

Constant	a	b	c	d
Value	-88.15	-7.041e-4	4.469e-4	2.282

- **RC Specimen Boundary**

All the other boundaries were characterised as insulating conditions, both the fluxes of all the ionic species and the electric current were assumed to be zero on all these boundaries of RC specimen.

6.3 Results and Analysis

6.3.1 Ionic Distribution under Cathodic Protection

When CP is applied to chloride contaminated RC structures, all the ionic species dissolved in the concrete pore solution will be redistributed under the externally applied electric field. The ionic distribution of chloride and hydroxyl ions at the steel-concrete interface are the major concern, the chloride content is directly related to the steel corrosion state and the hydroxyl content is closely connected to the steel corrosion protection.

- **Chloride Ion Redistribution in Concrete**

Figures 6.4 and 6.5 show the chloride ion concentration redistribution in concrete with different CP operation times under current densities of 10mA/m^2 and 20mA/m^2 for the RC specimen with 1% NaCl, respectively. Chloride ion concentration redistribution in concrete obtained for the RC specimen with different NaCl contents under different CP operation time for the current densities of 10mA/m^2 and 20mA/m^2 are contained in Appendix A.

It can be seen that the chloride ion concentration presents a significant change in concrete under the different CP operation time, the chloride ions have migrated from the steel bars to the anode under the applied electric field. Chloride ions in the region around rebars have been reduced steadily with the CP operation time and the increase of CP current density. For example, under the current density of 10mA/m^2 , the chloride ion concentrations at the steel-concrete interface are about 436.2mol/m^3 and 432.3mol/m^3 corresponding to the CP operation time of 24 hours and 90 days, respectively. On the other hand, for the same CP operation time of 30 days, the chloride ion concentrations at the steel-concrete interface are about 433mol/m^3 and 427.2mol/m^3 corresponding to the applied current density of 10mA/m^2 and 20mA/m^2 , respectively.

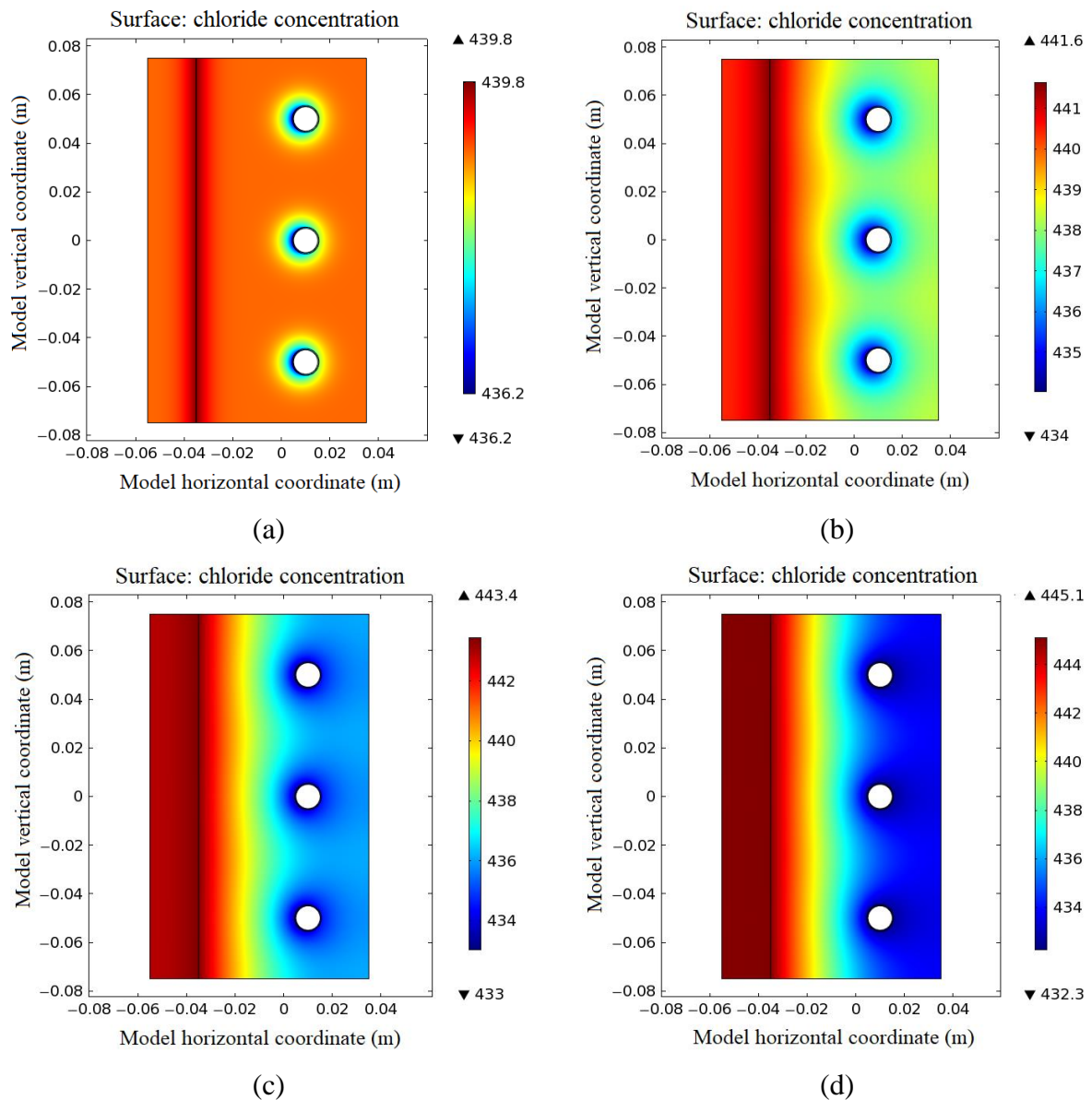


Figure 6.4 Redistribution of chloride ion concentration in concrete under 10mA/m^2 (1% NaCl). (a) $t = 24$ hours, (b) $t = 10$ days, (c) $t = 30$ days, (d) $t = 90$ days.

The results have confirmed the beneficial effects of protection current. Under the CP application, the electric current circulation in concrete can induce the removal of chloride ions at the steel surface. Most importantly, the applied electric field can stop the diffusion of chloride ions from the external environment toward the rebar in concrete, this is the effect known as CP chloride barrier effect (Pedefferri, 1996). In summary, the results have demonstrated that the chloride removal degree depends on the applied CP current density and its operation time.

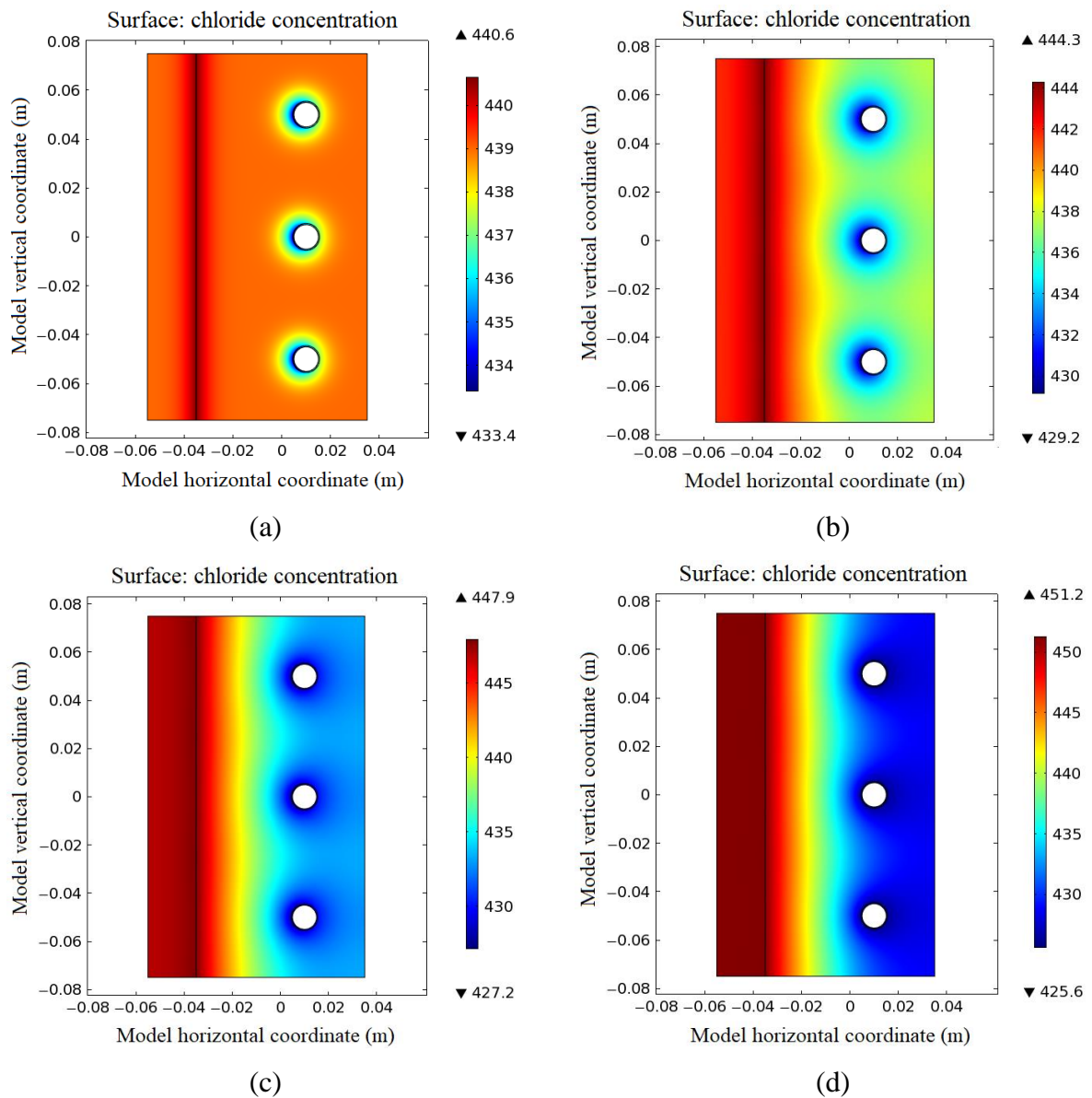


Figure 6.5 Redistribution of chloride ion concentration in concrete under 20mA/m^2 (1% NaCl). (a) $t = 24$ hours, (b) $t = 10$ days, (c) $t = 30$ days, (d) $t = 90$ days.

- **Chloride and Hydroxyl Ions Distribution at Steel-Concrete Interface**

Figures 6.6 and 6.7 show the concentration distribution of chloride and hydroxyl ions at steel-concrete interface with the different CP operation time under the current densities of 25mA/m^2 and 45mA/m^2 for the RC specimen with 1% NaCl, respectively. The chloride and hydroxyl ion concentration distribution at steel-concrete interface obtained for the RC specimen with different NaCl contents under different CP operation time for the current densities of 25mA/m^2 and 45mA/m^2 are contained in Appendix B.

At first, we can observe that the chloride ions at the steel-concrete interface have been redistributed under the applied electric field. In general, the chloride ion concentration decreases with the CP operation time and the increase of current density. However, it also can be seen that the chloride ions along the steel surface is unevenly distributed under the CP process, that directly facing the anode are more easy to be moved while that at the location behind the rebar are reduced in a less degree. As a result, a chloride ion concentration gradient is formed along the circumference of the rebar at the steel-concrete interface which increases with the CP operation time and the increase of protection current density. For example, the ion concentration gradient is 4.5mol/m^3 under the current density of 25mA/m^2 for 24 hours (Figure 6.6a); as the CP operation time enlarged to 10 days under the same current density, the ion concentration gradient increased to 6.2mol/m^3 (Figure 6.6b); as the current density increased from 25mA/m^2 to 45mA/m^2 for 24 hours, the ion concentration gradient increased from 4.5mol/m^3 to 8.4mol/m^3 (Figure 6.7a).

The results indicate non-uniformity of chloride ions removal at the steel-concrete interface under the CP process. The migrating rates of chloride ions at the steel-concrete interface near and remote from the anode are both increased with the CP operation time and current density but at the different speeds. These phenomena can be ascribed to the following reasons: the connectivity, tortuosity and saturation degree of concrete pore network; chloride ions distribution in concrete; uneven distribution of the current intensity of applied electric field. The uneven distribution of chloride ions under CP process should be taken into account in CP design, particularly considering that the pitting corrosion character under chloride attack.

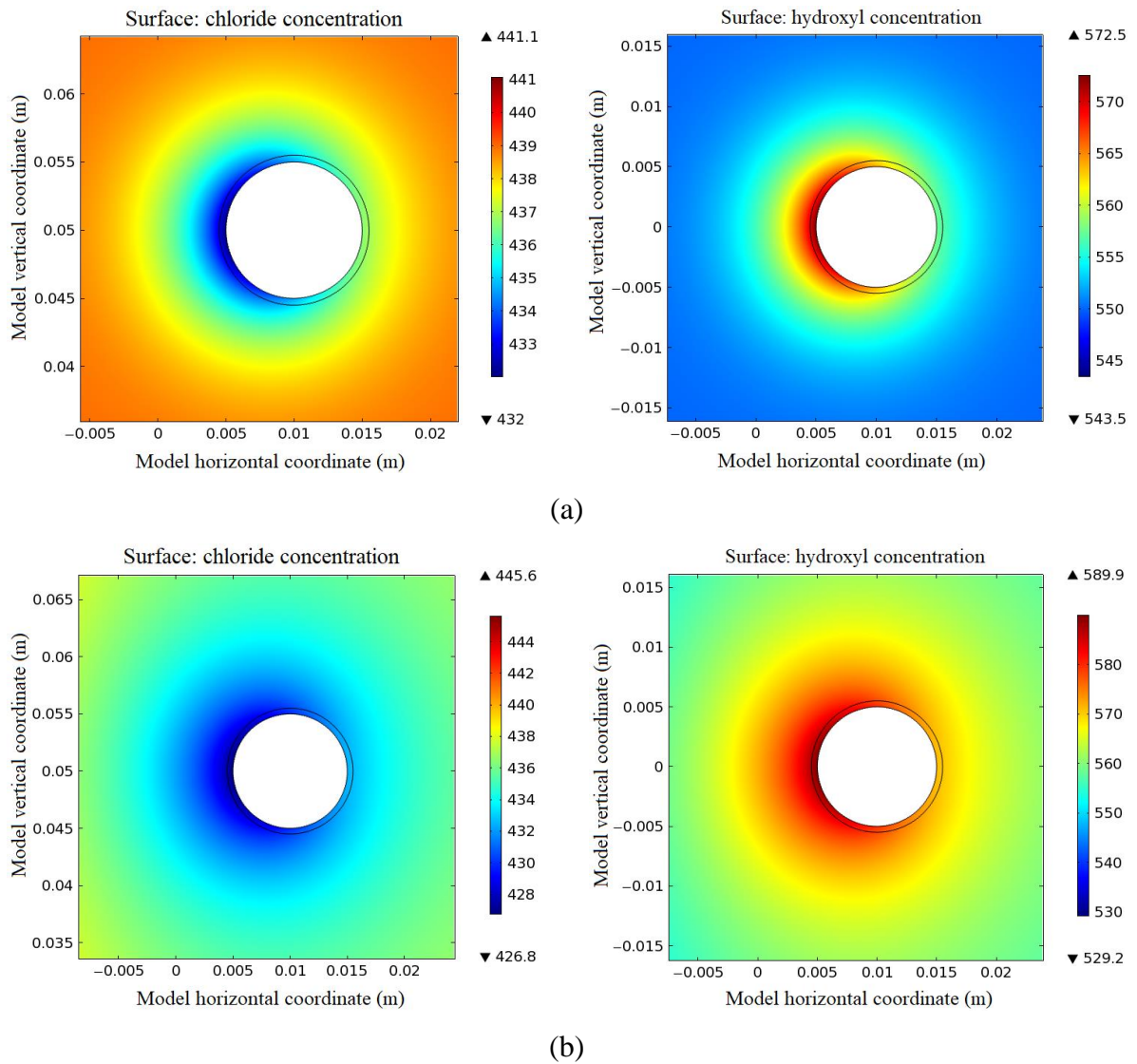


Figure 6.6 Distribution of chloride and hydroxyl ion concentration at steel-concrete interface under 25mA/m^2 (1% NaCl). (a) $t = 24$ hours (b) $t = 10$ days.

Secondly, it can be seen that the hydroxyl ion concentration around steel bar increases with the CP operation time. For instance, under the current density of 25mA/m^2 , the hydroxyl ion concentrations are about 565mol/m^3 and 580mol/m^3 corresponding to the CP running for 24 hours and 10 days, respectively. Comparing Figures 6.6 and 6.7, the growth degree of hydroxyl ion concentration at the steel-concrete interface is enhanced under the higher current density, such as, under the CP operation time of 10 days, the hydroxyl ion concentration increased from 580mol/m^3 to 600mol/m^3 when the applied current density increased from 25mA/m^2 to 45mA/m^2 .

The results represent that, the applied CP current density provides the electrons to accelerate the electrochemical cathodic reaction (oxygen reduction) at the steel-concrete interface to help

increase the alkaline environment around the steel bar, and then promotes the steel repassivation in concrete. In short, the results demonstrate that CP will be able to reinstate the alkaline nature of concrete.

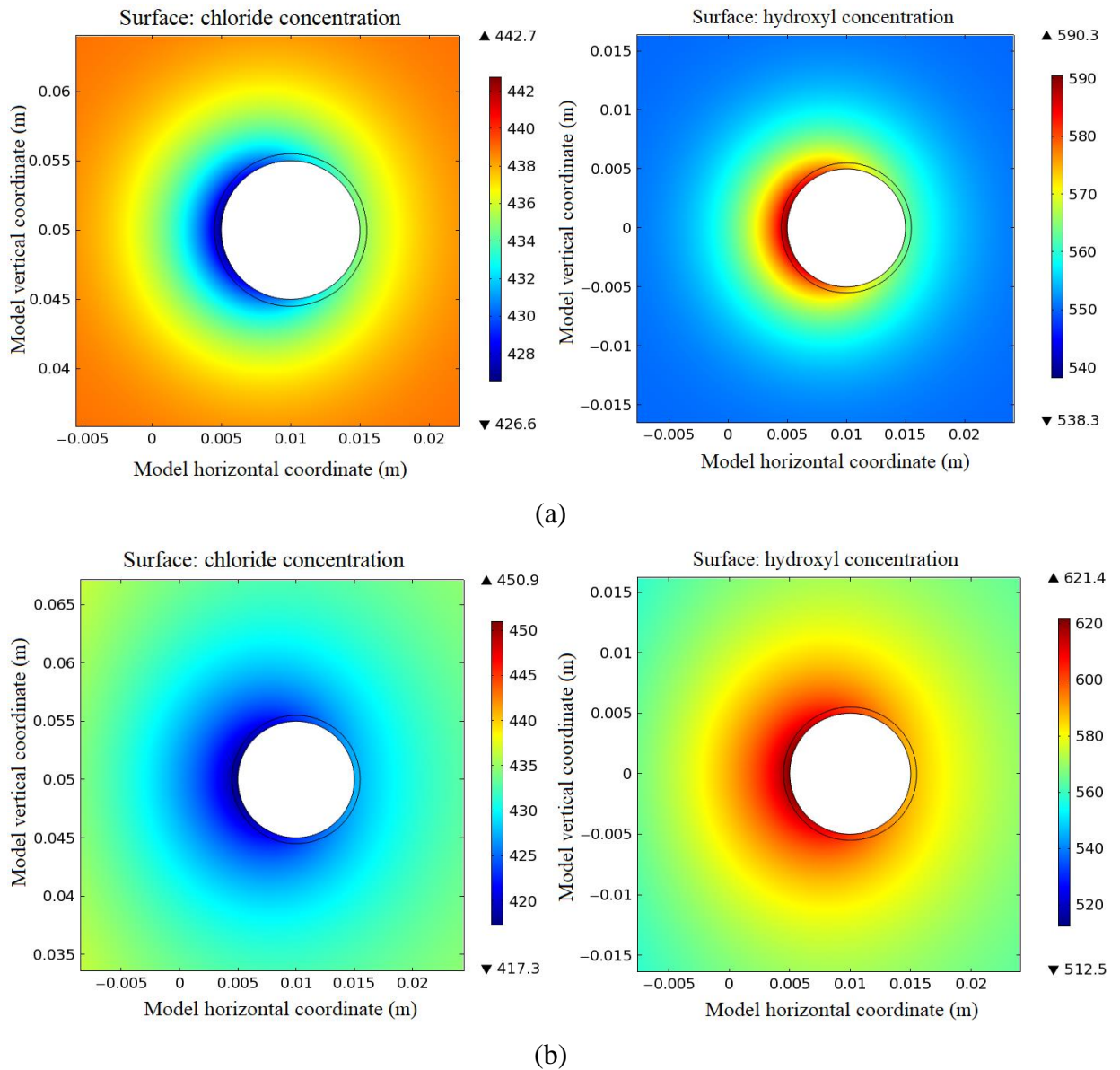


Figure 6.7 Distribution of chloride and hydroxyl ion concentration at steel-concrete interface under 45mA/m^2 (1% NaCl). (a) $t = 24$ hours (b) $t = 10$ days.

6.3.2 Ionic Condition under Cathodic Protection

In view of the chloride ion distribution at the steel-concrete interface in section 6.3.1, it can see that, although the total chloride removal degree depends on the applied CP current density and its operation time, but the chloride ions at the steel-concrete interface remote from the

anode are difficult to remove. Therefore, it is a big interest to quantitatively determine the variation of ionic concentration at the location under different applied CP current densities and operation time.

- **Chloride Ion Concentration at Steel-Concrete Interface under Different Current Densities**

Figure 6.8 shows the variation of chloride ion concentration at the position of the steel-concrete interface remote from the anode at the CP operation time of 90 days, under different CP current densities for the RC specimens with 1, 2, 3.5 and 5% NaCl, respectively.

It can be seen that the chloride ion concentrations of different cases present the different values under each CP current density, which all reduce progressively with the increased applied current density. For example, under the current densities of 5mA/m^2 and 75mA/m^2 , for the case of 1% NaCl, chloride ion concentrations are 436mol/m^3 and 395.2mol/m^3 , the reduction are 3mol/m^3 and 43.8mol/m^3 (compared with the initial chloride ion concentration of 439mol/m^3), respectively; for the case of 5% NaCl, chloride ion concentrations are 1804mol/m^3 and 1725mol/m^3 , the reduction are 5mol/m^3 and 83.8mol/m^3 (compared with the initial chloride ion concentration of 1809mol/m^3), respectively.

The results have displayed that, for the air exposed chloride contaminated RC structure, the chloride ions removal at the steel-concrete interface remote from the anode is a very slow progress under the CP process, even it can be enhanced by increasing the applied current density, however, the effect is not very effective. It can be explained by that the chloride ions removal in concrete is not only related to the intensity of applied current density, but also affected by the concrete pore size distribution, saturation degree of concrete pore water and the external environment (or RH).

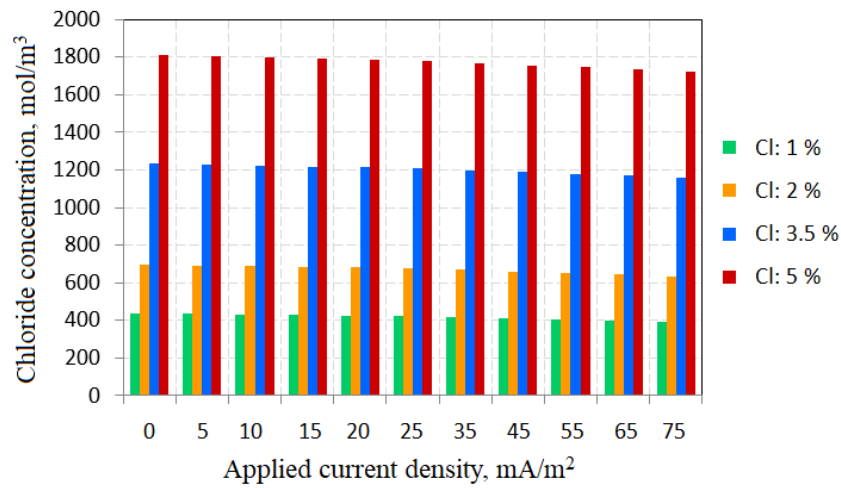


Figure 6.8 Variation of chloride ion concentration at steel-concrete interface remote from the anode under different current densities for CP operation time of 90 days (1, 2, 3.5 and 5% NaCl).

- **Chloride and Hydroxyl Ion Concentration at Steel-Concrete Interface under Different CP Operation Time**

Figures 6.9 and 6.10 show the concentration variation of chloride and hydroxyl ions at the steel-concrete interface with the different CP operation time under the applied current densities of 15mA/m² and 75mA/m² for the RC specimen with 1% NaCl, respectively, in which the chloride ion condition has been considered in two cases, one is at the steel-concrete interface near the anode; the other is at the steel-concrete interface remote from the anode.

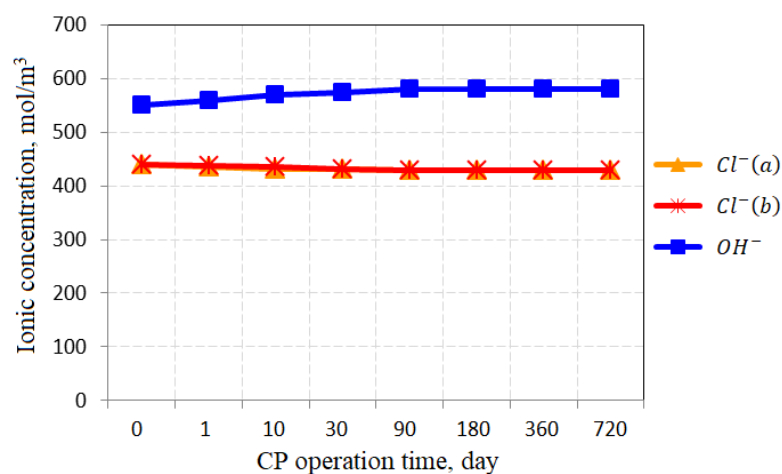


Figure 6.9 Variation of chloride and hydroxyl ion concentrations at steel-concrete interface under different CP operation time at current density of 15mA/m² (1% NaCl).

(a) steel-concrete interface near anode (b) steel-concrete interface remote from anode.

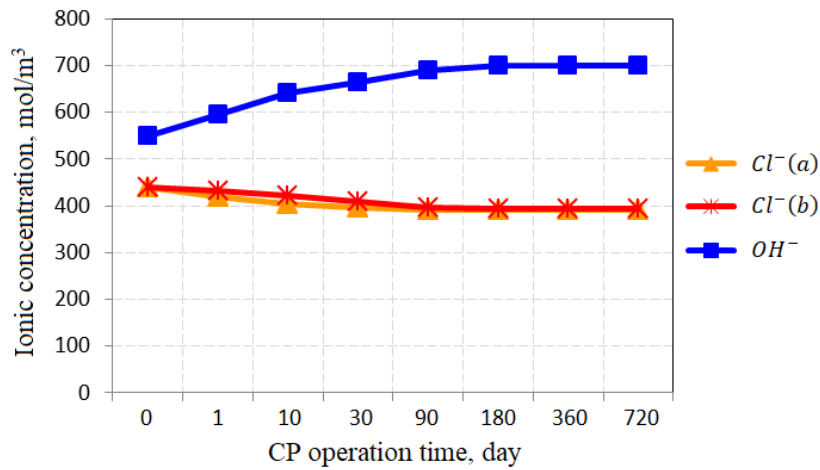


Figure 6.10 Variation of chloride and hydroxyl ion concentrations at steel-concrete interface under different CP operation time at current density of 75mA/m^2 (1% NaCl).
 (a) steel-concrete interface near anode (b) steel-concrete interface remote from anode.

Figure 6.9 shows that, at a low CP current density of 15mA/m^2 , the hydroxyl ion concentration increases slowly with CP operation time. However, the concentration values of chloride ions are very close in the two cases while in both which slightly decreases with the CP operation time.

At the higher current density of 75mA/m^2 (Figure 6.10), the hydroxyl ion concentration gradually increases with the CP operation time in the first 90 days and then remains constant thereafter regardless of increasing time; the two cases of chloride ion concentrations are tapering off with CP operation time in the first 90 days, during this period, those ions concentration at the steel-concrete interface remote from the anode is slightly higher than the ionic concentration at the steel-concrete interface near the anode and the difference decreases with time, 90 days later two cases of chloride ion concentration values become very close and nearly keep constant along with further increasing CP time.

The results demonstrate that both the increase of hydroxyl ion concentration and the decrease of chloride ion concentration at the steel-concrete interface with the applied current density and CP operation time are limited. When the applied current density is relatively high and after a certain amount of CP operation time, the hydroxyl ion concentration will remain at a fixed value, in the meantime, the chloride ion concentration stops reducing and also keeps at a fixed value, forming a dynamic balance between the hydroxyl and chloride ion concentration at the steel-concrete interface. Similar phenomenon also can be observed in Figures 6.11 and 6.12, which considered the RC specimen with 2% NaCl.

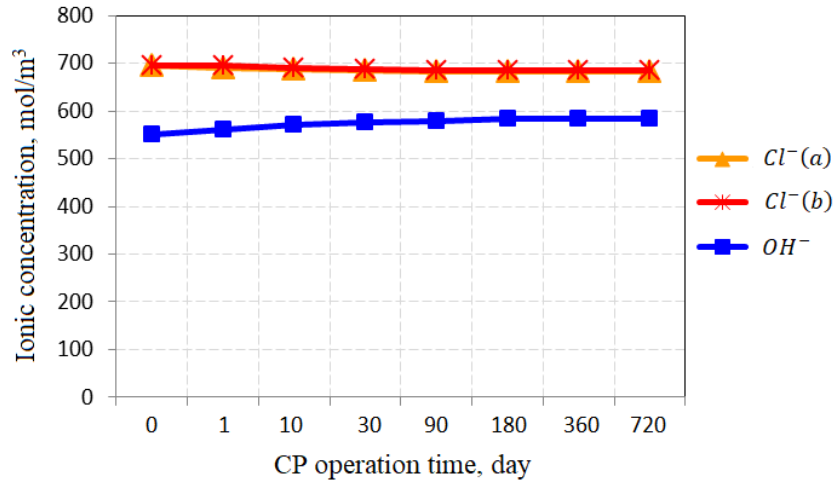


Figure 6.11 Variation of chloride and hydroxyl ion concentrations at steel-concrete interface under different CP operation time at current density of 15mA/m^2 (2% NaCl).

(a) steel-concrete interface near anode (b) steel-concrete interface remote from anode.

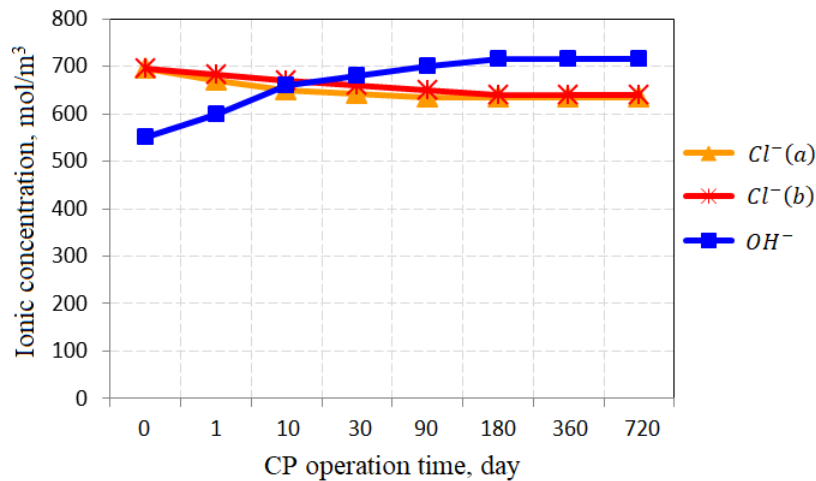


Figure 6.12 Variation of chloride and hydroxyl ion concentrations at steel-concrete interface under different CP operation time at current density of 75mA/m^2 (2% NaCl).

(a) steel-concrete interface near anode (b) steel-concrete interface remote from anode.

The results have clearly indicated the influence of the cathodic reaction under the coupling effect of activation and concentration controlled kinetics. There are a large numbers of electrons provided by the high current density, which will speed up the electrochemical cathodic reaction (oxygen reduction) at the steel-concrete interface, and then consume all the available oxygen content at the steel surface, since the oxygen diffusion through the bulk concrete to the steel surface is slower than the charge transfer rate, the cathodic reaction rate (the increase rate of hydroxyl ion concentration) will stop increasing and remain at the

maximum rate (as mentioned in Chapter 2). The chloride ion concentration reaching a constant rate is directly related to the hydroxyl ion concentration, which can be explained by the local electric neutrality in bulk concrete. This phenomenon also revealed that the chloride ions motion is not only decided by the applied CP current density and operation time, but also affected by the local hydroxyl ion concentration.

6.3.3 Steel Corrosion Rate under Cathodic Protection

The main purpose of applying the CP to chloride contaminated RC structures is to mitigate or stop the steel corrosion rate, that is to change the corroding steel from the corrosion to passivation state. For this reason, the steel corrosion rate under CP application is the major concern, which is directly related to CP effectiveness.

- **Steel Corrosion Rate Distribution at the Steel-Concrete Interface**

Figures 6.13 and 6.14 show the steel corrosion rate along the circumference of the rebar cross section varies with CP operation time under the applied current densities of 35mA/m^2 and 75mA/m^2 for the RC specimen with 1% NaCl, respectively. The steel corrosion rate along the circumference of the rebar cross section obtained for the RC specimen with varying NaCl contents under different CP operation time for the current densities of 35mA/m^2 and 75mA/m^2 are contained in Appendix C.

The horizontal axis shows the positions on the circumference of the steel cross section, which starts anticlockwise from the point near to the anode ($x = 0$). It can be seen that the steel corrosion rate along with the cross section circumference of rebar is not uniformly distributed under the CP process, but presents a similar shape of the sine function. The closest point to the anode has the smallest corrosion rate, whilst the furthest point to the anode has the largest corrosion rate.

It also can be observed that the steel corrosion rate degrades with continuing CP operation time. For instance, under the current density of 35mA/m^2 , the largest corrosion rate decreased to 0.84mA/m^2 and 0.8mA/m^2 under CP operation time of 10 days and 90 days, respectively. The legends in Figures 6.12 and 6.13 demonstrate the developmental stages of the model with time presented by multiple curve variations. Comparing Figures 6.13 and 6.14 show that the

degradation of steel corrosion rate also increases with increasing current density, such as, under the same CP operation time of 90 days, the largest corrosion rate decreased to 0.8mA/m^2 and 0.052mA/m^2 under the current densities of 35mA/m^2 and 75mA/m^2 , respectively.

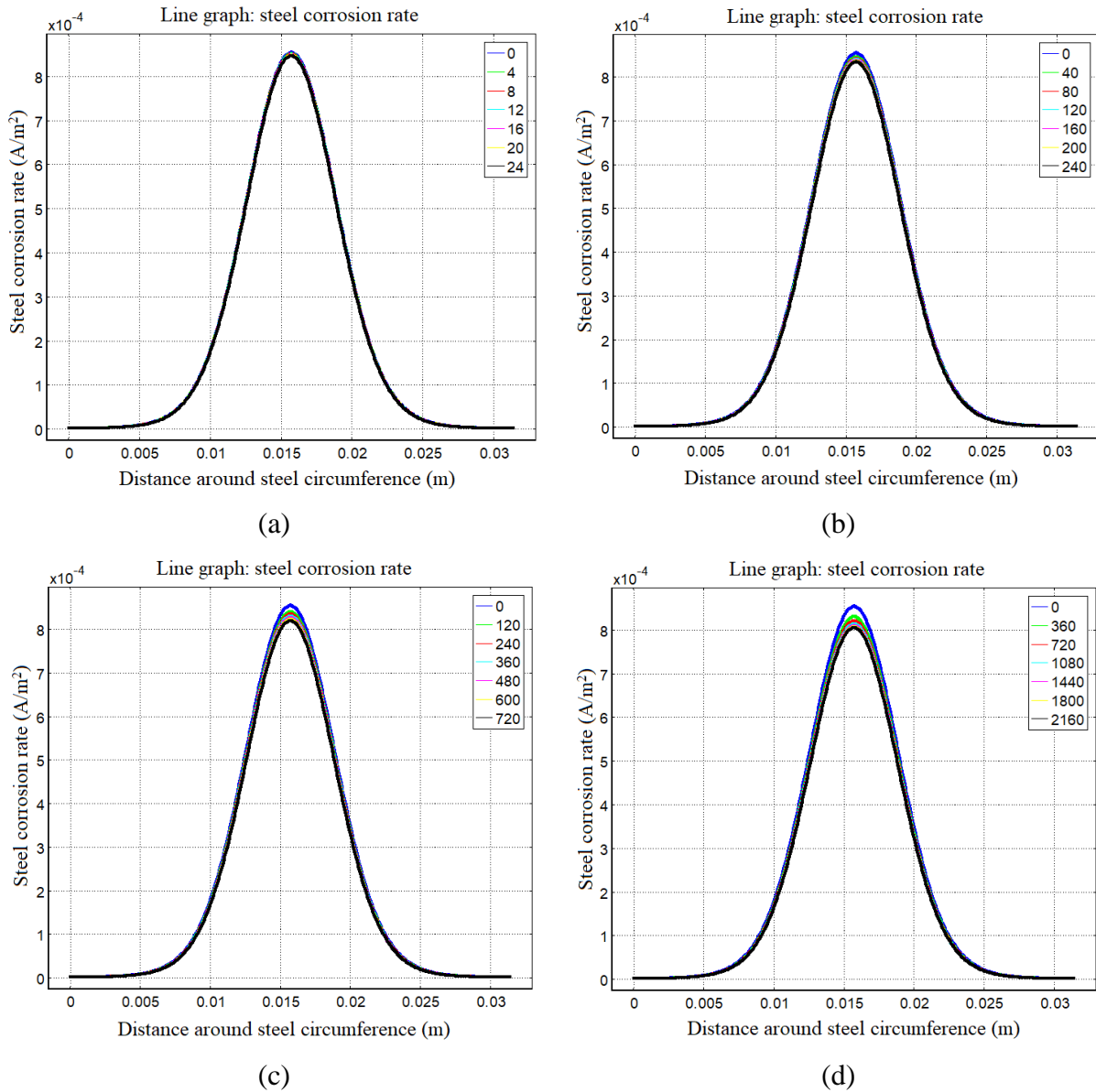


Figure 6.13 Distribution of steel corrosion rate along the circumference of steel bar cross section under 35mA/m^2 (1% NaCl).

(a) $t = 24$ hours, (b) $t = 10$ days, (c) $t = 30$ days, (d) $t = 90$ days.

The results show that, under the CP process, the profile of corrosion rate along the cross section circumference of rebar is similar to that of the profile of chloride ions. These results have verified that the closer the corroding rebar is to the anode, the easier it is to protect. It

proves that the structural geometry, anode position and configuration are important factors that should be considered in the CP design.

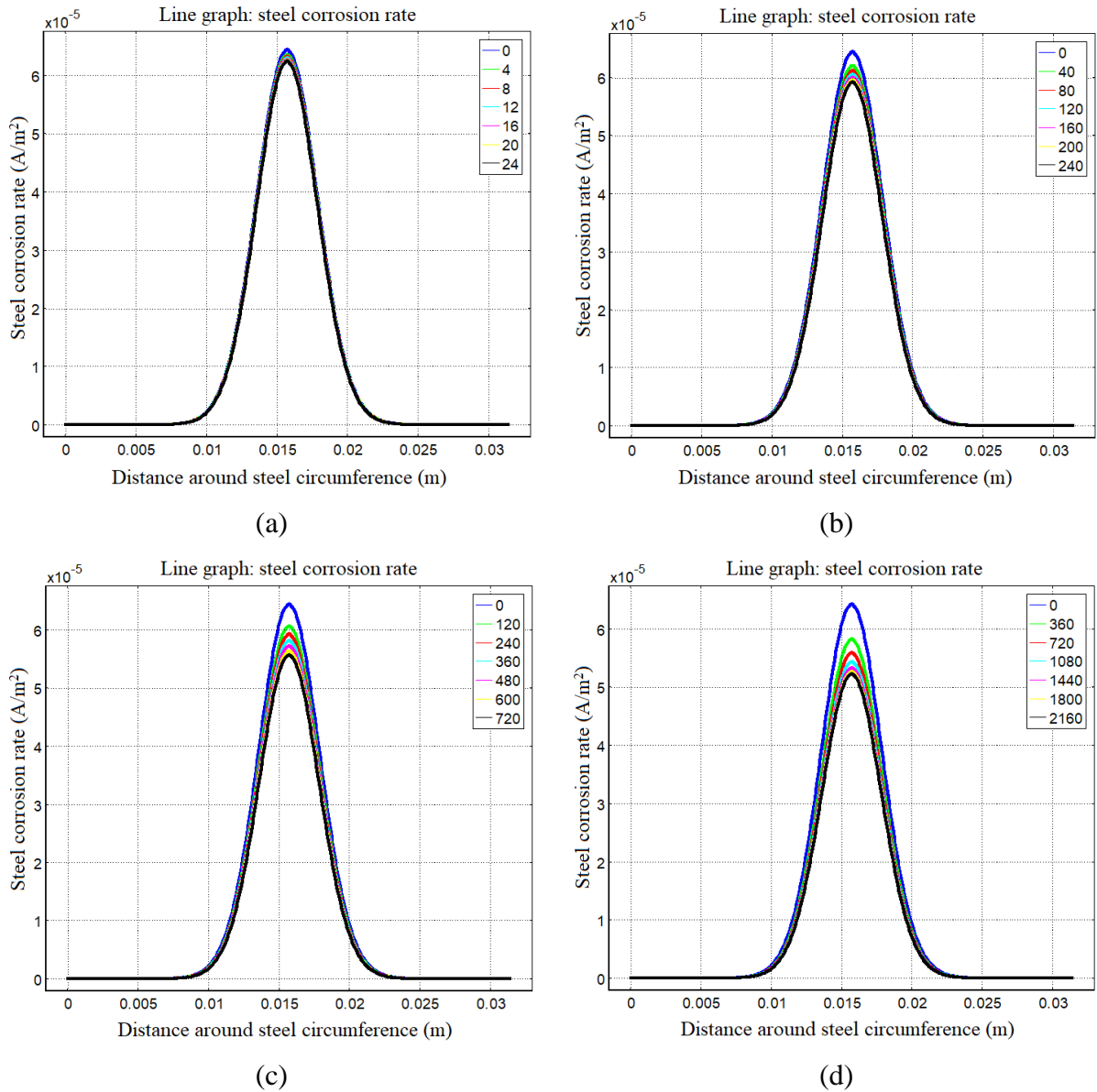


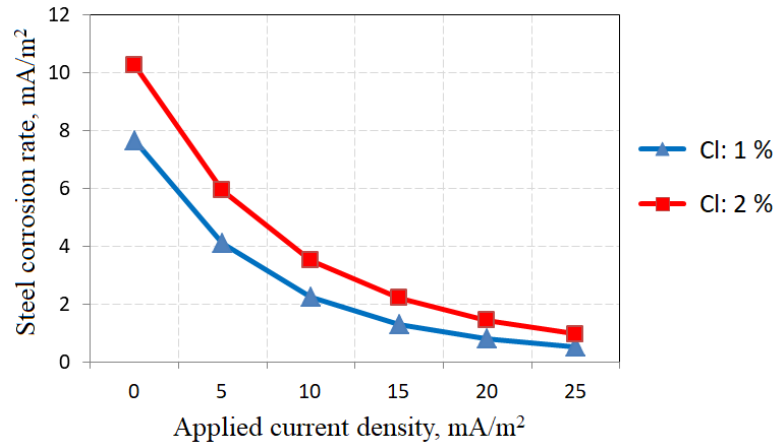
Figure 6.14 Distribution of steel corrosion rate along the circumference of steel bar cross section under 75mA/m^2 (1% NaCl).

(a) $t = 24$ hours, (b) $t = 10$ days, (c) $t = 30$ days, (d) $t = 90$ days.

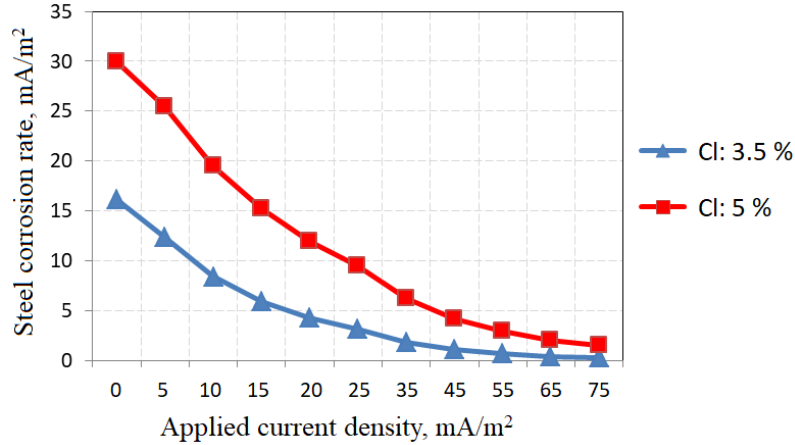
- **Steel Corrosion Rate under Different CP Current Densities**

Figure 6.15(a) shows the variation of steel corrosion rate at steel-concrete interface under five different CP current densities (5, 10, 15, 20, and 25mA/m^2) at 24 hours of CP operation for the RC specimen with 1 and 2% NaCl, respectively.

It can be seen that the steel corrosion rates are 10.5mA/m^2 and 7.8mA/m^2 when there is no CP installed for the two specimens. When CP is active, the steel corrosion rate decreases with increase of the applied current density. Theoretically, when the steel corrosion rate is less than 2mA/m^2 , the steel bar can be regarded as in a passive state. The results show that the higher the chloride content, the higher the CP current density needed to drive the steel bar into a passive state. The required CP current densities are about 18.5mA/m^2 and 12.5mA/m^2 for the two cases of 2 and 1% NaCl, respectively.



(a)



(b)

Figure 6.15 Variation of steel corrosion rate under different CP current densities for 24 hours.

(a) 1, 2% NaCl, (b) 3.5, 5% NaCl.

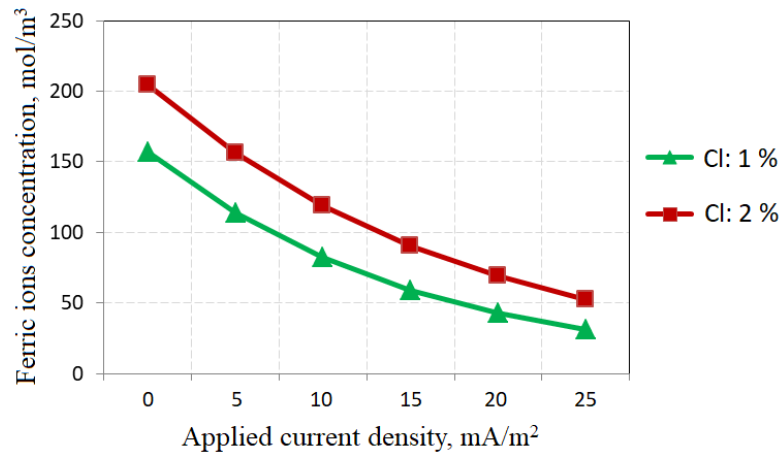
Figure 6.15(b) shows the steel corrosion rate at steel-concrete interface under ten different CP current densities (5, 10, 15, 20, 25, 35, 45, 55, 65, and 75 mA/m²) at 24 hours of CP operation for the RC specimen with 3.5, 5% NaCl, respectively.

Similar results as that in Figure 6.15(a) can be noticed. However, due to the higher chloride contents in the two cases, the required CP current densities are about 75mA/m^2 and 42mA/m^2 to achieve the steel corrosion protection, to bring the steel corrosion rate lower than 2mA/m^2 .

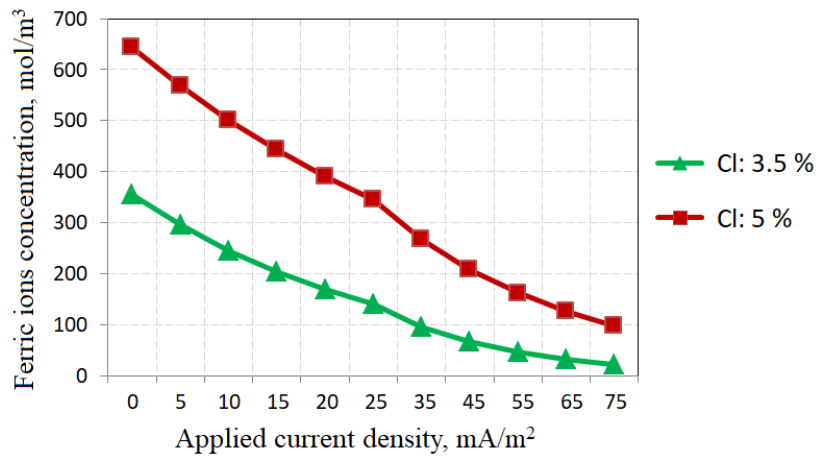
- **Ferric Ions Production at Steel-Concrete Interface**

In this study Equation (6.1) is used to describe the dynamic balance between the ferric and ferrous ions in the concrete pore solution. Therefore, a quantitative estimation of the concentration of ferric ions under different applied current densities can be obtained.

Figure 6.16 shows the ferric ion concentration at steel-concrete interface under different CP current densities. It can be seen that before the CP energisation, the highest ferric ion concentration corresponds to the highest chloride content. This is due to the high chloride content induces a high ferrous ion concentration due to the high steel corrosion rate, once the concentration of ferrous ions exceeds its solubility in pore solution, the extra ferrous ions will further react with oxygen and water to be oxidised to ferric hydroxide, and eventually which will converted to hydrated ferric oxide, rust. After CP energisation, the decreasing steel corrosion rate is accompanied by a decrease of ferrous and ferric ion concentrations.



(a)



(b)

Figure 6.16 Variation of ferric ion concentrations at steel-concrete interface under different CP current densities for 24 hours. (a) 1, 2% NaCl, (b) 3.5, 5% NaCl.

6.3.4 Comparison with Experimental Study

Figure 6.17 shows the comparison of numerical and experimental results for the minimum required CP current density to protect the rebar in the RC specimen with 1, 2, 3.5, and 5% NaCl. The relative errors of results are listed in Table 6.6, which is within 10% (ranges between 3.8 - 9.7%), which demonstrates a reasonably good agreement. The result has validated the developed CP model and justified its potential in real world application.

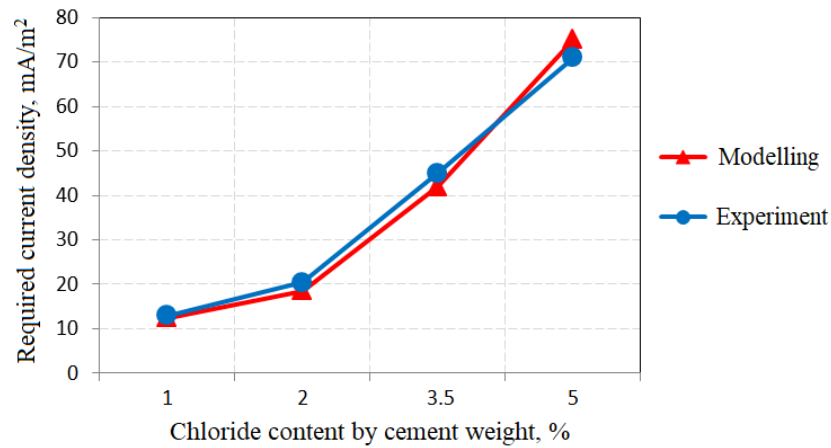


Figure 6.17 Comparison of the numerical and experimental results of required current density under different chloride contents.

Table 6.6 Results of numerical simulation and experimentation about the required CP current density for steel corrosion protection (mA/m²).

Specimens (NaCl)	Simulated Results	Experimental Results	Relative Errors
1%	12.5	13	3.8%
2%	18.5	20.5	9.7%
3.5%	42	45	6.6%
5%	75	71	5.6%

The experimental results are based on the study by Oleiwi (2018), where the required CP current density was determined in terms of the conventional CP criterion of 100mV potential decay. Figure 6.18 shows the experimentally measured steel potential decay of four hours for RC specimens with 1, 2, 3.5 and 5% NaCl under different CP current densities, in which the horizontal solid line represents the base line of 100mV decay, blue points and red circles represent the corresponding steel potential decay of experimental and modelling results, respectively.

It can be seen that, except the case of 5% NaCl, the steel potential decay is very slightly greater than 100mV, in other cases, the steel potential decays are all less than 100mV but the steel corrosion protection have been achieved. The results prove that the criterion of 100mV potential decay presents an over protection, this conclusion is also consistent with the finding from Oleiwi (2018).

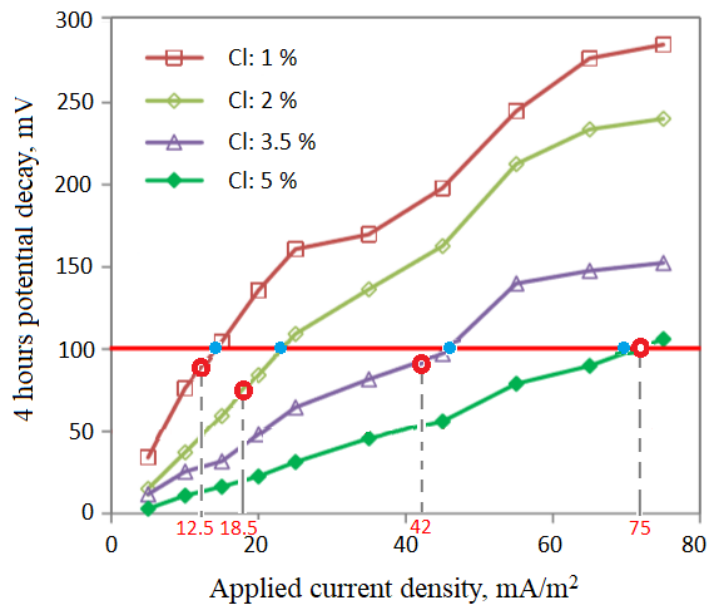
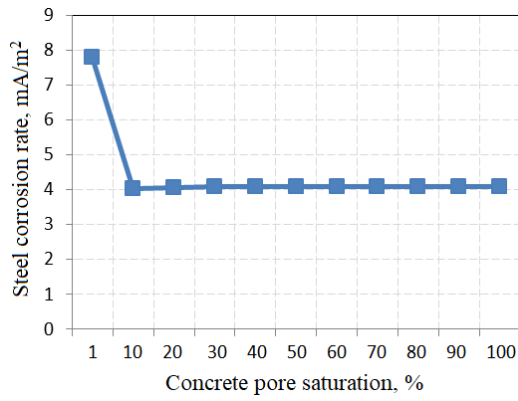


Figure 6.18 Four hours steel potential decay versus applied current density.

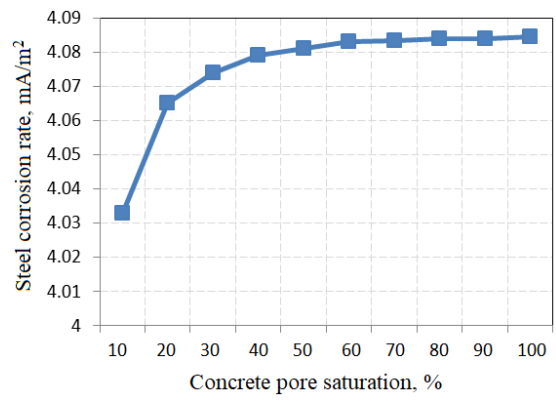
6.3.5 Parameter Study

Concrete Pore Saturation (PS) is closely linked to concrete electrical resistivity and oxygen transport mechanism in bulk concrete, therefore, which directly affects the effectiveness of CP systems. Since the RC structures are exposed to all kinds of environments, the concrete PS is subjected to large variations, it is a major parameter concerned in CP design and operation. In this study the developed CP numerical model was used to carry out the parameter study on the effect of concrete PS. Figures 6.19 to 6.21 show the variation of steel corrosion rate under different concrete PS and CP current densities at 24 hours of CP operation time for RC specimens with 1% NaCl.

It can be seen that the steel corrosion rate decreases with the increase of CP current density under the same concrete PS. However, the steel corrosion rate at the same CP current density presents the different value under different concrete PS: at PS of 1%, the steel corrosion rate does not change and remains at the initial corrosion rate; at PS range of 1%-10%, the steel corrosion rate decreases sharply (the effect of CP current enhanced greatly) with PS; at PS range of 10%-70%, the effect of CP current deteriorates slightly with PS; and at PS range of 70%-100%, the effect of CP is the same. Similar phenomenon can also be observed in Figures 6.22 to 6.24, which considered RC specimens with 2% NaCl.



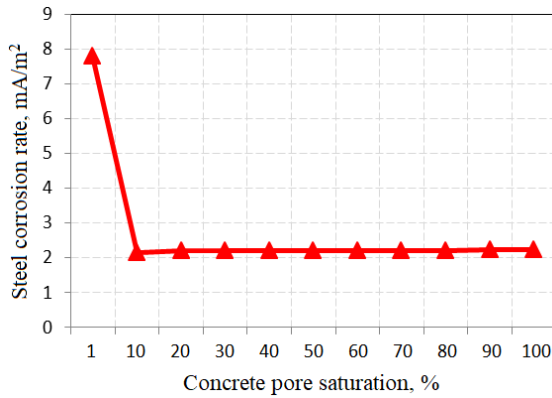
(a)



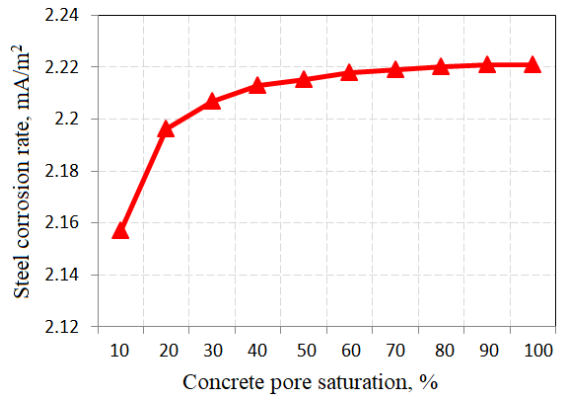
(b)

Figure 6.19 Variation of steel corrosion rate under 5mA/m^2 for 24 hours (1% NaCl).

(a) PS = (1~100)%, (b) PS = (20~100)%.



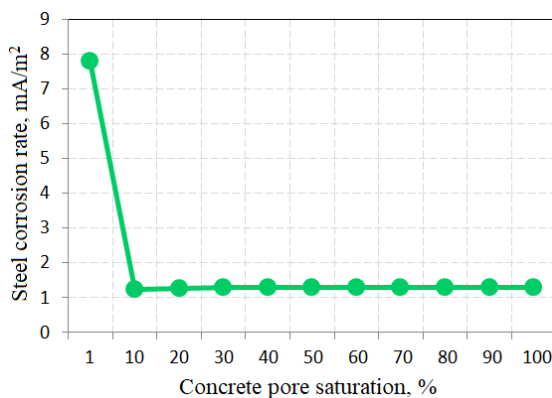
(a)



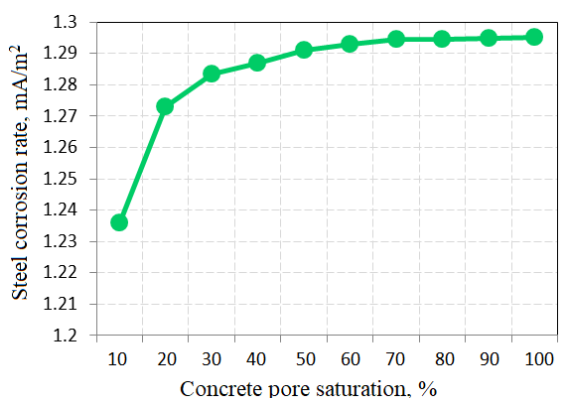
(b)

Figure 6.20 Variation of steel corrosion rate under 10mA/m^2 for 24 hours (1% NaCl).

(a) PS = (1~100)%, (b) PS = (20~100)%.



(a)



(b)

Figure 6.21 Variation of steel corrosion rate under 15mA/m^2 for 24 hours (1% NaCl).

(a) PS = (1~100)%, (b) PS = (20~100)%.

As reviewed in Chapter 4, the degree of concrete PS is an important influencing factor for concrete electrical resistivity. For the PS of 1%, the corresponding concrete electrical resistivity is very large, which limits the protection current flow in the bulk concrete, resulting in CP failure. For the PS range of 1%-10%, due to concrete electrical resistivity decreasing with increasing of PS, so the effective CP current density induced a significant decrease of steel corrosion rate. For the PS range of 10%-70%, the oxygen content available at steel-concrete interface decreasing with increasing of PS, the oxygen reduction rate may reach the maximum and along with the water reduction reaction, so the required CP current density increases. For the PS range of 70%-100%, the concrete electrical resistivity is virtually unchanged, which has no influence on the CP effect.

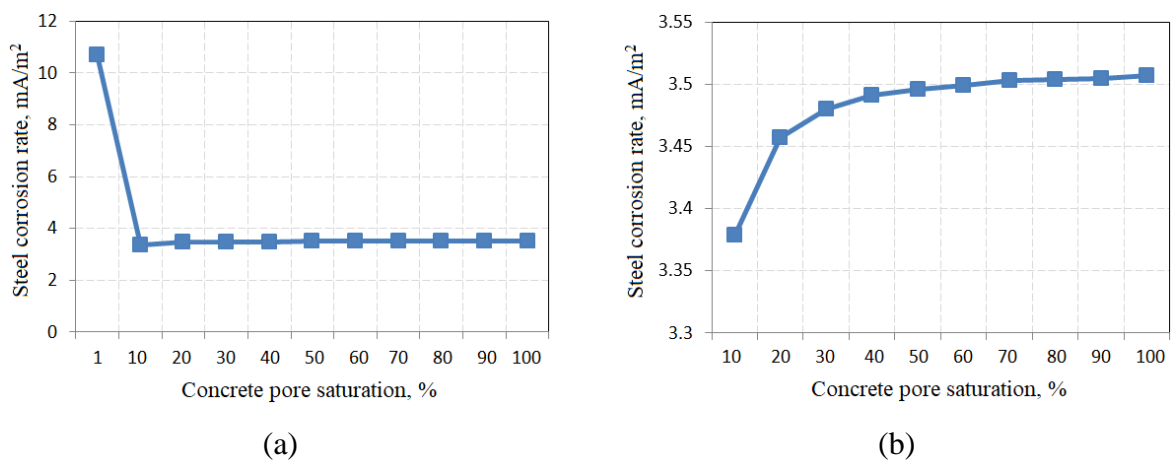


Figure 6.22 Variation of steel corrosion rate under 10mA/m^2 for 24 hours (2% NaCl).

(a) PS = (1~100)%, (b) PS = (20~100)%.

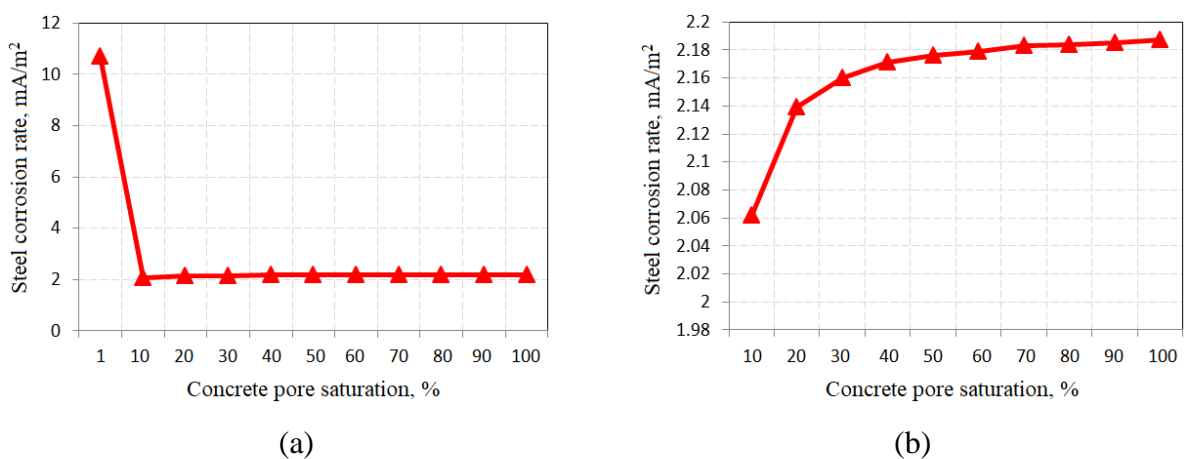


Figure 6.23 Variation of steel corrosion rate under 15mA/m^2 for 24 hours (2% NaCl).

(a) PS = (1~100)%, (b) PS = (20~100)%.

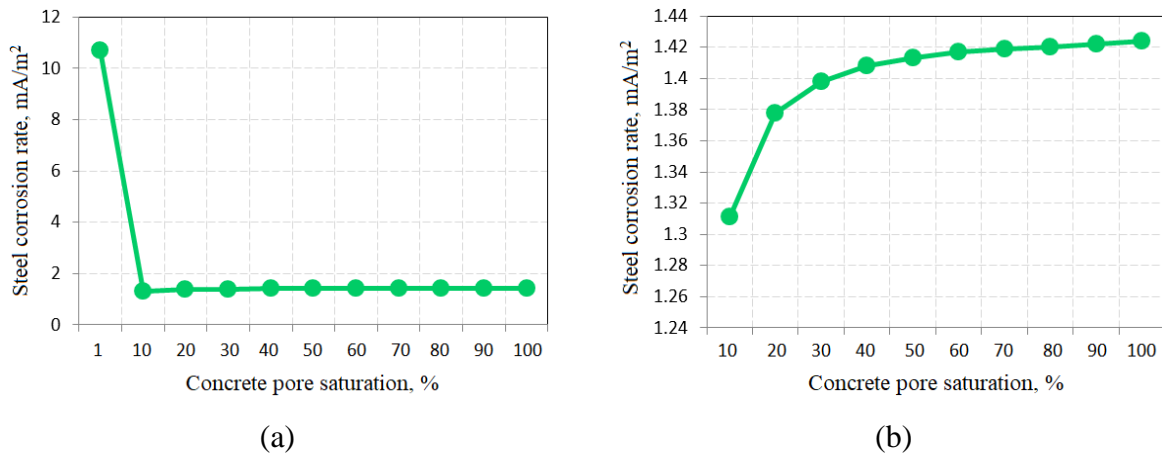


Figure 6.24 Variation of steel corrosion rate under 20mA/m^2 for 24 hours (2% NaCl).

(a) PS = (1~100)%, (b) PS = (20~100)%.

6.4 Discussion

6.4.1 Ionic Distribution and Concentration Variation

1. According to the existing fundamental theory of CP applied to chloride contaminated RC structures, which only qualitatively describes the migration trend of chloride ions that, the chloride ions at the steel-concrete interface can be moved away from the rebar by the externally applied current due to the chloride ions being negatively charged, which migrate in the opposite the direction of the protection current. In this study, the CP numerical modelling considered the variation of concrete electrical resistivity, the coupling effect of the ionic behaviour in concrete and the applied electric field, therefore, the simulated results have qualitatively and quantitatively described the chloride ion redistribution in concrete during the CP process, as below:

- the chloride ions at the steel-concrete interface remote from the anode are more difficult to disburse than those ions at the steel-concrete interface near the anode;
- the migration degree of chloride ions can be boosted by increasing the current density and/or extending the CP operation time, but the total amount of removable chloride ions compared with the initial chloride content is still small.

2. In the process of CP applied to RC structures, the hydroxyl ions are the main products of the electrochemical cathodic reactions (oxygen reduction) at the steel-concrete interface, which helps not only the steel corrosion protection but also to move the chloride ions away from the steel surface based on the electrical theory of like charges repel. In this study, the CP numerical simulation has qualitatively described the hydroxyl behaviour and the coupling effect between the hydroxyl and chloride ions, as follows:

- the hydroxyl ion concentration increases and the chloride ion concentration decreases at the steel-concrete interface with time under a lower protection current;
- the hydroxyl ion concentration at the steel-concrete interface will increase to a maximum value and remains at this value with time under a higher protection current;
- when the hydroxyl ion concentration is fixed, the chloride ion concentration at the steel-concrete interface will simultaneously stop decreasing and remains the same, forming a dynamic balance between the hydroxyl and chloride ions.

In short, for a chloride contaminated RC structure under CP application, it is impossible to get rid of all the harmful chloride ions at the steel-concrete interface. In this numerical study, the total quantity of chloride ion removal is small even under a very high applied current density (75mA/m^2) for a long CP operation time (2 years). The magnitude of applied current density and the CP operation time are only the secondary reasons, the concrete interior structure and the internal microenvironment are one of the main reasons to retard the chloride ion removal process. In addition, the hydroxyl ion concentration also significantly affects the chloride ion migration. When the hydroxyl ion concentration is increasing, it has the effect of promoting chloride ion removal from the steel-concrete interface; however, if the hydroxyl ion concentration is stable, it has the effect of suppressing chloride ion removal, this is based on the local electric neutrality in bulk concrete.

6.4.2 Steel Corrosion

According to the existing standard of CP application for RC structures, the evaluation of steel corrosion protection is based solely on the potential of the steel-concrete interface under the CP process, using the potential value indirectly reflects the steel state. The standard states that

the steel protection is ensured if the instant-off potential value in a certain potential range or the potential decay reaches 100mV under a certain period. This criterion is theoretically based on the thermodynamics of steel corrosion (Pourbaix diagram) related to the pH value, chloride content and temperature.

In this study, the CP numerical modelling adopted the proposed new Butler-Volmer Equation based steel polarisation model (which is connected with the steel corrosion rate) as the boundary condition of the steel-concrete interface, and considered the coupling effect of the ionic behaviour and the applied electric field, therefore, the CP numerical simulation has qualitatively and quantitatively described the steel corrosion state under CP process, and presented the variation of ferric ion concentration as follows:

- the steel corrosion rate decreases with increasing protection current density, the required CP current density for the steel corrosion protection is proportional to the steel corrosion state;
- the steel corrosion rate can be arrested by the CP current density which is less than the current density specified by the standard (based on the 100 mV potential decay) and the current CP standard provides overprotection for the corroding steel in chloride contaminated RC structure;
- the ferric ion concentration at the steel-concrete interface is proportional to the steel corrosion state, which decreases with the increasing protection current density.

In brief, CP technology is a reliable corrosion prevention method, the impressed protection current can effectively arrest the steel corrosion rate. Under CP application, the steel corrosion state was compared with the corresponding chloride ion distribution at the steel-concrete interface, a contradictory phenomenon can be observed that, the rebar has transformed from the active state to the passive state but the chloride ion concentration at the steel-concrete interface is still very high. This is because when the steel corrosion rate has been restrained by the protection current, and changed to the steel bar to the passive state, the chloride ion removal and production of hydroxyl ions in the CP process enlarge the steel passive range and then increases the chloride threshold concentration (which can induce the initiation of steel corrosion), therefore, the chloride ion concentration at the steel-concrete interface is very high

but the steel bar can still attain the passive state under CP application. This is also the fundamental mechanism of cathodic prevention.

Based on the numerical study, it was found that the required CP current density for steel corrosion protection was less than the specified current density, the specified 100mV potential decay criterion therefore gives an over protection. This is because the CP standard specifications link to the potential values, aiming to make the rebar potential reach a state where the steel corrosion is thermodynamically impossible to take place. That is, dropping the steel potential under the base line of protection potential, where the steel will be passivated. However, the specification does not take account of the long-term beneficial effects of CP current density. The chloride ion removal and the production of alkalinity can arrest the steel corrosion rate and also can widen the steel passivity region. That is, they can further move the base line of protection potential in the positive direction. As a result, the required CP current density up to the existing CP standard can be reduced.

Furthermore, the improved CP numerical model can directly describe the ferric ion state, its capability to quantify rust production has given the developed model a potential for application to real world problems, which can predict the RC structural spalling process and service life span when incorporated with a fracture mechanism model.

6.4.3 Effect of Concrete Pore Saturation on Cathodic Protection

The research results shown that the lower concrete PS (less than 10%) affects the CP effectiveness greatly, this conclusion is in line with the study of Koretsky et al. (1999) that the electrical resistivity of drier concrete limits the flow of protection current. When the concrete PS greater than 70%, corresponding to a very small concrete electrical resistivity, which has no obvious effect on CP effectiveness, this conclusion confirmed the research result between concrete electrical resistivity and pore saturation degree (Lopez and Gonzalez, 1993). The required CP current density increases with PS, which verified the study of Koretsky et al. (1999) that at high values of PS, the CP system is limited by oxygen transport in concrete and water reduction becomes the important cathodic process, therefore, a higher CP current density is needed. Also this conclusion is in agreement with the study of Oleiwi (2018), who stated that the required CP current density increases with decreasing concrete electrical resistivity.

6.5 Conclusion

In this study, an improved numerical modelling which considered variation of concrete electrical resistivity, steel polarisation state under CP process, and coupling effect of the ionic behaviour and the applied electric field has been proposed and investigated. It has been demonstrated that the developed model not only can describe the chloride and hydroxyl ion behaviours in concrete, but most importantly, it also can reflect the steel corrosion rate under CP application. The proposed model considers the electrochemical mechanism of the corrosion reactions at the steel surface, it provides an effective tool which can directly make assessment for the steel corrosion rate and the corresponding corrosion products. This model can provide more insight and accurate information for the CP design and operation on RC structures.

CHAPTER 7

CONCLUSIONS AND RECOMMENDATIONS FOR FUTURE RESEARCH WORK

7.1 Conclusions

The present work has developed a mathematical model for concrete electrical resistivity, which comprises the main factors related to the varied water and chloride contents in concrete. As applications, this mathematical model has been applied in the governing equation to describe the electric field inside concrete for the cathodic protection (CP) numerical modelling of reinforced concrete (RC) structures to simulate the ionic transportation in concrete pore solution under the CP process.

The present work also has characterized a Butler-Volmer Equation based rebar polarisation model, which involves the main factors related to the varied chloride contents and applied protection current densities under CP conditions. As applications, this polarisation model has been used as the boundary condition in the CP numerical model of RC structures to describe the electrochemical reaction at the steel-concrete interface under the CP process.

This study has improved the CP numerical modelling of RC structures by involving the above two developed models and considering the coupling effect of the ionic behaviour in concrete pore solution and externally applied electric field effect. As applications, numerical modelling of CP for chloride contaminated RC structures has been conducted to investigate the related ionic states in concrete and steel corrosion under CP conditions; a parameter study based on the improved model has been carried out to research the effect of concrete pore saturation on CP effectiveness.

For the case of ionic distribution and concentration variation: the chloride ions at the steel-concrete interface remote from the anode are more difficult to be moved away than those ions at the steel-concrete interface near the anode, the total amount of removable chloride ions

under CP is small; the hydroxyl ion concentration at the steel-concrete interface increases with the increase of CP current density, which will increase to a maximum value under a higher protection current; meanwhile, the chloride ion concentration at the steel-concrete interface will simultaneously remain the same, forming a dynamic balance between the hydroxyl and chloride ions. The ferric ion concentration at the steel-concrete interface is proportional to the steel corrosion state, which decreases with the increasing protection current density.

Steel corrosion rate decreases with increasing protection current density, the required CP current density for steel corrosion protection is proportional to the steel corrosion state. The steel corrosion rate can be arrested by the required CP current density which is less than the specified current density stated in the standard.

From the parameter study, the concrete pore saturation (PS) significantly influences the CP effectiveness when its value is small, the required CP current density to achieve steel corrosion protection increases with increasing pore saturation.

In conclusion, the improved numerical modelling can not only describe the chloride and hydroxyl ions behaviours in concrete but also directly reflect the steel corrosion rate under CP application. It provides an effective tool which can directly assess the steel corrosion rate and corresponding corrosion products, and then provide more insight and accurate information for CP design and operation of RC structures.

7.2 Recommendation for Future Research Work

A CP numerical investigation was carried out in this study, the developments made through the course of this study have directly helped improve our understanding in underlying electrochemical mechanisms of the CP process in RC structures. This research area of CP of RC structures is related to ionic behaviour in concrete pore solution, electrochemical reaction at electrode-concrete interface studies. Future numerical research work for development in CP technology of RC structures could address the following:

1. The developed mathematical model of concrete electrical resistivity only considered the effects of varied water and chloride contents, a comprehensive model with the additional considerations of the effects of pH value and temperature is needed.
2. The characterisation of the steel polarisation model was based on the experimental data of air exposed RC specimens, which does not describe the steel state of underwater RC structures. A comprehensive polarisation model with the additional consideration of the effect of water content is needed.
3. In the CP numerical modelling, the electrochemical reactions (time, moisture dependent polarisations) at anode-concrete interface was neglected, instead the anode potential was set to a reference point and assigned a value of zero. An anode polarisation model under CP conditions is a key direction for future CP numerical investigation.
4. In this study, the numerical model only involved the corroding steel bar state (microcell corrosion), a model comprising both the corroding steel bars and the passive steel bars is needed, to comprehensively evaluate the steel macrocell corrosion state under CP, and the effect of passive steel bars on CP effectiveness.
5. In this study, the numerical research was based on a two-dimensional model, the steel corrosion state was therefore based on a plane analysis. The CP numerical model needs to be extended from a two-dimensional to a three-dimensional model to comprehensively characterise the steel corrosion state and the CP effectiveness.

REFERENCES

- Ahmad, S. (2003). Reinforcement corrosion in concrete structures, its monitoring and service life prediction - a review. *Cement and Concrete Composites*, 25(4-5), pp. 459-471.
- Alonso, M. C., and Sanchez, M. (2009). Analysis of the variability of chloride threshold values in the literature. *Materials and Corrosion*, 60(8), pp. 631–637.
- Al-Sulaimani, G. J., Kaleemullah, M., Basunbul, I. A., and Rasheeduzzafar. (1990). Influence of corrosion and cracking on bond behavior and strength of reinforced concrete members. *ACI Structural Journal*, 87(2), pp. 220-231.
- Andrade, C., Keddad, M., Novoa, X. R., Perez, M. C., Rangel, C. M., and Takenouti, H. (2001). Electrochemical behaviour of steel rebars in concrete: influence of environmental factors and cement chemistry. *Electrochimica Acta*, 46(24-25), pp. 3905-3912.
- Andrade, M. C., Bolzoni, F., and Fullea, J. (2011). Analysis of the relation between water and resistivity isotherms in concrete. *Materials and Corrosion*, 62(2), pp. 130-138.
- Angst, U., Elsener, B., Larsen, C. K., and Vennesland, Ø. (2009). Critical chloride content in reinforced concrete—a review. *Cement and Concrete Research*, pp. 1122-1138.
- Araujo, A., Panossian, Z., and Lourenco, Z. (2013). Cathodic protection for concrete structures. *Ibracon structures and materials journal*, 6(2), pp. 178-193.
- Archie, G. E. (1942). The electrical resistivity log as an aid in determining some reservoir characteristics. *Transactions of the American Institute of Mining and Metallurgical Engineers*, 146(1), pp. 54-62.
- ASCE. (2009). Report Card for America’s Infrastructure – Facts about Transportation – Bridges, American Society of Civil Engineers.
- Ashworth, V. (2010). *Principles of Cathodic Protection*. Vol. 2, pp. 10:3–10:28.
- Atkins, E. R., and Smith, G. H. (1961). The significance of particle shape in formation resistivity factor-porosity relationships. *Transactions of the American Institute of Mining and Metallurgical Engineers*, 13(3), pp. 285-291.

- Azarsa, P., and Gupta, R. (2017). Electrical resistivity of concrete for durability evaluation: a review. *Advances in Materials Science and Engineering*.
- Bartholomew, J., Bennett, T., Turk, T., Hartt, W. H., Lankard, D. R., Sagues, A. A., et al. (1993). *Control criteria and materials performance studies for CP of reinforced concrete*. Strategic Highway Research Program Report.
- Banea, P. I. (2015). Study of Electrical Resistivity of Mature Concrete. MSc thesis.
- Berkeley, K. G., and Pathmanaban, S. (1990). *Cathodic protection of reinforcement steel in concrete*. Butterworths.
- Bertolini, L., Bolzoni, F., Pedferri, P., Lazzari, L., and Pastore, T. (1998). Cathodic protection and cathodic prevention in concrete: principles and applications. *Journal of applied electrochemistry*, 28(12), pp. 1321-1331.
- Bertolini, L., Elsener, B., Pedferri, P., and Polder, P. (2004). *Corrosion of Steel in Concrete: Prevention, Diagnosis, Repair*. Wiley-VCH.
- Bertolini, L., Elsener, B., Pedferri, P., Redaelli, E., and Polder, R. B. (2013). *Corrosion of steel in concrete: prevention, diagnosis, repair (Second edition)*. John Wiley and Sons.
- Bertolini, L., Elsener, B., Pedferri, P., Redaelli, E., and Polder, R. B. (2014). *Corrosion of Steel in Concrete: Prevention, Diagnosis, Repair, 2nd Edition*. Wiley VCH.
- Bertolini, L., Gastaldi, M., Pedferri, M., and Redaelli, E. (2002). Prevention of steel corrosion in concrete exposed to seawater with submerged sacrificial anodes. *Corrosion Science*, 44(7), pp. 1497-1513.
- Brandt, A. M. (2014). *Cement-based Composites: Materials, Mechanical Properties and Performance*. CRC Press.
- Broomfield, J. P. (1997). *Corrosion of steel in concrete: understanding, investigation and repair*. CRC Press.
- Bruns, M., and Raupach, M. (2010). Protection of the opposite reinforcement layer of RC-structures by CP - results of numerical simulations. *Materials and Corrosion*, 61(6), pp. 505-511.
- BS EN ISO. (2016). Cathodic protection of steel in concrete: British European Standards Institution.

- BSI. (2012). ISO 12696:2012, Cathodic protection of steel in concrete.
- Buffle, J., Zhang, Z., and Startchev, K. (2007). Metal flux and dynamic speciation at (Bio) interfaces. Part I: Critical evaluation and compilation of physicochemical parameters for complexes with simple ligands and fulvic/humic substances. *Environmental Science and Technology*, 41(22).
- Byrne, A., Holmes, N., and Norton, B. (2016). State-of-the-art review of cathodic protection for reinforced concrete structures. *Magazine of Concrete Research*, 68(13), pp. 664-677.
- Carmona, C. J., Climent, L. M., and Garces, T. P. (2017). Influence of different ways of chloride contamination on the efficiency of cathodic protection applied on structural reinforced concrete elements. *Journal of Electroanalytical Chemistry*, 793, pp. 8-17.
- Chang, M. T., Montanari, L., Suraneni, P., and Weiss, W. J. (2018). Expression of cementitious pore solution and the analysis of its chemical composition and resistivity using x-ray fluorescence. *Journal of Visualized Experiments*, 139.
- Chen, C.-T., Chang, J.-J., and Yeih, W.-C. (2014). The effects of specimen parameters on the resistivity of concrete. *Construction and Building Materials*, 71, pp. 35-43.
- Chess, P. M., and Broomfield, J. P. (2014). *Cathodic Protection of Steel in Concrete and Masonry*. CRC Press.
- Cheung, M. M., and Cao, C. (2013). Application of cathodic protection for controlling macrocell corrosion in chloride contaminated RC structures. *Construction and Building Materials*, 45, pp. 199-207.
- Christodoulou, C., Glass, G., Webb, J., Austin, S., and Goodier, C. (2010). Assessing the long term benefits of impressed current cathodic protection. 52(8), pp. 2671-2679.
- CIA. (2009). The World Fact Book, Country Comparison of GDP.
- Cicek, V. (2013). Cathodic Protection of Reinforced Concrete Steels. In V. Cicek, *Cathodic Protection : Industrial Solutions for Protecting Against Corrosion*. John Wiley and Sons.
- Cussler, E. L. (2009). *Diffusion: Mass Transfer in Fluid Systems*. Cambridge University Press.

- Elkey, W., and Sellevold, E. J. (1995). Electrical Resistivity of Concrete. *Norwegian Road Research Laboratory*.
- FHWA. (1982). Memorandum on FHWA Position on Cathodic Protection Systems, US Federal Highway Administration.
- Fonna, S. H., Huzni, S., Putra, M. A., and Kurniawan, R. (2018). Simulation the effect of anode-cathode displacement and anode type on reinforced concrete cathodic protection using BEM. *Matec Web of Conferences*.
- Frankel, G. S. (2016). Fundamentals of Corrosion Kinetics. In A. E. Hughes, J. M. Mol, M. L. Zheludkevich, and R. G. Buchheit, *Active Protective Coatings: New-Generation Coatings for Metals* (pp. 17-32). Springer Netherlands.
- Gao, X. J., Yang, Y. Z., and Deng, H. W. (2011). Electrochemical Changes of Pre-Corroded Steel Reinforced Concrete Due to Electrochemical Chloride Extraction. *International Journal of Electrochemical Science*, 6, pp. 1797-1809.
- Ge, J., and Isgor, O. B. (2007). Effects of Tafel slope, exchange current density and electrode potential on the corrosion of steel in concrete. *Materials and Corrosion*, 58(8), pp. 573-582.
- Gjørv, O. E., Vennesland, Ø. E., and El-Busaidy, A. H. (1977). Electrical resistivity of concrete in the oceans. *Offshore Technology Conference*, pp. 581-588.
- Glass, G. K., and Buenfeld, N. R. (1997). The presentation of the chloride threshold level for corrosion of steel in concrete. *Corrosion Science*, 39(5), pp. 1001-1013.
- Glass, G. K., Page, C. L., and Short, N. R. (1991). Factors affecting the corrosion rate of steel in carbonated mortars. *Corrosion Science*, 32(12), pp. 1283-1294.
- Gulikers, J. (2005). Theoretical considerations on the supposed linear relationship between concrete resistivity and corrosion rate of steel reinforcement. *Materials and Corrosion*, 56(6), pp. 393-403.
- Hansson, C. M., Poursaee, A., & Jaffer, S. J. (2012). Corrosion of reinforcing bars in concrete. *Portland Cement Association (PCA)*.
- Hansson, C. M. (1984). Comments on electrochemical measurements of the rate of corrosion of steel in concrete. *Cement and Concrete Research*, 14(4), pp. 574-584.

- Hansson, I. L., and Hansson, C. M. (1993). Electrochemical extraction of chlorides from concrete part I - A qualitative model of the process. *Cement and Concrete Research*, 23(5), pp. 1141-1152.
- Hassanein, A. M., Glass, G. K., and Buenfeld, N. R. (2002). Protection current distribution in reinforced concrete cathodic protection systems. *Cement and Concrete Composites*, 24(1), pp. 159-167.
- Helm, C., and Raupach, M. (2016). Development of a numerical simulation model considering the voltage drops within CP anode systems in RC structures. *Materials and Corrosion*, 67(6), pp. 621-630.
- Henry, R. L. (1964). *Water vapor transmission and the electrical resistivity of concrete*. Technical report R314.
- Hong, D., Fan, W., Luo, D., Ge, Y., and Zhu, Y. (1993). Study and application of impressed current cathodic protection technique for atmospherically exposed salt-contaminated reinforced concrete structures. *Aci Materials Journal*, 90(1), pp. 3-7.
- Hornbostel, K., Larsen, C. K., and Geiker, M. R. (2013). Relationship between concrete resistivity and corrosion rate—a literature review. *Cement and Concrete Composites*, 39, pp. 60-72.
- Hunkeler, F. (1996). The Resistivity of Pore Water Solution—A Decisive Parameter of Rebars Corrosion and Repair Methods. *Construction and Building Materials*, 10(5), pp. 381-398.
- Jan, Bijen. (2003). *Durability of Engineering Structures: Design, Repair and Maintenance*.
- Jiang, J., and Yuan, Y. (2012). Prediction model for the time-varying corrosion rate of rebar based on micro-environment in concrete. *Construction and Building Materials*, pp: 625–632.
- Jiang, J. H., and Yuan, Y. S. (2013). Relationship of moisture content with temperature and relative humidity in concrete. *Magazine of Concrete Research*, 65(11), pp. 685-692.
- Jin, H., Wang, Y., Zheng, Q., Liu, H., and Chadwick, E. (2017). Experimental study and modelling of the thermal conductivity of sandy soils of different porosities and water contents. *Applied Sciences*.

- Kean, R. L., and Davies, K. G. (1981). Cathodic Protection, Guide Prepared British Department Trade and Industry. Vols. 2–4.
- Kepler, J. L., Darwin, D., and Locke, C. E. (2000). *Evaluation of corrosion protection methods for reinforced concrete highway structures*. University of Kansas Center for Research, Inc.
- Kerkhoff, B. (2007). Effects of substances on concrete and guide to protective treatments. *Portland Cement Association*.
- Koch, G. H., Brongers, M. P. H., Thompson, N. G., Virmani, Y. P., and Payer, J. H. (2002). Corrosion costs and preventive strategies in the United States.
- Koretsky, M. D., Aboameri, F., and Westall, J. C. (1999). Effect of Concrete Degree of pore water saturation on Cathodic Protection of Steel-Reinforced Concrete Bridges. *Corrosion*, 55(1), pp. 52-64.
- Lambert, P. (1995). Cathodic protection of reinforced concrete. *Anti-Corrosion Methods and Materials*, pp: 4-5.
- Laurens, S., and Francois, R. (2017). Cathodic protection in reinforced concrete structures affected by macrocell corrosion: a discussion about the significance of the protection criteria. *RILEM Technical Letters*, 2, pp. 27-32.
- Layssi, H., Ghods, P., Alizadeh, A. R., and Salehi, M. (2015). Electrical resistivity of concrete. *Concrete International* , pp: 41-46.
- Liu, Y., and Shi, X. M. (2012). Modeling cathodic prevention for unconventional concrete in salt-laden environment. *Anti-Corrosion Methods and Materials*, 59(3), pp. 121-131.
- Lopez, W., and Gonzalez, J. A. (1993). Influence of the degree of degree of pore water saturation on the resistivity of concrete and the corrosion rate of steel reinforcement. *Cement and Concrete Research*, 23(2), pp. 368-376.
- Loziquez, E. B., Barthélémy, J. F., Bouteiller, V., and Desbois, T. (2018). Contribution of Sacrificial Anode in reinforced concrete patch repair:. *Construction and Building Materials*, pp. 405-417.

- Masuda, M., Arita, M., Ju, L. E., Hanada, K., Minagawa, H., and Kawamata, K. (2004). The Application of FEM to Cathodic Corrosion Protection of Steel Reinforcement in Concrete. *Materials Transactions*, 45(12), pp. 3349–3355.
- Montemor, M. F., Simoes, A. M., and Ferreira, M. G. (2003). Chloride-induced corrosion on reinforcing steel: from the fundamentals to the monitoring techniques. *Cement and Concrete Composites*, 25(4-5), pp. 491-502.
- Morgan, B., and Lahav, O. (2007). The effect of pH on the kinetics of spontaneous Fe(II) oxidation by O₂ in aqueous solution - basic principles and a simple heuristic description. *Chemosphere*, 68(11), pp. 2080-2084.
- Morris, W., Vico, A., and Vazquez, M. (2004). Chloride induced corrosion of reinforcing steel evaluated by concrete resistivity measurements. *Electrochimica Acta*, 49(25), pp. 4447–4453.
- Muehlenkamp, E. B., Koretsky, M. D., and Westall, J. C. (2005). Effect of Moisture on the Spatial Uniformity of Cathodic Protection of Steel in Reinforced Concrete. *Corrosion*, 61(6), pp. 519-533.
- Newman, J. (1973). *Electrochemical Systems*, Prentice-Hall, Englewood Cliffs.
- Olewi, H. M. (2018) Using cathodic protection to control corrosion of reinforced concrete structures. Doctoral thesis.
- Page, C. L., Short, N. R., and Holden, W. H. (1986). The influence of different cements on chloride-induced corrosion of reinforcing steel. *Cement and Concrete Research*, 16(1), pp. 79-86.
- Paul Guyer, J., E, P., A., R., Fellow ASCE, and Fellow AEI. (2014). An introduction to cathodic protection principles.
- Pedefferri, P., and Bertolini, L. (2000). Durability of Reinforced Concrete. *McGraw-Hill Italia*.
- Pedefferri, P. (1996). Cathodic protection and cathodic prevention. *Construction and Building Materials*, 10(5), pp. 391-402.
- Polder, R. B. (1996). The influence of blast furnace slag, fly ash and silica fume on corrosion of reinforced concrete in marine environment. *Heron*, PP: 287-300.

- Polder, R. B., Peelen, W. H., Stoop, B. T., and Neeft, E. A. (2011). Early stage beneficial effects of cathodic protection in concrete structures. *Materials and Corrosion*, 62(2), pp. 105-110.
- Polder, R. B., Peelen, W. H. A., Lollini, F., Redaelli, E., and Bertolini, L. (2008). Advanced numerical design for economical cathodic protection. In *Tailor Made Concrete Structures: New Solutions for our Society*, by Walraven and Stoelhorst (eds), pp. 691-696. CRC Press.
- Pradhan, B. (2014). Corrosion behavior of steel reinforcement in concrete exposed to composite chloride–sulfate environment. *Construction and Building Materials*, 72, pp. 398-410.
- Qiao, G. F., Guo, B. B., and Ou, J. P. (2015). Numerical Simulation of the Impressed Current Cathodic Protection System for a Reinforced Concrete Structure. *2015 Fifth International Conference on Instrumentation and Measurement*, pp. 836-839.
- Qiao, G. F., ASCE, M., Guo, B. B., and Ou, J. P. (2017). Numerical Simulation to Optimize Impressed Current Cathodic Protection Systems for RC Structures. *Journal of Materials in Civil Engineering*.
- Qiao, G. F., Guo, B. B., Ou, J. P., Xu, F., and Li, Z. H. (2016). Numerical optimization of an impressed current cathodic protection system for reinforced concrete structures. *Construction and Building Materials*, 119, pp. 260-267.
- Redaelli, E., Bertolini, L., Peelen, W., and Polder, R. (2006). FEM-models for the propagation period of chloride induced reinforcement corrosion. *Materials and Corrosion*.
- Roberge, P. R. (2008). *Corrosion engineering : principles and practice*. McGraw-Hill Education.
- Roy, D. M., Brown, P. W., Shi, D., Scheetz, B. E., and May, W. (1993). Concrete Microstructure Porosity and Permeability. *Strategic Highway Research Program*.
- Saleem, M., Shameem, M., Hussain, S. E., and Maslehuddin, M. (1996). Effect of moisture, chloride and sulphate contamination on the electrical resistivity Portland cement concrete. *Construction and Building Materials*, 10(3), pp. 209-214.

- Schmitt, G. (2009). *Global Needs for Knowledge Dissemination, Research, and Development in Materials Deterioration and Corrosion Control*, World Corrosion Organisation.
- Schutter, G. D. (2012). *Damage to concrete structures*. CRC Press.
- Schweitzer, P. A. (2009). *Fundamentals of corrosion: mechanisms, causes, and preventative methods*. CRC Press.
- Shaikhon, O. (2015). The effect of chloride and sulfate ions on the resistivity of concrete. MSc dissertation.
- Sims, I. (1994). The assessment of concrete for carbonation. *Concrete*.
- Srinivasan, R., Gopalan, P., Ronald Zarriello, P., Myles-tochko, C. J., and Meyer, J. H. (1996). Design of Cathodic Protection of Rebars in Concrete Structures An Electrochemical Engineering Approach. *Applied Research*, 17(4), pp. 362-370.
- Stumm, W., and Morgan, J. J. (1996). *Aquatic Chemistry: Chemical Equilibria and Rates in Natural Waters, 3rd Edition*. John Wiley and Sons, New York.
- Stratfull, R. F. (1974). Cathodic protection of a bridge deck-preliminary investigation. *Materials performance*, pp. 24-25.
- Su, J.-K., Yang, C.-C., Wu, W.-B., and Huang, R. (2002). Effect of moisture content on concrete resistivity measurement. *Journal of the chinese institute of engineers*, 25(1), pp. 117-122.
- Sun, G. D., Qiao, G. F., and Xu, B. (2010). Corrosion Monitoring Sensor Networks With Energy Harvesting. *IEEE Sensors Journal*, 11(6), pp. 1901-1902.
- Tilly, G. P., and Jacobs, J. (2007). *Concrete repairs - performance in service and current practice*. IHS BRE Press.
- Torres-Acosta, A. A., Sen, R., and Martínez-Madrid, M. (2004). Cathodic Protection of Reinforcing Steel in Concrete Using Conductive-Polymer System. *Journal of Materials in Civil Engineering*, 16(4), pp. 315-321.
- Trethewey, K. R., & Chamberlain, J. (1995). *Corrosion for science and engineering*.
- Tuutti, K. (1980). Service life of structures with regard to corrosion of embedded steel. *Special Publication*, 65, pp. 223-236.

- Villagran, Z. Y., and Di Maio, A. A. (2014). Electrical resistivity measurement of unsaturated concrete samples. *Magazine of Concrete Research*, 66(10), pp. 484-491.
- Villagran, Z. Y., Fullea Garcia, J., Huelamo, P., and Di Maio, A. A. (2009). Influence of temperature and humidity on Portland cement mortar resistivity monitored with inner sensors. *Materials and Corrosion*, 60(4), pp. 294-299.
- Wang, Y. (2001). *Mathematical modelling of chloride ingress into concrete and electrochemical chloride removal from concrete*. Doctoral Thesis.
- Wang, Y., and Wu, G. (2008). Understanding and modelling of soil-water characteristic curves. *Chinese Journal of Geotechnical Engineering*, pp. 1282–1290.
- Wang, Y., Grove, S. M., and Anderson, M. G. (2008). A physical-chemical model for the static water retention characteristic of unsaturated porous media. *Advances in Water Resources Research*, pp. 723–735.
- Wang, Y., Wang, X. Y., Scholz, M., and Ross, D. K. (2012). A physico-chemical model for the water vapour sorption isotherm of hardened cementitious materials. *Construction and Building Materials*, pp. 941–946.
- Wang, Y., and Li, L. Y. (2000). Efficiency investigation of chloride removal from concrete by using electrochemical method. *10th Concrete Communication Conference Birmingham*, (pp. 223-235).
- Warkus, J., and Raupach, M. (2008). Numerical modelling of macrocells occurring during corrosion of steel in concrete. *Materials and Corrosion*, 59(2), pp. 122-130.
- Whiting, D. A., and Nagi, M. A. (2003). Electrical Resistivity of Concrete – A Literature Review. *Portland Cement Association*.
- Whittington, H. W., McCarter, J., and Forde, M. C. (1981). The conduction of electricity through concrete. *Magazine of Concrete Research*, 33(114), pp. 48-60.
- Wilson, K., Jawed, M., and Ngala, V. (2013). The selection and use of cathodic protection systems for the repair of reinforced concrete structures. *Construction and Building Materials*, 39, pp. 19-25.

- Xu, J., and Yao, W. (2009). Current distribution in reinforced concrete cathodic protection system with conductive mortar overlay anode. *Construction and Building Materials*, 23, pp. 2220-2226.
- Zaccardi, Y. A. V., and Maio, A. A. D. (2014). Electrical resistivity measurement of unsaturated concrete samples. *Magazine of Concrete Research*, pp. 484–491.
- Zaccardi, Y. A. V., García, J. F., Huéllamo, P., and Maio, Á. A. D. (2009). Influence of temperature and humidity on Portland cement mortar resistivity monitored with inner sensors.” *Materials and Corrosion*, pp. 294–299.
- Zhou, Y., Gencturk, B., Willam, K., and Attar, A. (2014). Carbonation-induced and chloride-induced corrosion in reinforced concrete structures. *Journal of Materials in Civil Engineering*.
- Zhu, J. H., Zhu, M., Han, N., Liu, W., and Xing, F. (2014). Electrical and Mechanical Performance of Carbon Fiber-Reinforced Polymer Used as the Impressed Current Anode Material. *Materials*, 7(8), pp. 5438-5453.

APPENDIX A

Chloride Ion Concentration Redistribution in Concrete

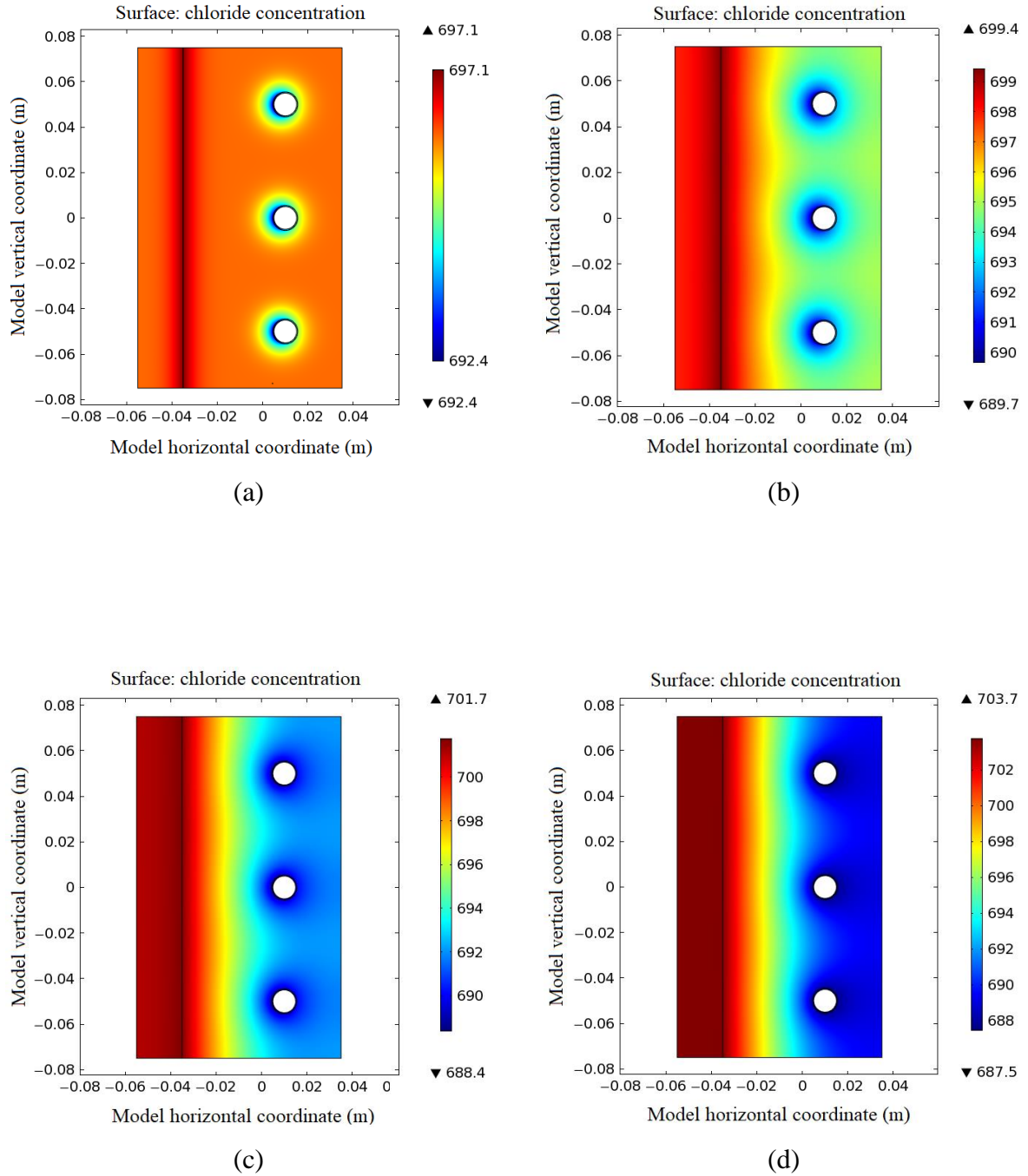


Figure A.1 Redistribution of chloride concentration in concrete under 10mA/m^2 (2% NaCl).

(a) $t = 24$ hours, (b) $t = 10$ days, (c) $t = 30$ days, (d) $t = 90$ days.

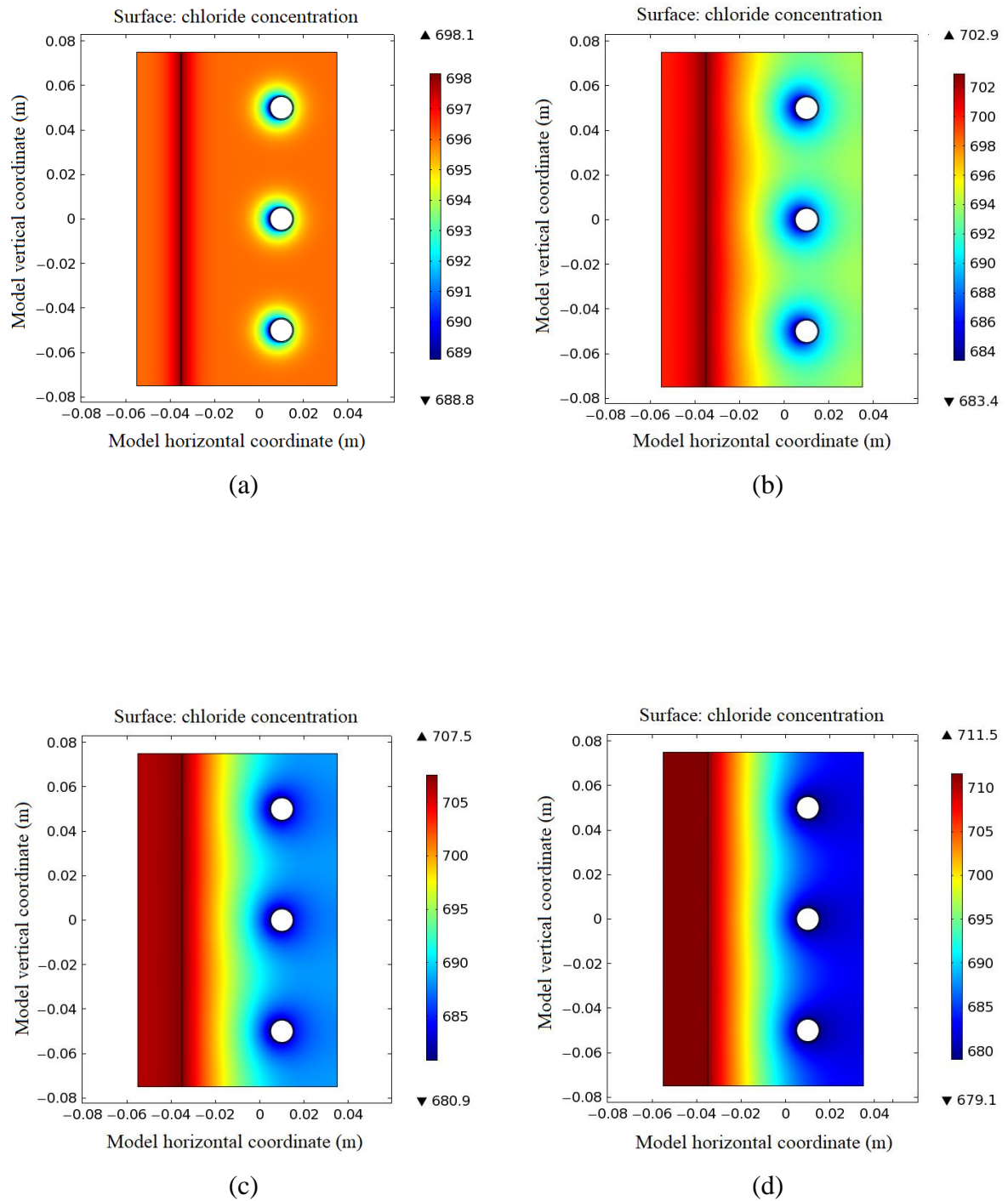


Figure A.2 Redistribution of chloride concentration in concrete under 20mA/m^2 (2% NaCl).
 (a) $t = 24$ hours, (b) $t = 10$ days, (c) $t = 30$ days, (d) $t = 90$ days.

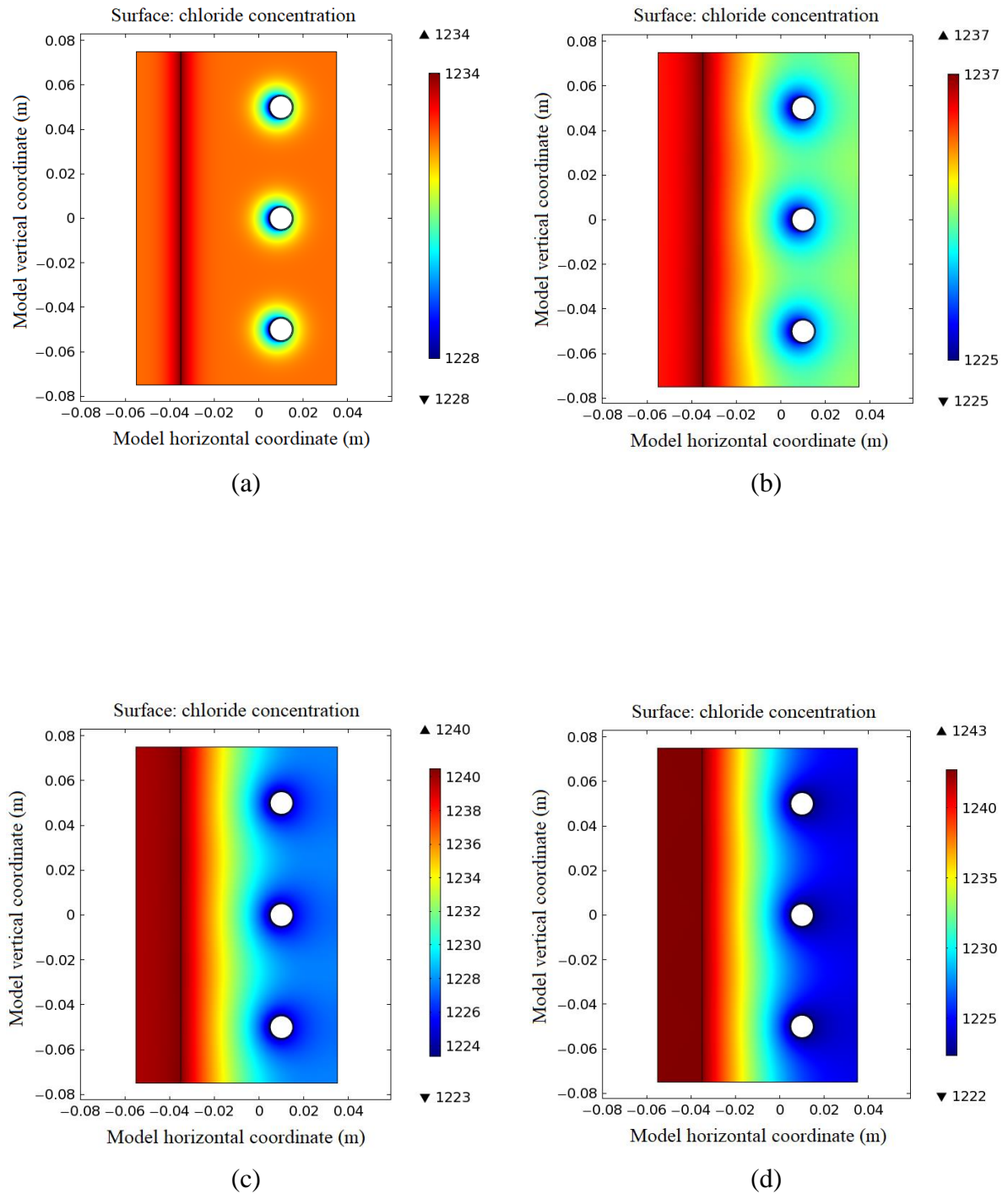


Figure A.3 Redistribution of chloride concentration in concrete under 10mA/m^2 (3.5% NaCl).
 (a) $t = 24$ hours, (b) $t = 10$ days, (c) $t = 30$ days, (d) $t = 90$ days.

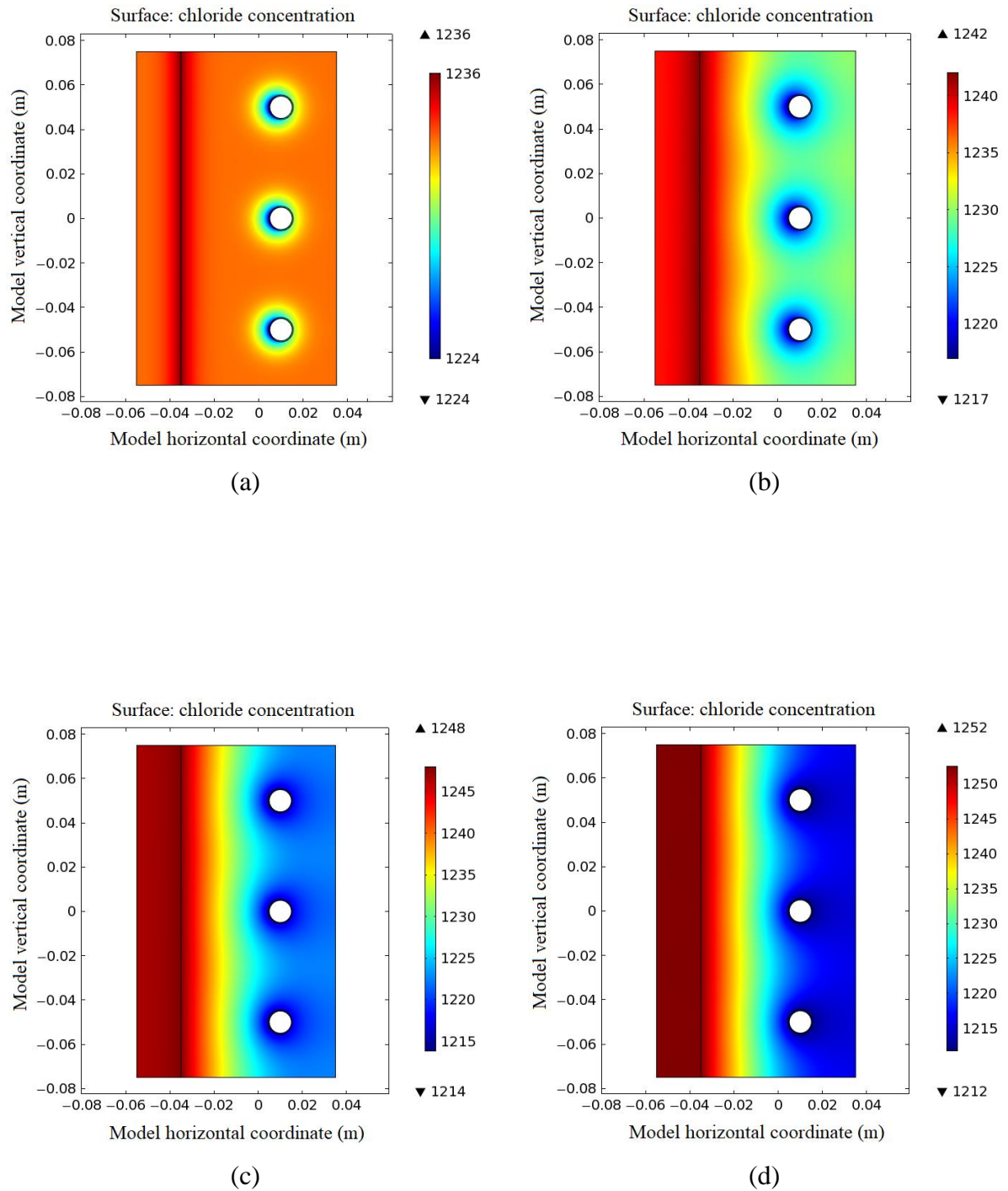


Figure A.4 Redistribution of chloride concentration in concrete under 20mA/m^2 (3.5% NaCl).
 (a) $t = 24$ hours, (b) $t = 10$ days, (c) $t = 30$ days, (d) $t = 90$ days.

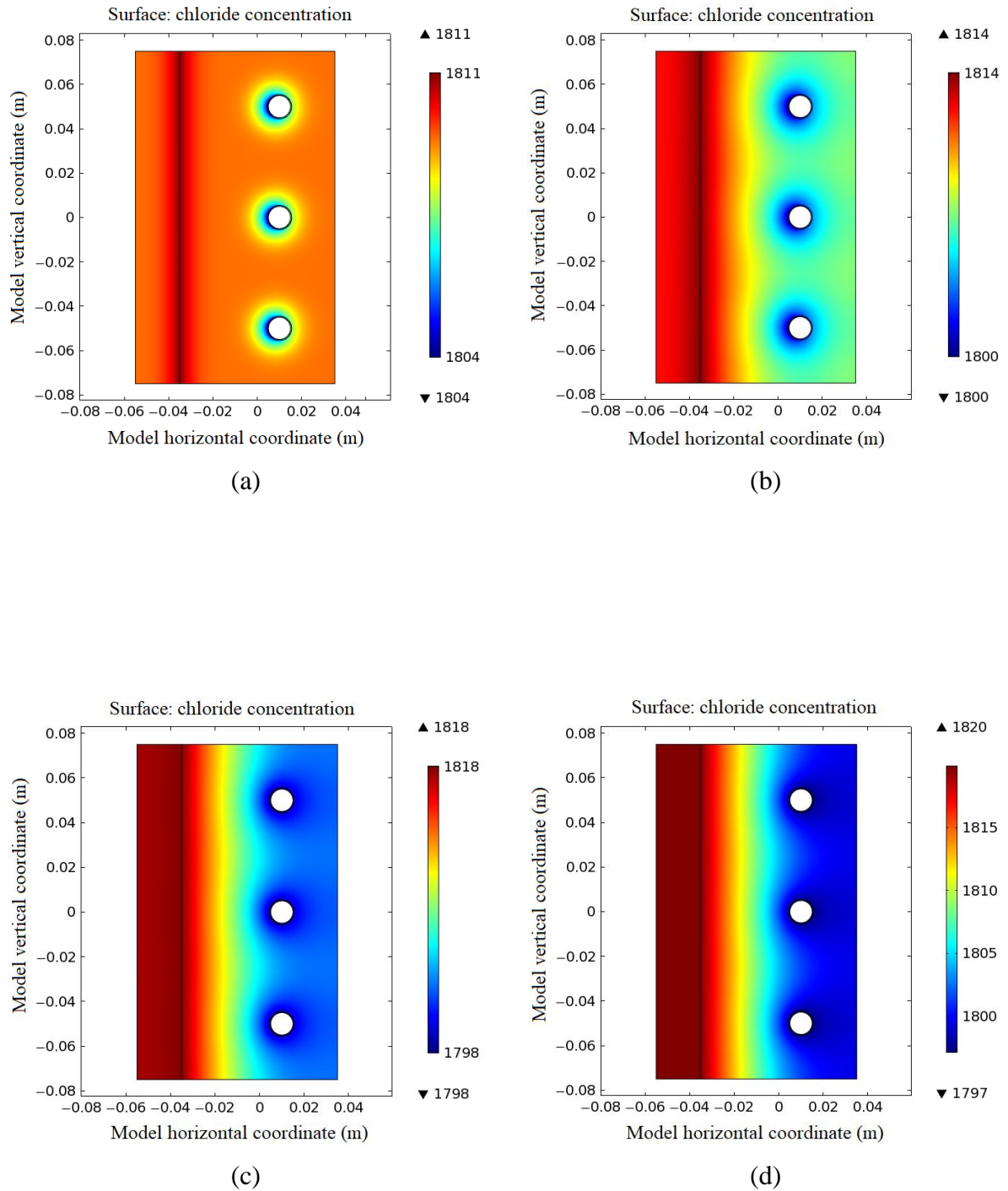


Figure A.5 Redistribution of chloride concentration in concrete under 10mA/m² (5% NaCl).
 (a) $t = 24$ hours, (b) $t = 10$ days, (c) $t = 30$ days, (d) $t = 90$ days.

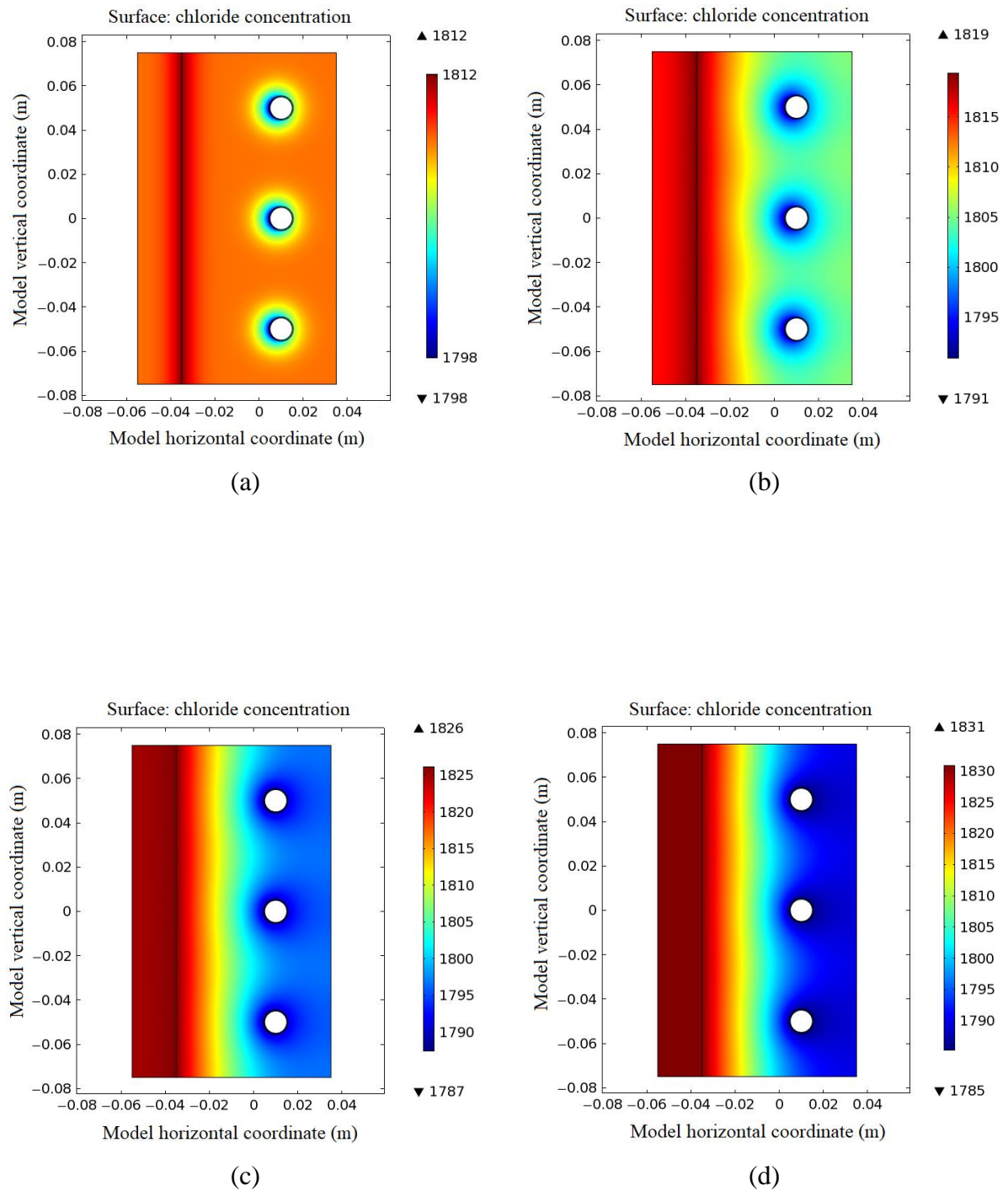
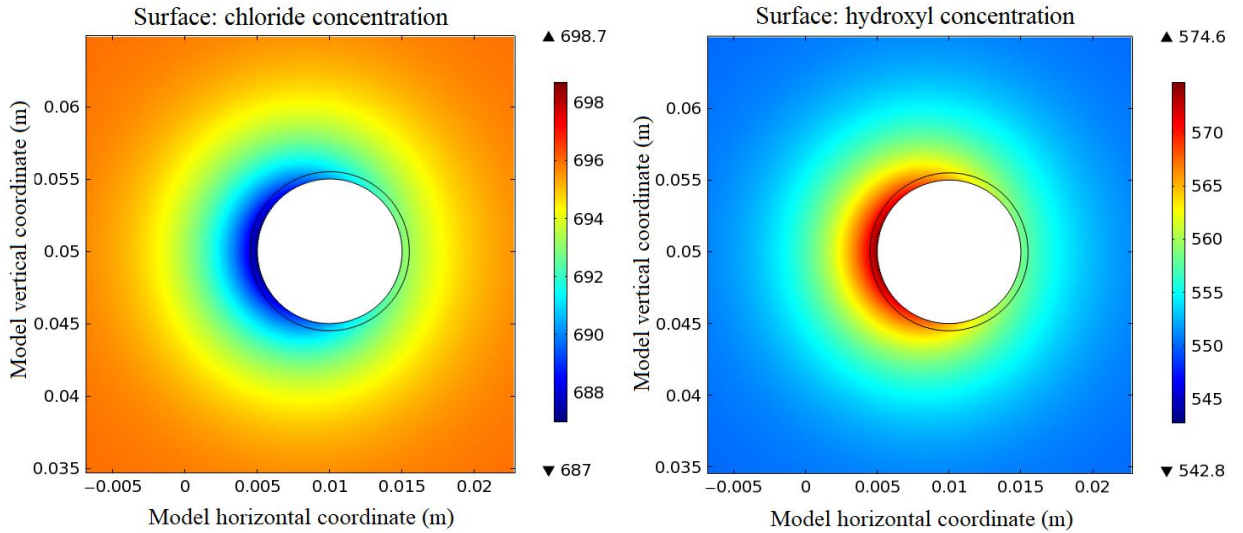


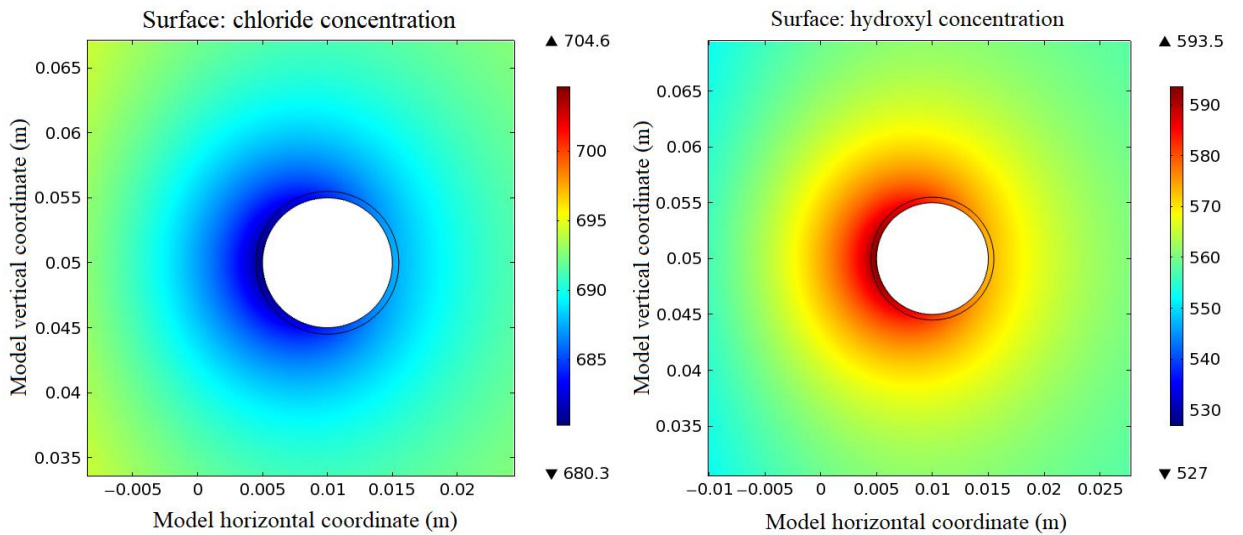
Figure A.6 Redistribution of chloride concentration in concrete under 20mA/m^2 (5% NaCl).
 (a) $t = 24$ hours, (b) $t = 10$ days, (c) $t = 30$ days, (d) $t = 90$ days.

APPENDIX B

Distribution of Chloride and Hydroxyl Ion Concentration at Steel-Concrete Interface

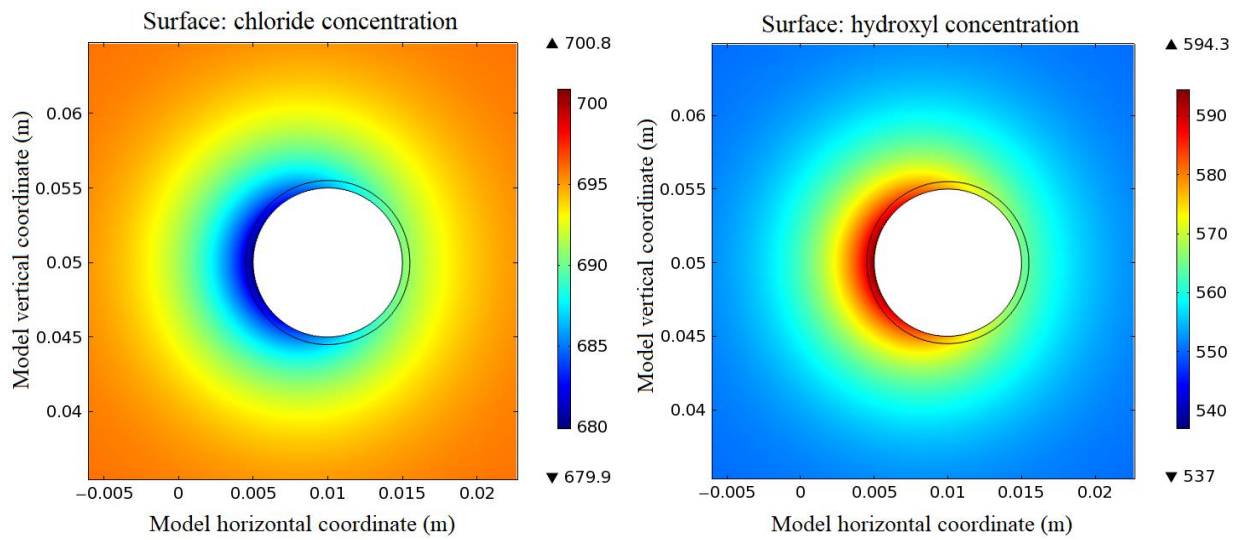


(a)

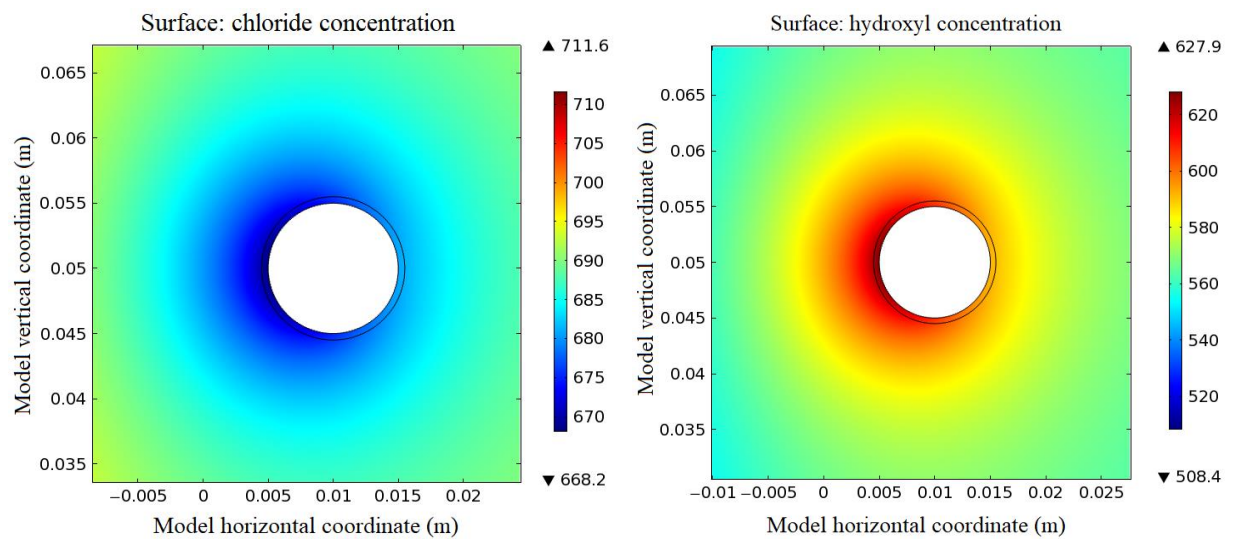


(b)

Figure B.1 Distribution of chloride and hydroxyl ions concentration at steel-concrete interface under 25mA/m^2 (2% NaCl). (a) $t = 24$ hours (b) $t = 10$ days.

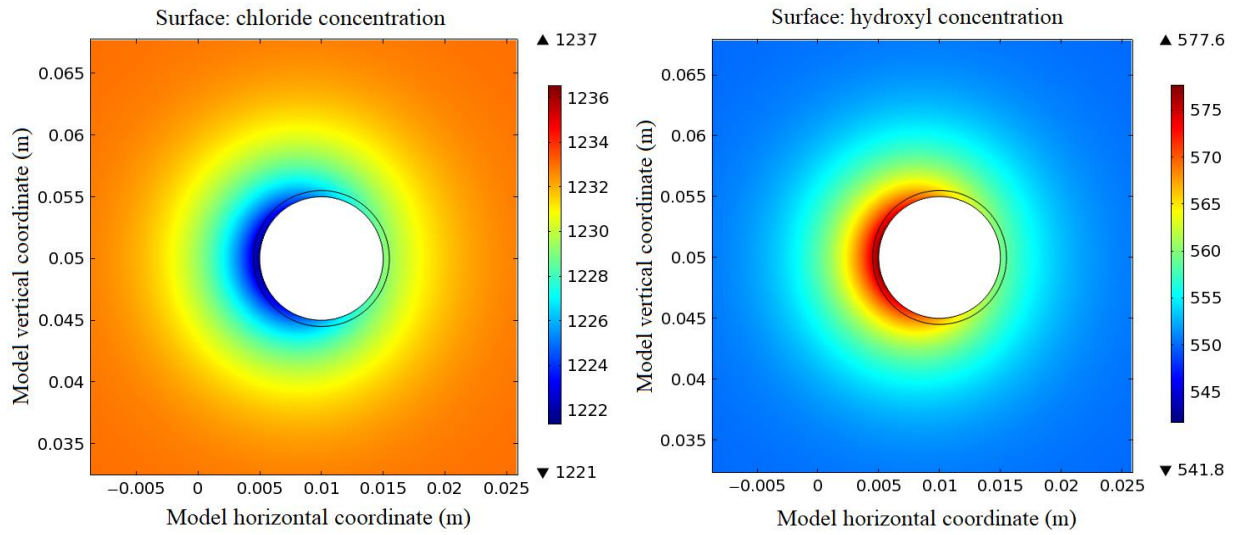


(a)

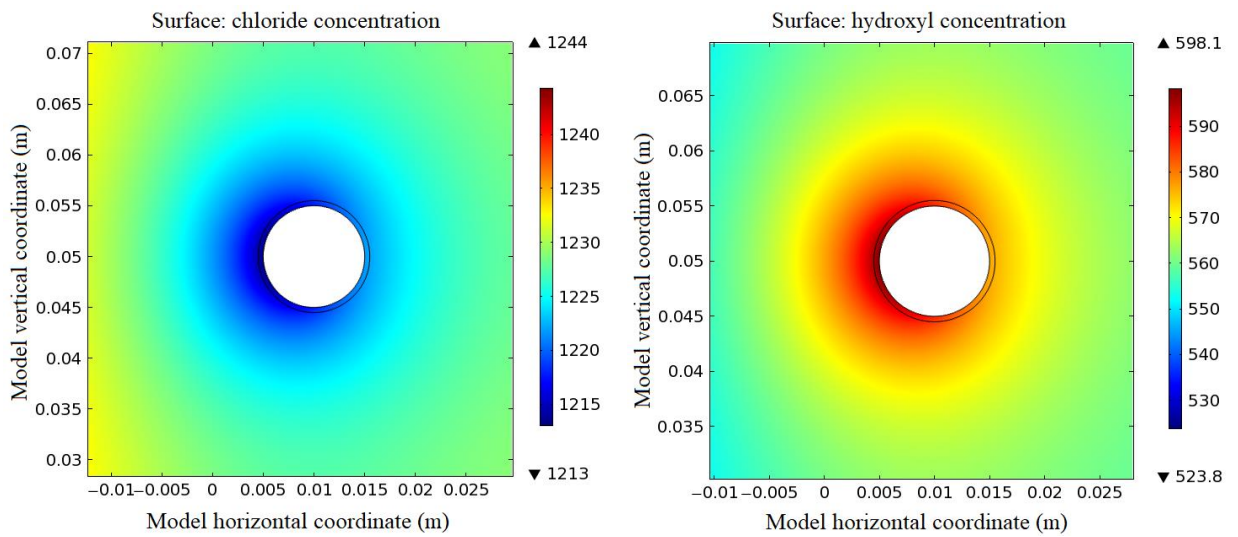


(b)

Figure B.2 Distribution of chloride and hydroxyl ions concentration at steel-concrete interface under 45mA/m^2 (2% NaCl). (a) $t = 24$ hours (b) $t = 10$ days.

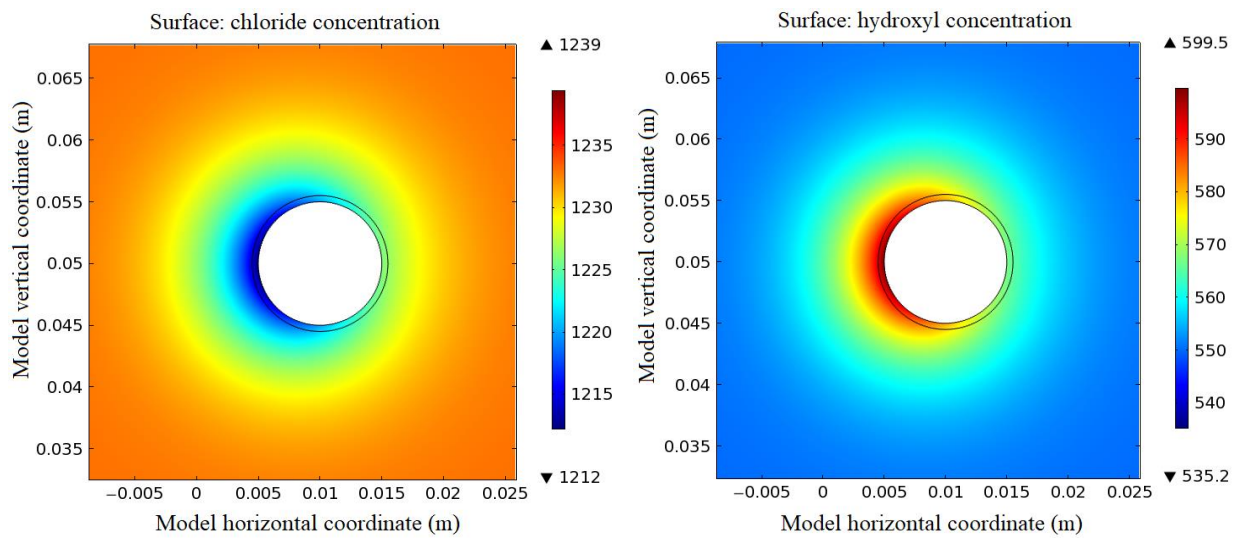


(a)

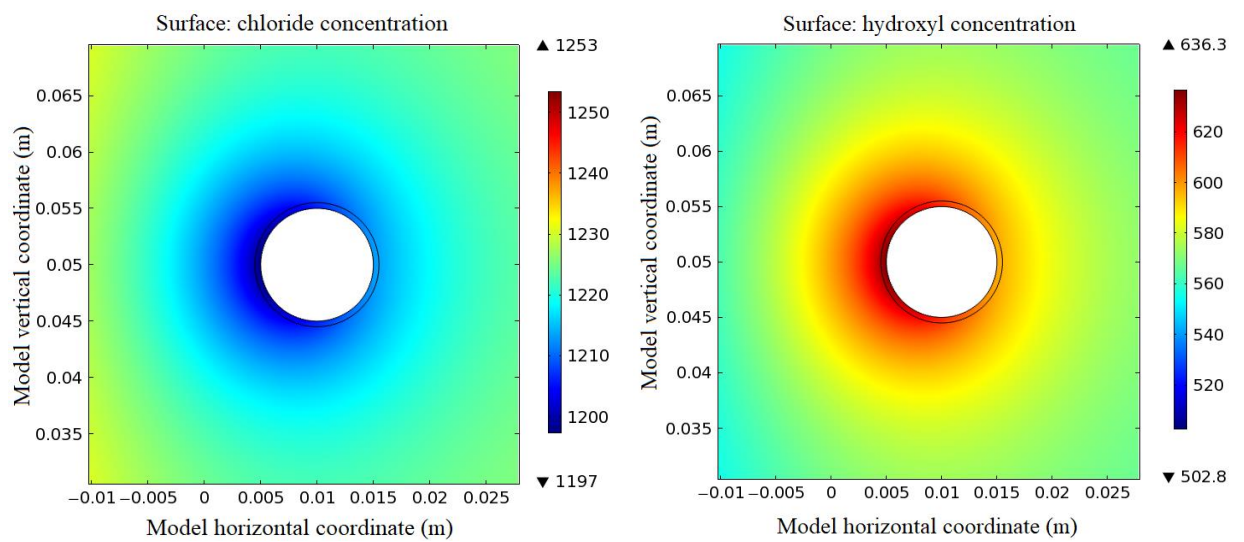


(b)

Figure B.3 Distribution of chloride and hydroxyl ions concentration at steel-concrete interface under 25mA/m^2 (3.5% NaCl). (a) $t = 24$ hours (b) $t = 10$ days.

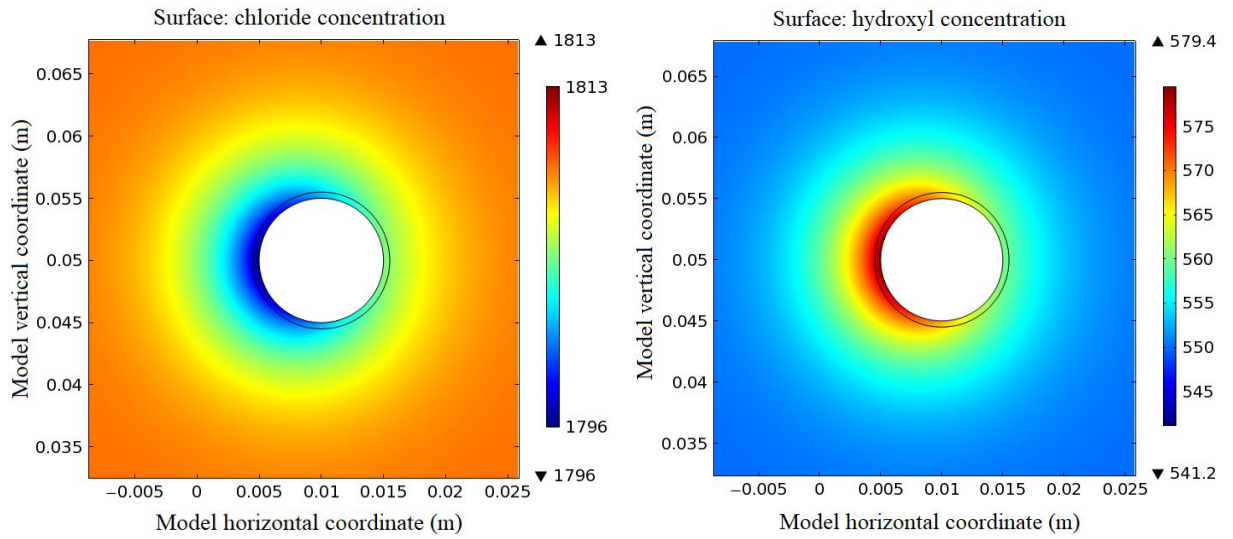


(a)

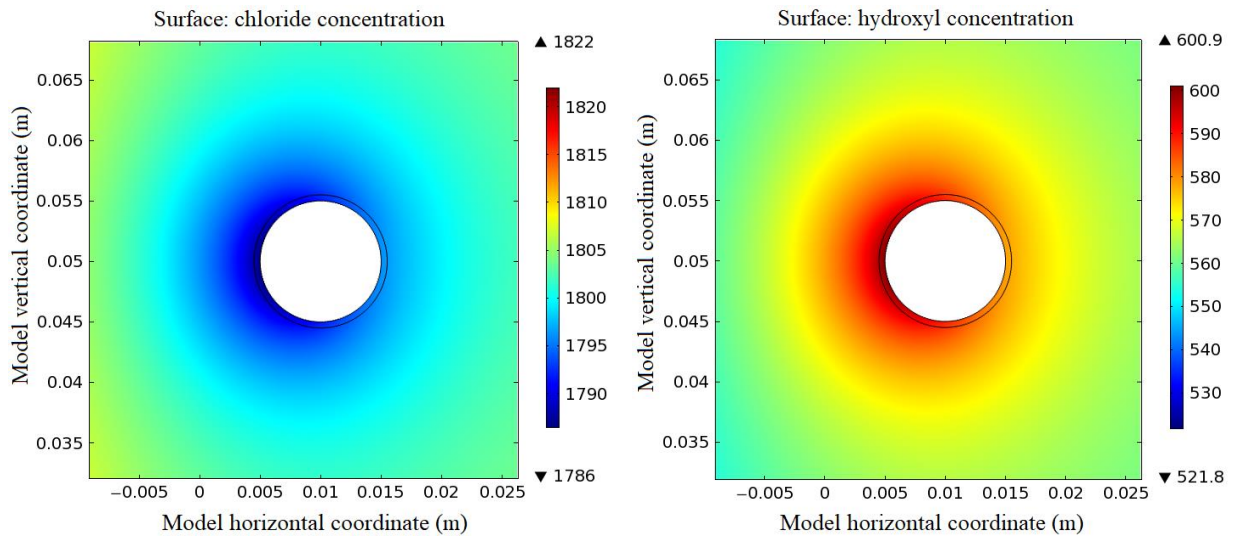


(b)

Figure B.4 Distribution of chloride and hydroxyl ions concentration at steel-concrete interface under 45mA/m^2 (3.5% NaCl). (a) $t = 24\text{ hours}$ (b) $t = 10\text{ days}$.

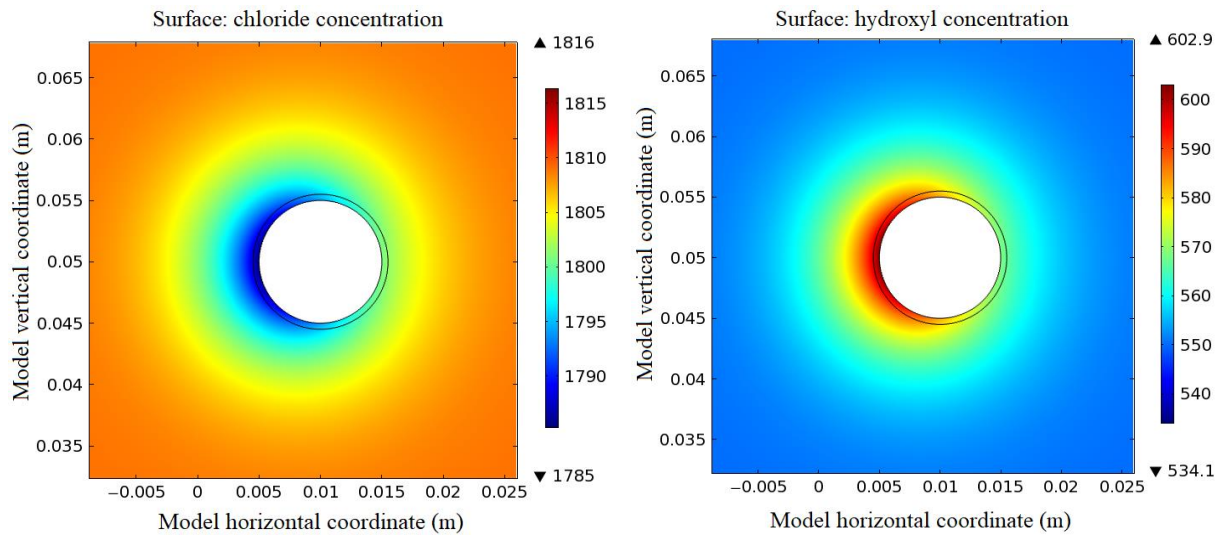


(a)

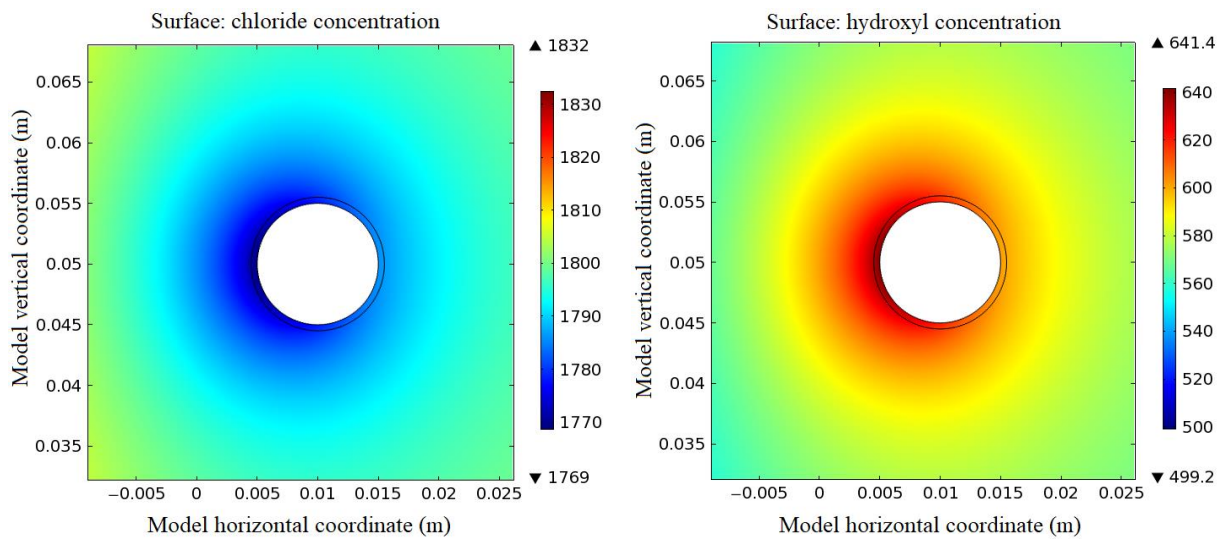


(b)

Figure B.5 Distribution of chloride and hydroxyl ions concentration at steel-concrete interface under 25mA/m^2 (5% NaCl). (a) $t = 24$ hours (b) $t = 10$ days.



(a)

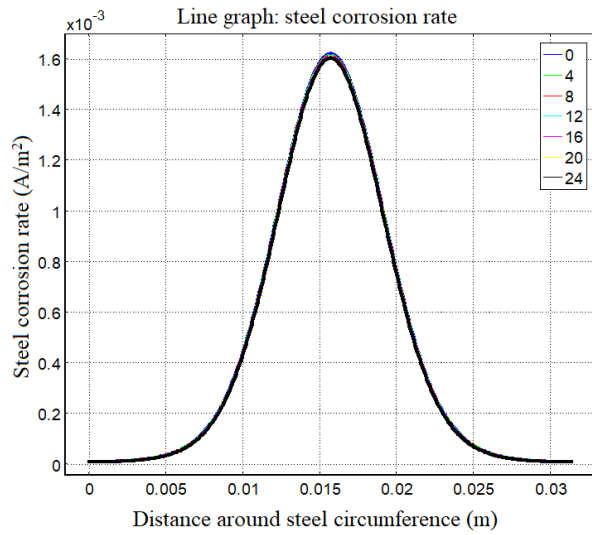


(b)

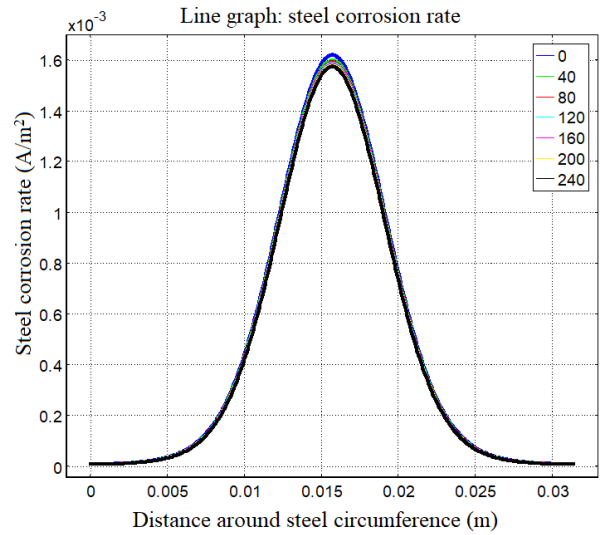
Figure B.6 Distribution of chloride and hydroxyl ions concentration at steel-concrete interface under 45mA/m^2 (5% NaCl). (a) $t = 24$ hours (b) $t = 10$ days.

APPENDIX C

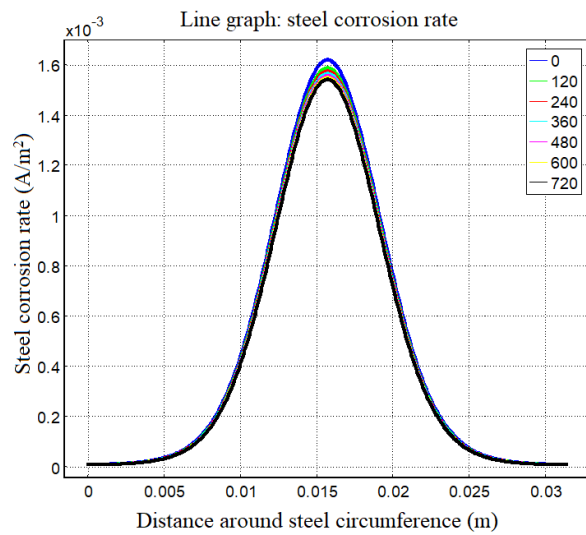
Distribution of Steel Corrosion Rate along the Circumference of Steel Bar Cross Section



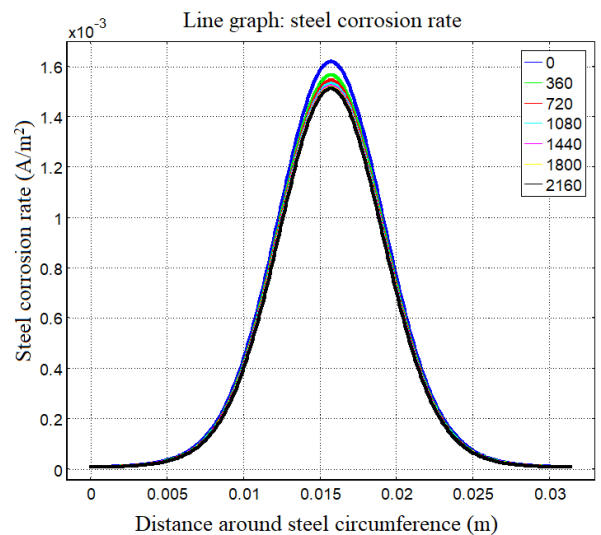
(a)



(b)



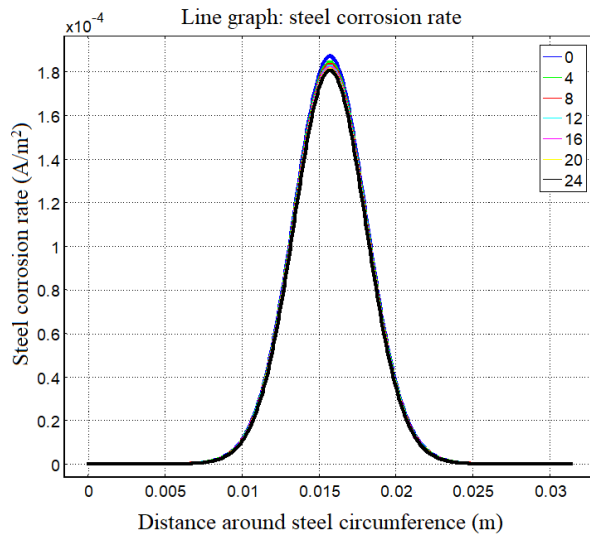
(c)



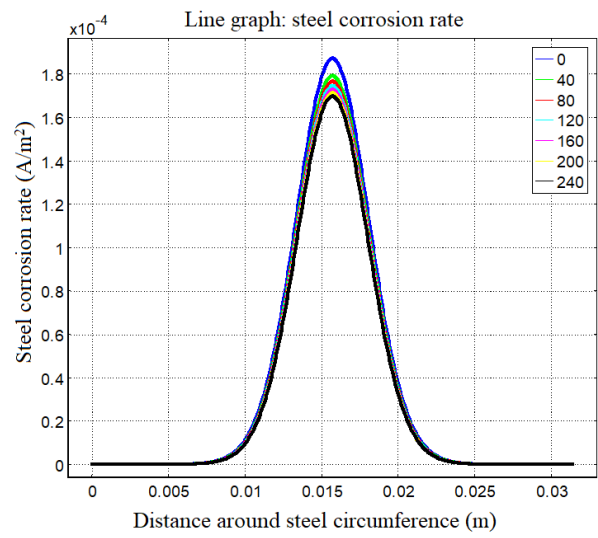
(d)

Figure C.1 Distribution of steel corrosion rate along the circumference of steel bar cross section under $35mA/m^2$ (2% NaCl).

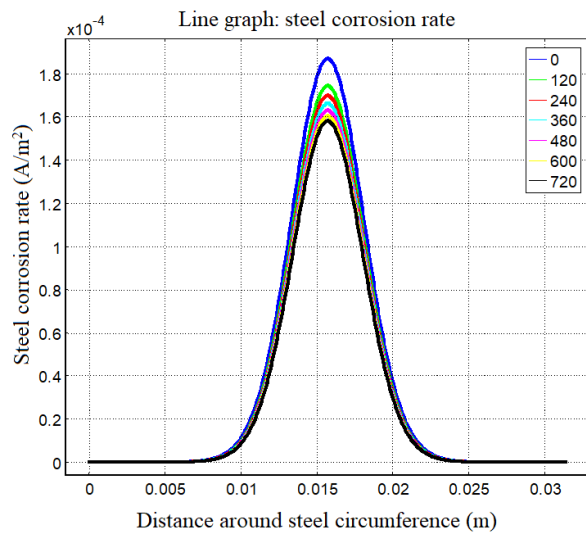
(a) $t = 24$ hours, (b) $t = 10$ days, (c) $t = 30$ days, (d) $t = 90$ days.



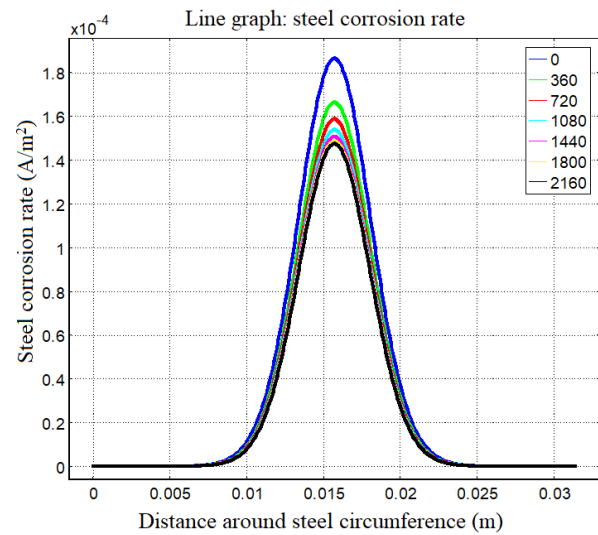
(a)



(b)



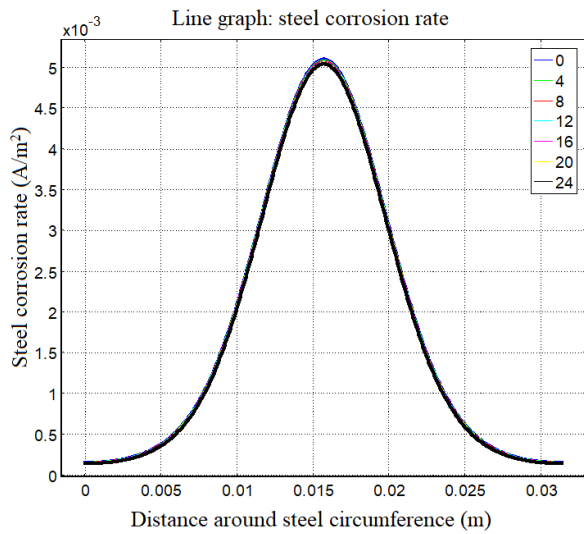
(c)



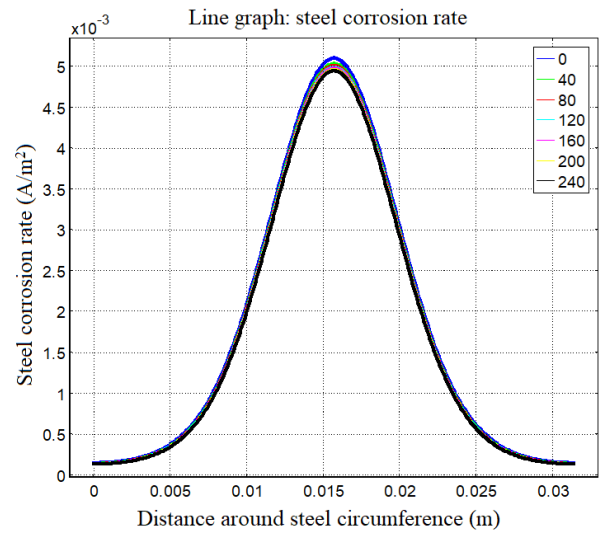
(d)

Figure C.2 Distribution of steel corrosion rate along the circumference of steel bar cross section under $75mA/m^2$ (2% NaCl).

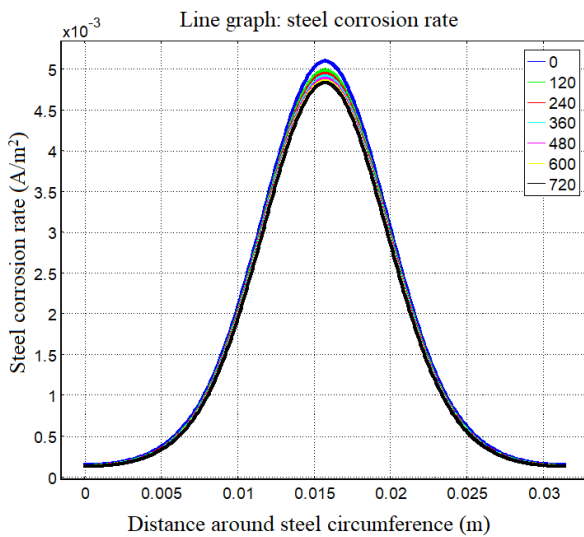
(a) $t = 24$ hours, (b) $t = 10$ days, (c) $t = 30$ days, (d) $t = 90$ days.



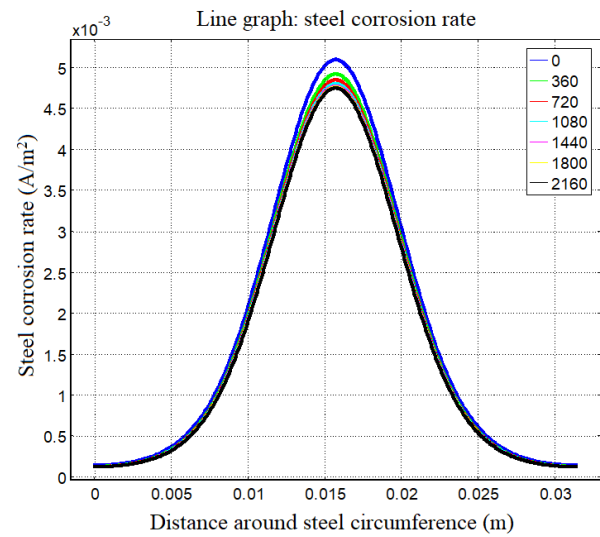
(a)



(b)



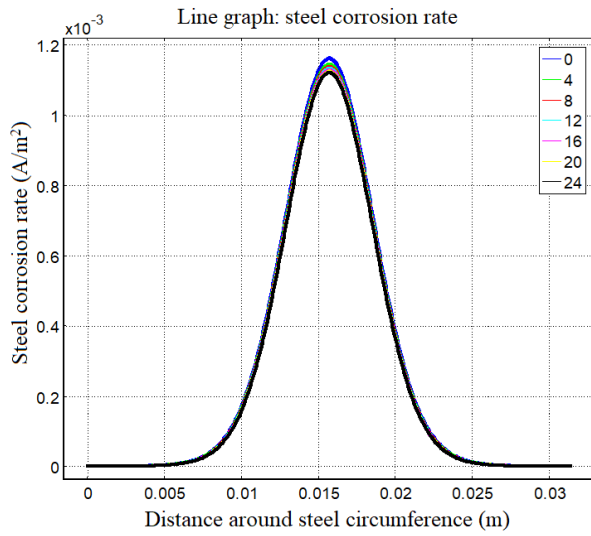
(c)



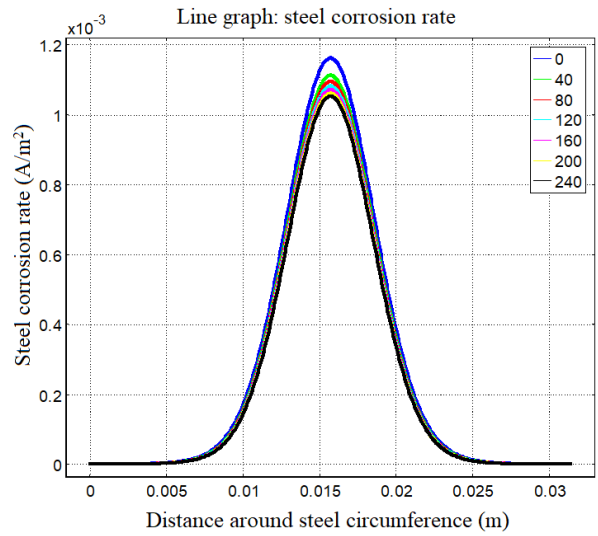
(d)

Figure C.3 Distribution of steel corrosion rate along the circumference of steel bar cross section under $35mA/m^2$ (3.5% NaCl).

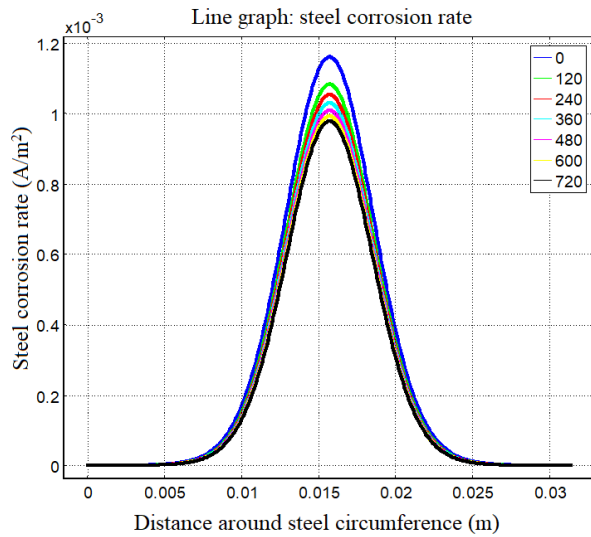
(a) $t = 24$ hours, (b) $t = 10$ days, (c) $t = 30$ days, (d) $t = 90$ days.



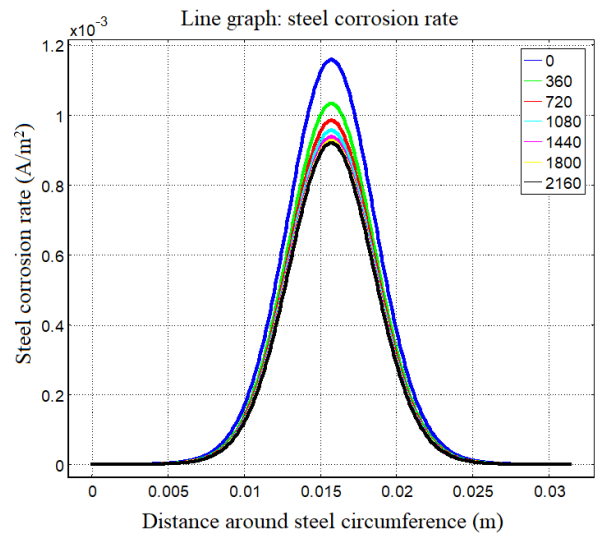
(a)



(b)



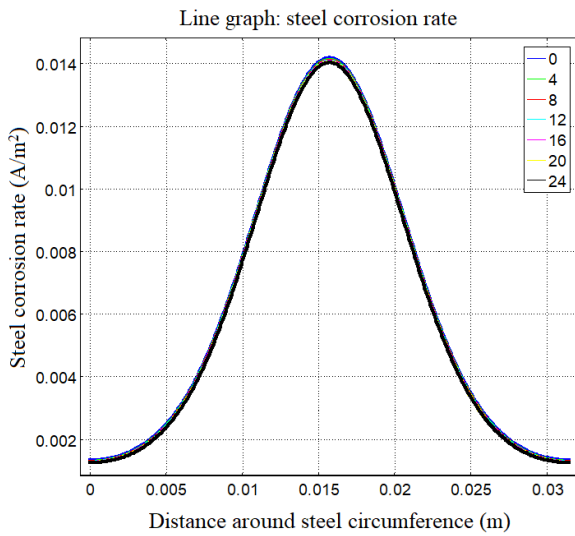
(c)



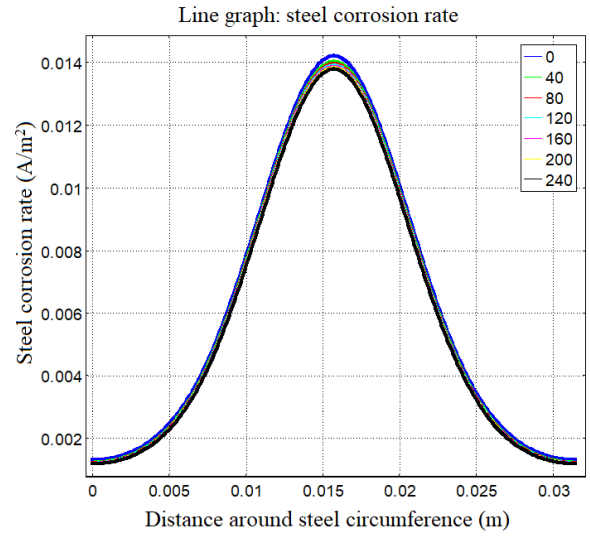
(d)

Figure C.4 Distribution of steel corrosion rate along the circumference of steel bar cross section under 75mA/m^2 (3.5% NaCl).

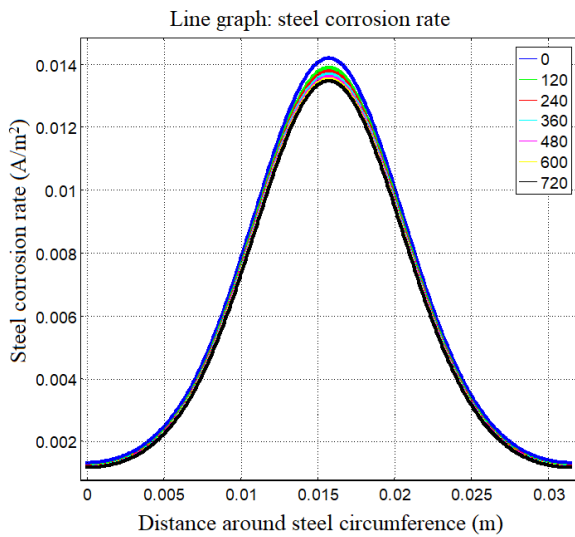
(a) $t = 24$ hours, (b) $t = 10$ days, (c) $t = 30$ days, (d) $t = 90$ days.



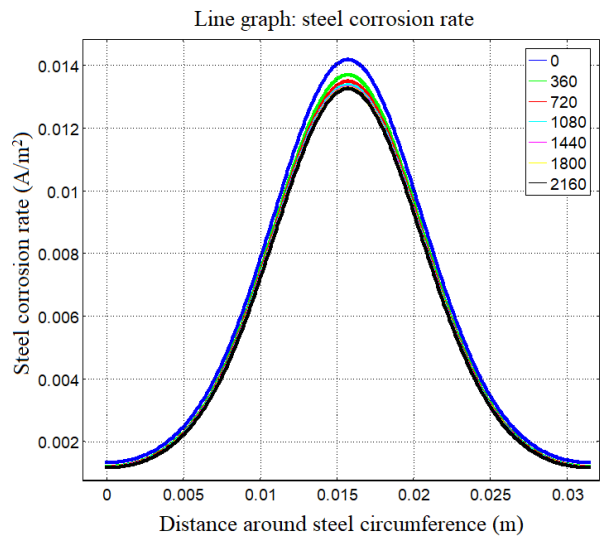
(a)



(b)



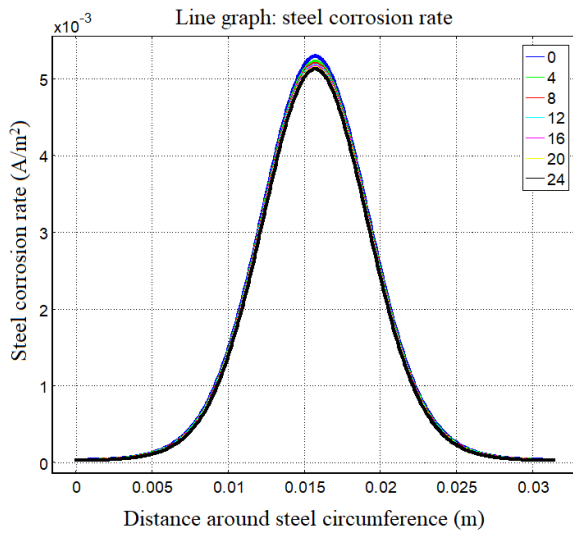
(c)



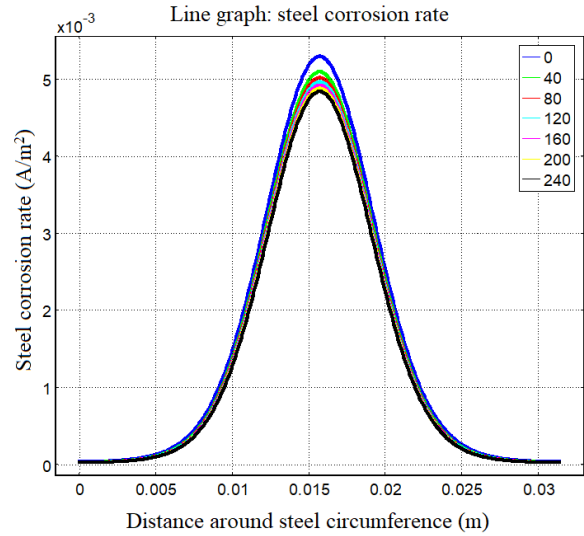
(d)

Figure C.5 Distribution of steel corrosion rate along the circumference of steel bar cross section under $35mA/m^2$ (5% NaCl).

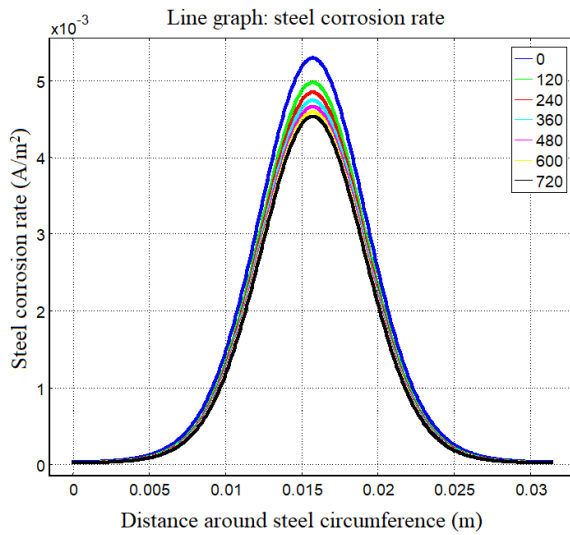
(a) $t = 24$ hours, (b) $t = 10$ days, (c) $t = 30$ days, (d) $t = 90$ days.



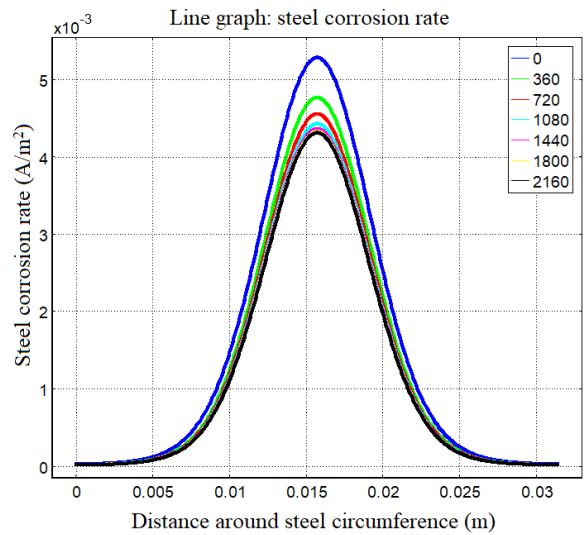
(a)



(b)



(c)



(d)

Figure C.6 Distribution of steel corrosion rate along the circumference of steel bar cross section under 75mA/m^2 (5% NaCl).

(a) $t = 24$ hours, (b) $t = 10$ days, (c) $t = 30$ days, (d) $t = 90$ days